

8-1-2018

# Comprehensive Study of Spray-Painting and 3d Printing Fabrication Methods for Nafion® and Nafion® Equivalents in Ionic Polymer-Metal Composite Actuators and Sensors

Sarah Trabia  
sarahtrabia@gmail.com

Follow this and additional works at: <https://digitalscholarship.unlv.edu/thesesdissertations>



Part of the [Mechanical Engineering Commons](#)

---

## Repository Citation

Trabia, Sarah, "Comprehensive Study of Spray-Painting and 3d Printing Fabrication Methods for Nafion® and Nafion® Equivalents in Ionic Polymer-Metal Composite Actuators and Sensors" (2018). *UNLV Theses, Dissertations, Professional Papers, and Capstones*. 3389.  
<https://digitalscholarship.unlv.edu/thesesdissertations/3389>

This Dissertation is protected by copyright and/or related rights. It has been brought to you by Digital Scholarship@UNLV with permission from the rights-holder(s). You are free to use this Dissertation in any way that is permitted by the copyright and related rights legislation that applies to your use. For other uses you need to obtain permission from the rights-holder(s) directly, unless additional rights are indicated by a Creative Commons license in the record and/or on the work itself.

This Dissertation has been accepted for inclusion in UNLV Theses, Dissertations, Professional Papers, and Capstones by an authorized administrator of Digital Scholarship@UNLV. For more information, please contact [digitalscholarship@unlv.edu](mailto:digitalscholarship@unlv.edu).

COMPREHENSIVE STUDY OF SPRAY-PAINTING AND 3D PRINTING FABRICATION  
METHODS FOR NAFION® AND NAFION® EQUIVALENTS IN IONIC POLYMER-  
METAL COMPOSITE ACTUATORS AND SENSORS

By

Sarah Trabia

Bachelor of Science in Engineering – Mechanical Engineering  
University of Nevada, Las Vegas  
December 2012

Master of Science in Engineering – Mechanical Engineering  
University of Nevada, Las Vegas  
August 2014

A dissertation submitted in partial fulfillment  
of the requirements for the

Doctor of Philosophy in Engineering– Mechanical Engineering

Department of Mechanical Engineering  
Howard R. Hughes College of Engineering  
The Graduate College

University of Nevada, Las Vegas  
August 2018



## **Dissertation Approval**

The Graduate College  
The University of Nevada, Las Vegas

May 14, 2018

This dissertation prepared by

Sarah Trabia

entitled

COMPREHENSIVE STUDY OF SPRAY-PAINTING AND 3D PRINTING  
FABRICATION METHODS FOR NAFION® AND NAFION® EQUIVALENTS IN  
IONIC POLYMERMETAL COMPOSITE ACTUATORS AND SENSORS

is approved in partial fulfillment of the requirements for the degree of

Doctor of Philosophy in Engineering– Mechanical Engineering  
Department of Mechanical Engineering

Kwang Kim, Ph.D.  
*Examination Committee Chair*

Kathryn Hausbeck Korgan, Ph.D.  
*Graduate College Interim Dean*

Woosoon Yim, Ph.D.  
*Examination Committee Member*

Jaeyun Moon, Ph.D.  
*Examination Committee Member*

Brendan O'Toole, Ph.D.  
*Examination Committee Member*

Michael Pravica, Ph.D.  
*Graduate College Faculty Representative*

## Abstract

Ionic Polymer-Metal Composites (IPMC) are smart materials that are useful in different applications because of their low voltage requirements and light weight. IPMC are made of ion-conducting polymer (ionomer) plated with a noble metal, such as platinum. When a voltage potential is applied to the surface of the IPMC, it creates an electro-mechanical effect, causing it to actuate. This is due to the motion of the cations towards the negatively charged side of the IPMC, causing it to swell, and in turn, bend. Conversely, deforming an IPMC moves cations within it, which produces a small voltage that can be amplified as a sensing signal (mechano-electrical effect).

There are three forms of ionomers available on the market: sheets, precursor pellets, and water-based dispersion. Current fabrication processes limit the shapes that can be made using these forms. The goals of this research are:

1. Develop fabrication methods to allow for the possibility of creating new shapes, contours, and structures of ionomer to broaden their applications.
2. Consider an alternative candidate for IPMC base, *Aquivion*, instead of *Nafion* which is commonly used, to improve the actuation performance of IPMCs.

Two fabrication methods are presented: spray-painting and additive manufacturing (3D printing). While spray-painting gives more control in the thickness of the membrane and detailed outlines, 3D printing allows the creation of new 3D IPMC structures. Material characteristics of *Nafion* and *Aquivion*, both the activated and precursor forms, are studied to optimize the fabrication processes, such as Young's modulus, damping coefficient, melting temperature, and viscosity. It was found

that each fabrication method produces ionomers with altered properties, such as the Young's Modulus and thermal degradation temperature. As a result of this research, IPMCs were fabricated using these two developed methods. The performance of these actuators was compared to traditionally-made IPMCs using a set of standardized tests. It was shown that the proposed fabrication processes did not alter the ionomers negatively. It was also shown that it was possible to improve the performance of IPMCs by using *Aquivion* as the base of the IPMC and through 3D printing, a high performance IPMC was produced.

Additionally, a National Advisory Committee for Aeronautics (NACA) inspired hydrofoil shape was 3D printed with precursor *Aquivion*. The structure was designed to have curved features and is relatively thick for an IPMC. The largest thickness in the cross section is 1.63 mm. The 3D Printed *Aquivion* Hydrofoil was activated by hydrolysis and plated with platinum. It was then tested for actuation and blocking force capabilities. The 3D Printed *Aquivion* IPMC Hydrofoil was able to actuate up to 3 mm peak-to-peak and had good blocking force output.

## **Acknowledgements**

I would first like to thank my family for the constant support throughout my academic career. To my parents, I don't think I can ever repay you for everything you have done for me. To Suzy and Kareem, thank you for being my best friends since day one. I would like to thank my dad for helping me grow within my field and always being open to discuss research and experiments.

I would also like to thank my advisor, Dr. Kwang Kim. Without your experience, knowledge, and continuous encouragement, I would not be as well rounded of a researcher as I am now. I truly appreciate all of your advice throughout my career and everything you have provided to me during my Ph.D. studies.

Dr. Viljar Palmre and Dr. Taeseon Hwang, thank you for training me in IPMC fabrication, wet lab practices, material characterization, prototype manufacturing, and more. I have learned so much from you both and now know how to completely design an experiment, from the first stages of development, to collecting data and results, and finally putting together a manuscript. I would also like to thank my lab colleagues for great discussions and fun memories. I will always be proud of the work we have conducted together at Active Materials and Smart Living Laboratory (AMSL).

To the Department of Mechanical Engineering and College of Engineering that has been there for every aspect of my life, thank you for continually supporting me and pushing me to be my best. Thank you, Joan Conway, for always being there to help with any question I may have had. Thank you to all the professors that taught me throughout all three of my degrees here at UNLV. Thank you, Julie Longo and Sue Wainscott, for training me to be an effective writer and a more thorough

researcher. Thank you, Kari Locke, for always helping out whenever I ran into issues with the programs I needed to use. Thank you, Jeff Markle, for being a great resource in experimental setups and any other random questions I had. But overall, thank you all for the wonderful conversations that we've shared after we were done talking shop.

Finally, this work would not be possible without funding agencies. This work is partially funded by the National Science Foundation and National Aeronautics and Space Administration.

## Table of Contents

Abstract.....	iii
Acknowledgements.....	v
Table of Contents.....	vii
List of Figures.....	xi
List of Tables.....	xxiii
Chapter 1. Introduction.....	1
1.1. Basics of Ionic Polymer-Metal Composites.....	1
1.2. History of Ionic Polymer-Metal Composites.....	1
1.3. Applications of Ionic Polymer-Metal Composites.....	3
1.4. Current Fabrication Methods.....	4
1.4.1. Rectangular IPMCs using membrane sheets.....	5
1.4.2. Hot-pressing membranes and pellets.....	6
1.4.3. Casting Nafion Water Dispersion.....	6
1.4.4. Extruding tubes using pellets.....	7
1.5. Rationale for Advanced Fabrication Methods.....	8
1.6. Improving the performance of Ionic Polymer-Metal Composites.....	8
1.7. Objectives and Significance of the Work Presented.....	9
1.7.1. Objectives.....	9
1.7.2. Significance of the Work Presented.....	10
Chapter 2. Exploring the Possibility of Improving the Performance Abilities of Ionic Polymer-Metal Composites: Searching for an alternative ionomer.....	12
2.1. A hypothesis regarding the need to increase performance of IPMC.....	12



2.2. Physics of Ion Transport Within Ionomers.....	13
2.3. Comparison of Nafion and Aquivion Characteristics.....	15
2.4. Theoretical Consideration of IPMC Modelling Regarding Nafion versus Aquivion .....	18
2.4.1. Brief Summary of the 1D COMSOL Model.....	18
2.4.2. Diffusion Coefficient as a Parameter to Affect the Performance of an IPMC .....	20
2.5. Experimental data of N-IPMC and A-IPMC .....	23
Chapter 3. Understanding the Thermal Properties of Precursor-Ionomers to Optimize Fabrication Processes for Ionic Polymer-Metal Composites (IPMCs).....	28
3.1. Introduction.....	28
3.2. Methods.....	33
3.3. Results.....	34
3.4. Discussion .....	42
3.5. Conclusions.....	44
3.6. Acknowledgement .....	45
Chapter 4. A Fabrication Method of Unique Nafion Shapes by Painting for Ionic Polymer-Metal Composites.....	46
4.1. Introduction.....	46
4.2. Methodology .....	49
4.3. Results.....	51
4.3.1. Comparison of the Physical Characteristics of P-Nafion® and Nafion® 117.....	51
4.3.2. Comparison of Paintable-IPMC and Traditional IPMC .....	57
4.4. Discussion .....	67
4.5. Conclusions and Future Work .....	69

4.6. Acknowledgements.....	69
Chapter 5. Searching for A New Ionomer for 3D Printable Ionic Polymer-Metal Composites:	
Aquivion® As A Candidate.....	70
5.1. Introduction.....	70
5.1.1. Basics of IPMCs .....	70
5.1.2. Potential Applications of IPMCs .....	71
5.1.3. Traditional fabrication methods for the ionomer base.....	72
5.1.4. Advanced fabrication methods for the ionomer base .....	73
5.2. Objectives .....	74
5.3. Approaches .....	75
5.4. Methods.....	75
5.4.1. Comparing Nafion® and Aquivion® .....	75
5.4.2. Filament production and 3D Printing of Aquivion® .....	76
5.4.3. Activation and platinum plating.....	78
5.4.4. IPMC performance testing.....	80
5.5. Results and Discussion .....	82
5.5.1. Comparing Nafion® and Aquivion® .....	82
5.5.2. Filament production.....	90
5.5.3. 3D printing Aquivion® .....	91
5.5.4. Material characterization of the printed Aquivion® .....	97
5.5.5. IPMC performance comparison.....	99
5.6. Conclusions and Future Work .....	107
5.7. Acknowledgements.....	108

Chapter 6. Demonstration: 3D Printed NACA-inspired Hydrofoil-shaped IPMC .....	109
6.1. Introduction.....	109
6.2. Hydrofoil Design .....	110
6.3. Printing Process .....	113
6.4. Activating and plating the Printed-Aquivion Hydrofoil .....	116
6.5. Performance of the 3D Printed-Aquivion Hydrofoil-shaped IPMC .....	120
6.6. Conclusions and Future Work .....	126
Chapter 7. Conclusion.....	128
Chapter 8. Future Work .....	130
Appendix A. Permission to use portion of a book chapter in Chapter 1 from CRC Press .....	132
Appendix B. Permission to reuse figures in Chapter 2.....	133
Appendix C. Considered Multi-Physics for IPMC Actuators and COMSOL Procedure.....	134
Appendix D. Permission to use full article in Chapter 4 from IOP Publishing .....	153
Appendix E. Permission to use full article in Chapter 5 from IOP Publishing .....	160
Appendix F. Injection Molding Ionomers .....	167
Appendix G. Frequency Response for IPMCs in Sensing Applications .....	179
Bibliography .....	181
Curriculum Vitae .....	195

## List of Figures

Figure 2.1. Diagram of an ion cluster, recreated from Hsu and Gierke [44]. The typical diameter of a water molecule is around 2.75 Å [45].	13
Figure 2.2. Relationship between the EW and cluster diameter, with a data point included to show where Aquivion would be on the curve (diamond).	14
Figure 2.3. Relationship between the EW and water content, with a data point included to show where Aquivion would be on the curve (diamond).	15
Figure 2.4. Chemical structure of activated forms of Nafion and Aquivion. Reprinted with permission from IOP Publishing [46].	17
Figure 2.5. FT-IR results that compare the chemical structures for activated forms of Nafion and Aquivion. The peaks that match signify symmetric $\text{CF}_2$ ( $1213 \text{ cm}^{-1}$ ), asymmetric $\text{CF}_2$ ( $1153 \text{ cm}^{-1}$ ), and $\text{S-O}_3$ ( $1060 \text{ cm}^{-1}$ ) bonds. Reprinted with permission from IOP Publishing [46].	17
Figure 2.6. TGA results showing the two activated ionomers have similar thermal degradation points at $300^\circ\text{C}$ . Reprinted with permission from IOP Publishing [46].	18
Figure 2.7. 1D component with the domains named for the boundary conditions applied.	19
Figure 2.8. 2D component with the domains named for the boundary conditions applied.	20
Figure 2.9. Results for the two cases of diffusion coefficients with a sinusoidal voltage input (0.5 V, 1 Hz), where the solid line is Nafion-based IPMC and the dotted line is Aquivion-based IPMC.	22
Figure 2.10. Results for the two cases of diffusion coefficients with a square voltage input (0.5 V, 1 Hz), where the solid line is Nafion-based IPMC and the dotted line is Aquivion-based IPMC.	22

Figure 2.11. Results for the two cases of diffusion coefficients with a triangular voltage input (0.5 V, 1 Hz), where the solid line is Nafion-based IPMC and the dotted line is Aquivion-based IPMC. .... 23

Figure 2.12. IPMCs fabricated using off-the-shelf Nafion (left) and Aquivion (right) membranes. .... 24

Figure 2.13. Experimental data for an N-IPMC and A-IPMC with a voltage input of 3 Volts at 100 mHz. Reprinted with permission from IOP Publishing [46]. .... 24

Figure 2.14. Experimental data for an N-IPMC and A-IPMC with a voltage input of 3 Volts at 500 mHz. Reprinted with permission from IOP Publishing [46]. .... 25

Figure 2.15. Experimental data for an N-IPMC and A-IPMC with a voltage input of 3 Volts at 1 Hz. Reprinted with permission from IOP Publishing [46]. .... 26

Figure 3.1. COMSOL Multi-physics simulation of a parameter sweep to predict the actuation capabilities of a Nafion-based IPMC (solid line) and an Aquivion-based IPMC (dotted line). The applied voltage is 0.5 V at a frequency of 1 Hz. The IPMC modeled is 51.07 mm long, 9.94 mm wide, and 0.586 mm thick. The model has two components: the transport, electric current, and general form of partial differential equation (PDE) were used to model Poisson-Nernst-Planck system, which was coupled to a model for the solid mechanics to obtain the tip deflection [59].30

Figure 3.2. Chemical structure of Nafion (a) and Aquivion (b) activated, membrane forms [60], [61]. .... 30

Figure 3.3. Chemical structure of Nafion (a) and Aquivion (b) un-activated, precursor forms [62], [63]. .... 31

Figure 3.4. Injection molding setup heating to the set temperature (150°C) (a) and a modified 3D printer (Lulzbot Mini) to print precursor Aquivion filament heating up the to set temperatures (the extruder set to 260°C and the bed set to 180°C) (b).....	32
Figure 3.5. A precursor Nafion membrane printed with inner channels for potential implementation of liquid sensors (a) and a precursor Aquivion membrane being printed in typical dimensions for IPMC applications (b).....	32
Figure 3.6. FT-IR results comparing Nafion and Aquivion precursor pellets.....	34
Figure 3.7. TGA results showing that both precursor ionomers have the same thermal degradation temperature at 330°C. ....	35
Figure 3.8. DTG results from the TGA tests for precursor Nafion and precursor Aquivion.....	35
Figure 3.9. Results from the rheology tests showing the melting temperature of precursor Aquivion (a) and precursor Nafion (b). ....	37
Figure 3.10. Results for $\tan(\delta)$ from the rheology tests to understand the viscous behavior of precursor Aquivion and precursor Nafion. ....	38
Figure 3.11. Complex viscosity results from the rheology tests conducted on the precursor ionomers.....	38
Figure 3.12. Rheology tests with applied shear rate to measure the shear stress and shear viscosity of the precursor-ionomers. Precursor Nafion was tested at 200°C and precursor Aquivion was tested at 240°C.....	39
Figure 3.13. Rheology tests with an applied strain to measure the storage and loss modulus of the precursor-ionomers. Precursor Nafion was tested at 200°C and precursor Aquivion was tested at 240°C at a frequency of 1 Hz.....	39

Figure 3.14. Rheology tests with an applied angular frequency to measure the complex viscosity and storage and loss modulus. Precursor Nafion was tested at 200°C and precursor Aquivion was tested at 240°C.....	40
Figure 3.15. Damping coefficient as the temperature increases to find the glass transition temperature range for the precursor ionomers.....	41
Figure 3.16. Young's Modulus as the temperature increases for each precursor ionomer. ....	41
Figure 4.1. Conceptual drawing of proposed new fabrication method by means of painting Nafion onto a surface. 1: Master Airbrush Model G22. 2: Canister for Nafion water dispersion. 3: Sprayed Nafion water dispersion, 4: Vinyl stencil. 5: Substrate (Acrylonitrile butadiene styrene, ABS). ....	48
Figure 4.2. Nafion water dispersion painted onto an Acrylonitrile butadiene styrene (ABS) weighing dish to create a maple leaf shaped membrane.....	50
Figure 4.3. Stencils made for custom Nafion shape. Left: Maple leaf shape. Right: Crescent moon with a void. They stencils are about ~3 inches tall and ~3 inches wide.....	51
Figure 4.4. Leaf and moon shaped dehydrated Nafion made using the painting method. ....	51
Figure 4.5. P-Nafion® (left) and N117 (right). ....	52
Figure 4.6. SEM images of the cross sections of P-Nafion® (left) and N117 (right), x300.....	52
Figure 4.7. SEM images of the cross sections of P-Nafion® (left) and N117 (right), x5,000. ....	53
Figure 4.8. SEM images of the cross sections of P-Nafion® (left) and N117 (right), x10,000. ..	53
Figure 4.9. XRD results for P-Nafion® sample.....	55
Figure 4.10. TGA results. ....	55
Figure 4.11. FT-IR results.....	56
Figure 4.12. DMA results for Young's Modulus (left) and Damping Coefficient (right). ....	57

Figure 4.13. P-IPMC (left) and traditional IPMC (right).....	59
Figure 4.14. Probe placement for measuring the surface resistance (left) and resistance through the IPMC (right).....	60
Figure 4.15. IPMC surface (left) and P-IPMC surface (right) viewed using an optical microscope at 500 times magnification. The surface of the IPMC (left) is much smoother and shows minimal cracking. The P-IPMC (right) shows a lot of cracking on the surface. ....	60
Figure 4.16. Experimental setups for IPMC being tested for displacement (a and b) and blocking force (c and d). ....	61
Figure 4.17. Voltage and displacement measurements from actuation experiments.....	62
Figure 4.18. Voltage drop across sample and current for IPMC and P-IPMC. ....	63
Figure 4.19. Comparison of the displacement for IPMC and P-IPMC measurements from actuation experiments. ....	63
Figure 4.20. Voltage and blocking force measurements from blocking force experiments. ....	64
Figure 4.21. Comparison of the blocking force for IPMC and P-IPMC measurements.....	65
Figure 4.22. Calculated strain from displacement measurements for IPMC and P-IPMC.....	66
Figure 4.23. Strain rate from differentiating the strain curves for IPMC and P-IPMC. ....	66
Figure 4.24. Displacement versus voltage for IPMC and P-IPMC to check for hysteresis effects. ....	67
Figure 4.25. Crack fracture SEM imaging of P-Nafion®, 55x magnification.....	68
Figure 4.26. Crack fracture SEM imaging of P-Nafion®, 220x magnification.....	68
Figure 4.27. Conceptual illustration of painting an airfoil-shaped P-Nafion® with active-skin-like texture. ....	69



Figure 5.1. Polymer structure for Nafion® (left) and Aquivion® (right) membranes comparing the side chain lengths.....	75
Figure 5.2. IPMC actuation test setup (for both back relaxation and frequency-based displacement) with a laser sensor performed in DI water.....	81
Figure 5.3. IPMC performance testing for blocking force capabilities in air.....	81
Figure 5.4. IPMC performance sensing test conducted in DI Water.....	81
Figure 5.5. FT-IR comparison of Nafion® 115 and Aquivion® P87S membranes.....	83
Figure 5.6. TGA results of Nafion® 115 and Aquivion® P87S membranes for the thermal degradation temperature.....	84
Figure 5.7. SEM images at a magnification of x800 of N-IPMC (left) and A-IPMC (right).....	85
Figure 5.8. SEM images at a magnification of x3,000 of N-IPMC (left) and A-IPMC (right)....	85
Figure 5.9. Actuation test results with 3 Volts at a frequency of 100 mHz applied.....	87
Figure 5.10. Actuation test results with 3 Volts at a frequency of 500 mHz applied.....	88
Figure 5.11. Actuation test results with 3 Volts at a frequency of 1 Hz applied.....	88
Figure 5.12. Power Input for the three cases of input. From top to bottom, 3 Volts at 100 mHz, 3 Volts at 500 mHz, and 3 Volts at 1 Hz.....	89
Figure 5.13. Aquivion® precursor pellets drawn into filament (left) and cross-sectional view of the filament with measurement showing the diameter to be around ~3 mm (right).....	90
Figure 5.14. Aquivion® filament printed onto double-sided Kapton tape using the Raised N2 Plus Printer. 1: Extruder hot end. 2: Printed Aquivion. 3: Heated glass plate.....	94
Figure 5.15. Printed Aquivion® in a rectangular shape with a brim to help with bed adhesion (each square on the grid is 6 mm x 6 mm).....	95
Figure 5.16. Star-shaped Aquivion® membrane printed on the Raised N2 Plus Printer.....	95

Figure 5.17. Aquivion<sup>®</sup> printed with the Lulzbot Mini and Flexystruder. 1: Extruder hot end on the Flexystruder. 2: Cooling fan (turned off for our print settings). 3: Printed Aquivion. .... 96

Figure 5.18. Four Aquivion<sup>®</sup> membrane samples printed using the Lulzbot Mini with the Flexystruder. .... 96

Figure 5.19. Printed Aquivion<sup>®</sup> sample chemical structure compared with an Aquivion<sup>®</sup> precursor pellet using FT-IR results. Each wavelength correlates to a specific bond that is present in the polymer: 1465 cm<sup>-1</sup> represents the C-F bond, 1213 cm<sup>-1</sup> represents the symmetric CF<sub>2</sub> bond, 1153 cm<sup>-1</sup> represents the asymmetric CF<sub>2</sub> bond, 986 cm<sup>-1</sup> represents the C-F<sub>3</sub> bond, 800 cm<sup>-1</sup> represents the S-O bond..... 98

Figure 5.20. TGA results for the thermal degradation temperature of the printed Aquivion<sup>®</sup> and an Aquivion<sup>®</sup> precursor pellet..... 98

Figure 5.21. FT-IR results for the chemical structure of activated, printed Aquivion<sup>®</sup> and an Aquivion<sup>®</sup> membrane..... 99

Figure 5.22. DMA results for activated, printed Aquivion<sup>®</sup> compared with an Aquivion<sup>®</sup> membrane..... 99

Figure 5.23. Four Printed Aquivion IPMCs (Pr-Aq-IPMC) plated with platinum using the electroless plating process (top) and surface of one of the samples at 100x magnification (bottom)..... 101

Figure 5.24. Back relaxation test for the IPMC samples with an applied voltage of -3 Volts DC (top) and the calculated strain from the results (bottom)..... 102

Figure 5.25. Actuation tests for the IPMC samples at 3 Volts, 500 mHz..... 103

Figure 5.26. Frequency response plot at 3 Volts driven at 0.1 Hz, 0.5 Hz, 1 Hz, and 5 Hz. .... 104

Figure 5.27. Blocking force tests for the IPMC samples with an applied voltage of -1 Volts DC (top) and the calculated stress from the results (bottom)..... 105

Figure 5.28. Sensing data from oscillating the IPMC samples with input of 3 mm (peak to peak amplitude) at 2 Hz..... 106

Figure 6.1. Hydrofoil wing given by the Navy, with scaled down 3D printed replications. .... 112

Figure 6.2. CAD of the Hydrofoil-shaped design to be printed..... 112

Figure 6.3. Hydrofoil-shaped design prepared for 3D printing using a Slicer program called Cura. The model has been broken down into 18 layers. The overall dimensions of the model is 39.6 mm long, 13.9 mm wide, and 1.8 mm thick. .... 113

Figure 6.4. First layer of the Hydrofoil printed on double sided Kapton tape, at a nozzle temperature of 295°C and bed temperature of 180°C. 1: Extruder hot end. 2: Cooling fan. 3: Double-sided Kapton tape. 4: Glass bed with heating pad underneath. .... 114

Figure 6.5. Completed precursor Aquivion print of the 3D Printed Hydrofoil-shaped Aquivion. .... 114

Figure 6.6. 3D Printed Hydrofoil-shaped Aquivion where the layers are visible, showing a curved surface. .... 115

Figure 6.7. Rounded edge of the 3D Printed Hydrofoil-shaped Aquivion viewed with an Optical Microscope at 100x magnification. Each layer can be distinctly seen, creating a rounded edge. .... 115

Figure 6.8. Top layer of the 3D Printed Hydrofoil-shaped Aquivion. The layers below can be seen through each layer, showing the cross-hatching infill. .... 116

Figure 6.9. Activation process to switch the SFVE end group of the precursor Aquivion to an acid group using a hydrolysis bath of 15% wt. of Potassium Hydroxide, 35% wt. of Dimethyl Sulfoxide, and 50% wt. of DI Water for three hours.....	117
Figure 6.10. 3D Printed Hydrofoil-shaped Aquivion during secondary plating.....	118
Figure 6.11. Top, curved side of the 3D Printed-Aquivion-Hydrofoil-shaped IPMC.....	119
Figure 6.12. Bottom, flat side of the 3D Printed-Aquivion-Hydrofoil-shaped IPMC.....	119
Figure 6.13. Trimmed edges of the 3D Printed-Aquivion-Hydrofoil-shaped IPMC to isolate the two sides.....	120
Figure 6.14. Experimental setup for actuation tests of the 3D Printed-Aquivion-Hydrofoil-shaped IPMC.....	121
Figure 6.15. Experimental setup for measuring blocking force of the 3D Printed-Aquivion-Hydrofoil-shaped IPMC.....	122
Figure 6.16. Various applied voltages to the 3D Printed-Aquivion-Hydrofoil-shaped IPMC. ..	124
Figure 6.17. Applied voltage of 8 Volts 100 mHz to the 3D Printed-Aquivion-Hydrofoil-shaped IPMC.....	124
Figure 6.18. Back relaxation data of the 3D Printed-Aquivion-Hydrofoil-shaped IPMC with an applied voltage of -4.5 VDC.....	125
Figure 6.19. Blocking force results for the 3D Printed-Aquivion-Hydrofoil-shaped IPMC measured at the tip. ....	126
Figure C.1. Cross-section of an IPMC with an applied voltage and the effects on the gradients present in the smart material. It should be noted that $\nabla V$ is the applied voltage potential. Figure redrawn from [47]......	135
Figure C.2. Solution flow chart for the sets of equations for IPMC modeling.....	137

Figure C.3. Parameters needed for the IPMC COMSOL model. ....	139
Figure C.4. Variables for the IPMC COMSOL model. ....	139
Figure C.5. Waveform to apply different kinds of voltage potential. ....	140
Figure C.6. 1D Component geometry breakdown. ....	141
Figure C.7. 2D Component geometry breakdown. ....	142
Figure C.8. Variables for 1D component. ....	142
Figure C.9. Linear extrusion set up to map the PNP results to the 2D domain. ....	143
Figure C.10. Settings for General Form PDE. ....	144
Figure C.11. Settings for the Electric Currents. ....	145
Figure C.12. Settings for Transport of Diluted Species. ....	146
Figure C.13. Variables for the 2D component. ....	147
Figure C.14. Component list for this specific model. ....	147
Figure C.15. Settings for Solid Mechanics. ....	148
Figure C.16. Mesh for 1D Component (left) and zoomed in view of mesh (right). ....	149
Figure C.17. Mesh for 2D Component (left) and zoomed in view of mesh (right). ....	150
Figure C.18. Settings for parameter sweep. ....	150
Figure C.19. Settings for the Time Dependent Study. ....	151
Figure C.20. Settings for the Point Graph in 1D Plot Group. ....	152
Figure F.1. Sample from the work done by Nelson [27]. ....	167
Figure F.2. Injection molder setup. ....	168
Figure F.3. New mold for creating curved membranes with two parts, one to hold the cartridge heaters (stainless steel) and the other to mold the ionomers (aluminum). ....	169
Figure F.4. Aluminum machined curved membrane molds. ....	169

Figure F.5. Completed mold setup with the cartridge heaters installed.....	170
Figure F.6. IR image of the Injection Molder and Mold heated to 220°C for producing Nafion samples.....	171
Figure F.7. Nafion sample with many bubbles throughout the membrane.....	171
Figure F.8. Curved Nafion membrane.....	172
Figure F.9. An attempt at producing a Nafion puck with no bubbles using the vacuum oven...	172
Figure F.10. IR image of the Injection Molder and Mold heated to 255°C for producing Aquivion samples.....	173
Figure F.11. Aquivion curved membrane with many bubbles as well. ....	173
Figure F.12. Nafion membrane produced with bubbles present.....	174
Figure F.13. Aquivion membrane produced with large bubbles throughout.....	174
Figure F.14. Melted Aquivion pellets removed from the injection molder that has many bubbles. .....	175
Figure F.15. Nafion pellet heated up with a heat gun that shows de-gassing.....	175
Figure F.16. FT-IR scans for precursor Nafion and Injection Molded Nafion with these bond stretches: 1465 cm <sup>-1</sup> represents the C-F bond, 1213 cm <sup>-1</sup> represents the symmetric CF <sub>2</sub> bond, 1153 cm <sup>-1</sup> represents the asymmetric CF <sub>2</sub> bond, 986 cm <sup>-1</sup> represents the C-F <sub>3</sub> bond, 800 cm <sup>-1</sup> represents the S-O bond.....	176
Figure F.17. FT-IR scans for precursor Aquivion, printed Aquivion, and Injection Molded Nafion with these bond stretches: 1465 cm <sup>-1</sup> represents the C-F bond, 1213 cm <sup>-1</sup> represents the symmetric CF <sub>2</sub> bond, 1153 cm <sup>-1</sup> represents the asymmetric CF <sub>2</sub> bond, 986 cm <sup>-1</sup> represents the C-F <sub>3</sub> bond, 800 cm <sup>-1</sup> represents the S-O bond. ....	177

Figure F.18. TGA results for precursor Nafion and Nafion IM showing they have similar degradation temperatures and behaviors..... 177

Figure F.19. TGA results for precursor Aquivion, printed Aquivion, and Aquivion IM showing that the thermal degradation temperature shifts..... 178

Figure G.1. Frequency response plot for a Printed Aquivion-IPMC and Nafion-IPMC in sensing application under 3mm amplitude with varying frequencies..... 180

## List of Tables

Table 2.1. Calculated cluster diameter and water content for two values of EW for Aquivion forms available.....	15
Table 2.2. Material characteristics of activated forms of Nafion and Aquivion [42], [43]. .....	17
Table 2.3. IEC values found by conducting a titration test [46]. .....	18
Table 2.4. Dimensions for the N-IPMC and A-IPMC fabricated for testing.....	24
Table 2.5. Peak measurements from the data collected for the test with an applied voltage of 3 Volts at 100 mHz. ....	25
Table 2.6. Peak measurements from the data collected for the test with an applied voltage of 3 Volts at 500 mHz. ....	26
Table 2.7. Peak measurements from the data collected for the test with an applied voltage of 3 Volts at 1 Hz. ....	27
Table 3.1. Comparison of the mechanical characteristics of activated and precursor forms of the ionomers at room temperature. ....	42
Table 3.2. Parameter variables of modified-Carreau model (Equation (3)) for two precursor ionomers.....	43
Table 4.1. Measurements of P-Nafion® and N117 from figure 4.5. ....	52
Table 4.2. Water uptake comparison of P-Nafion® and N117.....	57
Table 4.3. Dimensions and resistances of P-IPMCs and IPMC tested. It should be noted that the resistances was measured using a 2-point probe multimeter. ....	59
Table 5.1. Cleaning process procedure for various points in the plating process.....	79
Table 5.2. Characteristics of Nafion® [114] and Aquivion® [115], [42]. ....	83
Table 5.3. Measured Ion Exchange Capacity results for Nafion® 115 and Aquivion® E87.....	84



Table 5.4. Thermal conductivities for Nafion <sup>®</sup> 1100 and Aquivion <sup>®</sup> P87S. ....	84
Table 5.5. Details of the analysis from the plots in Figure 5.9. ....	87
Table 5.6. Details of the analysis from the plots in Figure 5.10. ....	88
Table 5.7. Details of the analysis from the plots in Figure 5.11. ....	88
Table 5.8. Filament's Young's Modulus [115] and dimensions (measured directly from printers in-house) used for the calculations using Equation (9) to find the critical pressure for each printer. ....	93
Table 5.9. Dimensions of IPMC samples being tested. ....	101
Table 5.10. Calculated volumetric energy density for the samples. ....	105
Table 6.1. 3D Printer Settings. ....	112
Table C.1. Dimensions for the intervals in the 1D component geometry. ....	141
Table C.2. Dimensions for the rectangles used to build the 2D component. ....	142

## **Chapter 1. Introduction**

### **1.1. Basics of Ionic Polymer-Metal Composites**

Ionic Polymer-Metal Composite (IPMC) is a popular Electro-Active Polymer (EAP) that has been studied for about two decades [1], [2]. It is ionic polymer-membrane based, which is typically plated with a conductive metal, such as Platinum, Palladium, or Gold. When a voltage is applied to the surface of the IPMC, the free moving cations move to the negatively charged side, causing it to swell and force the IPMC to actuate. This effect is called electro-mechanic. Conversely, when an IPMC is deformed, the motion causes cations to move within the membrane that can be amplified and recorded as a sensor, which is called mechano-electric effect. IPMCs work well in water, since the cations pull the water molecules along with them, increasing the swelling and in turn, increasing the displacement. Also, IPMCs can work in air if encased with an ionic liquid. While other EAPs, such as dielectric elastomers, require a high voltage input (kV range) [3], IPMCs only need a low amount of voltage (1-5 Volts) [1], [4], [5].

### **1.2. History of Ionic Polymer-Metal Composites**

IPMCs were first studied in 1992 by Oguro *et. al* [6]. It was found that by adding an electrode to an ionomer, it could be possible to actuate the material. They showed that the IPMC was able to move with either a triangular or pulse input. Another group led by Sadeghipourt in 1992 showed that IPMCs can also be used as sensors [7]. Their results presented the IPMC as a vibration sensor with good sensitivity. Kanno *et al.* modeled the smart material, by breaking down the actuation effect into three “stages”: electrical, stress generation, and mechanical [8]. The applied current is directly related to the stress produced within the IPMC, which then causes a bending motion. Their model was able to closely match experimental results, though it responded faster. They attributed

this to the lack of internal friction in their model. One of the first applications published was a fin-like actuator by Mojarrad and Shahinpoor [9]. They attached an IPMC to a small boat and actuated it at high frequencies to create propulsion.

In 2000, two groups studied the underlying physics of how IPMCs work. The first group (de Gennes *et al.*) hypothesized that the water swelling the membrane can be connected to both the actuation and sensing modes of an IPMC [10]. Their basis is driven by the applied electric field and the pressure gradient due to water in the membrane and linear irreversible thermodynamics. The other group (Nemat-Nasser and Li) posits that the ion transport and electric field coupled with the elastic deformation can be used to predict the motion of an IPMC [11]. They compared their model with experimental results and saw minor differences in the values.

A four-part review article collection was published beginning in 2001 by Kim and Shahinpoor. The first review article discussed fundamentals of IPMCs and also proposed an idea in producing high-force-density IPMCs by adding dispersing agents [1]. The second review article presented detailed instructions on how to produce IPMCs and compared various methods and their effects on the resulting IPMCs [12]. The third review article discusses several different models for better understanding the physics of IPMCs, including continuum microelectromechanical models and continuum electrostatics of ionic polymeric gels swelling and de-swelling [4]. The last paper discusses the possible applications of IPMCs, such as mechanical grippers and bio-mimetic swimmers [5].

### 1.3. Applications of Ionic Polymer-Metal Composites

IPMCs have been used for bio-mimetic applications because of their flexibility and quick response. Palmre *et al.* built a robotic fin consisting of three IPMCs [13]. Because of the multiple IPMCs, not only can the fin bend, it can also twist, creating a more realistic fin motion. Chen *et al.* fabricated a robot manta ray using IPMCs [14]. The robot is able to swim in water easily. Yeom and Oh built a jellyfish inspired robot with a set of IPMCs [15]. It is able to move similarly to a jellyfish. Yim *et al.* designed a three-sectioned IPMC that was made to produce an undulating wave, similar to tadpoles [16]. They applied a control system to create an accurate motion.

IPMCs have also been shown to be useful for bio-medical applications. A tube IPMC with four sectored electrodes has been studied as an active catheter by Ruiz *et al.* [17]. It is able to move well in multiple directions with the applied control system, which was verified using a Finite Element Analysis program, COMSOL. Liu *et al.* designed a system of four IPMCs in a silicone tube for minimally invasive surgeries, which also moves in multiple directions [18]. By actuating certain IPMCs, they can control the direction of the tool. Artificial muscles have been designed by Lee *et al.* for the use in fingers [19]. They stacked Nafion films to produce thicker IPMCs and used them at the joints on a finger for an upward motion.

IPMCs are also used in robotic applications as well. Punning *et al.* produced a self-sensing IPMC [20]. It does this by measuring the surface resistance changes. Feng *et al.* designed an IPMC tweezer that is able to hold an object and lift, rotate, and squeeze it [21]. Jain *et al.* built a micro-gripper using IPMCs to help correct manufacturing errors [22]. Another group produced an IPMC-based micro-gripper using three IPMCs in a Polydimethylsiloxane (PDMS) sleeve [23].

#### **1.4. Current Fabrication Methods**

This section is a portion from a Book Chapter in “Advances in manufacturing and processing of materials and structures.” Copyright (2018) From (Advances in manufacturing and processing of materials and structures.) by (Stalbaum, T., Trabia, S., Hwang, T., Olsen, Z., Nelson, S., Shen, Q., Lee, D., Kim, K. J., Carrico, J., Leang, K., Palmre, V., Nam, J., Park, I., Tiwari, R., Kim, D., Kim, S.). Reproduced by permission of Taylor and Francis Group, LLC, a division of Informa plc.

Before diving into a discussion of how IPMCs are currently fabricated, it best to first start with how commercially available Nafion is produced by companies such as DuPont. There are two typical methods for producing Nafion membrane sheets: film-extrusion with precursor-ionomer pellets and film-casting with a dispersion of the activated ionomer. A non-acid form of the ionomer is produced in small, cylindrical pellets that is then melted and extruded into a film of the desired thickness. Then, the film is hydrolyzed in solution of 15% Potassium Hydroxide (KOH) and 30% Dimethyl Sulfoxide (DMSO). For film-casting, the dispersion is deposited onto a backing film and the solvents are allowed to evaporate out. Once the film is dry, it is covered with a protective layer. This is all done within a clean room to lower the risk of contamination. For a more thorough discussion of these processes, the reader is directed to a chapter called “Manufacture” in a book written by Walther Grot, one of the inventors of Nafion [24]. The naming procedure for Nafion is as such: the first two digits represent the Equivalent Weight and the last digit is the thickness in inches. An example to show how this is done is presented: Nafion 117 has an Equivalent Weight of 1100 and a thickness of 0.007 inches.

One of the industrial applications for Nafion is electrolytic cells. Nafion is a stable polymer that is able to withstand the harshest of environments. It also makes it a great candidate for electrolytic cells because it is water permeable, sensitive to ions, and can encourage chemical reactions [25]. Because of these characteristics, Nafion has been used quite extensively in fuel cells [25].

#### **1.4.1. Rectangular IPMCs using membrane sheets**

Due to their simplex geometric shapes, rectangular IPMCs are commonly made by cutting an existing membrane sheet of ionic polymer to a desired size, with thicknesses ranging from 25.4  $\mu\text{m}$  to 254  $\mu\text{m}$ . These membranes are chemically treated with an ionic salt solution of a metal then reduced to obtain the IPMC [26]. Shahinpoor and Kim describe the manufacturing of these IPMCs as incorporating two preparation processes, the initial compositing process the surface electroless plating process, and the exact execution of these can lead to significant differences in the precipitated metal morphologies.

Rectangular IPMCs made from membrane sheets are among the most common found in literature. Shahinpoor and Kim show that these types of IPMCs can yield large dynamic deformation when suitably constructed. These IPMCs serve as the basic actuator and sensor that many researchers use to advance the state of the art. Some limitations of the membrane sheet IPMCs are the geometric constraints imposed from using premade membranes. This can restrict the thickness of the IPMC and thus limit its use as a functional device for certain applications, such as high blocking force production or sensing capabilities.

### **1.4.2. Hot-pressing membranes and pellets**

There are a limited number of thicknesses available on the market for Nafion® membranes. The larger the thickness of the IPMC, the higher the blocking forces they can produce. To produce larger thicknesses, hot-pressing membranes and precursor pellets is a solution found to be successful by researchers. Nelson explored hot-pressing membranes using Nafion® membranes (N1110, thickness of 0.25 mm) to produce a 0.5 mm membrane [27]. The sample has a fairly uniform thickness of 0.48 mm but shows some discoloration, due to the fact that Nafion® membranes do not melt. If not properly heated through the fabrication process, the membrane will begin to degrade and could affect how it actuates as an IPMC.

Precursor pellets have a different end group ( $-\text{SO}_2\text{F}$ ) than the membrane form of the ionomer ( $-\text{HSO}_3$ ), which allows the polymer to melt. Palmre *et al.* [2013] used precursor pellets to produce and test IPMCs with two thicknesses (0.5 mm and 1 mm) [13]. The membranes produced from hot-pressing were activated to switch out the end group for a sulfonate group ( $-\text{SO}_3\text{-Na}^+$  or  $\text{K}^+$ ), then plated with platinum using an electroless process. Palmre *et al.* were able to use the specially produced IPMCs to produce a bio-mimetic fin, comprising of three IPMCs within a silicone boot that can bend and twist.

### **1.4.3. Casting Nafion Water Dispersion**

Nafion® water dispersion is solution of liquefied Nafion®, water, and alcohols. It can be purchased in a variety of weight percentages. The casting method is also used to produce large thickness membranes. As depicted by Kim *et al.*, the procedure for casting is to pour the solution into a mold and allow to dry to form the membrane [28]. Then it is thermally treated to remove

any of the water or alcohol that may not have evaporated out during the drying process and the membrane is ready for plating process. Another method allows for the electrodes to also be cast so that a complete IPMC can be produced. This process is described by Kim and Shahinpoor [29]. The conductive powder is mixed with the Nafion® water dispersion and cast first. Then, pure Nafion® water dispersion is cast on top of the first layer. Once that has dried, a second layer of conductive powder mixed with Nafion water dispersion is cast on the previous layer. The IPMC is thermally treated and ready for use.

These methods are successful in producing thick IPMCs for various applications. Kim and Shahinpoor produced a 2 mm thick octopus-like IPMC that can lift a US quarter with a step voltage of 2.5 V applied [29]. Kim *et al.* designed a micro-robot with 8 IPMC legs (1.15 mm thick) that is able to walk at a speed of 17 mm/min with a frequency of 0.8 Hz [30].

#### **1.4.4. Extruding tubes using pellets**

The extrusion of Nafion tubes for making tube-shaped IPMC devices is of great interest for multi-degree of freedom control and actuation. To process this shape, precursor Nafion is warm extruded through a die. Nafion precursor pellets are heated above glass transition temperature and are extruded until the desired length has been reached in the cross-sectional shape. The polymer is tensioned after extrusion to facilitate polymer chain realignment and to achieve the desired mechanical properties. After the polymer is cooled to room temperature, it can be cut into the desired length. The tube-shaped EAP is then activated by hydrolysis and plated with an electrode layer. The flanges can be removed to create the separated electrodes. Separating the electrodes



allow for multiple degree-of-freedom actuation motion when a voltage is applied and allows for sensing measurements in case of an applied deformation [31].

### **1.5. Rationale for Advanced Fabrication Methods**

Though the previous section introduces different ways of fabricating the base polymer of IPMCs, they are limited to the kinds of shapes possible. The problem of not having choices of shapes, contours, and structures can be addressed with the two methods to be explored: spray-painting and 3D printing. These fabrication methods can expand the applications of IPMCs through various ways. Spray-painting method provides the user with controlling the thickness of the membrane and creating intricate shaped IPMCs. 3D printing method gives the researcher the ability to build complex structures of IPMC using a CAD program. Furthermore, being able to optimize these methods tailored to this material, it is possible to produce the new desired shapes and not lose the valuable performance-characteristics. The research is built around the thorough study of the material before and after the processes to understand how the material has changed. Then, when the Nafion membranes are produced into IPMCs, those resulting soft actuators/sensors will need to be studied.

### **1.6. Improving the performance of Ionic Polymer-Metal Composites**

Another topic to be explored is improving the performance of IPMCs. Nafion<sup>®</sup> has been the typical choice for IPMCs because of its ideal material properties, including chemically stable, good mechanical properties, and high ionic conductivity [32], [33]. Nafion<sup>®</sup> is a perfluorosulfonic acid (PFSA) with a Teflon-like backbone, perfluorovinyl ether side group, and a sulfonate end group. Nafion<sup>®</sup>-based IPMCs perform well and have been used in many different applications. Some

work has been done in attempting to increase the performance of Nafion<sup>®</sup>-based IPMCs, including using different materials [34], [35], applying various solvents and cations [36], and trying different surface treatments [37]. Each method has affected the performance of an IPMC, however there is still room for improvement.

## **1.7. Objectives and Significance of the Work Presented**

### **1.7.1. Objectives**

First, an alternative ionomer will be introduced to potentially improve the performance of IPMCs. For this study, Aquivion will be the ionomer of interest. Aquivion is a Short-Side-Chain ionomer with a lower Equivalent Weight than Nafion. Because of these characteristics, Aquivion exhibits a higher ionic conductivity and ion exchange capacity. In theory, based on these values, an IPMC with Aquivion as the base polymer should have better performance. It will be important to first compare Aquivion and Nafion for their material characteristics, then explore the effects of their chemical structures directly and various manufacturing techniques on the performance of IPMCs made with either of these two materials. A preliminary assessment of the performance of Nafion-based and Aquivion-based IPMCs will be conducted theoretically, using Finite Element Analysis. This assessment will be followed by experimental evaluation, which is the major focus of this work. It should be noted that this dissertation is not centered around finite element modeling of IPMCs, which is an area that has attracted the attention of many researchers. A complete survey of this area is beyond the scope of this dissertation. Instead, a small section is included to provide a more thorough study, which will be discussed in Chapter 2.

Next, in order to optimize the advanced fabrication methods introduced, it is imperative to study the ionomers, especially the precursor form. This form can melt, but has not been studied thoroughly. Nafion and Aquivion precursor pellets will be studied to better understand how they react to thermal loads. The results will be presented in Chapter 3.

Then, two advanced fabrication methods will be presented. Spray-painting and 3D printing will be explored to gauge the feasibility of each method. Samples of ionomers will be characterized to ensure no contamination has occurred or that its material properties have not been adversely affected. Then, IPMCs will be fabricated, tested, and compared with traditionally made IPMCs. These will be discussed in Chapter 4 and Chapter 5, respectively.

Finally, using 3D printing, a small, National Advisory Committee for Aeronautics (NACA)-inspired hydrofoil will be explored. The design will feature asymmetry and curved features. The 3D-Printed-Aquivion Hydrofoil-shaped IPMC will be tested for its actuation capabilities. Chapter 6 will be for this portion of the work, as well as a discussion about printing issues and rooms for improvement.

### **1.7.2. Significance of the Work Presented**

The work in this dissertation offers new knowledge to the field about Nafion and Aquivion's material properties and advanced fabrication methods of ionomers for IPMCs. This dissertation provides information about the two ionomers that is not currently available. It provides an alternative ionomer to use for IPMCs depending on their application. The advanced fabrication

methods provide researchers with the ability to make different shapes that currently are too difficult to make.

## **Chapter 2. Exploring the Possibility of Improving the Performance Abilities of Ionic Polymer-Metal Composites: Searching for an alternative ionomer**

Some of the figures in this chapter are reprinted from “Searching for a new ionomer for 3D printable ionic polymer–metal composites: Aquivion as a candidate.” The reprint permission can be found in Appendix B.

### **2.1. A hypothesis regarding the need to increase performance of IPMC**

IPMCs have been usually made with Nafion as the base ionomer. Nafion is a great option as it is chemically stable, mechanically robust, and has good electrochemical characteristics [15], [38]–[41]. However, typical IPMCs have a low blocking force output and the displacement decreases as the thickness increases. This limits the applications possible for IPMCs. It would be beneficial to find a way to improve the performance of IPMCs, without losing any of the good qualities of the base ionomer.

An important characteristic of the base ionomer is its Equivalent Weight (EW), which is the mass per mole of  $\text{H}_2\text{SO}_4$ . By reducing the EW of the ionomer, it could be possible to increase the performance of the IPMC. Since it may be difficult to directly alter the ionomer’s structure, an alternative ionomer with a lower EW has been found to explore: Aquivion. Aquivion, a product by Solvay, has a shorter side chain, with similar properties, and is available in the same forms as Nafion. However, the major difference between the two is that Aquivion has nearly double the ionic conductivity of Nafion ( $\sim 228$  mS/cm and  $\sim 100$  mS/cm, respectively [42], [43]). This may give researchers a different material to consider when making their IPMCs.

To analyze and verify our approach, this chapter is organized as such:

- Discuss the physics of ion transport within ionomers,
- Comparing the material characteristics of Nafion and Aquivion,
- COMSOL Multiphysics simulation of the effect of the diffusion coefficient on an IPMC actuator, and
- Experimental data verifying our approach.

## 2.2. Physics of Ion Transport Within Ionomers

A paper was published in 1983 by Hsu and Gierke, where they analyze and discuss the relationship of the EW with the cluster diameter and the water content of Nafion [44]. Hsu and Gierke describe that the fluoro-carbon matrix and sulfonate ion sites interact with water molecules at the outer ring. Figure 2.1 shows the dimensions of an ion cluster, with the cluster diameter and the water molecule diameter clearly designated.

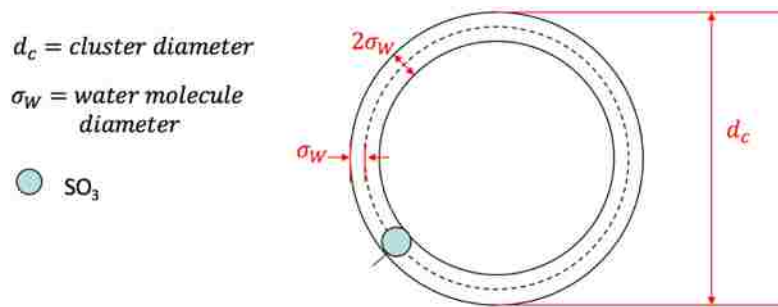


Figure 2.1. Diagram of an ion cluster, recreated from Hsu and Gierke [44]. The typical diameter of a water molecule is around  $2.75 \text{ \AA}$  [45].

They provide measurements of cluster diameter and water content for varying EW. The data was used to develop power regressions to find an equation to best describe the relationships. Figure 2.2

shows the relationship between the cluster diameter and the EW and Figure 2.3 shows the relationship between the water content and the EW. The cluster diameter shown in Figure 2.2 was calculated by first assuming the clusters are approximately spherical and estimating the size by measuring the water absorbed by Nafion. The water content data shown in Figure 2.3 was gathered through X-ray studies of the material. As the EW increases both the cluster diameter and the water content decrease. Referring back to the initial diagram for an ion cluster (Figure 2.1), it can be seen as the cluster diameter decreases, the circumference of the ion cluster would decrease as well, reducing the amount of water molecules that can fit in the along the outer ring. Aquivion's lower EW implies that it would have larger cluster diameter and water content. This is verified by calculating the values for two different Aquivion forms (Table 2.1).

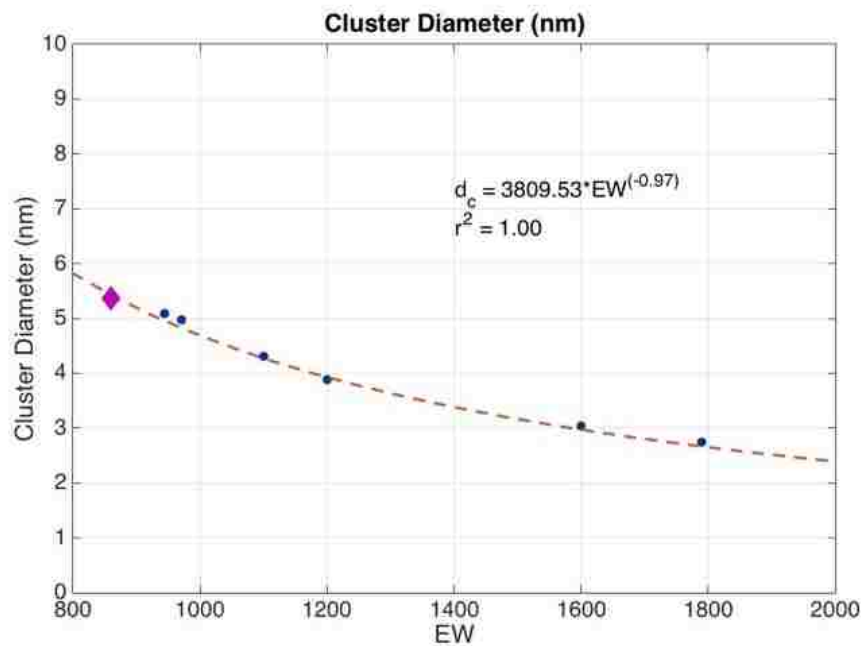


Figure 2.2. Relationship between the EW and cluster diameter, with a data point included to show where Aquivion would be on the curve (diamond).

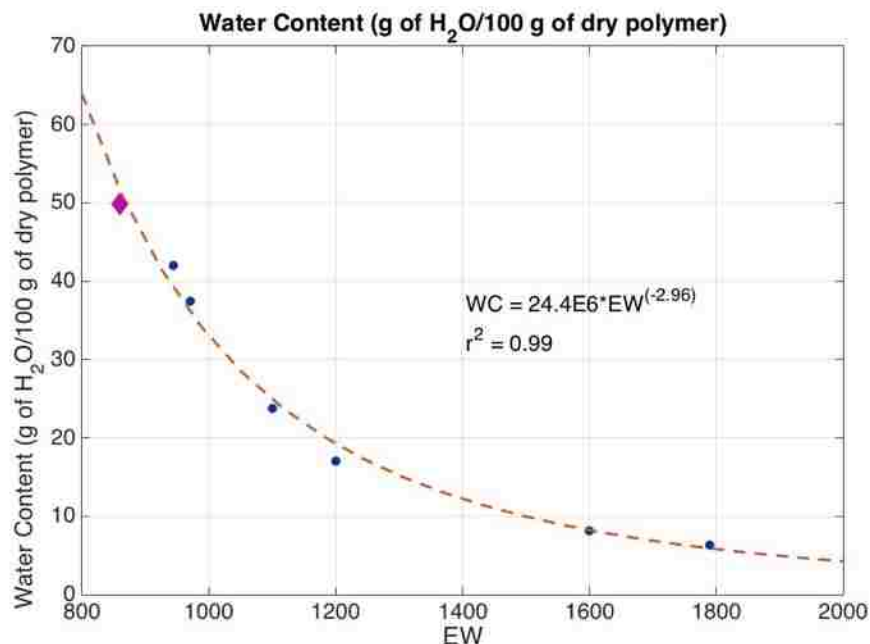


Figure 2.3. Relationship between the EW and water content, with a data point included to show where Aquivion would be on the curve (diamond).

Table 2.1. Calculated cluster diameter and water content for two values of EW for Aquivion forms available.

Aquivion	Cluster Diameter (nm)	Water Content (g of H <sub>2</sub> O/100 g of dry polymer)
EW=840	5.55	55.3
EW=870	5.36	49.8

### 2.3. Comparison of Nafion and Aquivion Characteristics

The next point of action is to show that the two ionomers have similar properties. Looking at the chemical structure, it can be seen that both have Teflon-like backbones (Figure 2.4). Nafion has a perfluorvinyl ether side group and a sulfonate end group, while Aquivion has a double ether perfluoro side chain and a sulfonic acid end group. Aquivion's side chain is smaller than Nafion's and this seems to affect the EW, as the other material characteristics match for the two ionomers (Table 2.2). The notable difference is the ionic conductivity, where Aquivion has over double the



conductivity to that of Nafion (~228 mS/cm and ~100 mS/cm, respectively). The higher ionic conductivity could provide the ionomer with the ability to move more ions for a given time, therefore increasing the mechanical output performance. This is most likely attributed to the lower Equivalent Weight and will be explored in the next section.

Their chemical structures are compared using a Fourier Transform-Infrared Spectroscopy (FT-IR) by scanning 60 times from 400 to 4000  $\text{cm}^{-1}$ . The bonds that are present are excited by specific wavelengths, causing it to stretch. These bond stretches are shown in the results through large peaks. The other wavelengths go through the material and do not have any distinction. The FT-IR results show they both have the distinct peaks, denoting the asymmetric and symmetric  $\text{CF}_2$  and the  $\text{S-O}_3$  bond stretches (Figure 2.5). Thermogravimetric Analysis (TGA) tests were conducted and showed that the two have similar thermal degradation temperatures at 300°C (Figure 2.6). The last test conducted was the Ionic Exchange Capacity (IEC) test. This was done through a simple titration method to calculate the amount of ions that can be held within the membrane per unit mass. The results showed that Aquivion had a higher capacity than Nafion, 1.25 meq/g versus 0.98 meq/g (Table 2.3).

Fundamentally, Nafion and Aquivion are different ionomers, though they are used in similar applications. Aquivion's shorter side chain allows for a smaller EW, giving it a higher IEC and ionic conductivity. These should potentially increase the actuator performance of an IPMC, without losing any of the ideal qualities of Nafion. Both ionomers are very stable polymers that can withstand harsh environments. Based on the material characterization tests, Aquivion should be a good candidate for IPMCs.

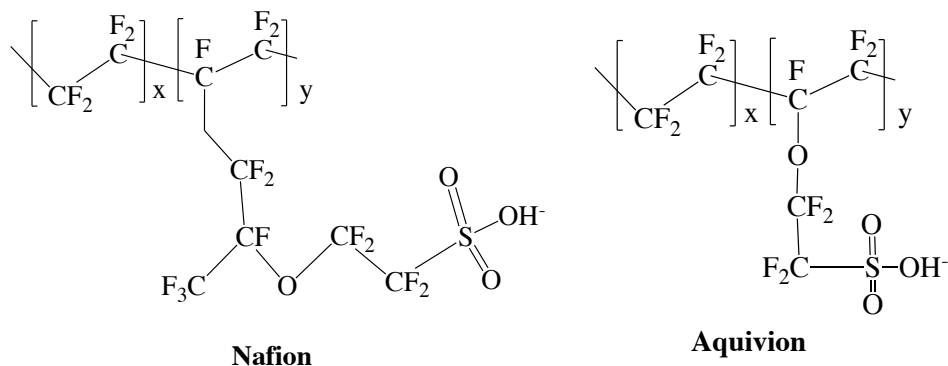


Figure 2.4. Chemical structure of activated forms of Nafion and Aquivion. Reprinted with permission from IOP Publishing [46].

Table 2.2. Material characteristics of activated forms of Nafion and Aquivion [42], [43].

	<b>Equivalent Weight (EW, g/eq)</b>	<b>Ionic Conductivity (mS/cm)</b>	<b>Young's Modulus, 50% RH, 23°C (MPa)</b>	<b>Water Uptake</b>
<b>Nafion 117</b>	1,100	100	249	38 wt. %
<b>Aquivion P87-12S</b>	870	>228	250	30 wt. %

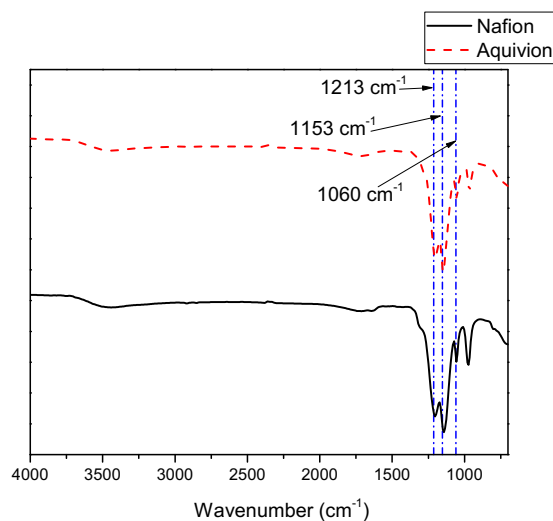


Figure 2.5. FT-IR results that compare the chemical structures for activated forms of Nafion and Aquivion. The peaks that match signify symmetric  $\text{CF}_2$  ( $1213 \text{ cm}^{-1}$ ), asymmetric  $\text{CF}_2$  ( $1153 \text{ cm}^{-1}$ ), and  $\text{S-O}_3$  ( $1060 \text{ cm}^{-1}$ ) bonds. Reprinted with permission from IOP Publishing [46].

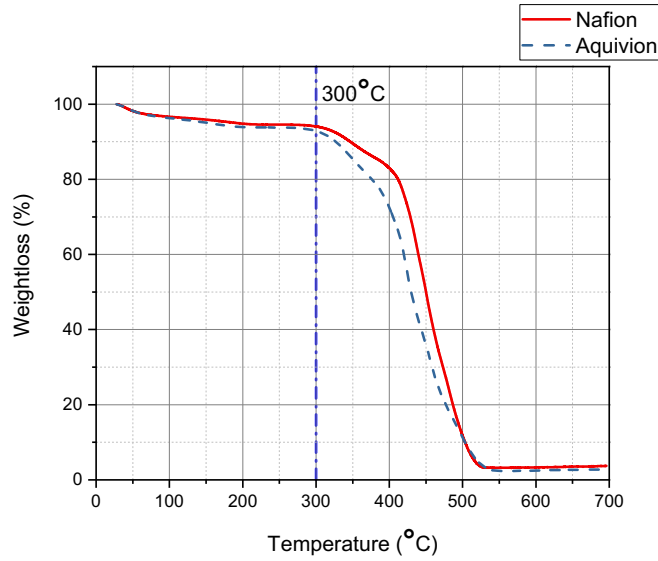


Figure 2.6. TGA results showing the two activated ionomers have similar thermal degradation points at 300°C. Reprinted with permission from IOP Publishing [46].

Table 2.3. IEC values found by conducting a titration test [46].

<b>Ion Exchange Capacity (meq/g)</b>	
<b>Nafion 117</b>	0.98±0.08
<b>Aquivion P87</b>	1.25±0.01

## 2.4. Theoretical Consideration of IPMC Modelling Regarding Nafion versus Aquivion

In order to verify the proposed approach that Aquivion could potentially enhance the performance of the IPMC, COMSOL Multiphysics was used to run a parameter sweep. It is based off the 2D, rectangular IPMC model presented by Pugal *et al.* [47], but has been since updated to be more efficient by Zakai Olsen [48].

### 2.4.1. Brief Summary of the 1D COMSOL Model

A complete, step-by-step procedure is provided in Appendix C. A simple, rectangular IPMC is built that is 51.07 mm long, 9.94 mm wide, and 0.586 mm thick. Boundary conditions applied

were set up to most appropriately mimic what an IPMC experiences. In the 1D portion of the model (Figure 2.7), the boundary condition for the applied voltage potential is set to the outer points of the IPMC. The “Transport of Diluted Species” physics includes the “No Flux” condition, which are the points between the “Platinum Electrodes” and “Membrane Buffer Regions,” and “Transport Properties” conditions are applied to the “Ionomer Membrane” and “Membrane Buffer Regions,” which is where the user gives the values for voltage potential, temperature, diffusion, mobility, and charge number. In the 2D portion of the model (Figure 2.8), only the membrane portions of the geometry are selected in the “Solid Mechanics.” The “Clamped Region” is fixed, while the “Free Region” is where the “External Stress” is applied. “External Stress” was used as it is a more appropriate force loading boundary condition to mimic what the IPMC feels.

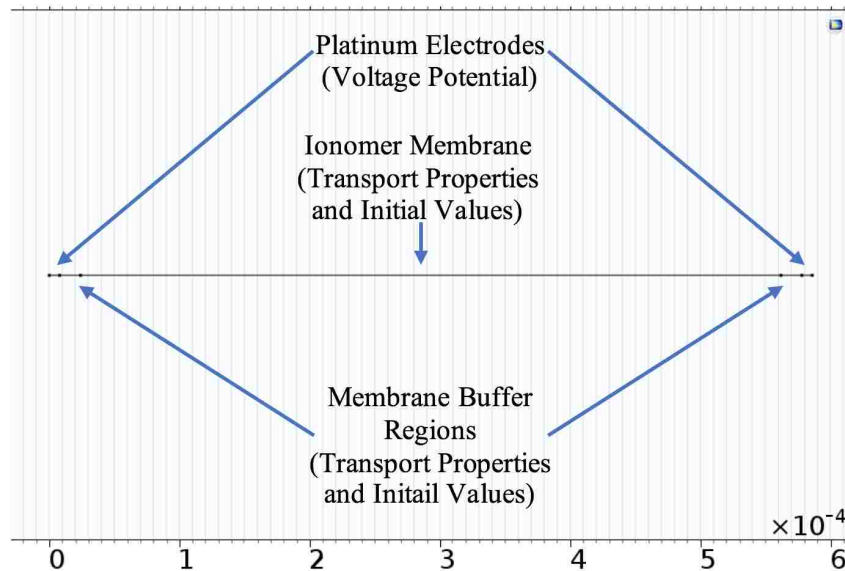


Figure 2.7. 1D component with the domains named for the boundary conditions applied.

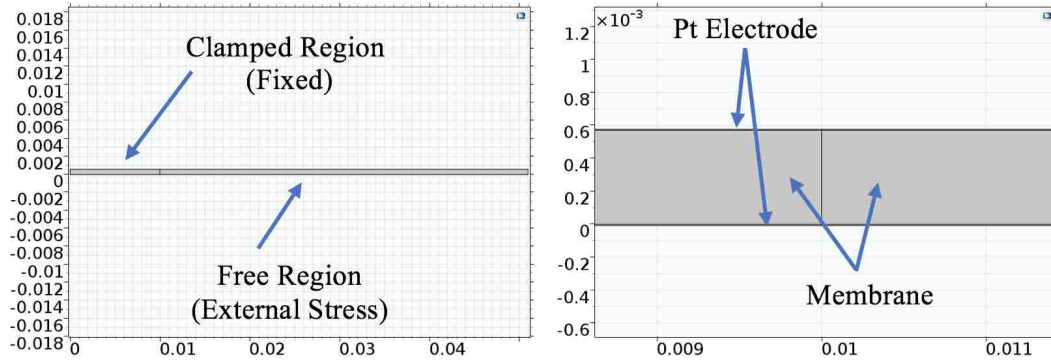


Figure 2.8. 2D component with the domains named for the boundary conditions applied.

#### 2.4.2. Diffusion Coefficient as a Parameter to Affect the Performance of an IPMC

The parameter to be swept is the ionic conductivity, which is not directly included in the equations provided above. However, there is a direct correlation between the diffusion coefficient and the ionic conductivity, which was discussed by Mochizuki *et al.* [49] and Peng and Zawodzinski [50]. The Nernst-Einstein equation, which can establish the relationship between the molar ionic conductivity ( $\sigma$ ) and the diffusivity ( $D$ ), is:

$$D = \frac{RT}{F^2 C} \sigma. \quad (1)$$

The Nernst-Einstein equation is a simple relation, but it has shown to be effectively correlate the two parameters [47], [50]. This equation gives an understanding of how easily the ions can flow through the polymer. It takes all of the characteristics of the mobile ion and predicts the rate at which they will move [50]. It is noted by Peng and Zawodzinski that the initial concentration ( $C$ ) plays a key role and the equation shows higher accuracy for high water content tests [50].

The ionic conductivity for Nafion is  $\sim 100$  mS/cm and for Aquivion is  $\sim 220$  mS/cm. The cation concentration,  $C$ , is difficult to be estimated as well and has been left as the same value for both ionomers. However, it should be noted that this value can also be a driving factor in the diffusion

coefficient. In the future, it may be of interest to study  $C$  for both ionomers and more accurately model their actuation capabilities. Since all the other coefficients are the same, it can be said that the ratio between the two diffusion coefficients is based entirely on the ionic conductivity. The ratio between two ionomers is shown to be:

$$\sigma_A = 2.2\sigma_N, \quad (2)$$

where  $\sigma_A$  and  $\sigma_N$  are the ionic conductivities for Aquivion and Nafion, respectively. This can be implemented into the COMSOL model. The new parameter “p” is introduced into mobility and the diffusion coefficient into the model to mimic the effects of the ionic conductivity increasing, which would in turn increase the diffusion coefficient.

The results are shown in Figure 2.9, Figure 2.10, and Figure 2.11. It can be seen that as the parameter “p” increases, the deformation increases. This verifies that Aquivion’s higher ionic conductivity creates a higher diffusion coefficient, which increases the performance of the IPMC. The varying waveform shapes show different responses from the IPMCs, but both of them respond similarly. The major differences between the two is the displacement amplitude and the response time, with Aquivion out-performing Nafion.

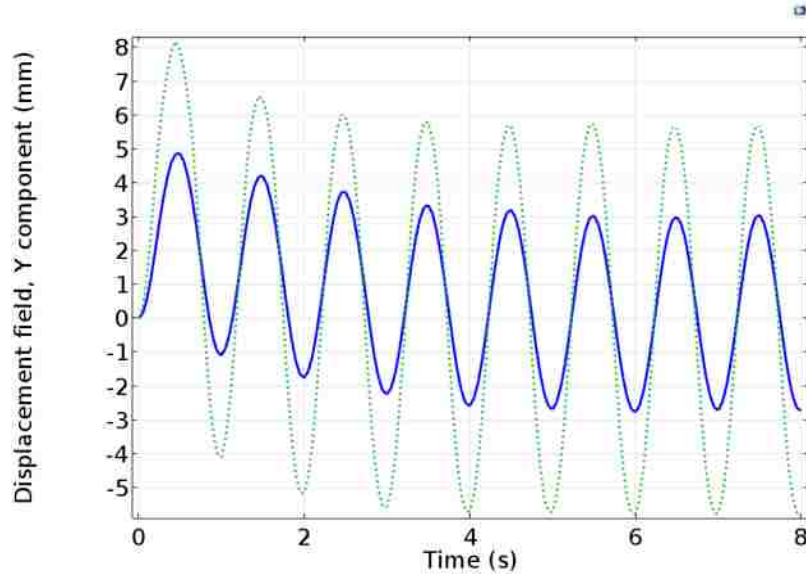


Figure 2.9. Results for the two cases of diffusion coefficients with a sinusoidal voltage input (0.5 V, 1 Hz), where the solid line is Nafion-based IPMC and the dotted line is Aquivion-based IPMC.

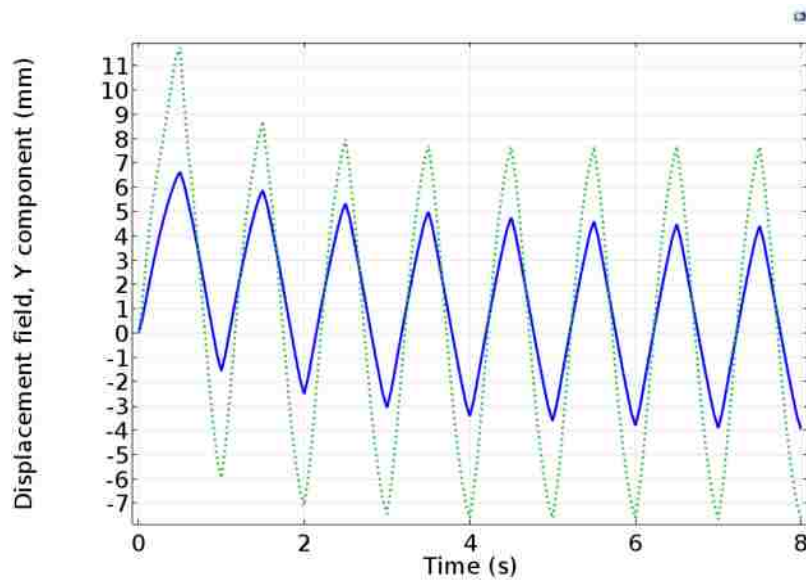


Figure 2.10. Results for the two cases of diffusion coefficients with a square voltage input (0.5 V, 1 Hz), where the solid line is Nafion-based IPMC and the dotted line is Aquivion-based IPMC.

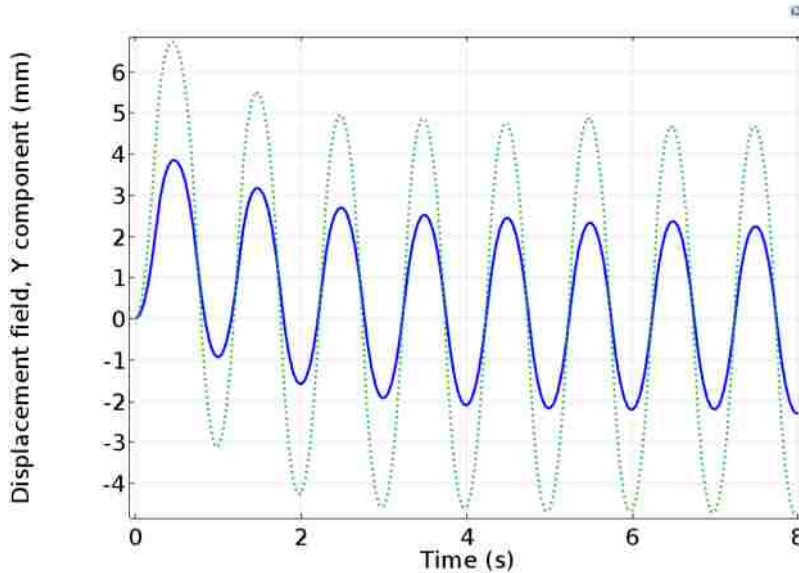


Figure 2.11. Results for the two cases of diffusion coefficients with a triangular voltage input (0.5 V, 1 Hz), where the solid line is Nafion-based IPMC and the dotted line is Aquivion-based IPMC.

## 2.5. Experimental data of N-IPMC and A-IPMC

The final step is to verify this effect experimentally. Off-the-shelf membranes were used to produce IPMCs (Figure 2.12). Nafion 115 (EW=1100) and Aquivion E98-15S (EW=980) were chosen because they have similar thicknesses ( $\sim 110 \mu\text{m}$ ). The fabricated Nafion IPMC (N-IPMC) and Aquivion IPMC (A-IPMC) were cut into similar dimensions (Table 2.4). The samples were tested using a sinusoidal input at 3 Volts with varying frequencies: 100 mHz, 500 mHz, and 1 Hz. For each data set, the displacement for both N-IPMC and A-IPMC are plotted together for comparison. The data for each test are shown in Figure 2.13, Figure 2.14, and Figure 2.15. The peaks are measured and the peak-to-peak amplitude and response times are summarized in Table 2.5, Table 2.6, and Table 2.7. It can be seen that there is an amplitude difference between the two IPMCs and that this difference decreases as the frequency increases. The response time of the A-



IPMC is slightly faster than the N-IPMC in all three cases. The data presented shows that Aquivion E98-15S is better performing than Nafion 115 in terms of actuation.

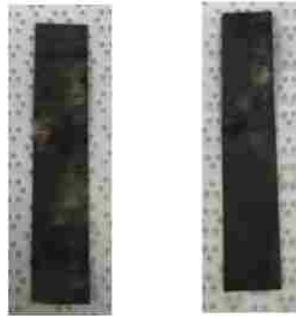


Figure 2.12. IPMCs fabricated using off-the-shelf Nafion (left) and Aquivion (right) membranes.

Table 2.4. Dimensions for the N-IPMC and A-IPMC fabricated for testing.

	<b>Length (mm)</b>	<b>Width (mm)</b>	<b>Thickness (mm)</b>
<b>N-IPMC</b>	10.47	50.23	0.2
<b>A-IPMC</b>	10	48.55	0.19

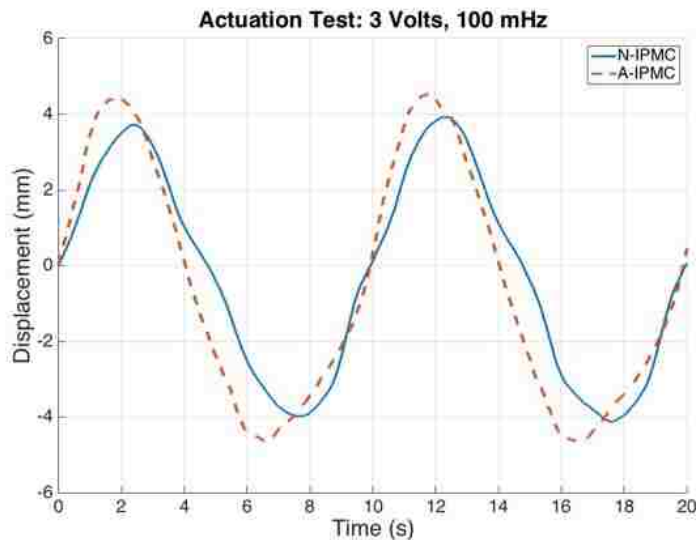


Figure 2.13. Experimental data for an N-IPMC and A-IPMC with a voltage input of 3 Volts at 100 mHz. Reprinted with permission from IOP Publishing [46].

Table 2.5. Peak measurements from the data collected for the test with an applied voltage of 3 Volts at 100 mHz.

3 Volts, 100 mHz			
	Peak to Peak Amplitude (mm)	Response Time (s)	
		Time to first peak	Time to second peak
N-IPMC	6.32	2.34	5.4
A-IPMC	11.02	1.79	4.78

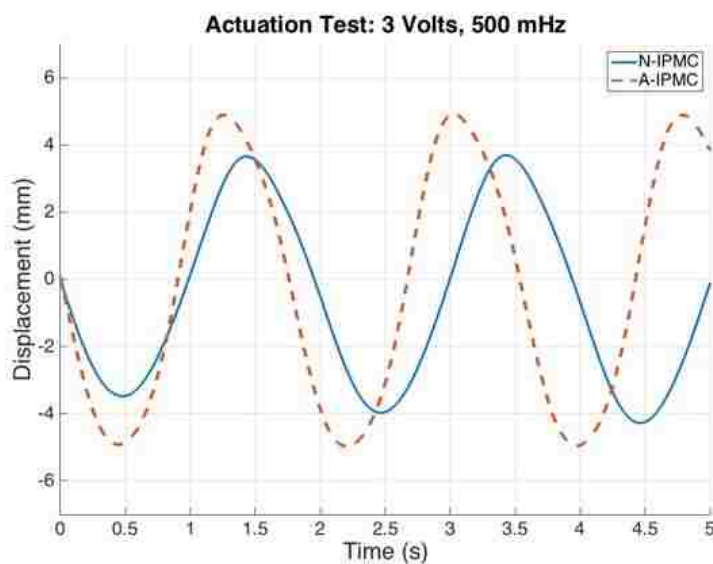


Figure 2.14. Experimental data for an N-IPMC and A-IPMC with a voltage input of 3 Volts at 500 mHz. Reprinted with permission from IOP Publishing [46].

Table 2.6. Peak measurements from the data collected for the test with an applied voltage of 3 Volts at 500 mHz.

<b>3 Volts, 500 mHz</b>			
	<b>Peak to Peak Amplitude (mm)</b>	<b>Response Time (s)</b>	
		<b>Time to first peak</b>	<b>Time to second peak</b>
N-IPMC	7.14	0.48	0.95
A-IPMC	9.82	0.44	0.82

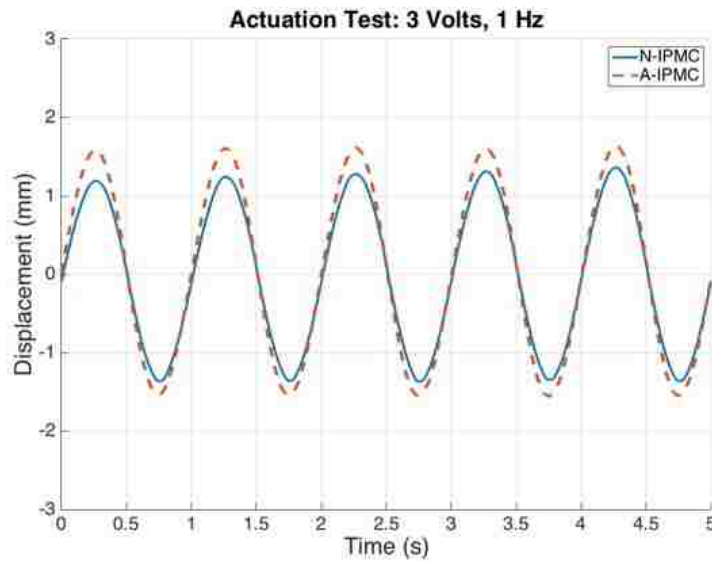


Figure 2.15. Experimental data for an N-IPMC and A-IPMC with a voltage input of 3 Volts at 1 Hz. Reprinted with permission from IOP Publishing [46].

Table 2.7. Peak measurements from the data collected for the test with an applied voltage of 3 Volts at 1 Hz.

<b>3 Volts, 1 Hz</b>			
	<b>Peak to Peak Amplitude (mm)</b>	<b>Response Time (s)</b>	
		<b>Time to first peak</b>	<b>Time to second peak</b>
N-IPMC	2.55	0.28	0.49
A-IPMC	3.11	0.25	0.49

### **Chapter 3. Understanding the Thermal Properties of Precursor-Ionomers to Optimize Fabrication Processes for Ionic Polymer-Metal Composites (IPMCs)**

This chapter is an accepted paper for an invited journal. The authors are Sarah Trabia, Kisuk Choi, Zakai Olsen, Taeseon Hwang, Jae-Do Nam, and Kwang J. Kim. The paper discusses the thermal characteristics of precursor Nafion and Aquivion measured using a Dynamic Mechanical Analyzer, Rotational Rheometer, and Thermogravimetric Analyzer. This paper's complete citation is: Trabia, S.; Choi, K.; Olsen, Z.; Hwang, T.; Nam, J.; Kim, K. Understanding the Thermal Properties of Precursor-Ionomers to Optimize Fabrication Processes for Ionic Polymer-Metal Composites (IPMCs). *Materials (Basel)*. **2018**, *11*, 665, doi:10.3390/ma11050665.

The experiments were conceived by KJK and JDN. Collecting all of the data and organizing the data was done by ST. The data collected from the Rotational Rheometer was conducted by KC and JDN. The COMSOL model included was made by ZO. All of the authors gave their input on the results.

#### **3.1. Introduction**

Ionic Polymer-Metal Composites (IPMCs) are one of the smart materials studied by many researchers [1], [2], [6], [51]. IPMCs have an ionomer base with a noble metal plated onto the surface. When a voltage is applied to the IPMC, the cations within the membrane are pulled towards the negatively charged side, causing it to swell and forcing a bending motion. The smart material can also act as a sensor when it is deformed [4], [10], [11]. The movement of the cations within an ionomer can generate a small amount voltage that can be amplified.

Nafion is usually the ionomer chosen for IPMCs. Nafion is an ideal option, as it is chemically stable and has good conductivity and material properties [32], [33], [44]. Many have studied ways to improve the properties of Nafion. However, the most critical characteristic of Nafion is its ionic conductivity and ion exchange capacity. Since there has not been a way to change this value directly other than in-depth chemistry approaches, a convenient solution is to choose another ionomer with a higher ionic conductivity and ionic exchange capacity. Recently, Aquivion has been shown to increase the IPMC's performance overall because it has a higher ionic conductivity and ionic exchange capacity [46]. The resulting performance measure is also estimated by a physic-based modeling (Figure 3.1) where it can be seen that as the diffusion coefficient increases due mainly to the increase in ion conductivity, the actuation abilities of IPMCs increase. Both ionomers are available in two forms: activated and un-activated (precursor). The activated forms of the ionomers have tetrafluoroethylene backbone, with Nafion having a perfluorovinyl ether side group and a sulfonate end group [38] and Aquivion having a double ether perfluoro side chain and sulfonic acid end group [52] (Figure 3.2). The acid end group is what deems the ionomers to be "activated" and able to conduct ions, but also causes the ionomers to be unable to melt [53], [54]. Their thermal properties have been studied thoroughly by researchers such as de Almeida and Kawano as well as Zhao and Benziger [55], [56]. The un-activated (precursor) forms of the ionomers have the following structure: tetrafluoroethylene backbone, with precursor Nafion has a perfluoro-3,6-dioxo-4-methyl-7-octenesulfonyl fluoride side chain, while precursor Aquivion has a shorter sulfonyl fluoride vinyl ether side chain (Figure 3.3). This different end group allows the precursor ionomer to melt, but cannot conduct ions [54], [57]. It is imperative to hydrolyze the ionomers to switch the end group to an acid form once the shape is made [58].

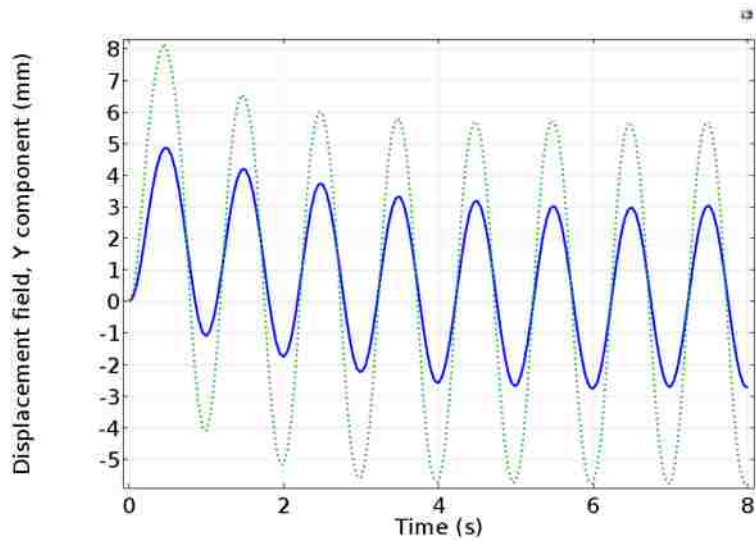


Figure 3.1. COMSOL Multi-physics simulation of a parameter sweep to predict the actuation capabilities of a Nafion-based IPMC (solid line) and an Aquivion-based IPMC (dotted line). The applied voltage is 0.5 V at a frequency of 1 Hz. The IPMC modeled is 51.07 mm long, 9.94 mm wide, and 0.586 mm thick. The model has two components: the transport, electric current, and general form of partial differential equation (PDE) were used to model Poisson-Nernst-Planck system, which was coupled to a model for the solid mechanics to obtain the tip deflection [59].

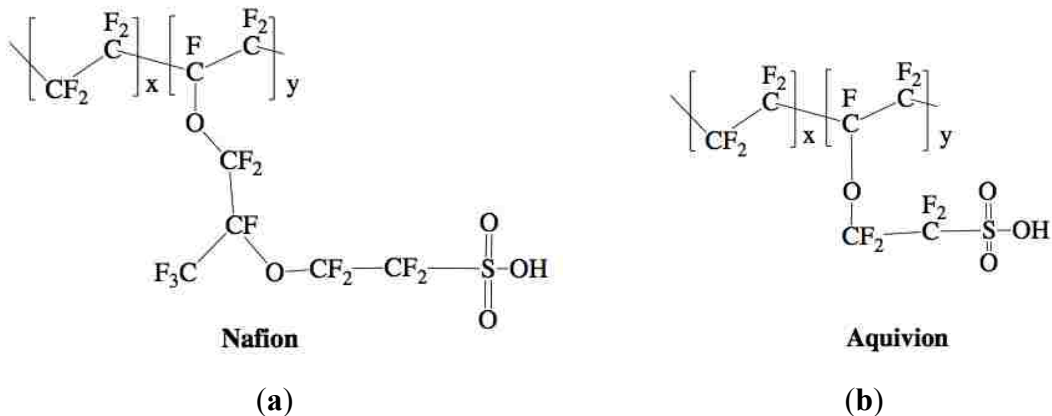


Figure 3.2. Chemical structure of Nafion (a) and Aquivion (b) activated, membrane forms [60], [61].

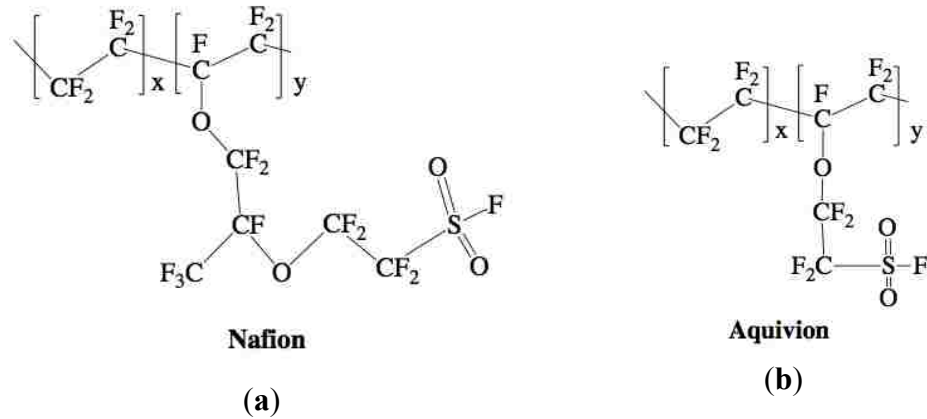


Figure 3.3. Chemical structure of Nafion (a) and Aquivion (b) un-activated, precursor forms [62], [63].

The un-activated form of the ionomers is available as precursor pellets. It has been used in extrusion [64] and hot-pressing [13]. More recently, newer fabrication methods were developed: injection molding [27] and 3D printing [46], [65] of precursor Nafion and precursor Aquivion. For all of these methods, it is important to understand how these ionomers behave with thermal loads. Though the precursor pellets can melt, if not heated properly or thoroughly during the process, it can cause degradation. For the injection molding process, the mold that the pellets enter needs to be at a similar temperature as the chamber where they are heated. This is done by heating the mold to the same temperature (Figure 3.4 (a)). Finding the correct temperature to set these two environments will help optimize the process. For 3D printing, the bed temperature needs to be high enough to encourage adhesion, while also allowing the print to cool down to have good layering (Figure 3.4 (b)). The best temperatures for Aquivion are 260°C for the extruder and 180°C for the bed [46]. The best temperatures for Nafion are 290°C for the extruder and 180°C for the bed [65]. Currently, there is no thorough study of the thermal characteristics of precursor Nafion and precursor Aquivion pellets. The key points that need to be clarified for researchers are the thermal degradation temperature, viscosity, melting temperature, and glass transition. The objective of this



study is to provide a clear guide of the ionomer precursor pellets in order to optimize various thermal-based fabrication processes. This can be done by conducting various tests to characterize the precursor ionomers.

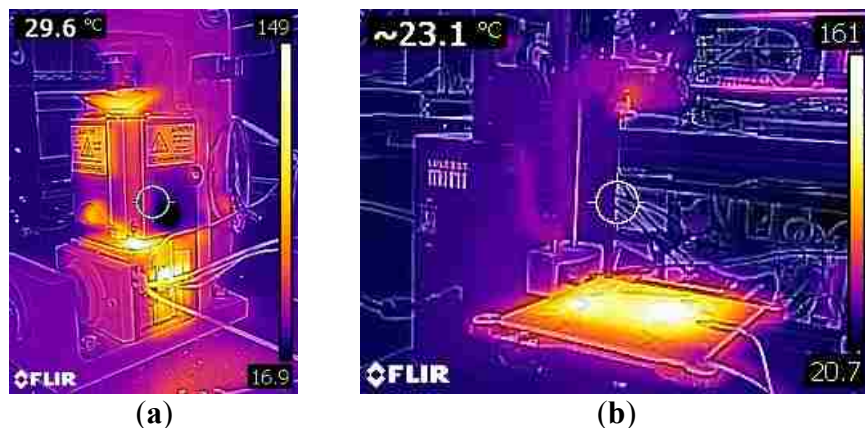


Figure 3.4. Injection molding setup heating to the set temperature (150°C) (a) and a modified 3D printer (Lulzbot Mini) to print precursor Aquivion filament heating up to set temperatures (the extruder set to 260°C and the bed set to 180°C) (b).



Figure 3.5. A precursor Nafion membrane printed with inner channels for potential implementation of liquid sensors (a) and a precursor Aquivion membrane being printed in typical dimensions for IPMC applications (b).

### 3.2. Methods

For these tests, Nafion precursor pellets with an Equivalent Weight (EW) of 970 g/eq (C.G. Processing) and Aquivion precursor pellets with an EW of 870 g/eq (P87S-SO<sub>2</sub>F, Solvay) were used. To characterize Nafion and Aquivion precursor pellets, a series of tests were conducted. First, the chemical structure of the two were studied using a Fourier Transform-Infrared Spectroscopy (FT-IR, IRTracer-100, Shimadzu). The thermal degradation temperature was measured using a Thermogravimetric Analyzer (TGA, Q500, TA Instruments) in a nitrogen atmosphere. The heat rate was 10°C/min and temperature range was set to start at room temperature to 650°C. The balance and sample purge flow of N<sub>2</sub> gas were set to 40 mL/min and 60 mL/min, respectively. Rheological tests were conducted with a rotational rheometer (MCR 300, Anton-Paar, Austria) using a parallel-plate geometry (D=25mm) to measure the change in shear viscosity as temperature increases and the melting temperature. From the steady shear test, the shear stress was measured as a function of shear rate in the range of 0.01-10 (1/s), while in an oscillatory shear measurement, an angular frequency from 0.6 to 600 (rad/s) was applied under a constant strain of 1%. To measure the glass transition range, samples were tested in a Dynamic Mechanical Analyzer (DMA, Pyris Diamond, Perkin Elmer) that has the ability to control the temperature of the test environment. The samples were annealed in the oven overnight at 140°C, following the procedure described by Tao [66]. He showed that by slowly heating and applying a displacement at a designated frequency, it is possible to plot the damping coefficient change with respect to temperature. From this curve, it is possible to find the glass transition range. The heat rate was set to 1°C/min and the heat range was set to start at 20°C to 100°C. The tests were conducted at a frequency of 1 Hz with an applied force of 50 mN.

### 3.3. Results

First, the chemical structures were analyzed with the FT-IR. Figure 3.6 shows the transmittance of the two precursor ionomers, which have similar structures based on this plot. The peaks at  $1465\text{ cm}^{-1}$ ,  $1213\text{ cm}^{-1}$ ,  $1153\text{ cm}^{-1}$ ,  $986\text{ cm}^{-1}$ , and  $800\text{ cm}^{-1}$  correlate to C-F, symmetric  $\text{CF}_2$ , asymmetric  $\text{CF}_2$ , C-F<sub>3</sub>, and S-O bonds respectively [46]. The thermal degradation temperature of the two ionomers is around  $330^\circ\text{C}$  (Figure 3.7). Both degrade at almost the same rate. To further investigate the degradation of the two precursor ionomers, the Differential Thermogravimetric (DTG) curves have been plotted (Figure 3.8). It can be seen that degradation more accurately begins at around  $400^\circ\text{C}$ . The peak for precursor Nafion is most likely due to vaporization. The peaks for precursor Aquivion are most likely correlated to a crystal structure change, followed by vaporization.

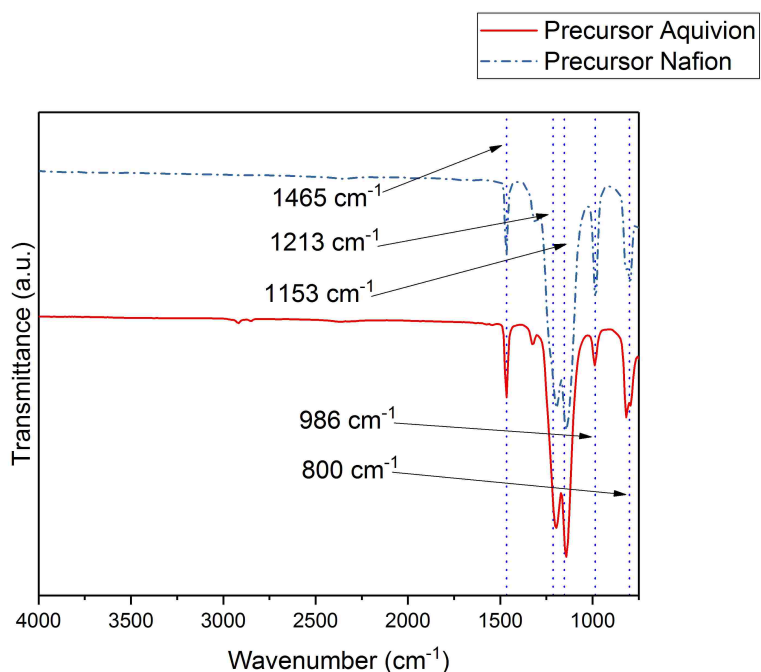


Figure 3.6. FT-IR results comparing Nafion and Aquivion precursor pellets.

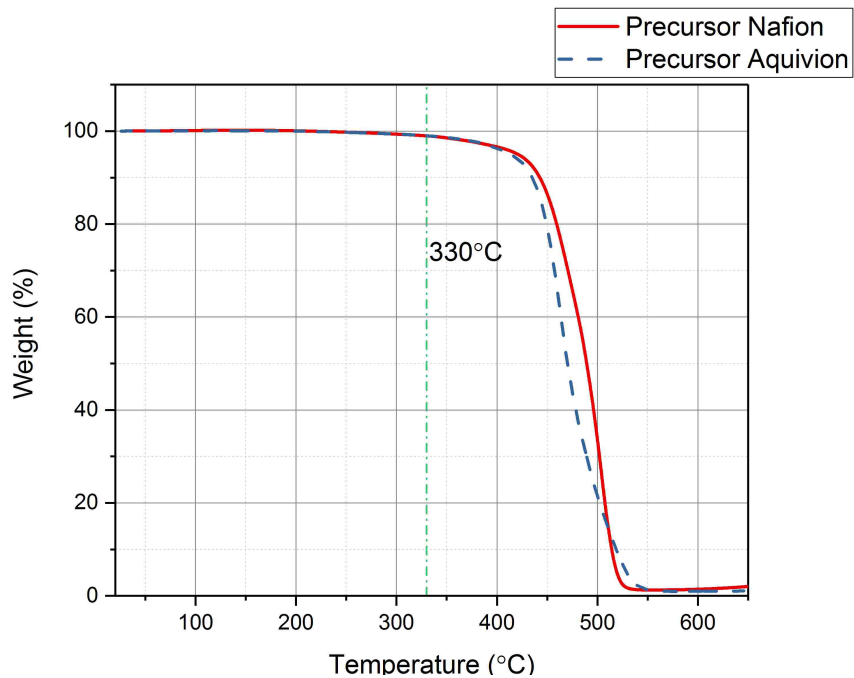


Figure 3.7. TGA results showing that both precursor ionomers have the same thermal degradation temperature at 330°C.

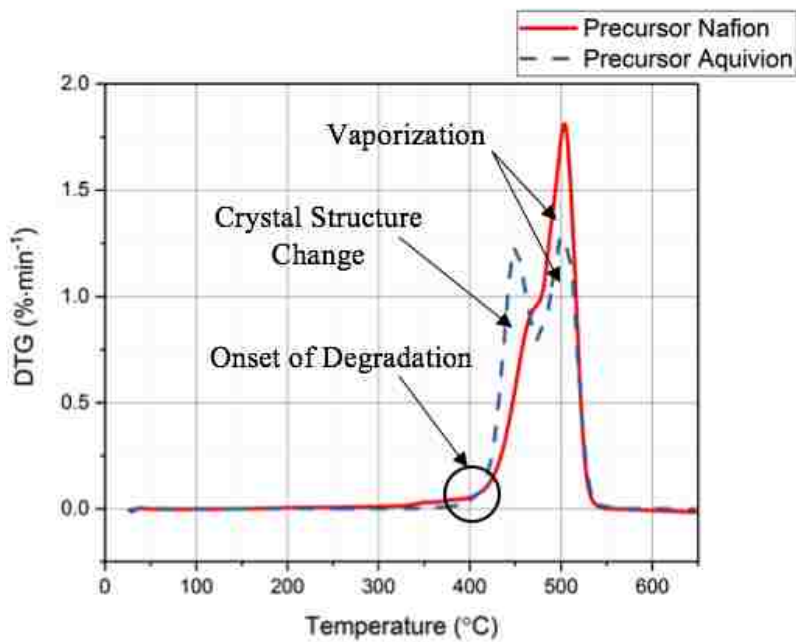


Figure 3.8. DTG results from the TGA tests for precursor Nafion and precursor Aquivion.

The rheology tests were run to gather data about the ionomers under different conditions. The data for the Storage Modulus and Loss Modulus for each ionomer and where the curves cross, denotes where the polymer is beginning to melt. From Figure 3.9, it can be seen that precursor Aquivion's melting temperature is about 240°C and for precursor Nafion's melting temperature is about 200°C. The melting temperature for precursor Aquivion matches what is provided by Solvay [63]. The plots in Figure 3.9 show that the two ionomers exhibit partially crystalline behavior, because after the two lines intersect, the loss modulus is larger than the storage modulus [67]. To further analyze the results, the ratio between storage and loss modulus is  $\tan(\delta)$  and this can give more information about the viscous behavior for the two precursor samples. When  $\tan(\delta)$  is less than 1, the sample has more of a gel-like behavior and when it is greater than 1, the behavior is more liquid-like [68]. In Figure 3.10, it can be seen that the values for precursor Nafion are greater than 1 at about 200°C and the values for precursor Aquivion are greater than 1 at about 240°C, which matches well with what is seen in Figure 3.9. It was also of interest to study the change in viscosity as the temperature increases. It was interesting to see that precursor Aquivion has a higher viscosity throughout the temperature sweep compared to precursor Nafion (Figure 3.11). With an applied shear rate (precursor Nafion was tested at 200°C and precursor Aquivion was tested at 240°C at a frequency of 1 Hz), it can be seen that precursor Aquivion has higher shear stress and shear viscosity than precursor Nafion (Figure 3.12). Both exhibit similar trends as the shear rate increases. With an applied strain (precursor Nafion was tested at 200°C and precursor Aquivion was tested at 240°C at a frequency of 1 Hz), precursor Aquivion still has higher storage and loss moduli (Figure 3.13). Based on the results, it can be noted that the two exhibit liquid-like characteristics, because the loss modulus is higher than the storage modulus [67]. As the angular frequency increases (precursor Nafion was tested at 200°C and precursor Aquivion was tested at

240°C), again precursor Aquivion has higher complex viscosity and storage and loss moduli than precursor Nafion (Figure 3.14). The angular frequencies between 1 and 1000 rad/s simulates an extrusion process and above  $\sim 100$  rad/s simulates an injection process [67]. The material characteristics can be found for ionomers in 3D printing and injection molding process using Figure 3.14.

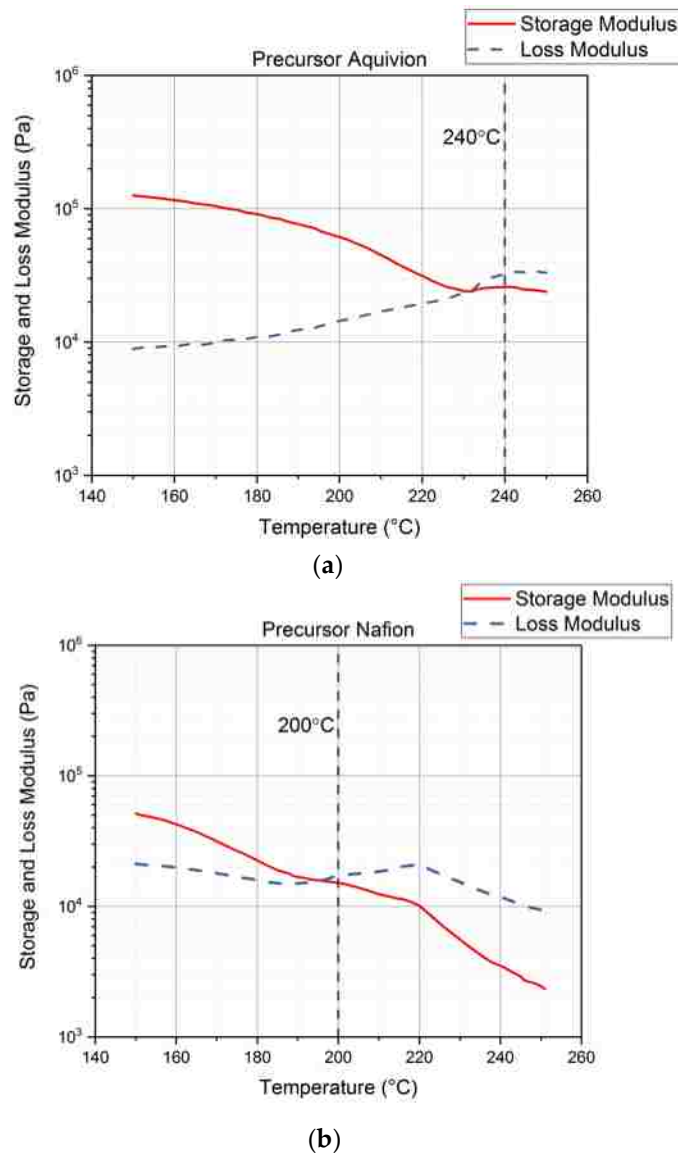


Figure 3.9. Results from the rheology tests showing the melting temperature of precursor Aquivion (a) and precursor Nafion (b).

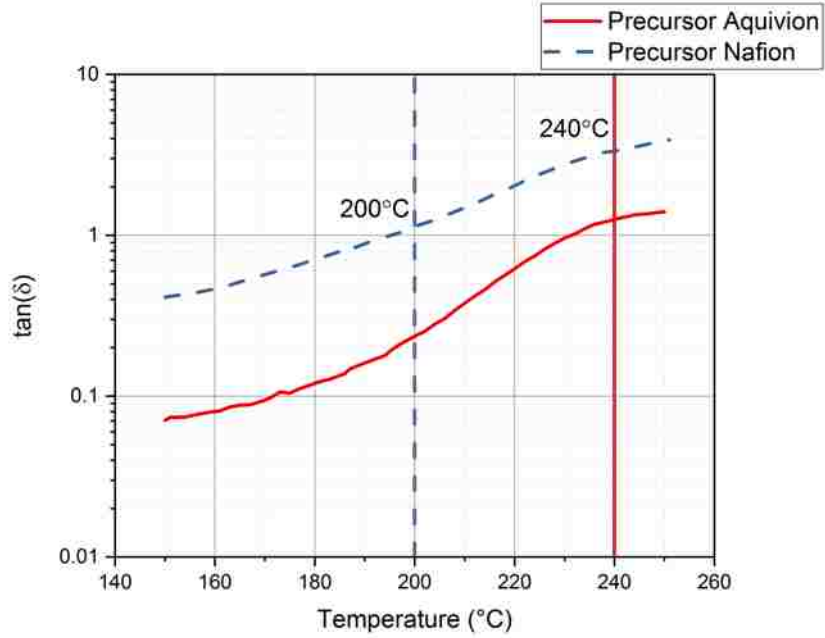


Figure 3.10. Results for  $\tan(\delta)$  from the rheology tests to understand the viscous behavior of precursor Aquivion and precursor Nafion.

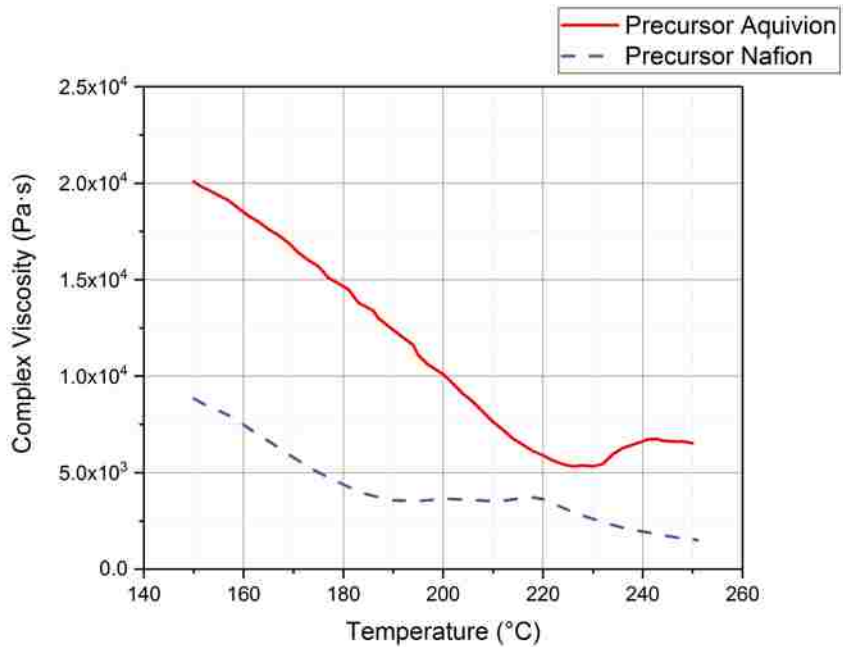


Figure 3.11. Complex viscosity results from the rheology tests conducted on the precursor ionomers.

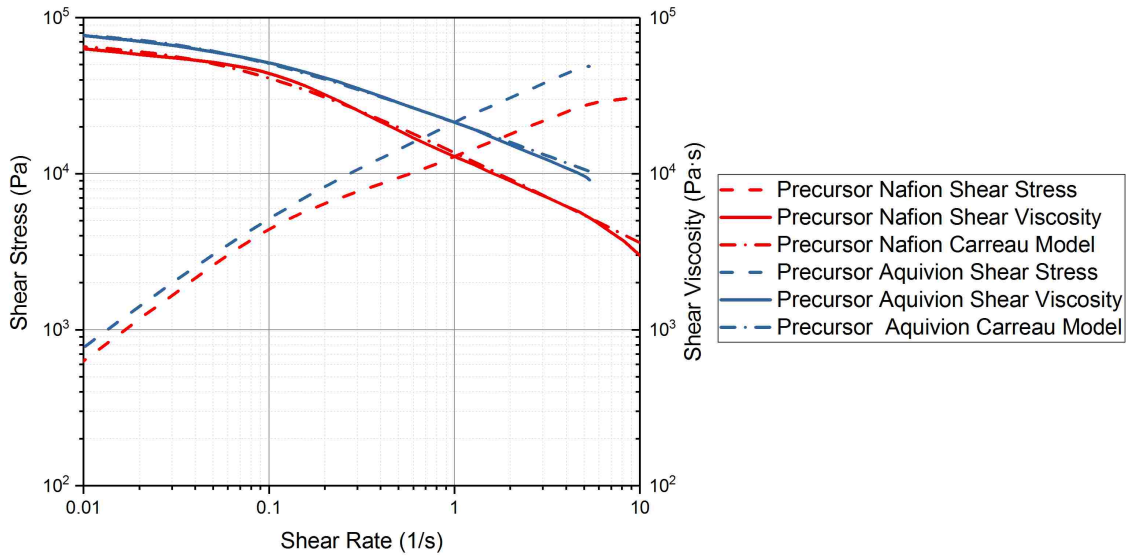


Figure 3.12. Rheology tests with applied shear rate to measure the shear stress and shear viscosity of the precursor-ionomers. Precursor Nafion was tested at 200°C and precursor Aquivion was tested at 240°C.

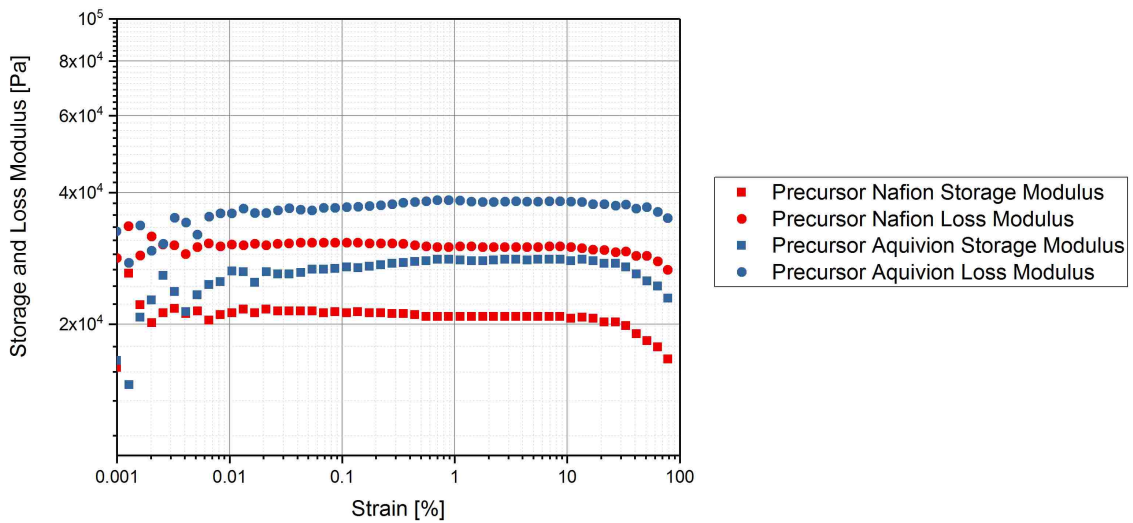


Figure 3.13. Rheology tests with an applied strain to measure the storage and loss modulus of the precursor-ionomers. Precursor Nafion was tested at 200°C and precursor Aquivion was tested at 240°C at a frequency of 1 Hz.



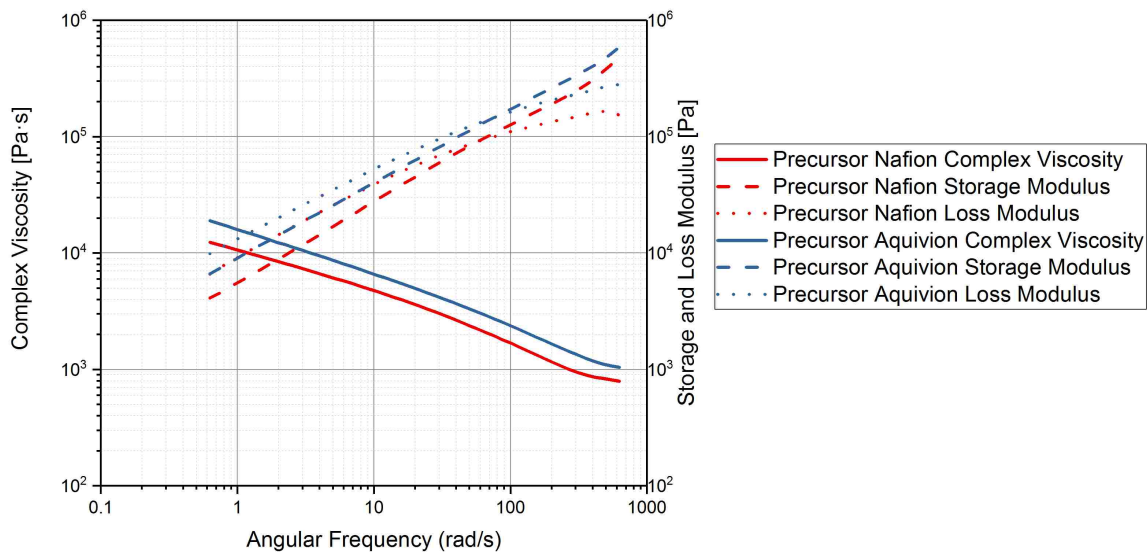


Figure 3.14. Rheology tests with an applied angular frequency to measure the complex viscosity and storage and loss modulus. Precursor Nafion was tested at 200°C and precursor Aquivion was tested at 240°C.

The DMA was used with thermal control to identify the glass transition range for each precursor ionomer [66]. This can be done by plotting the damping coefficient values as the temperature increases. Figure 3.15 shows the damping coefficient for precursor Aquivion and precursor Nafion. Precursor Aquivion has a larger range than precursor Nafion (32-65°C and 21-45°C, respectively). From this plot, it can also be noted that the precursor Aquivion sample is significantly stiffer than precursor Nafion. To verify this, the Young's Modulus for each was studied (Figure 3.16). It is clear from this plot that the precursor Aquivion sample is much stiffer at room temperature than precursor Nafion, but decreases to the same value as it is heated. To show how different the two types of ionomers are, Table 3.1 is presented compare the two damping coefficients and Young's Moduli of the activated and precursor forms. The activated forms are generally stiff, but it is interesting to note the vast difference in the precursor forms. Precursor Aquivion is significantly stiffer than the activated form, while precursor Nafion is significantly softer than the activated

form. These differences can further verify that precursor Aquivion may be easier to work with since there is a larger range in which the polymer becomes rubbery to liquid.

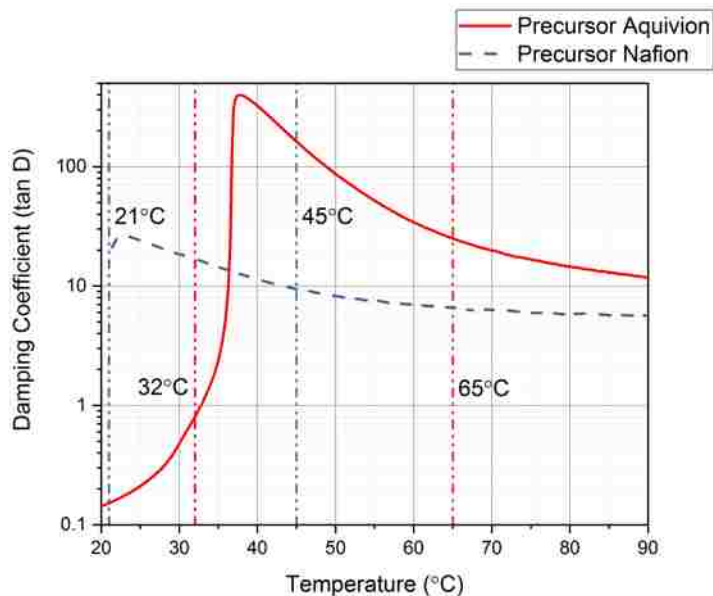


Figure 3.15. Damping coefficient as the temperature increases to find the glass transition temperature range for the precursor ionomers.

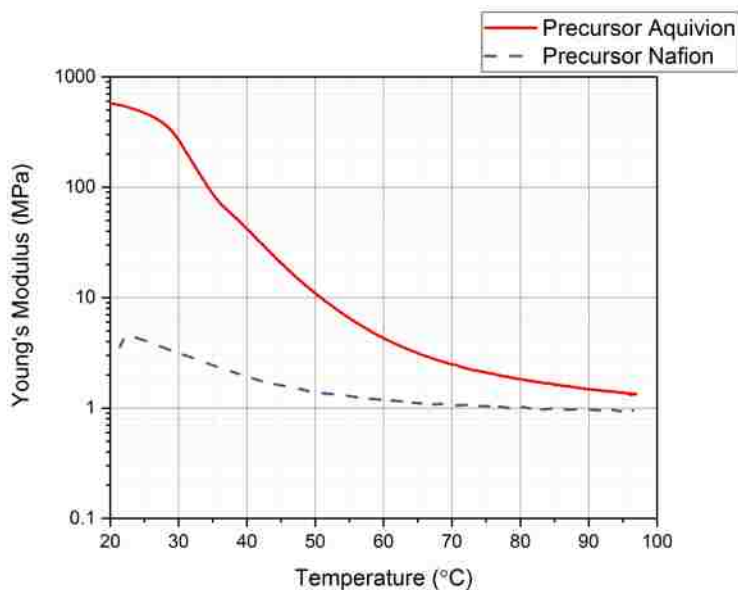


Figure 3.16. Young's Modulus as the temperature increases for each precursor ionomer.

Table 3.1. Comparison of the mechanical characteristics of activated and precursor forms of the ionomers at room temperature.

	<b>Aquivion</b>		<b>Nafion</b>	
	<b>Activated</b>	<b>Precursor</b>	<b>Activated</b>	<b>Precursor</b>
Damping Coefficient (tan D)	0.122±0.000085	0.144 ±0.00061	0.058±0.00012	21.1±8.74
Young's Modulus (MPa)	293±0.14	574±2.82	329±0.42	3.57±2.588

### 3.4. Discussion

Both of the precursor ionomers exhibit partially crystalline behavior based on the results in Figure 3.9. It is possible to see how the material will behave under certain angular frequencies that simulate different processes using Figure 3.14. The ranges of angular frequency mimic those that will be felt by precursor Nafion and precursor Aquivion. During the applied angular frequency test, the loss modulus was higher than the storage modulus for both precursor ionomers, indicating liquid-like behavior at the correlating temperatures chosen (Figure 3.14).

On the other hand, according to the shear viscosity as a function of precursor Nafion and precursor Aquivion in Figure 8, both ionomers show a non-Newtonian behavior (shear thinning) where the shear viscosity decreases with a shear rate. Note that the shear thinning property implies its solid-like behavior at a high shear rate with potential polymer chain alignment under a shear. The flow behavior of two precursor materials can be fitted using a weighted non-linear regression to a modified-Carreau model [69].

Table 3.2. Parameter variables of modified-Carreau model (Equation (3)) for two precursor ionomers.

<b>Ionomer</b>	$\eta_0$ (Pa·s)	$\lambda$ (s)	<b>n</b>	$r^2$
Precursor Nafion	$7.1 \times 10^4$	15.4	0.41	0.945
Precursor Aquivion	$8.4 \times 10^4$	21.5	0.56	0.977

$$\eta = \frac{\eta_0}{[1 + (\lambda\dot{\gamma})]^{(1-n)}} \quad (3)$$

Where  $\eta$  refers to the shear rate dependent shear viscosity,  $\eta_0$  is the zero-shear viscosity,  $\lambda$  is the characteristic time,  $\dot{\gamma}$  is a shear rate, and  $n$  is a dimensionless parameter. The slope of the power-law region with shear-thinning behavior is governed the exponent of  $(1-n)$ . The different flow behaviors with different degree of shear-thinning can be considered with various values of  $n$  in Equation 1. The value of  $n$  will be 1 for Newtonian fluids, while for typical shear thinning behavior is shown when  $n < 1$ . Newtonian fluids have an  $n$  value of 1 because there is no large change in shear viscosity as the shear rate increases. For non-Newtonian fluids, such as precursor Nafion and Aquivion, at low shear rates there will be minimal change in shear viscosity and once the polymer endures high shear rates, the power law comes into effect and begins show shear-thinning. The modified-Carreau model was well fitted with the experimental data as shown in Figure 3.12 with the calculated values of  $\eta_0$ ,  $\lambda$ , and  $n$  as illustrated in Table 3.2. The values for  $n$  for the two ionomers show that precursor Nafion has more shear-thinning abilities than precursor Aquivion, since it has a lower  $n$  value. From the shear stress measurement under different strains (Figure 3.14), both precursor ionomers illustrate the viscoelastic characteristics within the strain range of 1 and 10% which is used to conduct in oscillatory measurement. In addition, it can be also noted that the complex viscosity obtained from the dynamic oscillation test shows the similar trend to

the shear viscosity of two precursors where shear viscosity of precursor Aquivion is higher than that of precursor Nafion.

The precursor Nafion samples were very soft at room temperature. This is verified by the data from the DMA, showing that the glass transition temperature of precursor Nafion starts at room temperature. The melting temperature is also lower than expected (200°C). This data verifies what is noted by Grot in a book discussing fluorinated ionomers. He mentions that films made from Nafion precursor pellets are soft at room temperature and stretch easily [57]. This is verified by the data gathered from the DMA. The precursor Nafion sample is very soft at room temperature. Precursor Aquivion on the other hand has a higher glass transition and melting temperature. It seems that precursor Aquivion is a more thermally stable polymer. This can make it easier to work with since it is more moldable. It was noted throughout different processes, such as hot-pressing and filament extrusion, precursor Aquivion was easier to use and mold into the new desired shape.

### **3.5. Conclusions**

A thorough study of the behaviors of precursor Nafion and Aquivion has been provided. The melting temperature of both have been established for the ionomers. The ionomers have similar thermal degradation temperatures. The viscosity of the precursor ionomers has been studied versus temperature, strain rate, and angular frequency. Precursor Aquivion has higher viscosity than precursor Nafion. The shear viscosity was fit to a modified-Carreau model and showed that the precursor ionomers both have shear-thinning abilities. Precursor Nafion has more shear-thinning abilities due its lower  $n$  value than precursor Aquivion. Precursor Nafion is much softer at room temperature, which was verified using the DMA to find that its glass transition range starts at room

temperature and a Young's Modulus at around 3 MPa. Precursor Aquivion is significantly stiffer at room temperature (~574 MPa) and a larger glass transition range.

The gathered data showed that precursor Aquivion may be better to use in processes such as extrusion, hot pressing, and 3D printing. This is because precursor Aquivion has more of an ability to be molded into a shape after being heated. Precursor Nafion becomes much more liquid like, making it difficult to shape, such as in filament extrusion. However, the study has provided enough information for any researcher to use either precursor ionomer in a thermal-based fabrication process.

### **3.6. Acknowledgement**

This material is based upon work supported in part by the National Science Foundation under Grant #1545857. Any opinions, findings, and conclusions or recommendations expressed in this material are those of the author(s) and do not necessarily reflect the views of the National Science Foundation.

## **Chapter 4. A Fabrication Method of Unique Nafion Shapes by Painting for Ionic Polymer-Metal Composites**

This chapter includes the publication for the work on spray-painting of Nafion Water Dispersion. The goal is to have be able to produce intricate Nafion shapes by spray painting the dispersion into stencils. The authors are Sarah Trabia, Taeseon Hwang, and Kwang J. Kim. The paper discusses how the Nafion water dispersion was painted into a stencil to make new Nafion shapes. Reprinted with permission from Smart Materials and Structures: Trabia, S.; Hwang, T.; Kim, K. J. A fabrication method of unique Nafion® shapes by painting for ionic polymer–metal composites. *Smart Mater. Struct.* **2016**, *25*, 85006, doi:10.1088/0964-1726/25/8/085006. The copyright is included in Appendix C.

The fabrication of the samples was done by ST. Characterizing the samples made was conducted by ST and TH. All of the authors gave insight on the data.

### **4.1. Introduction**

Ionic Polymer-Metal Composites (IPMC) are a smart material made from Nafion®, an electro-active polymer, which is plated with platinum, palladium, gold, and/or other electric conducting materials. When a voltage is applied to the IPMC, the cations move to the negatively charged surface, causing the IPMC to bend [1]. It works best when hydrated as the movement of both the cations and water molecules causes the actuation. IPMC can also be used as sensors by reading the voltage produced by its motion. The applications of IPMCs can be determined by the shape and the thickness of the smart material [2], [5]. By making the IPMC thin, it can create a larger displacement when actuated. A thicker IPMC will not displace as much, but will produce a larger

blocking force. IPMCs work well in biomimicry because of how customizable they are and smoothness of the motion [13], [15], [70]–[75].

Nafion<sup>®</sup> membrane is the basis of most IPMC due to its electrical properties and porosity [15], [38]–[40], [76]. Nafion<sup>®</sup> is available in many forms, including sheets, pellets, and water dispersion. Each form is more suited for specific manufacturing techniques. For example, Nafion<sup>®</sup> sheets are already processed and can be purchased and cut to the desired dimensions, which is suited for producing rectangular IPMCs [73], [77], [78]. It is, however, difficult to create different shapes or thicknesses when using sheets. Nafion<sup>®</sup> precursor pellets are best for extrusion and injection molding to make rods or tube shaped Nafion<sup>®</sup> [79]. This process is fairly complicated and can take some time to produce perfectly within a typical lab environment.

Water dispersions can be used for casting Nafion<sup>®</sup> films, allowing for more control over various properties of the membrane. Chung *et al.* produced Nafion<sup>®</sup> films using 20 wt.% Nafion dispersion and studied the variation of crystalline structure by adding weights to the films [80]. They found it was possible to control the planar spacing with the weights to create the stiffness desired. In order to increase the blocking force of the IPMC, the thickness of the membrane is increased. Ryu *et al.* also used the casting method to produce thicker and stiffer membranes for their micro-robot [30]. Water dispersions also allow Nafion<sup>®</sup> to be mixed with other polymers for various reasons. He *et al.* fabricated a variety of samples with different thicknesses by pouring liquid mixtures of the Nafion<sup>®</sup> dispersion with dimethyl fluoride (DMF) in a container to create an azeotrope [81]. They verified that with an increase in thickness does indeed increase the blocking force as well as the Young's modulus, since both are related to the crystallinity of the



membrane. Hwang *et al.* mixed Nafion® with poly(vinyl-alcohol-co-ethylene) to create a cheaper ion exchange membrane for IPMC [82]. They found an optimal ratio between the two polymers to get comparable results with a Nafion®-based IPMC.

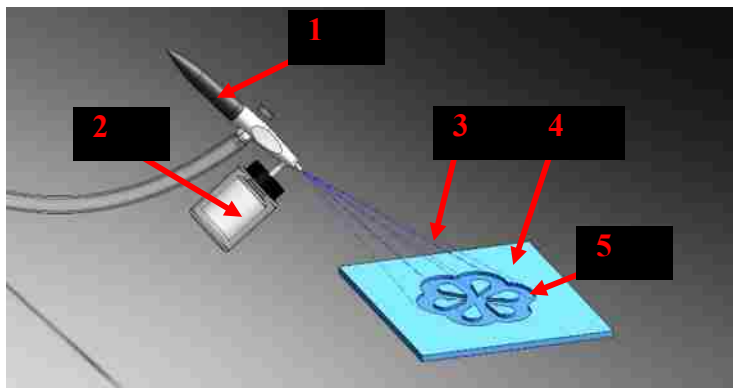


Figure 4.1. Conceptual drawing of proposed new fabrication method by means of painting Nafion onto a surface. 1: Master Airbrush Model G22. 2: Canister for Nafion water dispersion. 3: Sprayed Nafion water dispersion, 4: Vinyl stencil. 5: Substrate (Acrylonitrile butadiene styrene, ABS).

All of the papers mentioned above have given a lot of insight about casting Nafion®. However, it seems the issue of creating intricate shapes has not been explored. This paper proposes a new processing method using water dispersion by means of painting. Using an airbrush, the dispersion is painted onto a surface to create a unique shape (Figure 4.1). The process is conveniently customizable and can produce any shape that the user would like. This process of producing Nafion® membranes also gives the ability to control the thickness. Several samples of various shapes will be produced and their material characteristics will be compared with that of a commercial option. The tests conducted were Scanning Electron Microscope (SEM) imaging, X-Ray Diffraction (XRD), Thermogravimetric Analysis (TGA), Fourier Transform Infrared Spectroscopy (FT-IR), and Dynamic Mechanical Analysis (DMA). The Nafion shapes were then

incorporated into IPMCs and tested for a variety of characteristics including displacement, blocking force, and sensing.

#### **4.2. Methodology**

Using 5% wt. Nafion® water dispersion (1100 EW) from DuPont™ and an airbrush (Master Airbrush Model G22), several samples of painted Nafion® were made (Figure 4.2). The dispersion was sprayed onto an ABS weighing dish, allowing the Nafion® to easily peel off when completely dry. Each layer was allowed to dry before adding another. This ensured that the wet polymer would not move and tear or create bubbles. No heat was necessary for the process because heating causes the membrane to lift off the weighing dish too early. The membrane is difficult to build up if it has lifted because it will tear the thin membrane. To build up the membrane, it was important in the beginning to continuously add layers before it had fully dried to ensure tearing does not happen. The membrane is able to withstand cleaning and plating processes if the thickness is at least 300 microns. It has been noted that membranes around 100 microns will tear and break when in solvents. Once the desired thickness is reached, the Painted-Nafion® (P-Nafion®) is cut from the edges of the weighing dish and slowly peeled off the dish or allowed to come off the weighing dish on its own.



Figure 4.2. Nafion water dispersion painted onto an Acrylonitrile butadiene styrene (ABS) weighing dish to create a maple leaf shaped membrane.

The concept of this new procedure is being able to create custom shapes. Stencils were made using the Silhouette Cameo to cut out shapes on vinyl material with adhesive backing. To produce a membrane with the desired thickness, the vinyl can be layered to create a deeper stencil. One layer of vinyl is around 110 microns, so to create a membrane of about 300 microns, three layers were stacked together and then the shape was cut using the Silhouette Cameo. The stencil was placed onto a weighing dish and any air bubbles were pushed out (Figure 4.3). The void in the stencil was sprayed until the desired thickness was produced. In this case, a maple leaf shape with intricate points and a moon shape with a hole in the membrane were created (each around 100 microns thick) (Figure 4.4). The surface texture is uniform and no bubbles are present in the membrane. The two samples show that intricate and various shapes can be produced with this process.

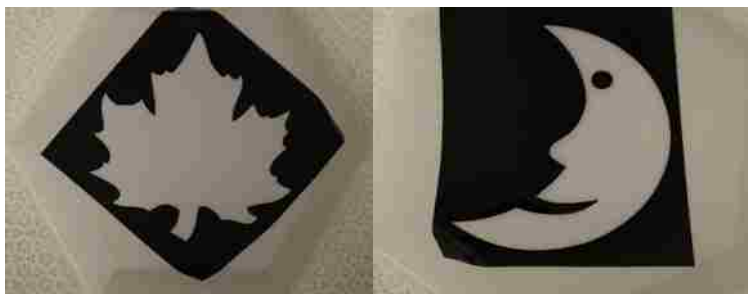


Figure 4.3. Stencils made for custom Nafion shape. Left: Maple leaf shape. Right: Crescent moon with a void. They stencils are about ~3 inches tall and ~3 inches wide.



Figure 4.4. Leaf and moon shaped dehydrated Nafion made using the painting method.

### 4.3. Results

#### 4.3.1. Comparison of the Physical Characteristics of P-Nafion® and Nafion® 117

Compared with the commercial Nafion® 117 (N117), the overall look and surface texture of the two samples are very similar (Figure 4.5). The two samples were measured and weighed to compare their densities (Table 4.1). The basic weights are comparable, when noting that the thickness is almost double for the P-Nafion® to N117 and that the basic weight from DuPont™ is said to be  $360 \text{ g/m}^2$ , the values seem to be reliable. To make sure that the airbrushing process does not affect the material characteristics Nafion®, a series of tests were conducted to provide feedback on the usefulness of this new manufacturing process. The first test done was comparing cross-sectional images of the two types of Nafion®. From Figure 4.6, Figure 4.7, and Figure 4.8, the two samples are almost identical. It should be noted that there are no air bubbles in the P-

Nafion® and both types of Nafion® have the similar amounts of dust particles. Visually, the two are indiscernible from each other.

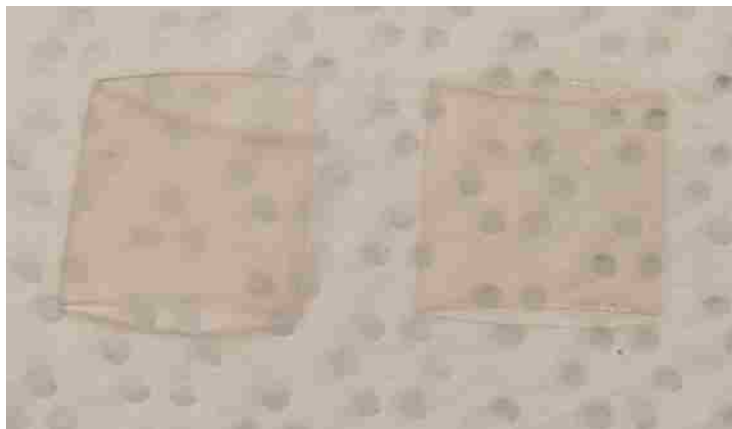


Figure 4.5. P-Nafion® (left) and N117 (right).

Table 4.1. Measurements of P-Nafion® and N117 from figure 4.5.

	<b>N117</b>	<b>P-Nafion</b>
Thickness (mm)	0.183	0.36
Width (mm)	10	10
Length (mm)	10	10
Mass (g)	0.0305	0.062
Basic Weight (g/m <sup>2</sup> )	305	620

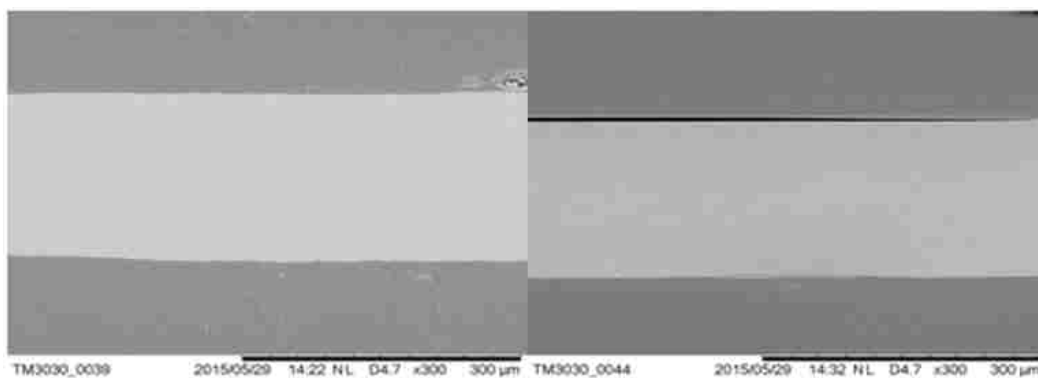


Figure 4.6. SEM images of the cross sections of P-Nafion® (left) and N117 (right), x300.

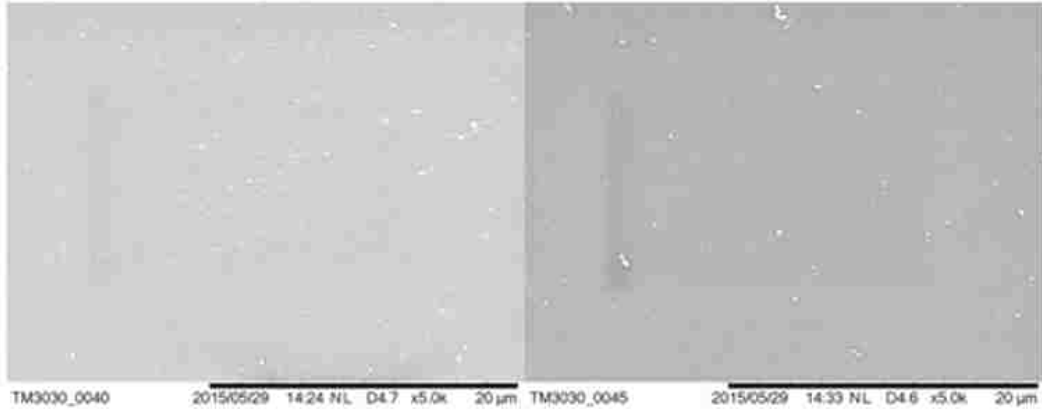


Figure 4.7. SEM images of the cross sections of P-Nafion® (left) and N117 (right), x5,000.

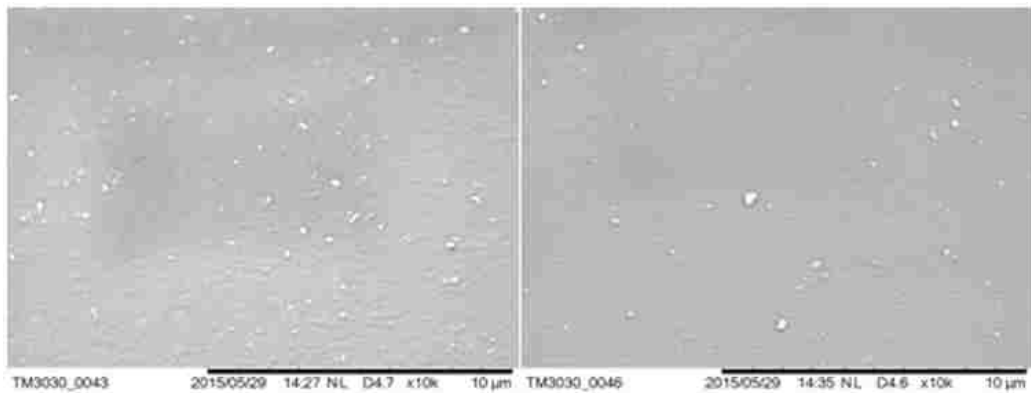


Figure 4.8. SEM images of the cross sections of P-Nafion® (left) and N117 (right), x10,000.

X-ray Diffraction (XRD) was used to show that there are no crystalline structures in the P-Nafion®, as well as to compare the chemical structure of the two samples. From Figure 4.9, the plot shows the results of the XRD test for the P-Nafion®. The curve is smooth and without small peaks throughout, showing that it is amorphous. The first peak of the P-Nafion® curve ( $17.5^\circ$ ) matches exactly with that of a casted Nafion® membrane, shown by Jiang *et al.*, Gierke *et al.*, and Moore and Martin [83]–[85]. This peak correlates to the backbone of the polymer (Teflon) [86].

In

Figure 4.9, the Full Width-Half Maximum (FWHM) is calculated for the first peak. The P-Nafion® FWHM is similar to that shown by Jiang *et al.* for their casted Nafion® sample [83].

A Thermogravimetric Analysis (TGA) test (Figure 4.10) shows that the two samples have similar thermal degradation points. Both samples begin to degrade around 300°C and have the same slope up until 400°C. P-Nafion® has a slower degradation slope and has not fully degraded until around 550°C, while N117 is fully degraded by 500°C. This is probably due to a slight thickness difference between the two samples. Neither type of Nafion® will be utilized at such high temperatures, so it is reassuring to see that P-Nafion is able to perform almost identically than N117. The curves are similar to those shown by many groups that have also tested N117 in a TGA [87]–[93].

Fourier Transform Infrared Spectroscopy (FT-IR) shows the transmittance of the samples within a range of wavelengths. Figure 4.11 shows that the samples have the same peaks and the curves are almost identical. The peaks are at 1153 cm<sup>-1</sup> and 1213 cm<sup>-1</sup>, which correlate to the asymmetric and symmetric CF<sub>2</sub> [88]. The peak at 1060 cm<sup>-1</sup> correlates to the SO<sub>3</sub> bond [88]. The two peaks are characteristic for Nafion®. They match what has been shown in various sources that have tested Nafion® [31,34,35].

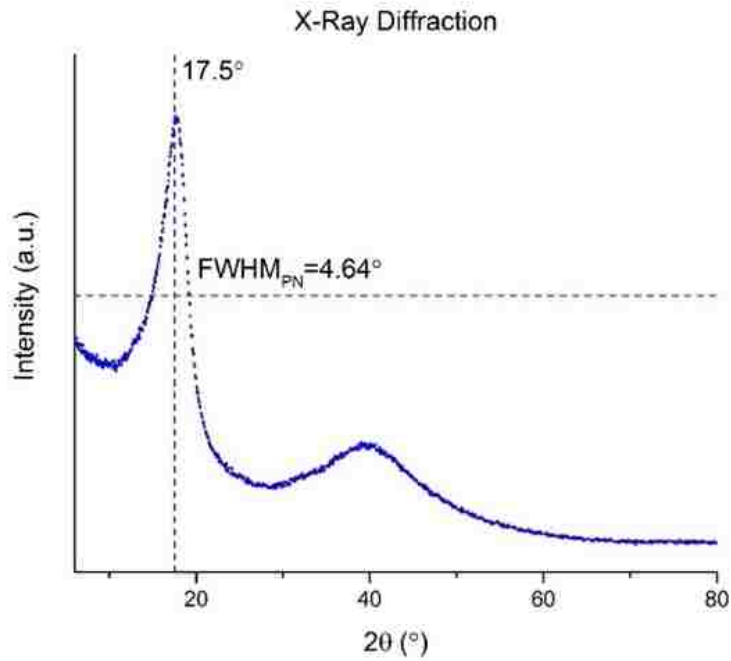


Figure 4.9. XRD results for P-Nafion® sample.

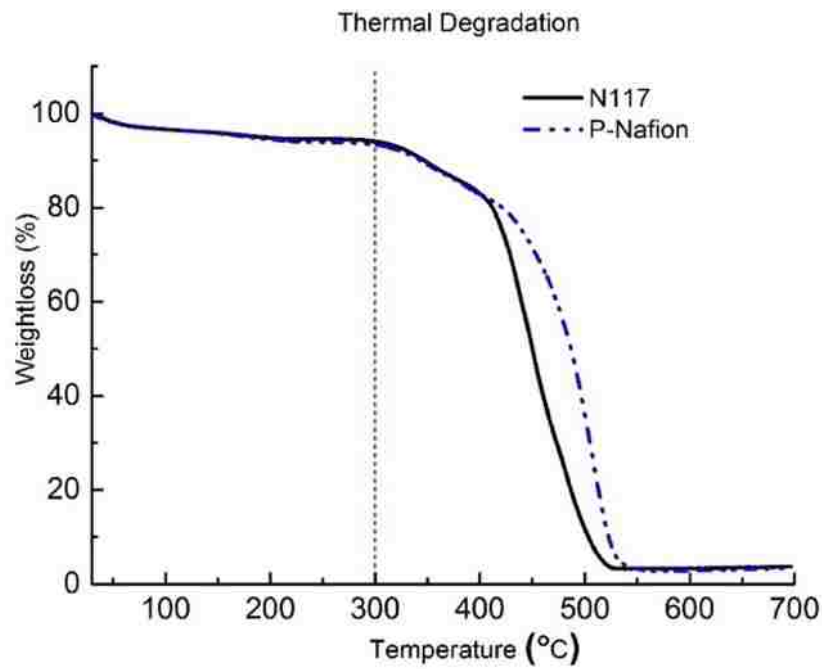


Figure 4.10. TGA results.



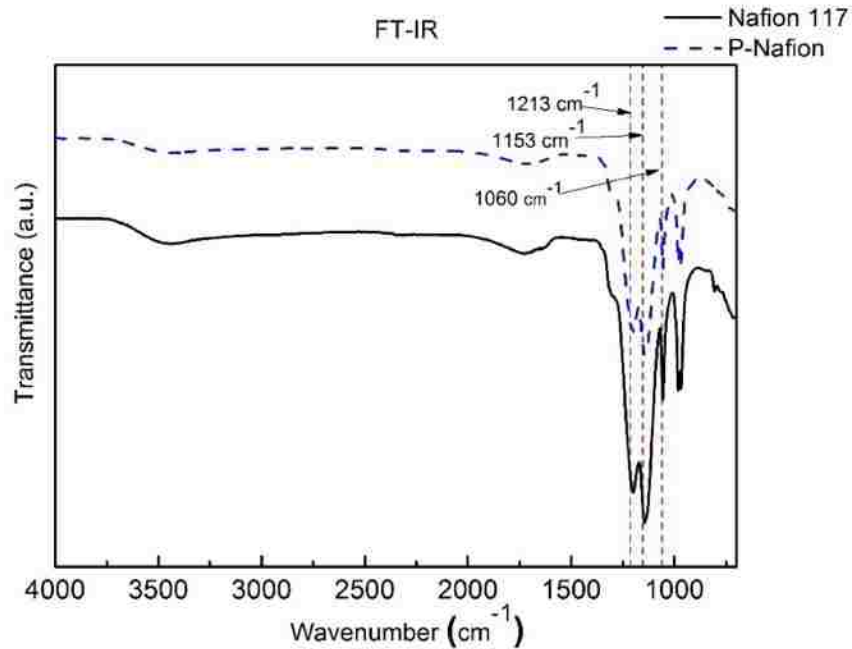


Figure 4.11. FT-IR results.

Dynamic Mechanical Analysis (DMA) tests the samples under dynamic loading under various frequencies. The two samples were tested three times in a row to ensure consistency of the results. The summary of these tests can be shown in Figure 4.12. The DMA gives the loss modulus ( $E''$ ) and storage modulus ( $E'$ ). Equation (4) is used to find the actual Young's Modulus. Interestingly, the results for damping coefficient are basically identical, however, there is a consistent shift between the results for Young's Modulus. This could be another indication that there are more crystalline structures in the P-Nafion® sample. It should be noted that the DMA tests were run in a non-controlled humidity environment and the relative humidity of the lab was recorded to be around 29%. The specifications from DuPont™ show that the modulus for N117 at 50% humidity are 249 MPa. The results seem reasonable for the recorded humidity of the day the experiments were conducted.

$$E = \sqrt{(E')^2 + (E'')^2} \quad (4)$$

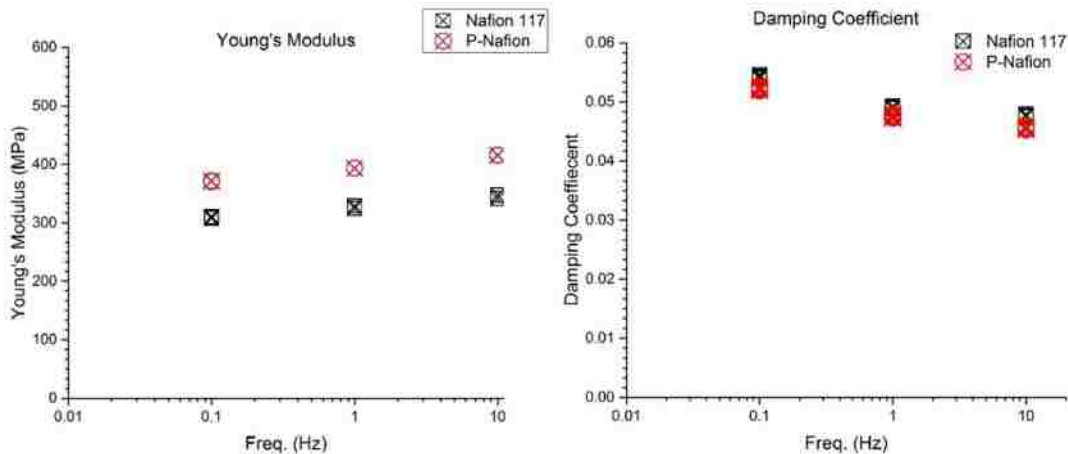


Figure 4.12. DMA results for Young's Modulus (left) and Damping Coefficient (right).

Another characteristic of interest is the water uptake of the membrane. The two samples used for the DMA testing were thoroughly dried and weighed. They were then placed in DI water for a few hours and weighed again. The results are shown in Table 4.2. P-Nafion® can absorb almost all of its weight while N117 absorbs about half of its weight. This could be because of the fabrication process of painting the Nafion® and allowing each layer to dry. It could be creating a more porous membrane with gaps from the evaporating gases. This becomes an issue that arises during the plating process and will be discussed later on.

Table 4.2. Water uptake comparison of P-Nafion® and N117.

	<b>P-Nafion® (mg)</b>	<b>N117 (mg)</b>
<b>Dry weight</b>	71.6	45.0
<b>Wet weight</b>	124.7	66.7
<b>Water uptake</b>	53.1	21.7
<b>Water uptake (%)</b>	74%	48%

#### 4.3.2. Comparison of Paintable-IPMC and Traditional IPMC

A sample of P-Nafion® was plated with platinum using the following process. First, the membrane was roughened using various grits of sandpaper to ensure it is even thickness throughout and to

facilitate of impregnation of the platinum. Then, the membrane was cleaned with 3% hydrogen peroxide ( $\text{H}_2\text{O}_2$ ), which eliminates organic impurities, and 1 M of sulfuric acid ( $\text{H}_2\text{SO}_4$ ), which eliminates metallic impurities. Both are heated to  $65^\circ\text{C}$  for 45 minutes. This is followed by two 45-minute De-Ionized water (DI water) baths heated at  $65^\circ\text{C}$ . Then, the P-Nafion<sup>®</sup> is immersed in a platinum salt solution ( $\text{Pt}(\text{NH}_3)_4\text{Cl}_2 \cdot \text{H}_2\text{O}$ ) for 3.5 hours, where it is flipped every half hour, to impregnate the membrane with the platinum. Once this was completed, the membrane was held in a sodium borohydride solution, causing the platinum to plate onto the membrane. The platinum impregnation and sodium borohydride bath process is repeated three times, with cleaning process completed after each sodium borohydride bath. The final bath is a platinum solution and hydroxylamine hydrochloride ( $\text{H}_2\text{NOH} \cdot \text{HCl}$ ) and hydrazine ( $\text{NH}_2\text{NH}_2 \cdot \text{H}_2\text{O}$ ) are added every half hour. This last step helps to reduce the surface resistance of the IPMC. A full and comprehensive procedure is presented by Kim et al. [12].

The Painted IPMC (P-IPMC) had an overall thickness of about 560 microns while the P-Nafion<sup>®</sup> sample was about 360 microns initially (Figure 4.13). This arises from the water uptake of the P-Nafion<sup>®</sup>. It seems to swell much more than N117. The dimensions and the resistances of P-IPMC and a traditional IPMC are shown in Table 4.3. It should be noted that the IPMC chosen for the experiments was chosen based on thickness and is not N117 based. The thickness of the IPMC affects how much it can displace and the blocking force it can induce. The resistance of the IPMCs were measured using a conventional, handheld multimeter with two point probes. The IPMCs were fully hydrated when the resistance was measured. The surface resistance of the IPMCs were measured by using each probe to contact each end of the IPMC (Figure 4.14 left). The resistance through the IPMC is measured using a two-point contact multimeter by contacting the IPMC where

it would be clamped for actuation tests (Figure 4.14 right). A more accurate reading could be obtained with a 4 point probe, but one was not available at the time. The resistances of the P-IPMC are significantly higher than traditional IPMCs. This can be an indication that the platinum has not penetrated far enough into the P-Nafion® membrane [1], [12]. Both samples were dehydrated in room temperature then viewed using an optical microscope. From the images in Figure 4.15, it can be seen that the P-IPMC's surface is rougher and cracked compared to the IPMC. This may also be an indication that the platinum did not penetrate fully into the P-Nafion® during the plating process.



Figure 4.13. P-IPMC (left) and traditional IPMC (right).

Table 4.3. Dimensions and resistances of P-IPMCs and IPMC tested. It should be noted that the resistances was measured using a 2-point probe multimeter.

	<b>Length (mm)</b>	<b>Width (mm)</b>	<b>Thickness (microns)</b>	<b>Surface Resistance (Ohms)</b>	<b>Resistance through IPMC (Ohms)</b>
<b>P-IPMC</b>	40	11	560	~150, ~25	~500
<b>IPMC</b>	42	9.9	500	~2 (both sides)	~200



Figure 4.14. Probe placement for measuring the surface resistance (left) and resistance through the IPMC (right).

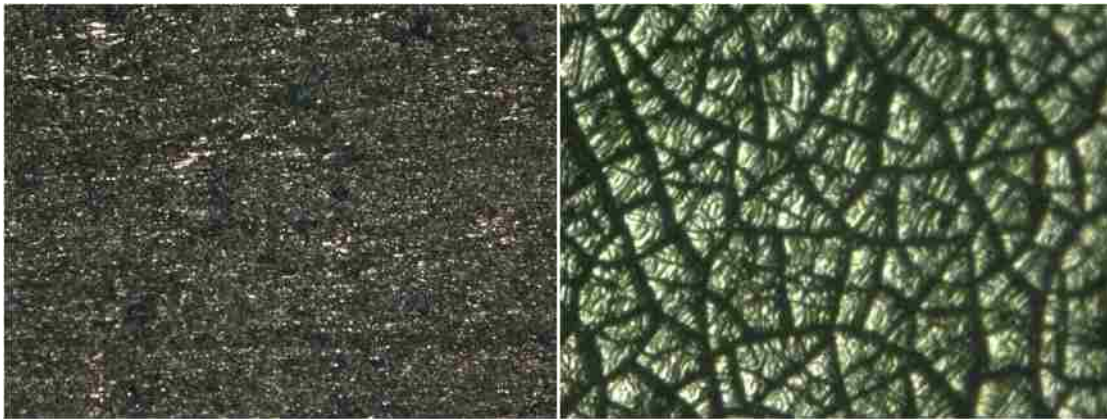


Figure 4.15. IPMC surface (left) and P-IPMC surface (right) viewed using an optical microscope at 500 times magnification. The surface of the IPMC (left) is much smoother and shows minimal cracking. The P-IPMC (right) shows a lot of cracking on the surface.

The P-IPMC sample and an IPMC were cut into similar dimensions and tested for displacement and blocking force, as well as sensing (Figure 4.16). A laser sensor was used to measure displacement and a load cell for blocking force, both at the tip of the IPMC. This ensures that the maximum displacement and blocking force are recorded. The contact length of the clamp used is 8 mm and it applies about 337 MPa of pressure, securely holding the IPMC. The DAQ systems used were from NI Instruments and the data was processed and saved through LabVIEW. For the

displacement tests, the IPMCs were in room temperature DI water and for the blocking force tests, the IPMCs were in air.

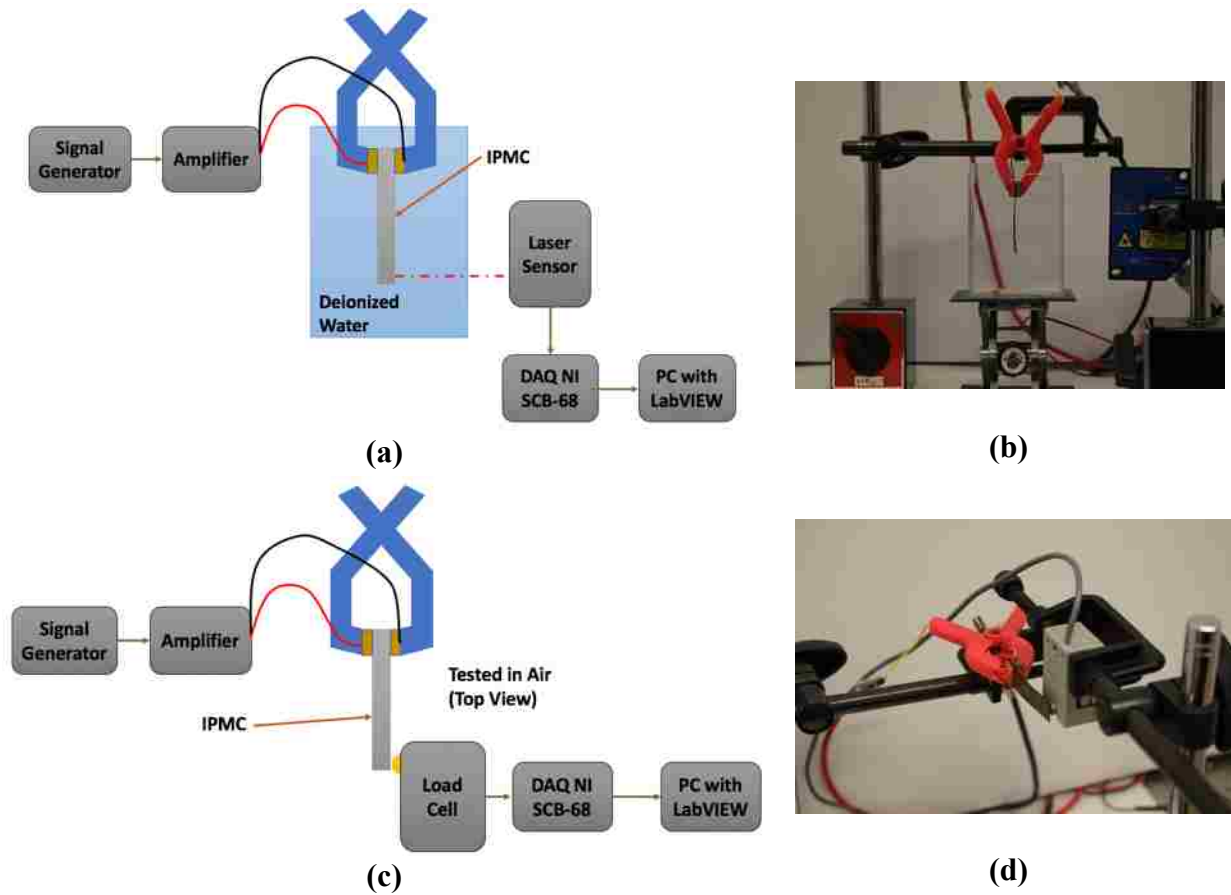


Figure 4.16. Experimental setups for IPMC being tested for displacement (a and b) and blocking force (c and d).

The results from the experiments were collected and plotted for comparison. 4 Volts AC were applied to both samples for the displacement tests. The results are shown in Figure 4.17. Both actuators move smoothly and consistently. The IPMC has a 6 mm peak-to-peak displacement, while the P-IPMC has a 2 mm peak-to-peak displacement. This is most likely due to the P-IPMC's higher Young's Modulus. IPMCs move similarly to a cantilever beam under a distributed load and the maximum displacement can be represented by Equation (5) where  $q$  is the distributed load,  $l$  is

the length of the IPMC,  $E$  is the Young's Modulus, and  $I$  is the area moment of inertia. Based on the equation, if  $q$  is constant (same applied voltage) and the length and area moment of inertia is known for both IPMCs and similar, then the driving factor of the maximum displacement is the Young's Modulus ( $E$ ). A larger modulus will cause a smaller displacement. Another point to note is that the voltage across the P-IPMC is higher than that of the IPMC. The voltage presented in these plots is the voltage drop after the sample. Since the P-IPMC has a much higher resistance through the membrane than that of the IPMC (~500 Ohms versus 200 Ohms), it has a larger impedance. This is further verified in Figure 4.18. A comparison of the two displacements is shown in Figure 4.19.

$$\delta_{max} = \frac{ql^4}{8EI} \quad (5)$$

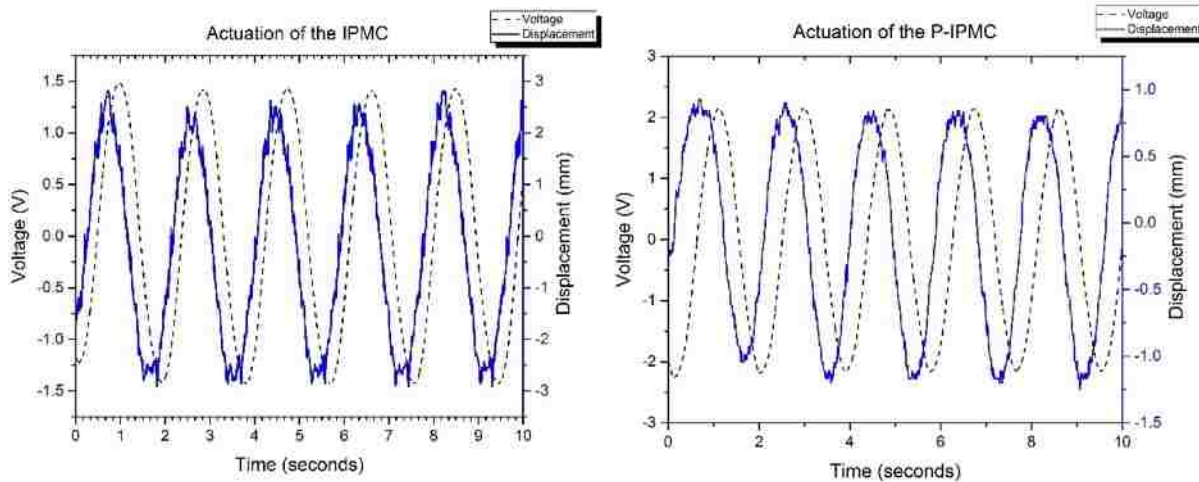


Figure 4.17. Voltage and displacement measurements from actuation experiments.

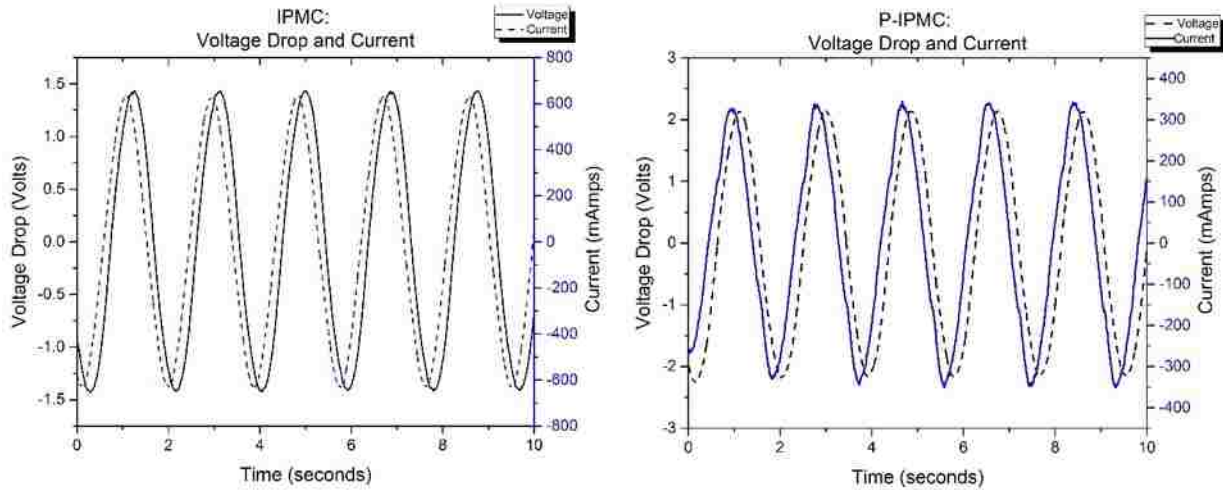


Figure 4.18. Voltage drop across sample and current for IPMC and P-IPMC.

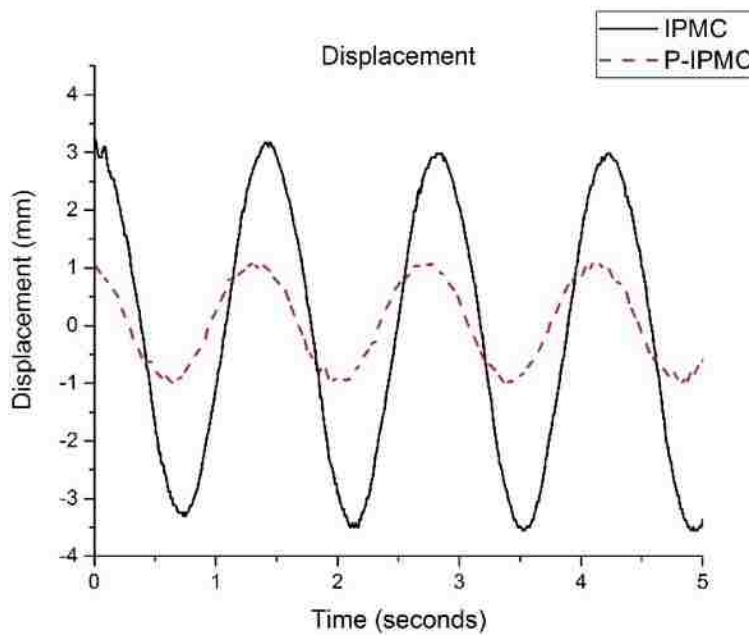


Figure 4.19. Comparison of the displacement for IPMC and P-IPMC measurements from actuation experiments.

The results from the blocking force experiments give more insight in the differences between the IPMC and P-IPMC. A low frequency voltage sine wave is applied to the samples to perform a pseudo-DC input. Figure 4.20 shows the voltage across the samples and the recorded blocking



force. The IPMC has a low surface resistance (2 Ohms) and a lower resistance through it (~200 Ohms) the P-IPMC. It acts more as a capacitor, while the P-IPMC acts more as a large resistor with its high surface resistance (150 and 25 Ohms) and high resistance through it (500 Ohms). Comparing the two first peaks of the blocking force curves in Figure 4.21, the P-IPMC is not able to reach as large of a force as that of the IPMC, probably because of its stiffness. However, it is able to hold a consistent load for longer than that of the IPMC. This could be useful in an application where this is needed, such as a soft robotic animal's actuator pushing itself forward.

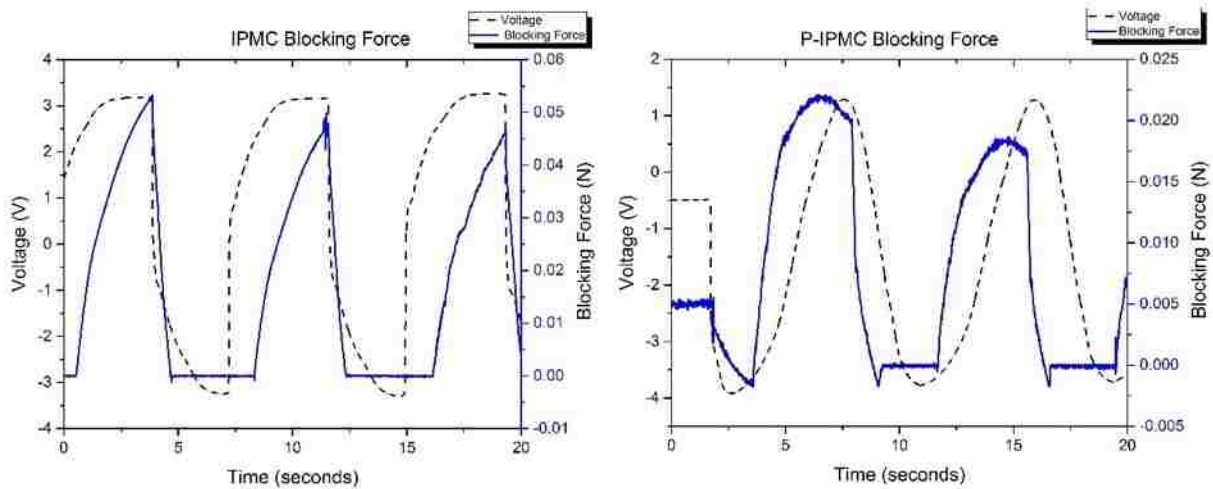


Figure 4.20. Voltage and blocking force measurements from blocking force experiments.

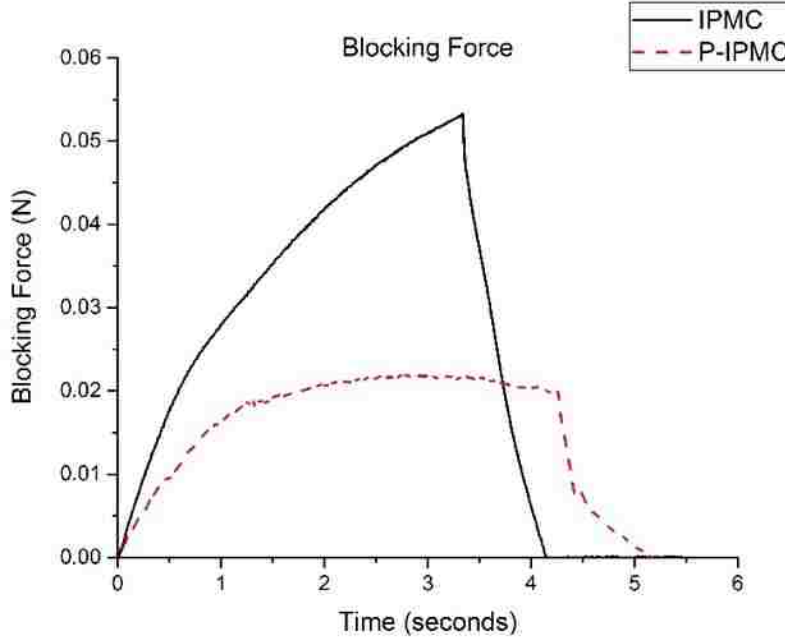


Figure 4.21. Comparison of the blocking force for IPMC and P-IPMC measurements.

The strain of the two samples was found by using the recorded displacement. First, the radius of curvature ( $\rho_r$ ) is calculated using Equation (6), where  $L$  is the length and  $\delta$  is the displacement recorded by the laser displacement sensor. Once that is calculated, it is used to find the strain ( $\varepsilon$ ) using Equation (7), where  $h$  is the thickness. The strain is plotted in Figure 4.22, while the strain rate, the differentiation of the strain plot, is shown in Figure 4.23. The strain for the IPMC is larger than that of the P-IPMC, another signifier that the P-IPMC is stiffer. The strain rate is similar for both samples.

$$\rho_r \cong \frac{L^2 + \delta^2}{2\delta} \quad (6)$$

$$\varepsilon \cong \frac{h}{2\rho_r} \quad (7)$$

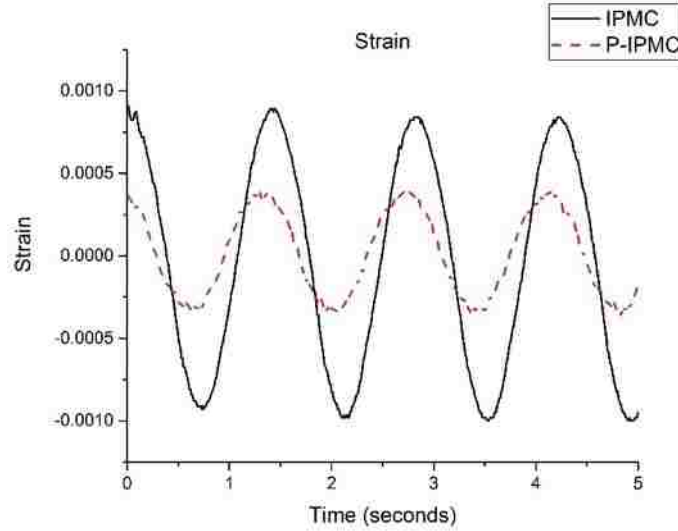


Figure 4.22. Calculated strain from displacement measurements for IPMC and P-IPMC.

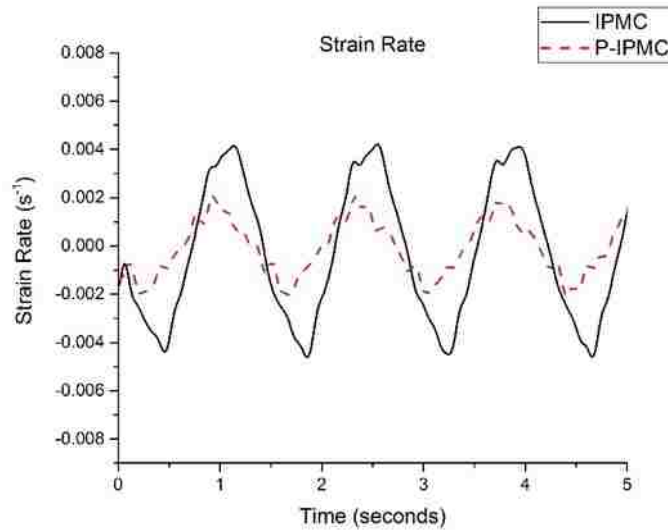


Figure 4.23. Strain rate from differentiating the strain curves for IPMC and P-IPMC.

The displacement versus voltage is plotted in Figure 4.24 to understand the hysteresis effects of the samples. Both the samples are consistent in its motion. There is some hysteresis for either sample as expected. This plot shows the difference in displacement and the amount of voltage across the samples. P-IPMC requires more voltage to move the same amount as the IPMC. Again, this could be due to the large difference in surface resistance of the two samples.

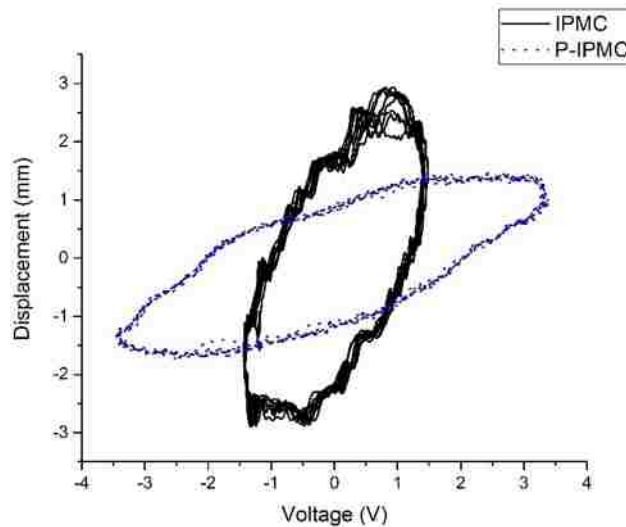


Figure 4.24. Displacement versus voltage for IPMC and P-IPMC to check for hysteresis effects.

#### 4.4. Discussion

The results P-Nafion® and P-IPMC vary only slightly from that of N117 and IPMC, respectively. These differences show up the most in porosity and Young's Modulus. The higher porosity helps the P-IPMC to actuate well, even though it's surface resistance is significantly higher than that of the IPMC. This does cause one hindrance in that the membrane swells to twice its size during the plating process. To reach the desired thickness, the P-Nafion® membrane should be at least half of what the actual thickness needed. This will allow for swelling during the plating process and the P-IPMC will be within a working range of thickness. The stiffness of the P-Nafion® is also due to the fabrication method. By spraying layer on top of layer, there could be some interfacial planes that is increasing the stiffness. To see if this is the case, crack fracture SEM imaging was conducted on a small sample of P-Nafion®. The sample was frozen in liquid nitrogen and broken in half, then lightly sputtered with gold (about 7 seconds). Figure 4.25 and Figure 4.26 show that the P-Nafion® membrane is fairly uniform. The top of the membrane is rougher probably because

of the fabrication method. The water and solvents evaporate from the surface causing it to be less uniform and bumpy compared to the bottom. The bottom of the membrane is much smoother with a few bumps. This could be from trapped air pockets or from the surface roughness of the ABS weighing dish that was used.

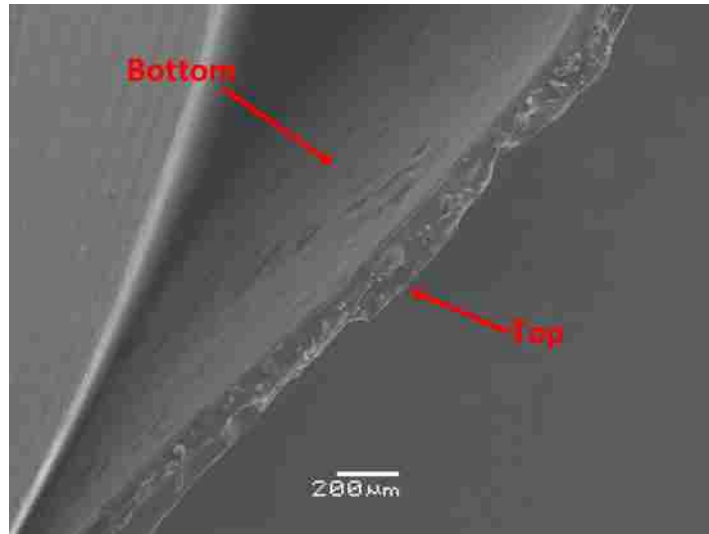


Figure 4.25. Crack fracture SEM imaging of P-Nafion®, 55x magnification.

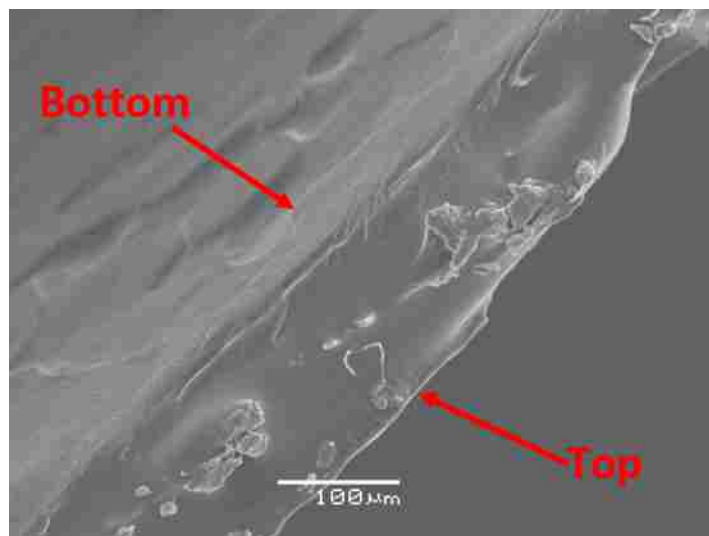


Figure 4.26. Crack fracture SEM imaging of P-Nafion®, 220x magnification.

#### 4.5. Conclusions and Future Work

The results from the P-Nafion® characterization show that the painting method can produce Nafion® that is almost identical to that of commercial options. The experiments for the P-IPMC demonstrate that it is a viable option for creating uniquely shaped actuators. With this new procedure, biomimicry can be expanded into reality by creating 3D P-Nafion® contours. For example, an airfoil P-Nafion with active skin texture could be created for an exploratory robot that can control its motion with P-IPMC fins while the skin texture can help control flow (Figure 4.27). The painting method may also be expanded to also painting the electrode onto the surface of the P-Nafion®, reducing the time needed to fabricate IPMCs.

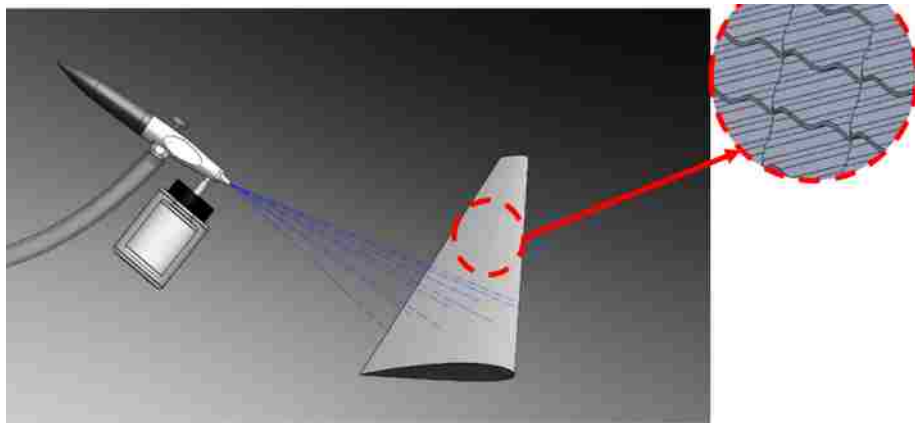


Figure 4.27. Conceptual illustration of painting an airfoil-shaped P-Nafion® with active-skin-like texture.

#### 4.6. Acknowledgements

This work was in part supported by National Aeronautics and Space Administration (NNX13AN15A) and Nevada NASA Space Grant Consortium. Also, K.J.K. thanks the partial financial support from the US National Science Foundation (#1545857) relating to robotic applications.

## **Chapter 5. Searching for A New Ionomer for 3D Printable Ionic Polymer-Metal**

### **Composites: Aquivion<sup>®</sup> As A Candidate**

This chapter is a paper that has been published in Smart Materials and Structures. The authors are Sarah Trabia, Zakai Olsen, and Kwang J. Kim. It first introduces Aquivion as an alternative base for IPMCs. Reprinted with permission: Trabia, S.; Olsen, Z.; Kim, K. J. Searching for a new ionomer for 3D printable ionic polymer–metal composites: Aquivion as a candidate. *Smart Mater. Struct.* **2017**, *26*, 115029, doi:10.1088/1361-665X/aa919f. The copyrights can be found in Appendix D.

The development of the process and production of samples was done by ST and ZO. The characterization of the samples was done by ST. Testing of the IPMCs and plotting the data was done by ST and ZO. All of the authors gave input and analyzed the data.

### **5.1. Introduction**

#### **5.1.1. Basics of IPMCs**

Ionic polymer-metal composites, IPMCs for short, are a class of electroactive polymers (EAPs) that have been studied for many years [2], [26]. IPMCs are ionomer-based, typically Nafion<sup>®</sup>, which is then plated with a noble metal. When an electric potential is applied to the surface, the negatively charged side attracts cations, causing it to swell. This swelling of one side forces a bending motion in the IPMC. This soft actuator is ideal for many applications because of its ability to work well in water and low voltage input to high deformation ratio [4], [5], [26].

### **5.1.2. Potential Applications of IPMCs**

#### **5.1.2.1. IPMCs as bio-medical, bio-mimetic, and robotic actuators.**

Extensive research has been made on the application of IPMC actuators in the bio-medical, bio-mimetics, and robotics fields. The IPMCs ability to be used as a mechanical gripper, utilizing 2, 4, or 8 IPMC actuators as tweezer and finger like manipulators was successfully demonstrated by Shahinpoor and Kim [5]. It was further demonstrated that rectangular IPMCs could be used as 3D manipulators, linear actuators, micro-catheter guidance tools [5]. Many researchers have developed IPMC based methods for locomotion, including underwater propulsion. Some designs utilize rectangular IPMC actuators as tail fins for swimming fish robots, underwater vehicles, and tadpole robots [5], [72], [73], [95]–[97], while sheet IPMC actuators have been cut to shape and embedded within a robotic manta ray fin [98]. Segmenting the electrodes of an IPMC has been shown to give more complex articulation in the tail fin actuators of these swimming bio-mimetic robots [99]. The use of both segmented IPMC electrodes and rectangular IPMCs as joint actuators have also been used to generate contractile and slithering type locomotion [5], [100]. Shahinpoor and Kim also demonstrated the ability to use IPMC actuators as diaphragm pumps and contractile heart compression assistive devices [5], [101].

#### **5.1.2.2. IPMCs as sensors.**

The use of IPMCs as sensors is a widely researched subject. A great deal of work can be found on the basic physics and fundamentals of the IPMCs sensing capabilities, electromechanical response, and use as mechano-electrical transducers can be found in [2], [4], [10], [11], [102]. Abdulsadda and Tan showed that an array of IPMC sensors could be utilized as an artificial lateral line, akin to what is found in many aquatic animals, to localize a dipole source [103]. Strazzeri *et al.*



demonstrated the use of an IPMC as a vibration sensor in a similar fashion to common mass-spring-damper sensor systems [104].

### **5.1.3. Traditional fabrication methods for the ionomer base**

The fabrication methods of IPMCs are continually advancing, but many of the traditional techniques are still used to construct these actuators and sensors. An overview of some traditional fabrication processes demonstrates the wide range of possible techniques for creating the ionomer membranes, all of which are applicable to IPMC manufacturing. Nafion<sup>®</sup> is typically available in sheet form from the manufacturer. This is useful cutting out generic shapes, such as rectangles. There are a variety of thicknesses (ranging from 25.4  $\mu\text{m}$  to 254  $\mu\text{m}$ ) available for purchase depending on what the user would like. This has been used a variety of ways, including cutting the sheets to mimic fins [105], [106]. Extrusion of ionomer materials has been shown to be a useful technique for IPMC fabrication [27], and the method has been used to fabricate Nafion<sup>®</sup> tube multi degree of freedom IPMC sensors [31]. The fabrication done by Palmre *et al.* with hot-pressing [107] and Stalbaum *et al.* with extrusion [31] further demonstrated the use of precursor pellets for thermal processing of the ionomer materials for IPMCs. Hot pressing may also be used to combining multiple membranes by compressing them together under high temperature to create a single, fused membrane. Injection molding is another thermal processing method shown to work with ionomer materials by Nelson [27]. Injection molding takes precursor pellets to mold a membrane of specified thickness and geometry. Dispersions of ionomer materials have been successfully used to manufacture IPMCs through film casting techniques. In this technique, a water dispersion of the ionomer material is cast as layers into a mold and dried or thermally cured [28]. This method can also be used to construct IPMCs by casting an ion conducting electrode solution, thus eliminating the need for the post processing of electrode coating [108].

#### 5.1.4. Advanced fabrication methods for the ionomer base

Though the traditional fabrication methods have been able to solve many problems, Nafion<sup>®</sup> is an expensive material and the current methods have limited the shapes that can be made. Researchers have been looking for solutions to find ways to reduce the amount of Nafion<sup>®</sup> used as well as creating new, intricate shapes to expand the actuation motions possible. Blending techniques have been presented that mix Nafion<sup>®</sup> with a cheaper polymer to create the base for IPMCs. Hwang *et al.* has blended Nafion<sup>®</sup> water dispersion with poly(vinyl alcohol-*co*-ethylene) (PVA-*co*-E) to produce membranes that were produced using a casting method [82]. They found a ratio between the two polymers (30:70, PVA-*co*-E:Nafion) that still had the advantageous characteristics of Nafion<sup>®</sup> and was able to produce IPMCs that were able to perform just as well as full Nafion<sup>®</sup> IPMCs, while reducing the amount of Nafion<sup>®</sup> being used. Nam *et al.* blended Nafion<sup>®</sup> water dispersion with polyamic acid (PAA), which is a precursor for polyimide (PI) [109]. These blends were also cast to produce the membranes. They showed that a ratio of 18:82 (PI:Nafion<sup>®</sup>) was ideal, producing IPMCs that were comparable to that of full Nafion<sup>®</sup> membranes. These two studies have shown the potential to reduce the amount of Nafion<sup>®</sup> used in IPMCs without losing the desired characteristics and abilities of Nafion<sup>®</sup> and IPMCs. The ability to produce different shapes has been recently explored. Since creating intricately shaped membranes is difficult with the current fabrication methods, spray-painting Nafion<sup>®</sup> water dispersion has been introduced to solve this. Trabia *et al.* were able to produce Nafion<sup>®</sup> membranes using vinyl stencils and an airbrush [110]. The produced shapes retained the detailed outlines of the stencils, as well as voids within the membrane if desired. The freedom of producing stencils allows the user to be able to produce any shape at a needed thickness using this method. The IPMCs produced with these membranes have been shown to actuate comparable to that of traditionally made IPMCs.

Additive manufacturing (3D printing) has been on the forefront of many research areas today. Carrico *et al.* have shown that this method of manufacturing is possible with Nafion<sup>®</sup> [65], [111]. They designed a 3D printer to work with filament that they have produced in-house. The shapes printed with their system are not possible, or could be very difficult to produce, using traditional methods. They were able to print parts for a soft robot that can crawl along a tube and a torsional actuator that can twist [111]. Their system has allowed researchers to potentially create complete robots by simply drawing their design in a Computer-Aided Design (CAD) program and a 3D printer.

## 5.2. Objectives

As previously discussed, Nafion<sup>®</sup> is usually the ionomer used for IPMCs. As mentioned, Nafion<sup>®</sup> is a good option for IPMCs, but the material has some issues in heat processing techniques. This study proposes to introduce another option for additive manufacturing of ionomers: Aquivion<sup>®</sup>. This ionomer has a shorter side chain, similar material properties, and nearly double the ionic conductivity of Nafion<sup>®</sup>. To show that Aquivion<sup>®</sup> is a viable option, the objectives of this research is to fully analyze and compare off-the-shelf Nafion<sup>®</sup> and Aquivion<sup>®</sup> membranes, then produce printed Aquivion<sup>®</sup> shapes.

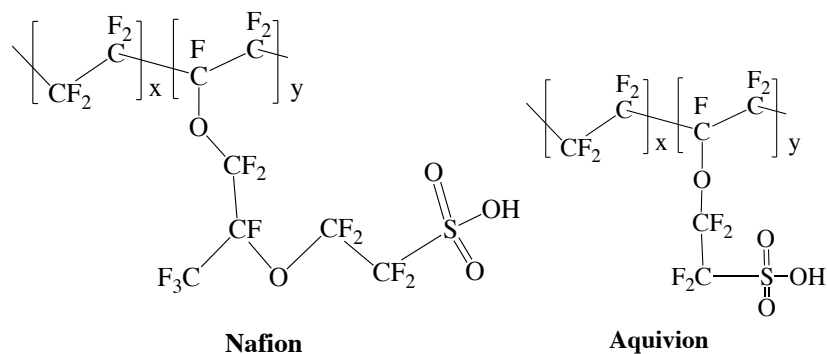


Figure 5.1. Polymer structure for Nafion® (left) and Aquivion® (right) membranes comparing the side chain lengths.

### 5.3. Approaches

To complete the objectives for this research, the following approaches are presented. A complete material characterization of Nafion® and Aquivion® membranes was conducted to show that the two are comparable. IPMCs were produced using the commercially membranes and performance testing will be conducted. For 3D printing Aquivion® ionomers, the physics of additive manufacturing and 3D printer design is discussed. The procedure for filament production and 3D printing is presented. Material characterization of the printed samples is conducted to show that the samples are similar to off-the-shelf membranes and are not contaminated or affected by the process. The printed samples are activated and plated with platinum. Printed Aquivion® IPMCs produced undergoes performance testing and a comparison to Nafion® based IPMCs.

### 5.4. Methods

#### 5.4.1. Comparing Nafion® and Aquivion®

An IRTracer-100 (Shimadzu) was used to compare chemical structure for Fourier Transform-Infrared Spectroscopy (FT-IR). To identify the thermal degradation temperature, a Thermogravimetric Analyzer (TGA), specifically the Q500 (TA Instruments). The thermal

conductivities of the two polymers were measured using a TCi Thermal Conductivity Meter (C-Therm).

First, the ion exchange capability of the ionomers is verified by an Ion Exchange Capacity (IEC) test. The membrane samples (2 cm x 2 cm) were dried in the oven at 80°C overnight. The samples were then weighed and the dry mass was recorded. The dried membranes are soaked in 50 mL of 1 M of sodium chloride (NaCl, Sigma-Aldrich) overnight. A drop of phenolphthalein (Sigma-Aldrich) is added to the solution and then it is titrated with 0.01 M of sodium hydroxide (NaOH, Sigma-Aldrich) until the solution is light pink. The volume of NaOH used is recorded for each sample. To find the IEC for each, the following equation is used:

$$IEC = \frac{VC}{M_{dry}} \quad (8)$$

where V is the volume of NaOH used in mL, C is the concentration of the titrant (0.01 M) and  $M_{dry}$  is the dry mass of the membranes in grams. Three samples of each membranes were tested. To view the samples fabricated, a Scanning Electron Microscope (SEM, TM3030 Hitachi) at 15 kV was used. For the samples viewed in the SEM, they were set in resin and the surface was polished. The surface was then sputtered with platinum for about 10 seconds.

#### **5.4.2. Filament production and 3D Printing of Aquivion®**

As discussed by Carrico *et al.*, fused filament fabrication, a type of additive manufacturing, requires polymer filament that can be extruded during the manufacturing process [65]. This filament is produced by melt processing a pelletized form of the polymer through the same method as seen in commercial filament production. The pelletized polymer is fed through a channel by a

feed auger. At the far end of the channel, a high temperature zone is created which melts the polymer and allows for extrusion through a die of specified diameter. Here, a small-scale filament production unit, the Noztek Pro, was used to process Aquivion<sup>®</sup> precursor pellets into filaments of 2 mm and 3 mm diameter. Once manufactured, the Aquivion<sup>®</sup> filament was used in appropriately modified 3D printers. Carrico *et al.* thoroughly discussed the challenges of printing of ionomer materials, specifically Nafion<sup>®</sup>, and how they were able to overcome the various issues in the manufacturing process [65]. Two 3D printing platforms, the Raised 3D N2 Plus and Lulzbot Mini, have been adapted to address the added complications and work with ionomer materials, such as Aquivion<sup>®</sup>. The Raised 3D N2 Plus is a medium format 3D printing system with a 12 x 12 x 24 in. build volume, whereas the Lulzbot Mini is small format platform with a 6 x 6 x 6 in. build volume. Each of these printers had to undergo different modifications in order to print Aquivion<sup>®</sup>. The Raised N2 Plus features a fully constrained 1.75 mm diameter filament path, which is known to play an important role in the printing of ionomer materials [111] and will be discussed further in a later part of this paper. Additionally, this system has a hot end that is capable of reaching 280°C, another key component to ionomer printing. To modify this printer to use Aquivion<sup>®</sup> a high temperature build platform was installed. This new heated build platform consisted of a 10 x 10 in flexible silicone heating pad (McMaster-Carr) with a 10 W/in<sup>2</sup> power output density which is insulated on its lower surface with a borosilicate glass plate (McMaster-Carr) placed on its upper surface. The constrained filament path of this printer is not exactly 1.75 mm but is in fact closer to 2 mm. This diameter should be matched as closely as possible to reduce the possibility of filament buckling.

The Lulzbot Mini is a smaller 3D printing system that has the ability to be upgraded to a different filament extruder. To address the issues of hot end temperatures and the constrained filament path, a Lulzbot Flexystruder mini was installed onto the Lulzbot Mini. The Flexystruder utilized a fully constrained 3 mm filament path and allows for maximum hot end temperatures of 280°C. This extruder is also specifically designed work with flexible materials, being fitted with deeper grooves in the pinch roller feed mechanism. The deep grooves reduce the possibility of filament slipping, which plays an important role in additive manufacturing physics. Similarly to the Raised N2 Plus, a 6 x 6 in flexible silicone heating pad (McMaster-Carr) with 10 W/in<sup>2</sup> power density and a borosilicate glass plate (McMaster-Carr) was installed. In both systems, the glass plate was coated with double sided Kapton tape to further promote bed adhesion, which is important to achieving high quality prints, as discussed by Turner *et al.* [112].

#### **5.4.3. Activation and platinum plating**

The Aquivion® precursor pellets are put through a hydrolysis process, to “activate” the membranes. This process exchanges the current end group (sulfonyl fluoride group) to a sulfonate end group, allowing the Aquivion to be able to carry water molecules. To do this, the membranes are suspended in an aqueous solution of 15% of potassium hydroxide (KOH, Sigma-Aldrich), 35% of dimethyl sulfoxide (DMSO, Sigma-Aldrich), and 50% deionized water (DI water, Millipore) at 75°C with proper stirring, until the samples have been activated fully. This process depends on the thickness of the membrane as Elliot *et al.* have mentioned in their studies [58]. After the activation process, the membranes are ready to be platinum plated by using the procedure detailed by Kim and Shahinpoor [12]. An electroless plating process is used for the samples fabricated. The

cleaning process is summarized in Table 5.1. Hydrogen peroxide removes the organic impurities, while the sulfuric acid removes the metallic impurities.

Table 5.1. Cleaning process procedure for various points in the plating process.

<b>Bath</b>	<b>Supplier</b>	<b>Temperature and Time</b>
3 wt. % Hydrogen peroxide (H <sub>2</sub> O <sub>2</sub> )	Sigma-Aldrich	65°C, 45 minutes
1 M of Sulfuric acid (H <sub>2</sub> SO <sub>4</sub> )	Sigma-Aldrich	65°C, 45 minutes
DI water	Filtered in lab (Millipore)	65°C, 45 minutes
DI water	Filtered in lab (Millipore)	65°C, 45 minutes

The primary plating process begins with the samples sitting in a platinum salt bath (Pt(NH<sub>3</sub>)<sub>4</sub>Cl<sub>2</sub>·H<sub>2</sub>O, tetraammineplatinum(II) chloride hydrate, Sigma-Aldrich) for 3.5 hours, where they are flipped every half hour. The primary plating process follows where the samples are suspended in 350 mL of DI water bath and 0.3 mL of ammonia (Sigma-Aldrich) with 0.2 grams of sodium borohydride (NaBH<sub>4</sub>, Sigma-Aldrich) added every half hour for a total of two hours. The solution is mixed at 130 rpm and it begins at 50°C with the temperature is increased by 2°C every half hour. After, the membranes are cleaned by a similar process to that in table 5.1, excluding the hydrogen peroxide bath. This whole process is repeated two more times. The secondary plating process uses a bath with 0.25 grams of the platinum salt and 0.3 mL ammonia in 350 mL of DI water, stirred at 90 rpm and heated to 50°C. The samples are suspended in this solution and two solutions are added every half hour for a total of four hours: 2 mL of hydroxylamine hydrochloride (H<sub>2</sub>NOH·HCl, Sigma-Aldrich) and 1 mL of hydrazine (NH<sub>2</sub>NH<sub>2</sub>·H<sub>2</sub>O, Sigma-Aldrich). The temperature is increased by 2°C every half hour as well. The membranes are rinsed off by DI water and the surface resistance is measured to ensure that both sides are between 1-3 Ω. If it is higher than this range, the secondary plating process is repeated and the surface resistance is measure again. Once this is between the designated range, the



membranes are cleaned using the process shown in Table 5.1, excluding the hydrogen peroxide. Finally, the samples are placed in a 1 M of LiCl bath for the ion exchange process for 24 hours.

#### **5.4.4. IPMC performance testing**

For the IPMC performance characterization tests, three tests were conducted: back relaxation, actuation, and blocking force. The signal for all three was generated with a signal generator (SDG1025, Siglent) and a power amplifier was also used (LVC-608, AE Techtron). For back relaxation and actuation tests, the displacement was measured using a laser displacement sensor (optoNCDT-1401, Micro-Epsilon), shown in Figure 5.2. For the blocking force tests (Figure 5.3), the force generated by the IPMC was measured using a load cell (GSO-30, Transducer Techniques). The data was collected with a Data Acquisition system (SCB-68, National Instruments) and LabVIEW was used to plot the data of the different values being collected as the test was being conducted and save the data at the end of a test. For the sensing experiments, an electrodynamic shaker (VR-5200, Vibration Research Corporation) moves an IPMC that is clamped at one end (Figure 5.4). The data is sent through a custom amplification circuit, then collected using a Data Acquisition system (USB-6008, National Instruments) and LabVIEW.

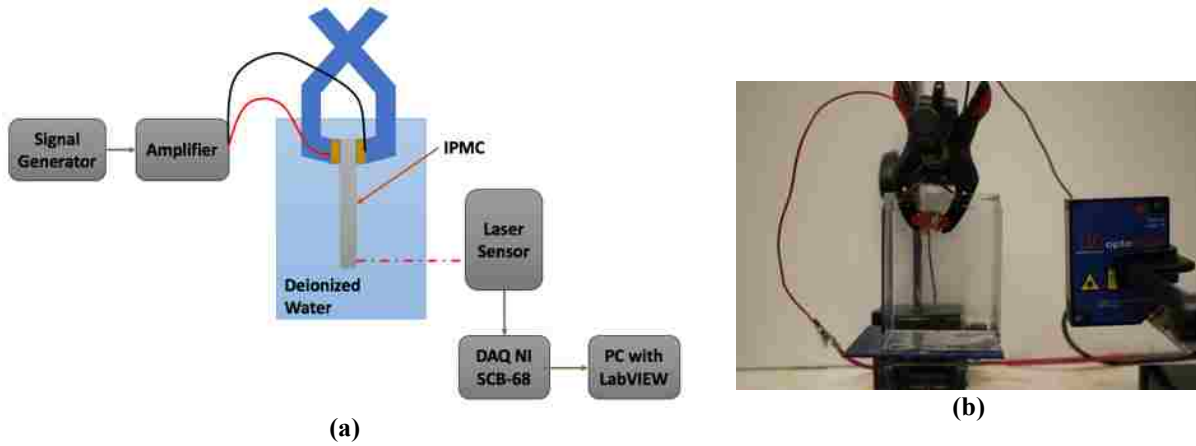


Figure 5.2. IPMC actuation test setup (for both back relaxation and frequency-based displacement) with a laser sensor performed in DI water.

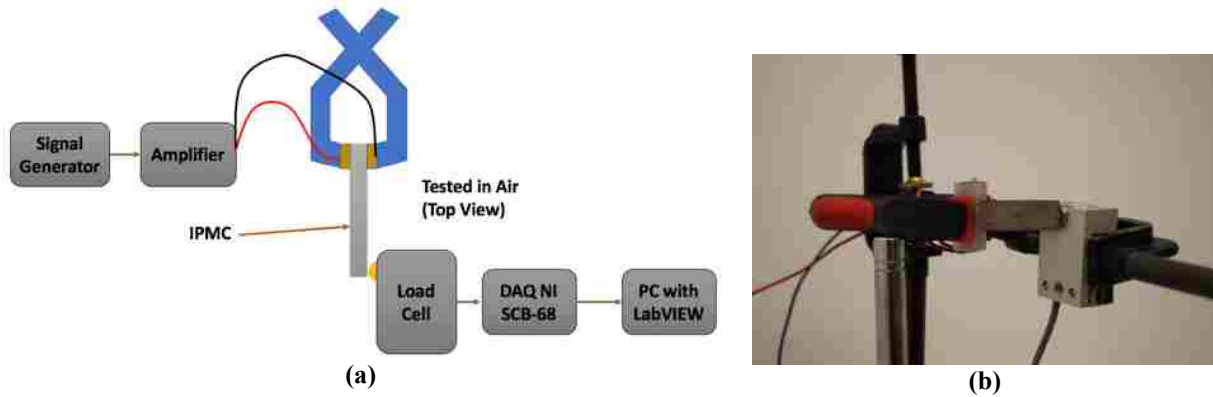


Figure 5.3. IPMC performance testing for blocking force capabilities in air.

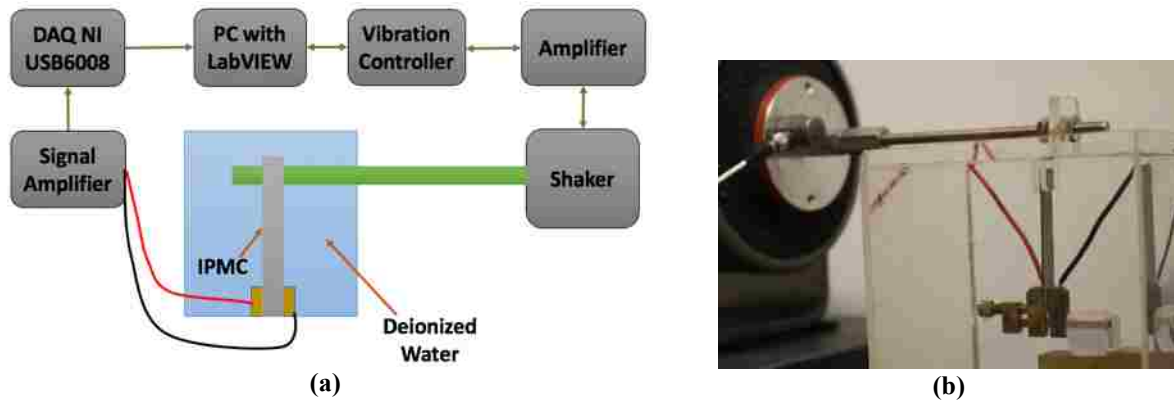


Figure 5.4. IPMC performance sensing test conducted in DI Water.

## 5.5. Results and Discussion

### 5.5.1. Comparing Nafion<sup>®</sup> and Aquivion<sup>®</sup>

Nafion<sup>®</sup> and Aquivion<sup>®</sup> are both perfluorosulfonic acids (PFSAs), with a Teflon-like backbone. Nafion<sup>®</sup> has a perfluorovinyl ether side group and a sulfonate end group. Aquivion<sup>®</sup> has a shorter side group: sulfonyl fluoride vinyl ether. This short side chain gives the polymer a lower equivalent weight, potentially creating a higher ionic conductivity than Nafion<sup>®</sup>. They have comparable Young's Moduli and water uptake. For the precursor pellets, the melting temperature of Aquivion<sup>®</sup> is lower than that of Nafion<sup>®</sup> pellets. The key points to take away from these comparisons is that Aquivion<sup>®</sup> has approximately double the ionic conductivity. Before IPMCs were made using the purchased membranes, the two polymers were characterized in-house. The two membranes are compared with an FT-IR to verify their chemical structure. They both have the same peaks at 1213  $\text{cm}^{-1}$ , 1153  $\text{cm}^{-1}$ , and 1060  $\text{cm}^{-1}$ , which correlates to the symmetric  $\text{CF}_2$ , asymmetric  $\text{CF}_2$ , and  $\text{SO}_3$  (Figure 5.5). These peaks have been confirmed by various researchers [88], [90], [93], [94]. The thermal degradation temperature was found to be the same for both ionomers with a TGA (Figure 5.6) and matches what has been noted by other researchers [87]–[93]. To understand the capability of each membrane to hold ions, Ion Exchange Capacity (IEC) tests were conducted. The samples tested showed Nafion to be as expected (0.98 meq/g), while Aquivion had a higher IEC value (1.25 meq/g) (Table 5.3). This value gives some insight to Aquivion's potential ability to perform better than Nafion. The thermal properties of the two polymers are important to understand because of the 3D printing process. Understanding how the pellets are affected by heat can help optimize the print settings, including the nozzle temperature, feed rate into the melt zone, and printer speeds. Samples of Nafion<sup>®</sup> and Aquivion<sup>®</sup> precursor pellets were tested for their thermal conductivities. Samples were made by hot pressing 3 grams of pellets to about 0.35 mm thick sheets. The samples

were tested with DI Water as the contact agent and a 500 gram weight on top to ensure there is complete contact with the sensor. Table 5.4 shows the results from the tests. The value for Nafion<sup>®</sup> matches what was recorded by Khandelwal and Mench [113]. The Aquivion<sup>®</sup> samples had a higher thermal conductivity than Nafion<sup>®</sup>, showing that it is able to conduct heat better than Nafion<sup>®</sup>. This helps during both the filament extrusion and 3D printing processes.

Table 5.2. Characteristics of Nafion<sup>®</sup> [114] and Aquivion<sup>®</sup> [115], [42].

	<b>Molecular Weight of Side Chain (g/mol)</b>	<b>Equivalent Weight (EW, g/eq)</b>	<b>Ionic Conductivity (mS/cm)</b>	<b>Young's Modulus, 50% RH, 23°C (MPa)</b>	<b>Water Uptake</b>	<b>Melting Temp. (Pellets) (°C)</b>
<b>Nafion</b>	330.10	1100	100	249	38 wt. %	~290
<b>Aquivion</b>	199.08	840	>228	250	30 wt. %	230-260

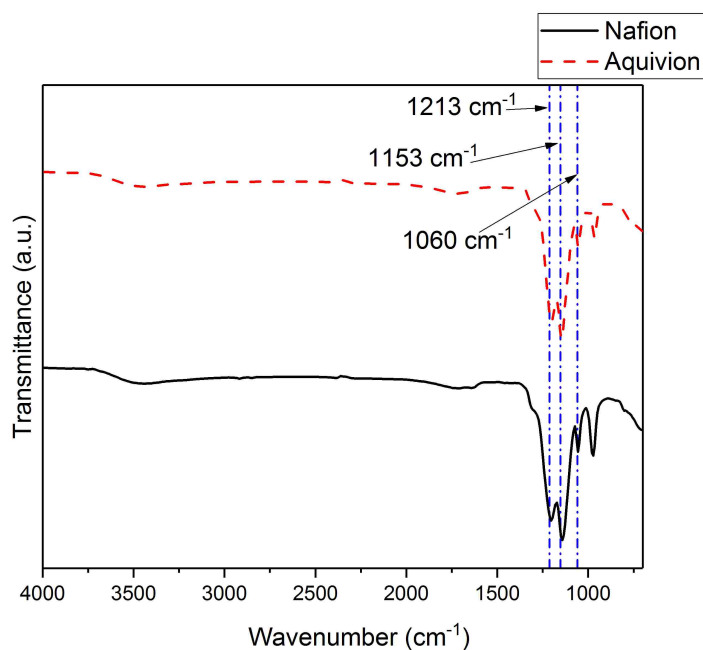


Figure 5.5. FT-IR comparison of Nafion<sup>®</sup> 115 and Aquivion<sup>®</sup> P87S membranes.

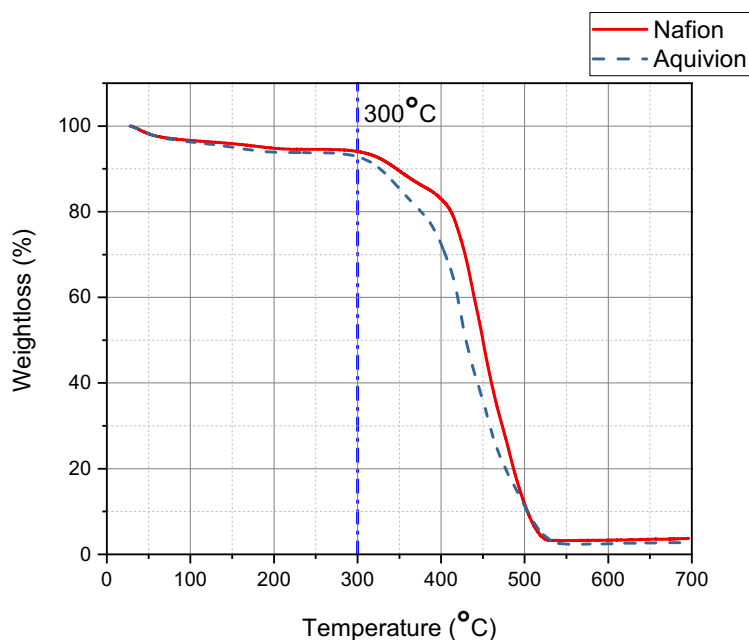


Figure 5.6. TGA results of Nafion<sup>®</sup> 115 and Aquivion<sup>®</sup> P87S membranes for the thermal degradation temperature.

Table 5.3. Measured Ion Exchange Capacity results for Nafion<sup>®</sup> 115 and Aquivion<sup>®</sup> E87.

	<b>Ion Exchange Capacity (meq/g)</b>
<b>Nafion 117</b>	0.98±0.08
<b>Aquivion E87</b>	1.25±0.01

Table 5.4. Thermal conductivities for Nafion<sup>®</sup> 1100 and Aquivion<sup>®</sup> P87S.

	<b>Thermal Conductivity (W/mK)</b>
<b>Nafion<sup>®</sup> 1100</b>	0.289±0.001
<b>Aquivion<sup>®</sup> P87S</b>	0.308±0.002

For IPMC fabrication, Nafion<sup>®</sup> 115 and Aquivion<sup>®</sup> E87 were used because they have comparable thicknesses (0.127 mm and 0.120 mm, respectively). The two ionomers were produced into IPMCs using the same electroless plating procedure and the samples were viewed in the SEM. The two

are indistinguishable in the SEM images shown in Figure 5.7. Comparing the electrodes, both of the samples show a roughened surface, as well as good contact with the Platinum (Figure 5.8). However, it is important to note that for these samples, N-IPMC has a thicker electrode than A-IPMC ( $\sim 10\ \mu\text{m}$  versus  $\sim 5\ \mu\text{m}$ ).

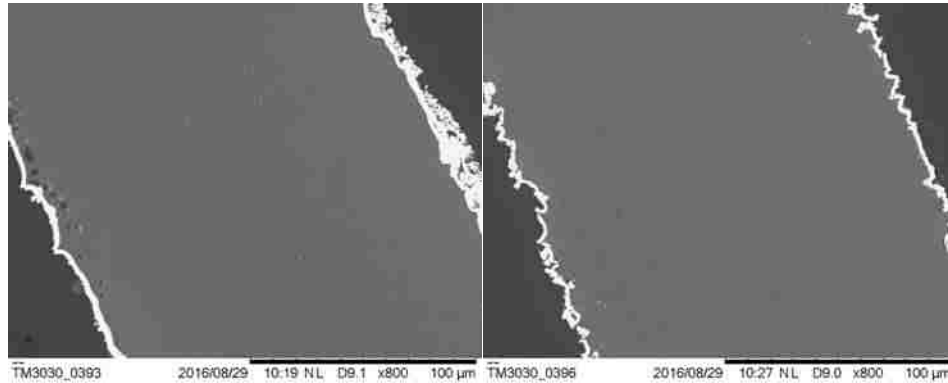


Figure 5.7. SEM images at a magnification of x800 of N-IPMC (left) and A-IPMC (right).

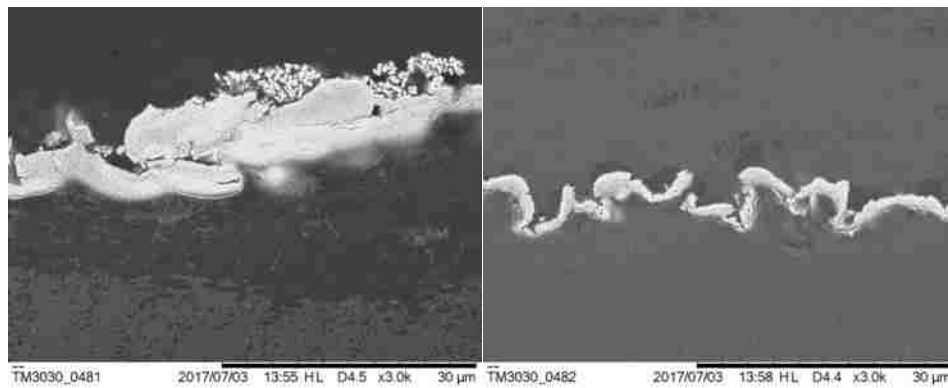


Figure 5.8. SEM images at a magnification of x3,000 of N-IPMC (left) and A-IPMC (right).

The samples are tested for their actuation capabilities with an input of 3 Volts at various frequencies: 100 mHz, 500 mHz and 1 Hz. The slowest applied voltage is 3 Volts at 100 mHz (Figure 5.9). The samples actuated similarly, however when comparing the two displacements, it can be seen that A-IPMC had a larger peak to peak amplitude and faster response times (Table

5.5). The next signal applied to the IPMC samples was 3 Volts at 500 mHz (Figure 5.10). The difference between the peak to peak amplitudes between N-IPMC and A-IPMC has decreased compared to the displacements in the previous test, but the A-IPMC is still actuating further and faster than the N-IPMC (Table 5.6). The last test is an applied voltage of 3 Volts at 1 Hz, which is the fastest signal (Figure 5.11). Typically, 1 Hz is quite a fast signal for an IPMC and the material is not able to reach its maximum displacement. Here it can be seen that the difference between the two peak to peak amplitudes has decreased even more so, but again the A-IPMC is still out performing the N-IPMC (

Table 5.7). Overall, A-IPMC has larger peak to peak amplitudes and faster response times compared to N-IPMC. In the case of blocking force capabilities, these IPMCs are very thin and it was not possible to test them as they cannot produce a large enough force to be measured by the load cell. The power input of the IPMC samples were plotted and the results are shown in Figure 5.12. At 500 mHz, both samples use about the same amount of power. At the slowest frequency, N-IPMC draws more power than the A-IPMC, while in the fastest frequency, this is reversed. This can be explained by the difference in ionic conductivity between the two samples. A-IPMC has a higher ionic conductivity so it does not need as much power to move the ions in the slowest case. However, in the fastest case, A-IPMC is able to move more ions to the other side than N-IPMC so it requires more power to move them back to the opposite end. The blocking force tests will be conducted on the printed samples versus a Nafion<sup>®</sup>-based IPMC of similar dimensions.

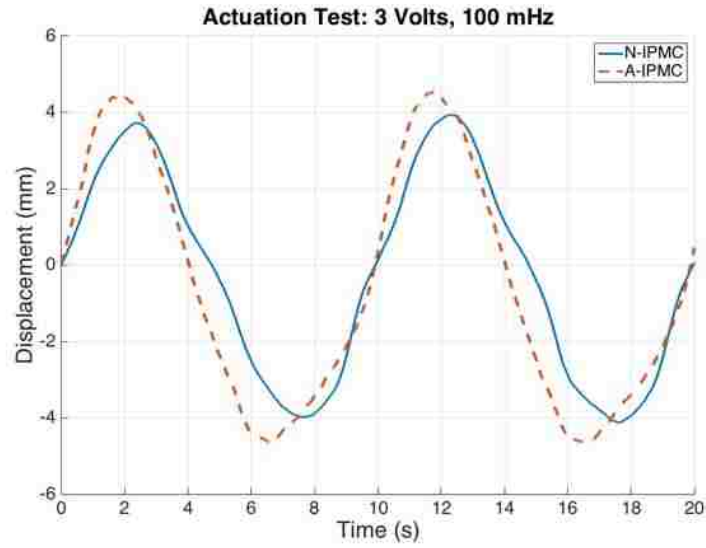


Figure 5.9. Actuation test results with 3 Volts at a frequency of 100 mHz applied.

Table 5.5. Details of the analysis from the plots in Figure 5.9.

<b>3 Volts, 100 mHz</b>			
	<b>Peak to Peak Amplitude (mm)</b>	<b>Response Time (s)</b>	
		<b>Time to first peak</b>	<b>Time to second peak</b>
<b>N-IPMC</b>	6.32	2.34	5.4
<b>A-IPMC</b>	11.02	1.79	4.78

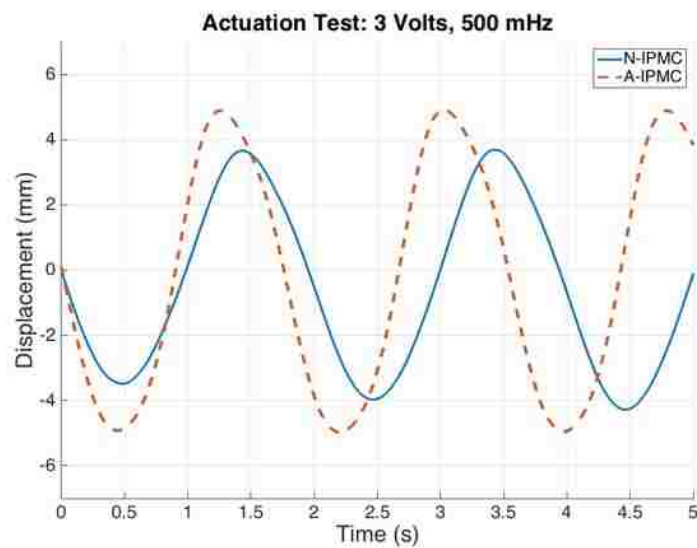




Figure 5.10. Actuation test results with 3 Volts at a frequency of 500 mHz applied.

Table 5.6. Details of the analysis from the plots in Figure 5.10.

<b>3 Volts, 500 mHz</b>			
	<b>Peak to Peak Amplitude (mm)</b>	<b>Response Time (s)</b>	
		<b>Time to first peak</b>	<b>Time to second peak</b>
<b>N-IPMC</b>	7.14	0.48	0.95
<b>A-IPMC</b>	9.82	0.44	0.82

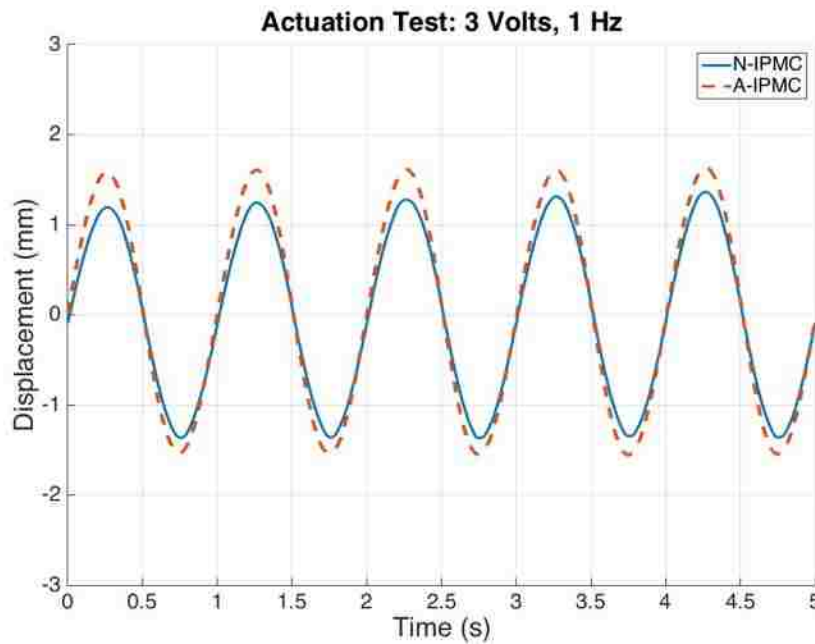


Figure 5.11. Actuation test results with 3 Volts at a frequency of 1 Hz applied.

Table 5.7. Details of the analysis from the plots in Figure 5.11.

<b>3 Volts, 1 Hz</b>			
	<b>Peak to Peak Amplitude (mm)</b>	<b>Response Time (s)</b>	
		<b>Time to first peak</b>	<b>Time to second peak</b>
<b>N-IPMC</b>	2.55	0.28	0.49
<b>A-IPMC</b>	3.11	0.25	0.49

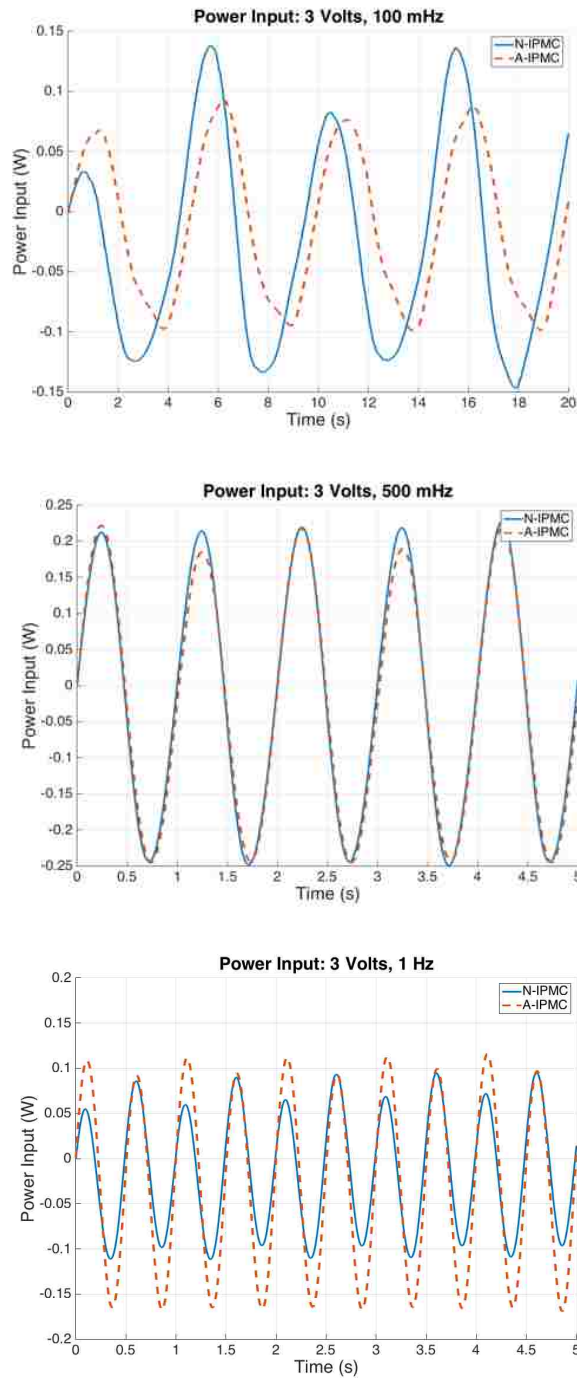


Figure 5.12. Power Input for the three cases of input. From top to bottom, 3 Volts at 100 mHz, 3 Volts at 500 mHz, and 3 Volts at 1 Hz.

### 5.5.2. Filament production

The filament made for these studies was made using Aquivion<sup>®</sup> P87 precursor pellets. The filament extruder, the Noztek Pro, was set to 230°C and allowed to reach temperature before turning on the motor for the feed auger. This filament extruder is at a 45° angle, helping the pellets and filament move easily. The pellets are filled into the hopper and the motor is turned on, moving the pellets towards the heating zone. It is very important to ensure that the pellets do not have any moisture absorbed because this can cause partial hydrolysis, bringing issues when the filament is being used in the 3D printer. This can be done by either storing the Aquivion<sup>®</sup> pellets in a desiccator or drying the pellets in a vacuum oven at 105°C for 20 hours, as described by Solvay. The diameter of the filament that can be produced are 2 mm and 3 mm. The filament produced is of similar color to the pellets and shows no signs of degradation (Figure 5.13).



Figure 5.13. Aquivion<sup>®</sup> precursor pellets drawn into filament (left) and cross-sectional view of the filament with measurement showing the diameter to be around ~3 mm (right).

### 5.5.3. 3D printing Aquivion®

#### 5.5.3.1. Additive manufacturing physics and 3D printer designs.

Though there are many 3D printers available, finding a printer that works well for Aquivion®, or Nafion® as discussed by Carrico *et al.* [65], can be difficult. Aquivion® filament is relatively soft compared to ABS or PLA filaments, which causes issues such as buckling or the drive gear tearing into the filament. The rate that the filament is fed through is very important as well to ensure that the filament is evenly and thoroughly heated. The nozzle's offset from the printer bed surface can cause too much pressure in the system, which in turn can cause buckling and clogging issues. These are the key issues to keep in mind when designing a 3D printer for either Aquivion® or Nafion®. Compared to typical plastic filaments that are used in 3D printing, Aquivion® and Nafion® have higher melting temperatures. To be able to print with these ionomers, the nozzle temperature needs to be at least 260°C. Though the Aquivion® precursor pellets have a melting temperature of 230°C, after the first thermal treatment during filament extrusion, the material has become “annealed” in a way so it is not able to melt at the lower temperature. In order to print with the filament, the printer has to be able to reach and hold a high temperature. In the case of printing Aquivion®, 260°C is the ideal extruder temperature. The other side of this issue is having a hot bed that is hot enough to encourage bed adhesion. The hot bed on commercially available printers is not able to reach high enough temperatures (usually 110°C is the maximum temperature) for the material to adhere to the bed. Since the extruder temperature is relatively high compared to most materials, the hot bed needs to be close in temperature to reduce the temperature drop after the material has exited the nozzle. The ideal temperature found to encourage bed adhesion is around 180°C.

Turner *et al.* thoroughly presents the physics of additive manufacturing [112]. Some key points gathered that have helped explain and solve issues encountered. Aquivion<sup>®</sup> filament has shown to be a sensitive material to moisture. If not stored in dry environment, the filament will absorb moisture from the air and partially hydrolyze during the printing process. This causes the filament to become unable to melt, leading to clogging and inability to adhere to the bed surface. A main key point from Turner *et al.* that was applied very well to issues with printing Aquivion<sup>®</sup> was the equation for critical pressure. The critical pressure is represented as:

$$P_{cr} = \frac{\pi^2 E d_f^2}{16 L_f^2} \quad (9)$$

where E is the elastic modulus of the filament,  $d_f$  is the diameter of the filament, and  $L_f$  is the distance from the drive gear to the entrance of the liquefier [112]. This value denotes the limit of the pressure that can be applied to the filament before it buckles. In fused filament deposition systems, the filament is pushed through the system by a drive gear. The distance between the drive gear and the entrance of the liquefier has shown to be important in successfully printing a soft filament such as Aquivion<sup>®</sup>. Initially, the printer being used was the Raised 3D N2 Plus printer. This printer was chosen because the entire path for the filament is constrained. However, this did not solve the issues of buckling. As shown in equation (9), the distance between the drive gear to the entrance of the liquefier needs to be as short as possible to increase the pressure built within the extrusion setup. In the Raised printer, this distance is about 10.8 cm (4.25 inches) diameter of the filament is 2 mm, resulting in a critical pressure of 53 kPa. Though it is possible to successfully print with this 3D printer, the pressure drop across the melt zone and nozzle exceeded this relatively low critical pressure, and thus filament buckling lead to unreliable printing. To lessen some of the pressure built up within the extruder system, the nozzle diameter was increased to 2

mm. This allowed for a few prints to be successful, but it was not as consistent as a typical 3D printer. A commercially available extruder that is designed to extrude flexible material, the Flexystruder, was purchased and added to the Lulzbot Mini. The distance between the drive gear and the entrance of the liquefier is 6.35 cm (2.5 inches) and the diameter of the filament is 3 mm, giving a critical pressure of 344 kPa. With this new extruder, the system is able to operate at 6.5 times more pressure drop than the Raised extruder, greatly reducing the likelihood of filament buckling. It is possible to keep the nozzle diameter as is (0.5 mm) and produce quality prints. Table 5.8 summarizes the dimensions measured off the 3D printers and values used for the calculations, as well the calculated critical pressure.

Table 5.8. Filament’s Young’s Modulus [115] and dimensions (measured directly from printers in-house) used for the calculations using Equation (9) to find the critical pressure for each printer.

	<b>Raised 3D Extruder</b>	<b>Flexystruder</b>
<b>Elastic Modulus (MPa)</b>		250
<b>d<sub>f</sub> (mm)</b>	2	3
<b>L<sub>f</sub> (cm)</b>	10.8	6.35
<b>P<sub>cr</sub> (kPa)</b>	53	344

### 5.5.3.2. 3D printing Aquivion® samples

The Raised 3D printer systems use the company’s proprietary software, ideaMaker, to slice and process STL models. A settings profile was created specifically for Aquivion® which included slower printing speeds to minimize back pressure in the nozzle and the use of a brim to promote bed adhesion. Ultimately, the profile was made to print 0.2 mm layers at a default speed of 5 mm/s and a 120% infill flow rate with 60% overlap and 100% infill. The first layer was printed at 10 mm/s and 160% flow rate to establish a sturdy foundation for the consecutive layers. The nozzle

was set to 260°C and the hot bed was set to 180°C. The hot bed was covered with double sided Kapton tape to encourage bed adhesion (Figure 5.14). The samples printed had even thicknesses and good layer adhesion (Figure 5.15 and Figure 5.16). Similarly, a profile was made to operate the Lulzbot Mini printer with Aquivion<sup>®</sup>. This printer used Cura (Lulzbot Edition) as the slicer, and the profile used similar settings. A 10 mm/s default print speed was used, along with a 100% first layer flow rate. Due to the larger filament diameter and shorter distance between drive gears and extruder nozzle, the Lulzbot profile did not require as many precautions to limit the filament back pressure. The nozzle was set to 260°C and the hot bed was set to 180°C to keep the temperature difference between the nozzle and bed as low as possible. The hot bed has a layer made out of polyetherimide (PEI), which helps with bed adhesion for typical printing materials. This was successful for Aquivion<sup>®</sup> but double sided Kapton tape worked as well. The Lulzbot Mini was able to print the Aquivion<sup>®</sup> filament consistently with good layer adhesion (Figure 5.17). Four samples were printed in sequence and shown in Figure 5.18 with minimal differences in dimensions.

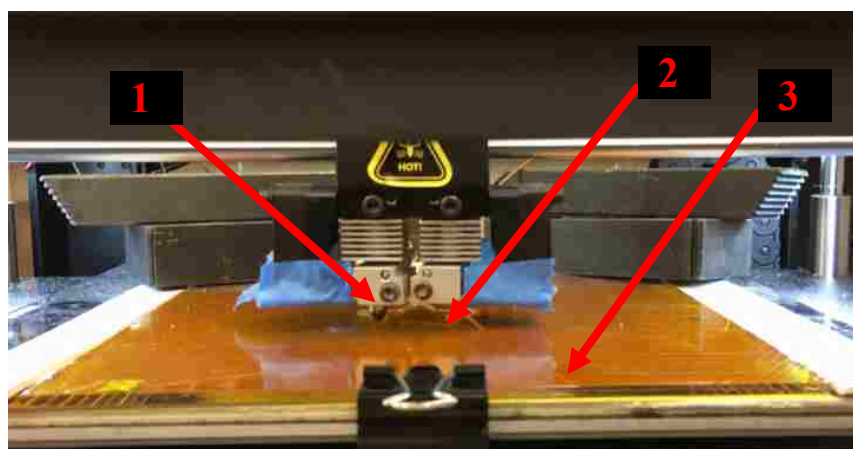


Figure 5.14. Aquivion<sup>®</sup> filament printed onto double-sided Kapton tape using the Raised N2 Plus Printer. 1: Extruder hot end. 2: Printed Aquivion. 3: Heated glass plate.

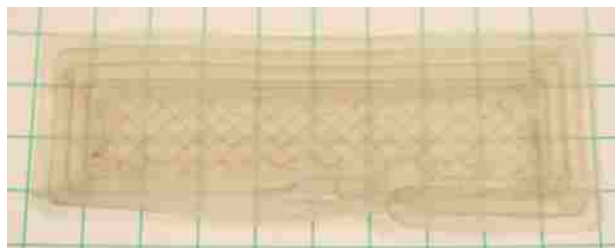


Figure 5.15. Printed Aquivion<sup>®</sup> in a rectangular shape with a brim to help with bed adhesion (each square on the grid is 6 mm x 6 mm).



Figure 5.16. Star-shaped Aquivion<sup>®</sup> membrane printed on the Raised N2 Plus Printer.



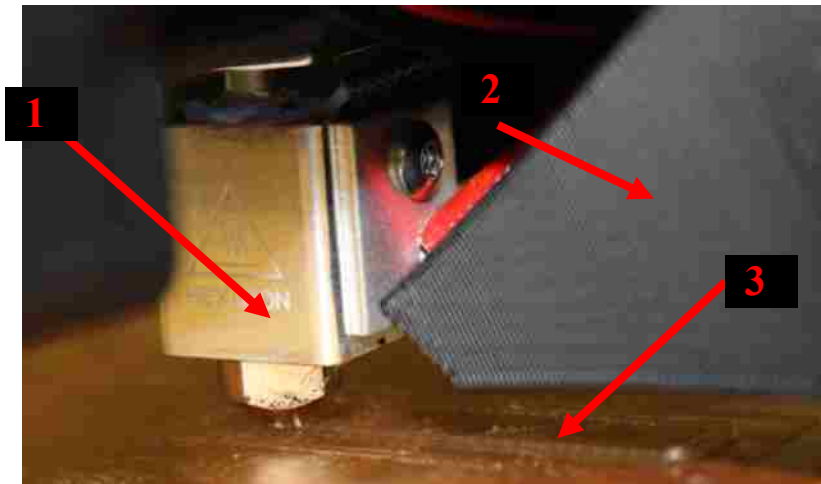


Figure 5.17. Aquivion<sup>®</sup> printed with the Lulzbot Mini and Flexystruder. 1: Extruder hot end on the Flexystruder. 2: Cooling fan (turned off for our print settings). 3: Printed Aquivion.

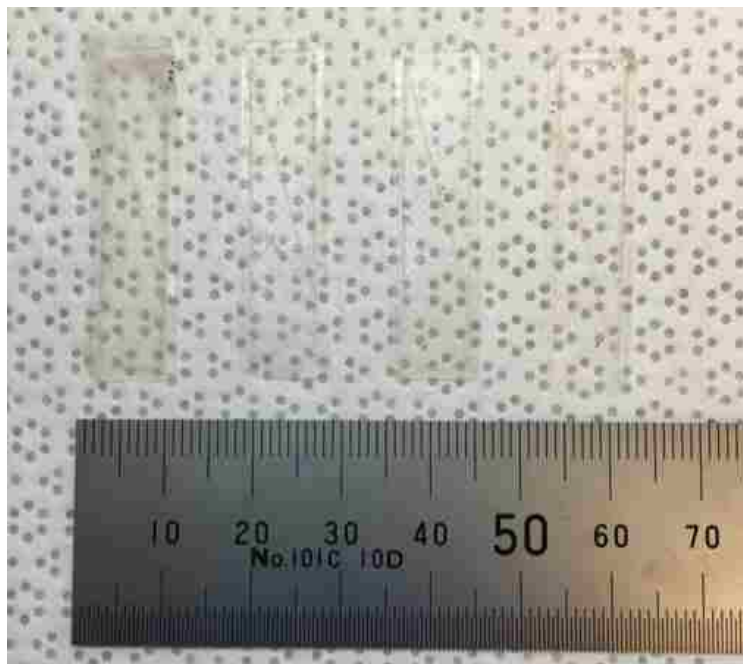


Figure 5.18. Four Aquivion<sup>®</sup> membrane samples printed using the Lulzbot Mini with the Flexystruder.

#### 5.5.4. Material characterization of the printed Aquivion®

To ensure that the printed Aquivion® sample was not contaminated, it was compared to a pure Aquivion® precursor pellet using the FT-IR (Figure 5.19). The two had the same peaks that correlate with the polymer's chemical composition. A sample from the printed Aquivion® was tested in the TGA to identify the thermal degradation temperature and compare to that of an Aquivion® precursor pellet. The results are compared in Figure 5.20 and it can be seen that the printed sample is able to withstand a higher temperature than the pellet (380°C compared to 300°C). This is probably because the ionomer has gone through two thermal treatments and has “annealed.” After the printed samples were activated, they were compared using the FT-IR to an Aquivion® membrane (Figure 5.21). The two have the same peaks at 1213  $\text{cm}^{-1}$ , 1153  $\text{cm}^{-1}$ , and 1060  $\text{cm}^{-1}$  corresponding to the symmetric  $\text{CF}_2$ , asymmetric  $\text{CF}_2$ , and  $\text{SO}_3$  bonds. The activated, printed membrane and the Aquivion® membrane were tested for their dynamic mechanical properties using the DMA in an environment of relative humidity of about 25% at room temperature. The samples had comparable Young's Moduli (Figure 5.22, left). The printed Aquivion® sample has a slightly higher Young's Modulus, but should not cause issues in actuation. The damping coefficient, however, differs between the two samples (Figure 5.22, right). When comparing the two samples, the printed Aquivion® has a lower damping coefficient, indicating less viscoelastic behavior. The printed Aquivion® is not as able to efficiently dissipate the energy absorbed. This could be because of the layering effect during the printing process, stiffening the membrane, causing it to not be able to absorb as much vibration as the off-shelf-membrane. However, the difference overall is minimal, when comparing the phase shifts between the two samples (such as 5.3° at 0.1 Hz).

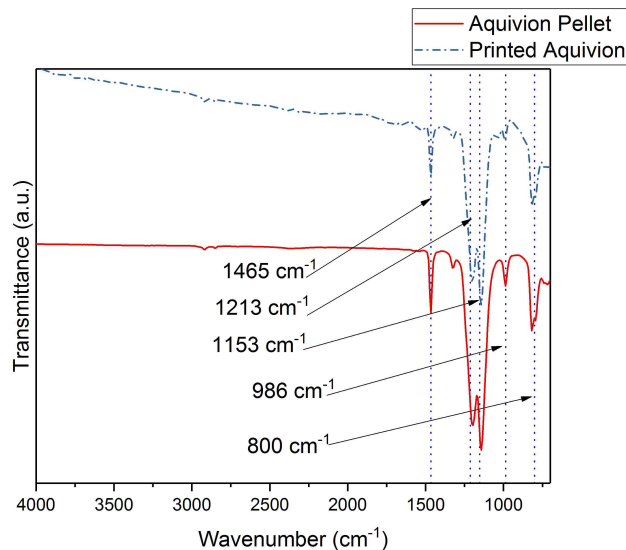


Figure 5.19. Printed Aquivion<sup>®</sup> sample chemical structure compared with an Aquivion<sup>®</sup> precursor pellet using FT-IR results. Each wavelength correlates to a specific bond that is present in the polymer: 1465  $\text{cm}^{-1}$  represents the C-F bond, 1213  $\text{cm}^{-1}$  represents the symmetric  $\text{CF}_2$  bond, 1153  $\text{cm}^{-1}$  represents the asymmetric  $\text{CF}_2$  bond, 986  $\text{cm}^{-1}$  represents the C-F<sub>3</sub> bond, 800  $\text{cm}^{-1}$  represents the S-O bond.

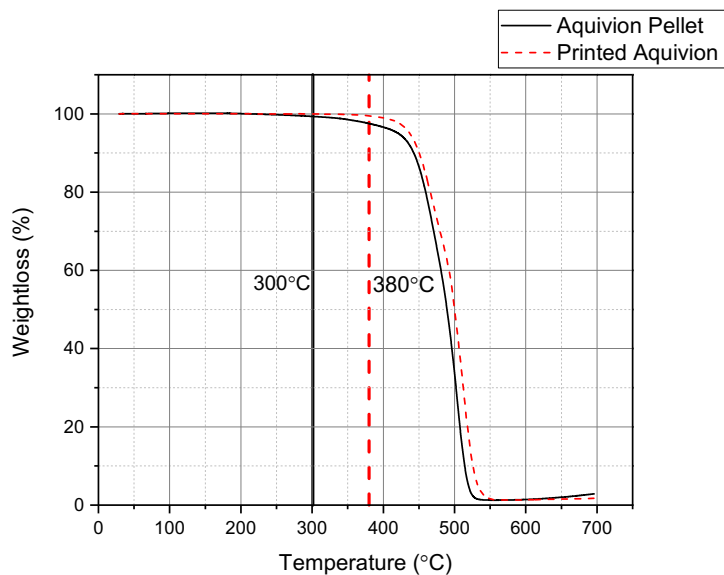


Figure 5.20. TGA results for the thermal degradation temperature of the printed Aquivion<sup>®</sup> and an Aquivion<sup>®</sup> precursor pellet.

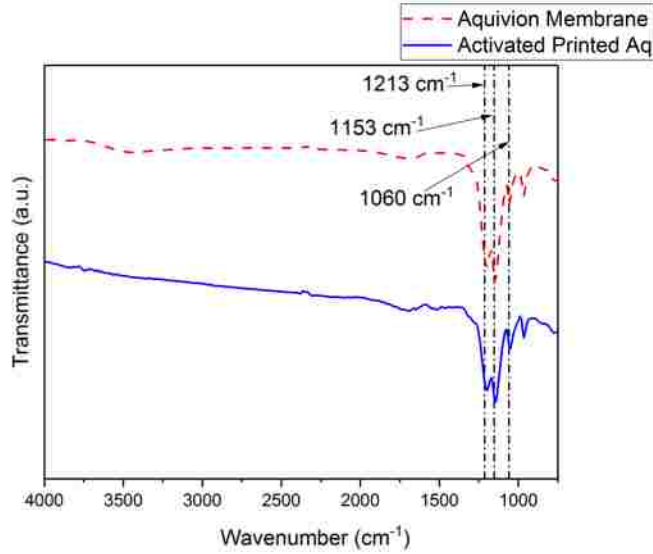


Figure 5.21. FT-IR results for the chemical structure of activated, printed Aquivion<sup>®</sup> and an Aquivion<sup>®</sup> membrane.

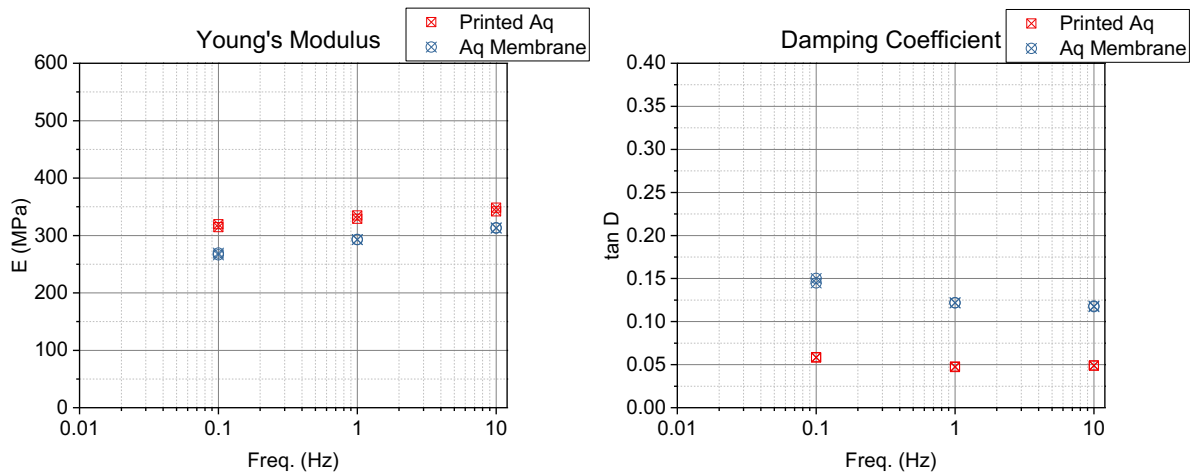


Figure 5.22. DMA results for activated, printed Aquivion<sup>®</sup> compared with an Aquivion<sup>®</sup> membrane.

### 5.5.5. IPMC performance comparison

The Printed Aquivion<sup>®</sup> IPMCs (Pr-Aq-IPMC, Figure 5.23) is compared to traditionally made, Nafion<sup>®</sup>-based IPMC (N-IPMC). Table 5.9 shows the similar dimensions and surface resistances

of the IPMC samples. It is important to compare samples that are as close as possible in shape, since the geometry of the IPMC can affect its performance greatly. The first point of interest was the back relaxation capabilities. This phenomenon occurs when a DC voltage is applied to an IPMC, forcing it to move to a maximum displacement, until it begins to move backwards to a different position than it initially started. The information from this test gives researchers an idea of how far an IPMC will displace until it no longer can as well as the position it returns to. The displacement is measured for analysis, including calculating the strain. Using the displacement data, the radius of curvature ( $\rho_r$ ) is calculated using Equation (10), where L is the length of the sample and  $\delta$  is the displacement recorded by the laser displacement sensor. Once that is calculated, it is used to find the strain  $\varepsilon$  using Equation (11), where h is the thickness.

$$\rho_r \cong \frac{L^2 + \delta^2}{2\delta} \quad (10)$$

$$\varepsilon \cong \frac{h}{2\rho_r} \quad (11)$$

Overall, the Pr-Aq-IPMC samples were able to actuate further than the N-IPMC (Figure 5.24). They also respond faster than the N-IPMC. The strains produced are within the typical ranges for an IPMC. Between the Pr-Aq-IPMC samples, they were able to perform well between each other.



Figure 5.23. Four Printed Aquivion IPMCs (Pr-Aq-IPMC) plated with platinum using the electroless plating process (top) and surface of one of the samples at 100x magnification (bottom).

Table 5.9. Dimensions of IPMC samples being tested.

	<b>Length (mm)</b>	<b>Width (mm)</b>	<b>Thickness (mm)</b>	<b>Surface Resistance (<math>\Omega</math>)</b>
<b>N-IPMC</b>	45.08	11.57	0.67	3,3
<b>Pr-Aq-IPMC 1</b>	45.28	11.08	0.67	2,2
<b>Pr-Aq-IPMC 2</b>	46.04	11.55	0.68	2,2
<b>Pr-Aq-IPMC 3</b>	45.66	11.44	0.64	2,2
<b>Pr-Aq-IPMC 4</b>	45.55	11.07	0.66	2,2

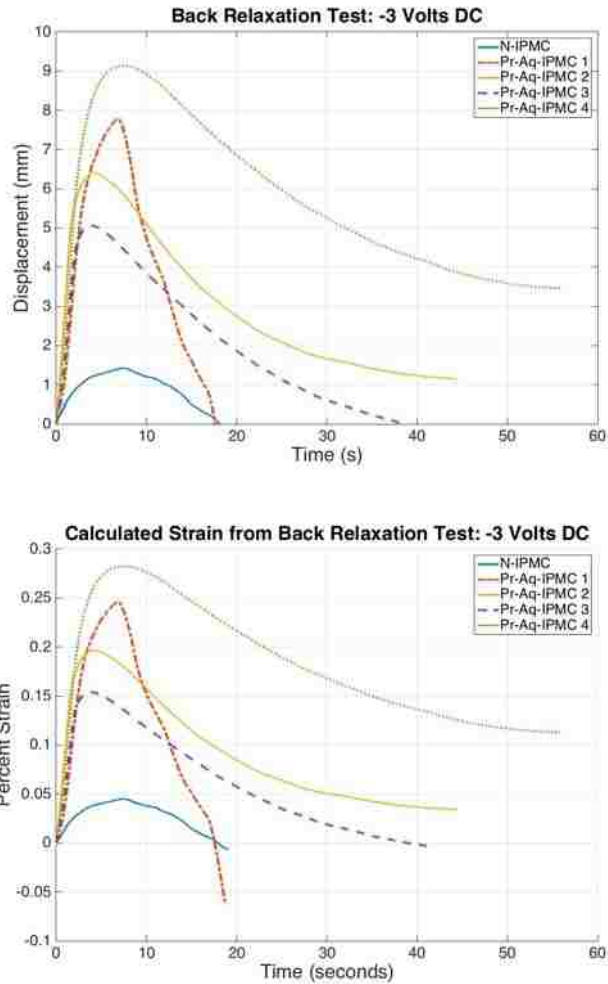


Figure 5.24. Back relaxation test for the IPMC samples with an applied voltage of -3 Volts DC (top) and the calculated strain from the results (bottom).

IPMCs are typically used in frequency-based applications. To determine how well the IPMCs respond to a sinusoidal voltage signal, the samples were placed in a DI water-filled tank with 3 Volts at 500 mHz applied. Figure 5.25 shows the results measured from the tests. Pr-Aq-IPMC samples perform better than the N-IPMC and similarly to each other. A frequency response test was conducted to further investigate the response performance of the samples. From Figure 5.26, it can be seen that the Pr-Aq-IPMC samples all responded faster compared to N-IPMC, within the same amount of time. The Pr-Aq-IPMC samples are all able to produce relatively large

displacements, even at 5 Hz, which is considered a fast input for this smart material. This is most likely due to its high ionic conductivity ( $\sim 228$  mS/cm). The final test that was conducted was the blocking force. The samples were tested in air in order to be in contact with the load cell. The samples were completely hydrated before the test was conducted. The input voltage was -1 Volt DC. From Figure 5.27, Pr-Aq-IPMC samples generated a much higher blocking force than the N-IPMC before back relaxation occurs. The stress was calculated by using a dividing the measured force by the cross-sectional area of the IPMC. Both of the samples produce comparable stresses within the IPMC. The volumetric energy density was calculated by taking the peak blocking force value multiplied by the distance the IPMC sample displaced, divided by the free moving volume (Table 5.10). Overall, the Pr-Aq-IPMC samples have higher energy densities than the N-IPMC. When compared to other smart material actuators, a paper written by Shankar *et al.* includes a summary plot of various actuators and it can be seen that the IPMC samples presented here perform below what is predicted [116]. This could be because the IPMCs tested for the plot could be thicker or of a different base.

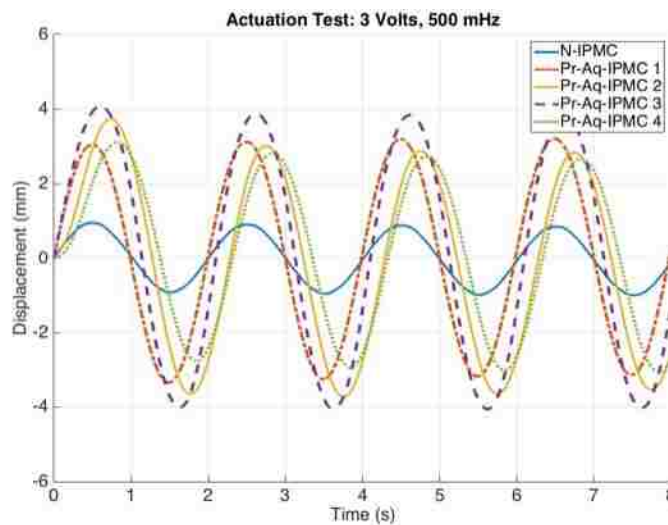


Figure 5.25. Actuation tests for the IPMC samples at 3 Volts, 500 mHz.



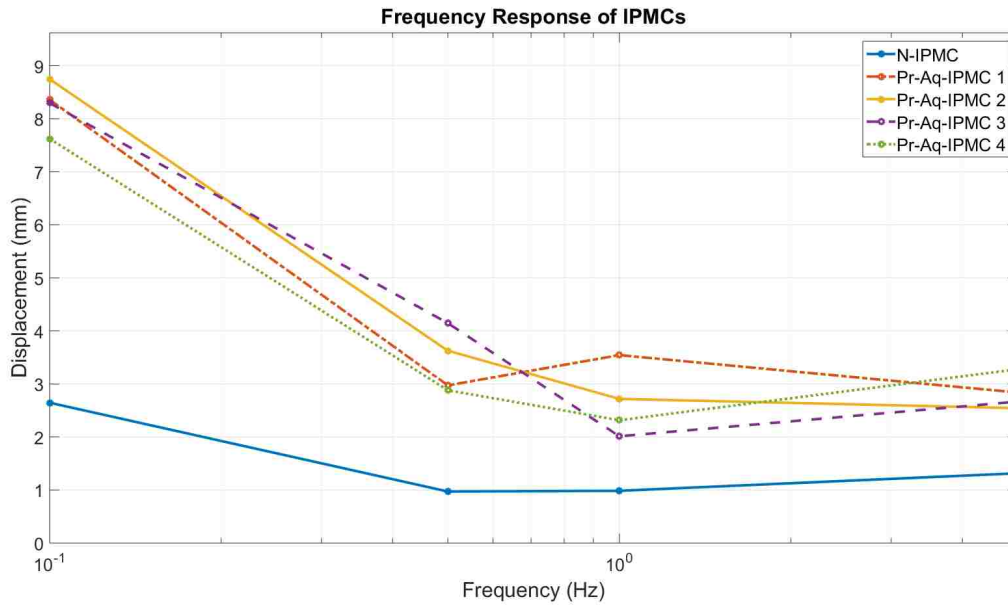


Figure 5.26. Frequency response plot at 3 Volts driven at 0.1 Hz, 0.5 Hz, 1 Hz, and 5 Hz.

The last test for IPMC performance characterization was the mechano-electric sensing test. The samples were oscillated with a sine wave of 3 mm (peak to peak) at a frequency of 2 Hz. From Figure 5.28, it can be seen that the N-IPMC performs as expected, while the Pr-Aq-IPMC samples vary from sensing close to N-IPMC to almost double that of the N-IPMC sample. The printed IPMCs show promise of introducing new shapes, similar to that of nature's sensors, that can push the field of biomimicry forward. A frequency response has been added into Appendix G.

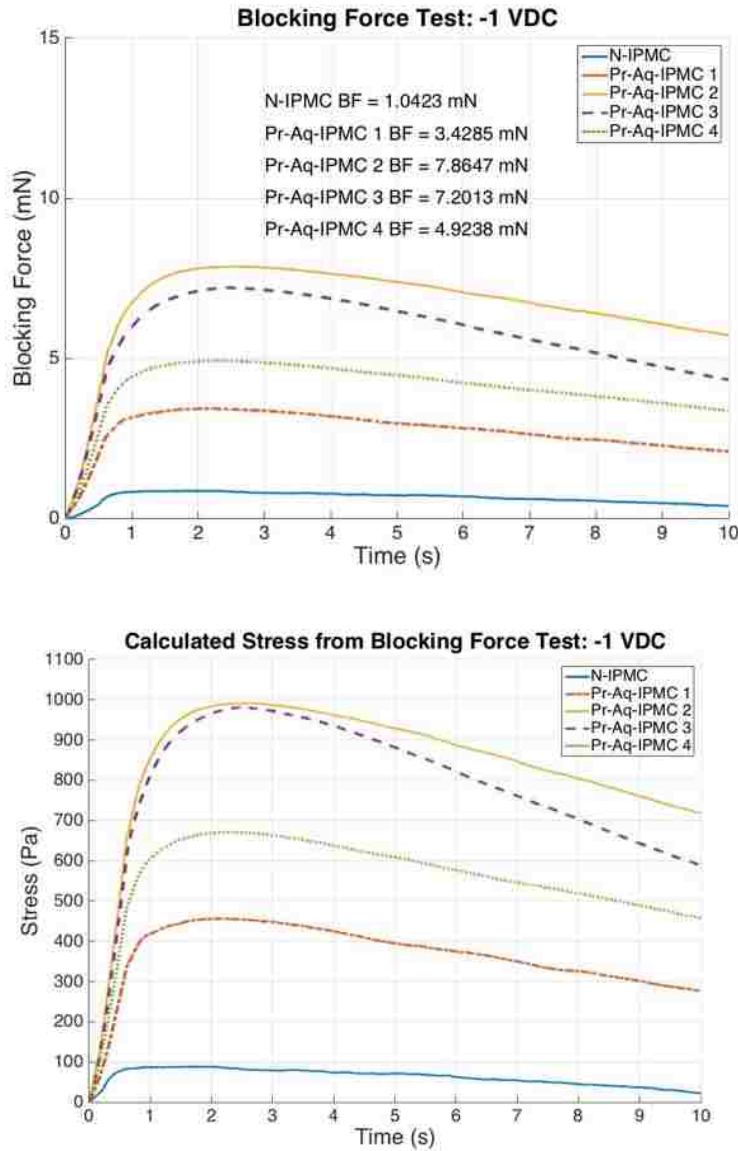


Figure 5.27. Blocking force tests for the IPMC samples with an applied voltage of -1 Volts DC (top) and the calculated stress from the results (bottom).

Table 5.10. Calculated volumetric energy density for the samples.

	<b>Volumetric Energy Density (J/m<sup>3</sup>)</b>
<b>N-IPMC</b>	9.6
<b>Pr-Aq-IPMC 1</b>	32.7
<b>Pr-Aq-IPMC 2</b>	69.5
<b>Pr-Aq-IPMC 3</b>	69.0
<b>Pr-Aq-IPMC 4</b>	47.4

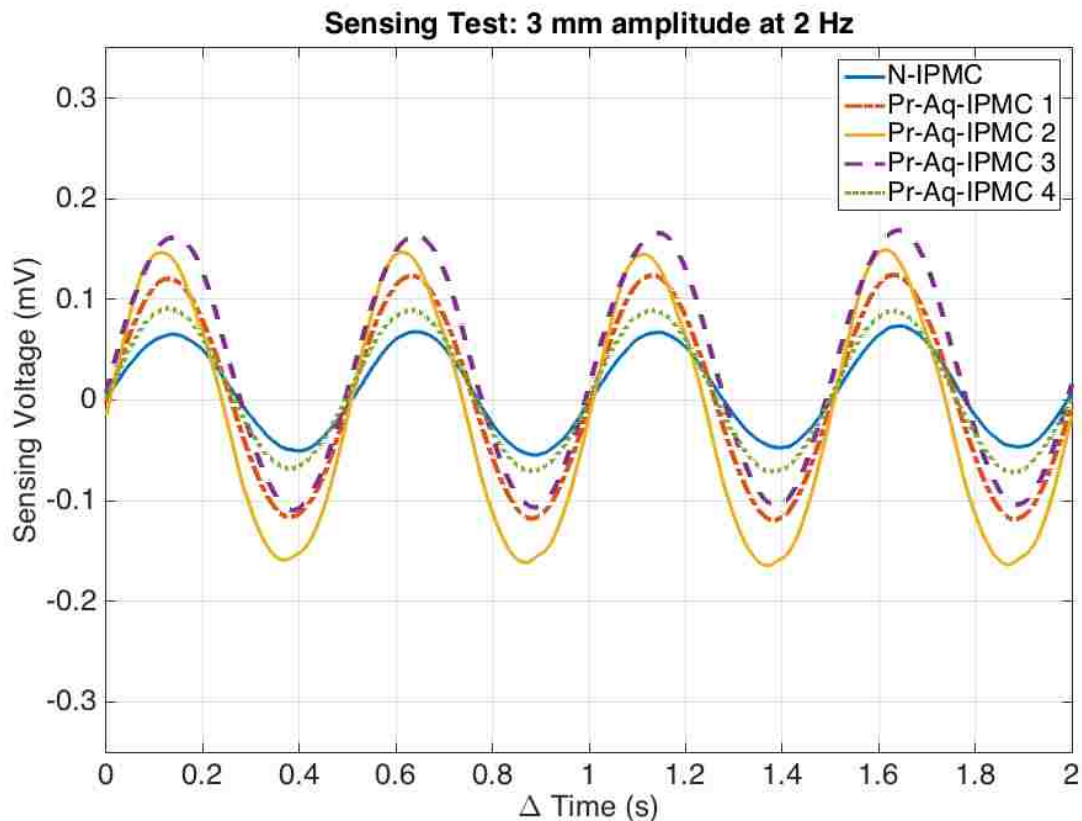


Figure 5.28. Sensing data from oscillating the IPMC samples with input of 3 mm (peak to peak amplitude) at 2 Hz.

Overall, the performance of the Pr-Aq-IPMCs have shown promise in their application compared to that of the N-IPMC. There are some differences in their responses which can be explained by a few different reasons. Traditionally made IPMCs that are cut into the desired dimensions from the same sheet can perform differently, even though they were manufactured at the same time, from the same membrane. This can be explained by not being able to completely control the manufacturing process of both the membranes, from the manufacturer, and the plating process, done in-house. Though a detailed procedure is followed, the entire sheet of IPMC may not be able to perform uniformly. A similar effect can be explained for the printed samples. Though we are

printing the same file several times in a row, every aspect of the printing process cannot be controlled. The adhesion between the layers can differ from very good connections to not if the printer bed has shifted. Though the membranes were left in the activation bath for several hours to ensure they have been completely activated, there is a potential issue that the membranes were not fully activated. The plating process though very carefully conducted, may not have evenly plated onto the surface, due to the unique surface texture of the printed samples. All of these factors could contribute to the difference in performance by each Pr-Aq-IPMC.

One aspect to note is the difference in peak to peak amplitude observed in Figure 5.10 and Figure 5.25. In Figure 5.10, the difference between the A-IPMC and N-IPMC peak to peak amplitude is small, but noticeable. In Figure 5.25, the peak to peak amplitude difference is much more noticeable. To explain this phenomenon, it should be noted that typically, very thin IPMCs will have large displacements, while thicker IPMCs will actuate less. The samples in Figure 5.10 have a thickness of about 120  $\mu\text{m}$ , so they are able to have large actuations. The N-IPMC in Figure 5.25 has a thickness of about 600  $\mu\text{m}$ , which is fairly thick for an IPMC. It actuates as expected, around 2 mm peak to peak. The Pr-Aq-IPMC samples are about the same thickness, but are able to outperform the traditional N-IPMC. This is most likely due to its high ionic conductivity, allowing the smart material to move more ions than the sample. The Pr-Aq-IPMC samples were able to overcome the hindrance of their large thickness.

## **5.6. Conclusions and Future Work**

The work in this paper introduces Aquivion<sup>®</sup> as a potential candidate for additive manufacturing of ionomeric polymers for the application of IPMCs. Aquivion<sup>®</sup> was characterized and shown to have similar material properties to Nafion<sup>®</sup> in general other than the ionic conductivity, where

Aquivion<sup>®</sup> has nearly double that of Nafion<sup>®</sup>. This difference shows when N-IPMC and A-IPMC were tested for their performance in frequency driven actuation, with the A-IPMC performing better. Two 3D printers were modified to successfully print Aquivion<sup>®</sup> filament. It was noted that the Lulzbot Mini was able to print consistently, without buckling issues. The printed membranes were activated and plated with platinum using an electroless process. The Pr-Aq-IPMC samples performed better to N-IPMC in back relaxation and strain production. In frequency driven actuation, the Pr-Aq-IPMC samples shows promise in its ability to respond faster and larger peak to peak amplitude. The Pr-Aq-IPMC samples is also able to generate a large blocking force before starting to back relax. Sensing tests showed promise for the application of Pr-Aq-IPMCs as sensors since they were able to perform better than the N-IPMC. Overall, it can be clearly seen that Aquivion<sup>®</sup> is a valid option for additive manufacturing. Future work includes studying the relationship between viscosity and temperature, expanding the shapes printed into 3D structures and studying the effects of printing asymmetric shapes on actuation and mechano-electric sensing performance.

## **5.7. Acknowledgements**

This material is based upon work supported in part by the National Science Foundation under Grant No. #1545875 (3D printing; ST, ZO, and KJK). Also, this work was supported in part by the Department of Energy Minority Serving Institution Partnership Program (MSIPP) managed by the Savannah River National Laboratory under SRNS contract TOA#0000332975 (robotics perspectives; KJK). Additionally, KJK acknowledges the partial financial support from the Office of Naval Research (N00014-16-1-2356; IPMC characterization; KJK). The authors would also like to thank Dr. Hyeunhwan An for assisting in the Ion Exchange Capacity tests.

## **Chapter 6. Demonstration: 3D Printed NACA-inspired Hydrofoil-shaped IPMC**

This chapter is a demonstration of how 3D printing can produce IPMC shapes that would otherwise be difficult to make using current fabrication methods. The process and design of the National Advisory Committee for Aeronautics (NACA)-inspired Hydrofoil is shown with a discussion on current limitations. The 3D Printed Aquivion Hydrofoil is activated and plated with platinum, then tested initially for basic performance testing. A discussion of bed adhesion issues and some potential solutions is included for the reader to consider.

The work was conducted with the assistance of Zakai Olsen, who had previously drawn the CAD models for the Hydrofoil and continued to work on 3D printing Aquivion.

### **6.1. Introduction**

Airfoils and hydrofoils are specifically designed to produce desired outputs such as lift force, velocity, thrust force [117]. By optimizing the design, wings for different types of vehicles have been produced [117]. One point of interest to many researchers is a flexible, potentially flapping wing. The first publication exploring the possibility of adapting bird's wings to engineering applications was shown by Lilienthal and Lilienthal [118]. From there, researchers have continued to study flapping airfoils. A group in the UK has studied the effects of stiffness on thrust generation on a flapping airfoil made of aluminum and steel and they found that airfoils with lower stiffness had higher thrust to input power ratio [119]. Another group from China studied the effects of the chord stiffness in different flow parameters and found that propulsive efficiency is related to the flexural amplitude of the chord [120]. A different group in Germany simulated a flapping airfoil

mimicking a seagull wing to study the effects of how flexible the wing is to thrust efficiency, drag, and lift [121].

The next area of interest for researchers is to produce a “smart” airfoil. Abdullah and Watkins present a discussion of what is needed from a smart material to make an adaptive airfoil [122]. From another reference [123], they saw that a smart airfoil needs quick response to an input, produce large strains as well as recover from them, efficiently transform input energy to mechanical energy, and have no fatigue issues. They continue on to give insight on how to properly design an airfoil using Shape Memory Alloys (SMA), which they conclude is the best option. Later, a group from France use a combination of SMAs and Macro-fiber composites (MFC) to produce an airfoil that can change its shape to control the shear layer [124].

Though SMAs are a good option for smart airfoils, another option is the Ionic Polymer-Metal Composites (IPMCs). Palmre *et al.* presented a controllable fin by using three IPMCs in a silicone boot [13]. By controlling each IPMC individually, the robotic fin was able to bend and twist to create different profiles. The IPMCs are hot-pressed, rectangular shapes which allowed for three to work together, but could be improved by making the IPMC into an airfoil-like shape. Presented here is a 3D Printed Aquivion Hydrofoil-shaped IPMC. By making the base ionomer into the shape needed, it could be possible to make a completely active, smart hydrofoil.

## **6.2. Hydrofoil Design**

See a hydrofoil wing (Figure 6.1). They were interested in producing this same fin in various scales and different forms. The profile is based on the NACA 0012, which is a symmetric airfoil

(designated by the first two digits, 00) with the last two digits being the maximum thickness to chord ratio. It is possible to 3D print this drawing in typical printing plastics, such as Polyactic Acid (PLA) and Acrylonitrile Butadiene Styrene (ABS), because these plastics have been studied thoroughly, most 3D printers can print them in high resolution, and they can be used as support material for themselves. Aquivion, as discussed in Reference [46], is not as easy to 3D print with. The ionomer easily buckles, requires very high printing temperatures, and should be printed slowly. Bed adhesion has not been completely solved, but some options have been explored. Since Aquivion needs a high bed temperature to continuously encourage bed adhesion, the design cannot be too tall. Another issue is during the activation process, thicker membranes are more difficult to completely activate, since the activation is based on hydrolysis. The goal is to keep the thickness below 2 mm, based upon our experiences. Figure 6.2 shows the completed design for the Aquivion-based hydrofoil. The hydrofoil from the Navy has been cut in half, to ensure that the bottom layer has good bed adhesion. Then, this design is input into a program for the 3D Printer, Cura, to generate the g-code. This is the tool path for the 3D printer to follow and place material in the correct positions to build the model. The settings are shown in Table 6.1. Only the bed temperature is controlled externally. The final “sliced” design is shown in Figure 6.3 and has a height of 1.8 mm which fits the design specifications. It can be seen that because of the small curvature present, the layers are terraced to mimic a curved surface.



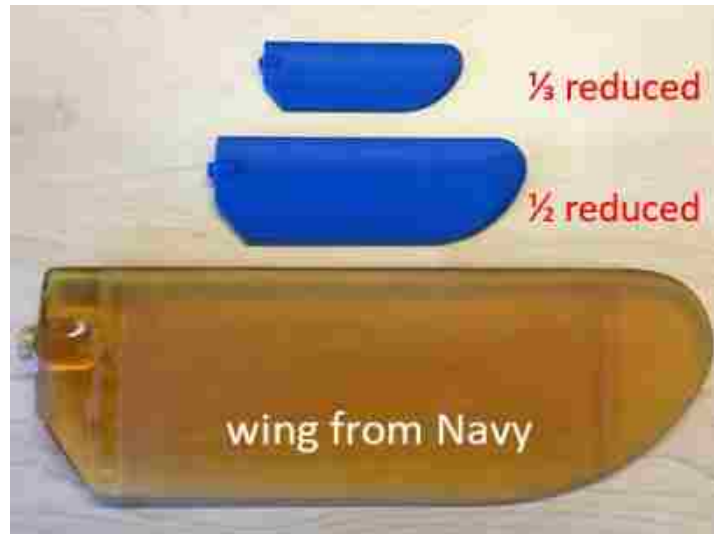


Figure 6.1. Hydrofoil wing given by the Navy, with scaled down 3D printed replications.

Table 6.1. 3D Printer Settings.

<b>Parameter</b>	<b>Value</b>
Extruder Temperature	295°C
Bed Temperature	180°C
Bottom Layer Height	0.2 mm
Layer Height	0.1 mm
Print Speed	10 mm/s



Figure 6.2. CAD of the Hydrofoil-shaped design to be printed.

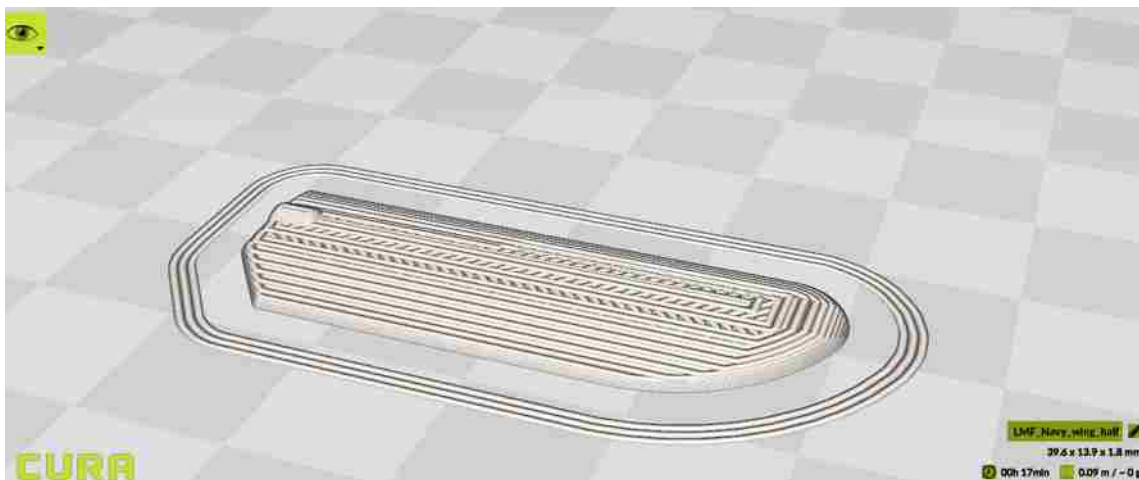


Figure 6.3. Hydrofoil-shaped design prepared for 3D printing using a Slicer program called Cura. The model has been broken down into 18 layers. The overall dimensions of the model is 39.6 mm long, 13.9 mm wide, and 1.8 mm thick.

### 6.3. Printing Process

The printing surface was double-sided Kapton tape (Figure 6.4). Kapton is a high temperature polymer that will not degrade or melt at the required temperatures for ionomers and the tackiness of the tape assists in adhesion for the bottom layer. The total print time was about 20 minutes. The complete print shown in Figure 6.5 was measured to have a thickness of 1.63 mm, which is smaller than the CAD file. This could be because the layers were compacted into each other during the printing process. However, the smaller thickness will assist in the activating process. In Figure 6.6, the layers are slightly visible, but is better viewed using an Optical Microscope. The rounded edge clearly shows the staggered layers to create a curved surface (Figure 6.7). The top layer shows the cross-hatching of the infill (Figure 6.8).

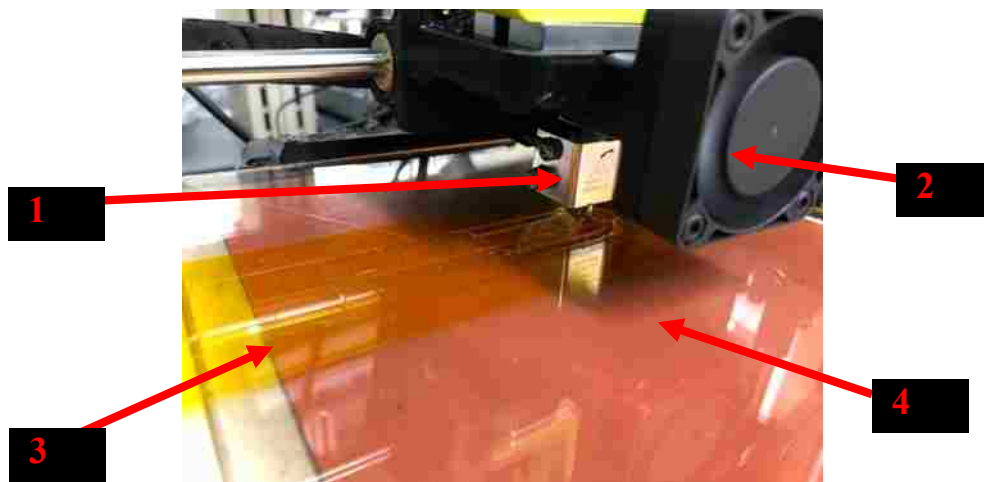


Figure 6.4. First layer of the Hydrofoil printed on double sided Kapton tape, at a nozzle temperature of 295°C and bed temperature of 180°C. 1: Extruder hot end. 2: Cooling fan. 3: Double-sided Kapton tape. 4: Glass bed with heating pad underneath.

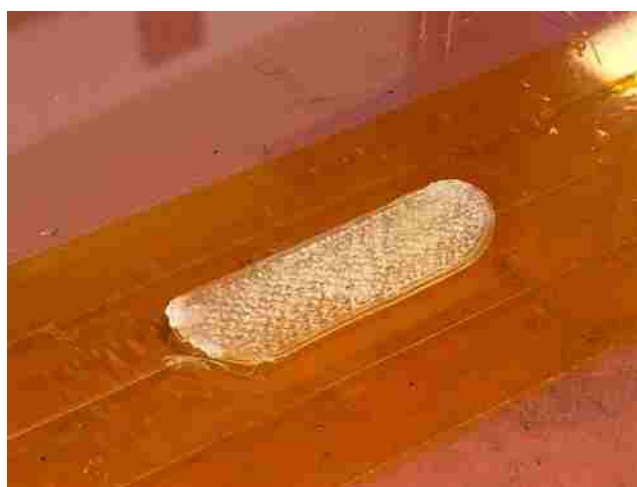


Figure 6.5. Completed precursor Aquivion print of the 3D Printed Hydrofoil-shaped Aquivion.



Figure 6.6. 3D Printed Hydrofoil-shaped Aquivion where the layers are visible, showing a curved surface.



Figure 6.7. Rounded edge of the 3D Printed Hydrofoil-shaped Aquivion viewed with an Optical Microscope at 100x magnification. Each layer can be distinctly seen, creating a rounded edge.



Figure 6.8. Top layer of the 3D Printed Hydrofoil-shaped Aquivion. The layers below can be seen through each layer, showing the cross-hatching infill.

#### **6.4. Activating and plating the Printed-Aquivion Hydrofoil**

Once a sample has been printed, the first step of IPMC fabrication is to “activate” the membrane. This is a hydrolysis process that switches the Sulfonyl Vinyl Ether (SFVE) end group of the precursor form of Aquivion with an acid group, allowing the polymer chains to carry cations and water molecules. The process used in this study bath of 15% wt. of Potassium Hydroxide (KOH, Sigma-Aldrich), 35% wt. of Dimethyl Sulfoxide (DMSO, Sigma-Aldrich), and 50% wt. of Deionized Water (DI Water, Millipore) for three hours. The time needed to complete the process depends on the thickness of the membrane [58]. Since the produced sample was around ~1.63 mm, it was left for three hours. A cleaning process is conducted with 1 M Sulfuric Acid bath (65°C for one hour) and two DI Water baths (60°C for 45 minutes).

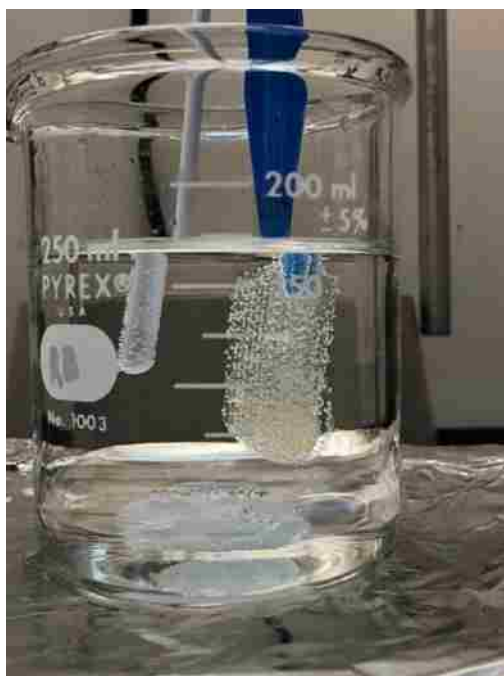


Figure 6.9. Activation process to switch the SFVE end group of the precursor Aquivion to an acid group using a hydrolysis bath of 15% wt. of Potassium Hydroxide, 35% wt. of Dimethyl Sulfoxide, and 50% wt. of DI Water for three hours.

The platinum plating process is made up of four major steps. The first is the cleaning process, which uses 3 wt. % Hydrogen Peroxide ( $\text{H}_2\text{O}_2$ , Sigma Aldrich) to remove chemical impurities, 1 M of Sulfuric Acid ( $\text{H}_2\text{SO}_4$ , Sigma Aldrich) to remove metallic impurities, and two DI Water baths. Next is primary plating, which allows the membrane to sit in 0.02 M of Platinum Salt ( $\text{Pt}(\text{NH}_3)_4\text{Cl}_2 \cdot \text{H}_2\text{O}$ , tetraammineplatinum(II) chloride hydrate, Sigma-Aldrich) for 3.5 hours and then the membrane is put through a reduction process using Sodium Borohydride ( $\text{NaBH}_4$ , Sigma Aldrich). It is followed by a cleaning process. The primary plating process is completed three times. The third step is secondary plating, where the platinum is deposited directly onto the surface. This step uses Platinum Salt, Hydroxylamine Hydrochloride ( $\text{H}_2\text{NOH} \cdot \text{HCl}$ , Sigma-Aldrich), and Hydrazine ( $\text{NH}_2\text{NH}_2 \cdot \text{H}_2\text{O}$ , Sigma-Aldrich). Secondary plating takes four hours and is then followed by a cleaning process. The last step is Ion Exchange using 1 M of Lithium Chloride ( $\text{LiCl}$ ,

Sigma Aldrich). The IPMC is left in the solution for at least 24 hours. Afterwards, the IPMC is ready for testing. For a thorough procedure, the reader is directed to references [12], [46].



Figure 6.10. 3D Printed Hydrofoil-shaped Aquivion during secondary plating.

The completed, 3D-printed Aquivion hydrofoil was left in LiCl to reintroduce ions before testing. Before tests were run, the active hydrofoil was viewed to get a thorough understanding of the printing process. From the top side, it can be seen layers have been adhered well and each layer is distinctly present (Figure 6.11). The brim is not attached very well, but is not important to the printed part. From the bottom side, the bed adhesion issues are easily seen (Figure 6.12). Portions of the first layer were not printed effectively, though there seems to be good adhesion between layers over all. The edges were trimmed using stainless steel scissors to isolate the two electrodes (Figure 6.13). That way, the IPMC will not short during testing. Enough was removed to isolate, but not destroy the small contour of the hydrofoil-shaped IPMC.



Figure 6.11. Top, curved side of the 3D Printed-Aquivion-Hydrofoil-shaped IPMC.



Figure 6.12. Bottom, flat side of the 3D Printed-Aquivion-Hydrofoil-shaped IPMC.

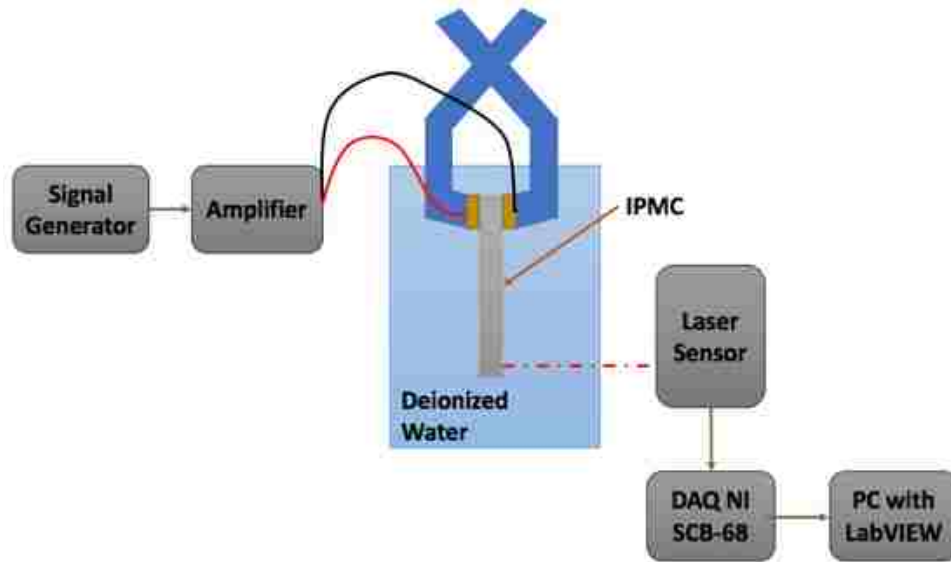




Figure 6.13. Trimmed edges of the 3D Printed-Aquivion-Hydrofoil-shaped IPMC to isolate the two sides.

### **6.5. Performance of the 3D Printed-Aquivion Hydrofoil-shaped IPMC**

Once the 3D Printed-Aquivion-Hydrofoil-shaped IPMC was completely activated, plated with platinum, and checked to have a surface resistance of  $\sim 1$  Ohm, it was tested in actuation and blocking force capabilities. The same set up was used for both tests as those previously discussed. For both tests, a signal generator (SDG1025, Siglent) and power amplifier (LVC-608, AE Techtron) were used. A laser sensor (optoNCDT-1401, Micro-Epsilon) was used to measure the displacement for the actuation and back relaxation tests. A load cell (GSO-30, Transducer Techniques) to measure the blocking force of the IPMC. For all the tests, the data was recorded with a Data Acquisition system (SCB-68, National Instruments) and LabVIEW program. The experimental setups are shown in Figure 6.14 and Figure 6.15.

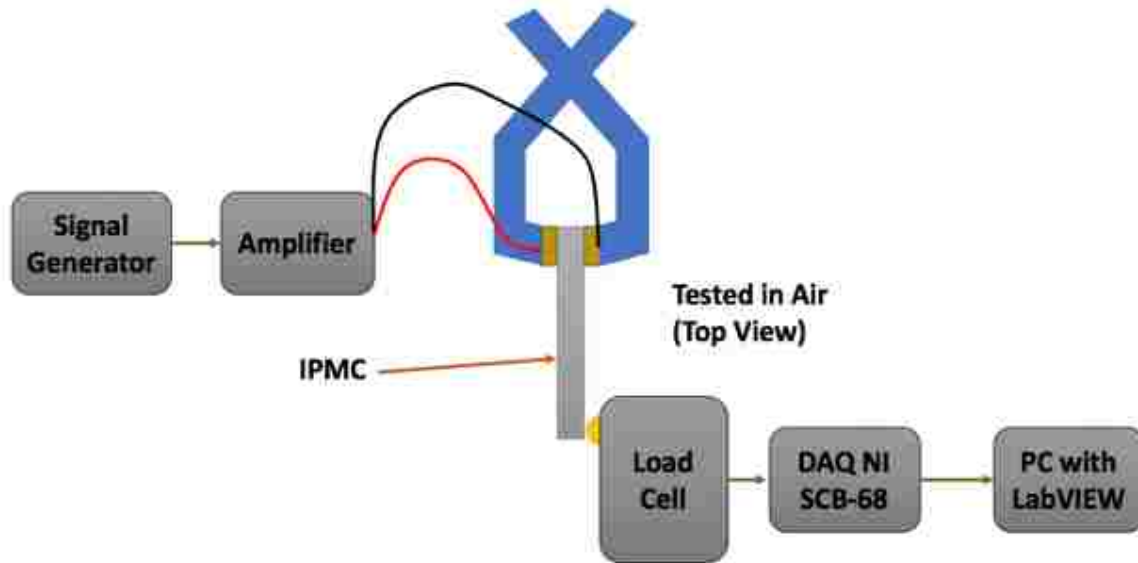


(a)



(b)

Figure 6.14. Experimental setup for actuation tests of the 3D Printed-Aquivion-Hydrofoil-shaped IPMC.



(a)



(b)

Figure 6.15. Experimental setup for measuring blocking force of the 3D Printed-Aquivion-Hydrofoil-shaped IPMC.

Actuation tests were conducted first. Typically, an applied voltage of 3 Volts 500 mHz should be enough to actuate an IPMC. The data recorded data from the 3D Printed-Aquivion-Hydrofoil-shaped IPMC shows some actuation, but it performed better with higher applied voltage (Figure 6.16). The IPMC was also tested with a slow input of 8 Volts 100 mHz, to see how far it would

displace (Figure 6.17). This test showed it could displace to about 3 mm peak-to-peak. In the back-relaxation test, the 3D Printed-Aquivion-Hydrofoil-shaped IPMC was able to displace further with a DC input of -4.5 Volts over 1.6 mm (Figure 6.18). As the 3D Printed-Aquivion-Hydrofoil-shaped IPMC is actuating, it can be seen that the thin edges curve out further than the thick, center portion. It should be noted that the thickest portion of the 3D Printed-Aquivion-Hydrofoil-shaped IPMC is about 1.63 mm, which is significantly larger than any IPMC currently fabricated in the lab. This portion hinders the rest of the 3D Printed-Aquivion-Hydrofoil-shaped IPMC to actuate to its full capability. If the Hydrofoil had been thinner overall, it would be able to actuate more. However, if this design had been made with the Nafion as the base, it may not have been able to actuate as well. The final test was to see the 3D Printed-Aquivion-Hydrofoil-shaped IPMC's blocking force capability. In Figure 6.19, the 3D Printed-Aquivion-Hydrofoil-shaped IPMC was tested with two DC inputs and showed it was able to produce a good blocking force output. This made sense since it is common for thicker IPMCs to produce large blocking force and lower displacements. However, it is important to note that by using Aquivion as the base, it was possible to get both blocking force and some actuation.

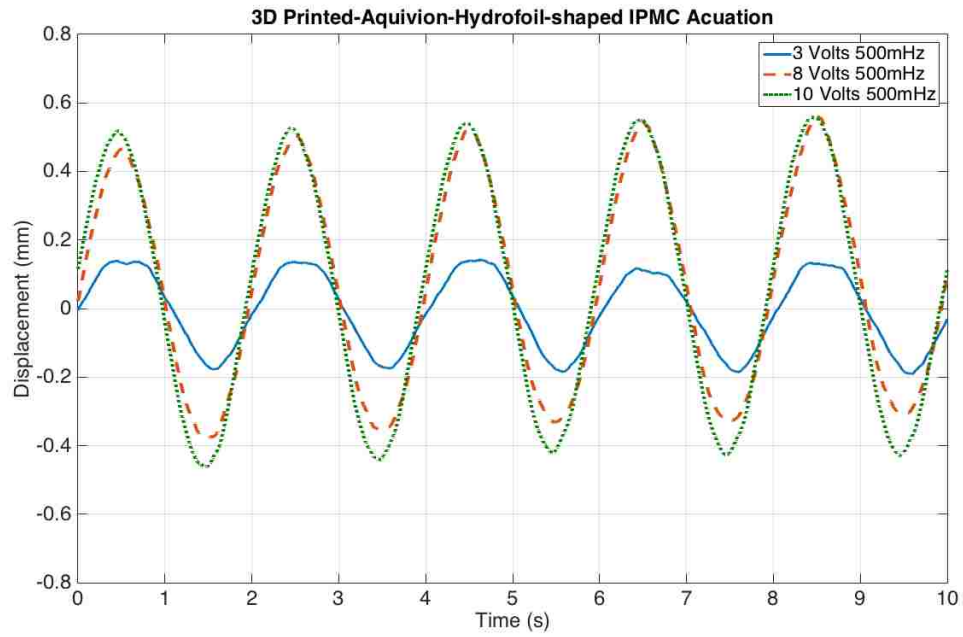


Figure 6.16. Various applied voltages to the 3D Printed-Aquivion-Hydrofoil-shaped IPMC.

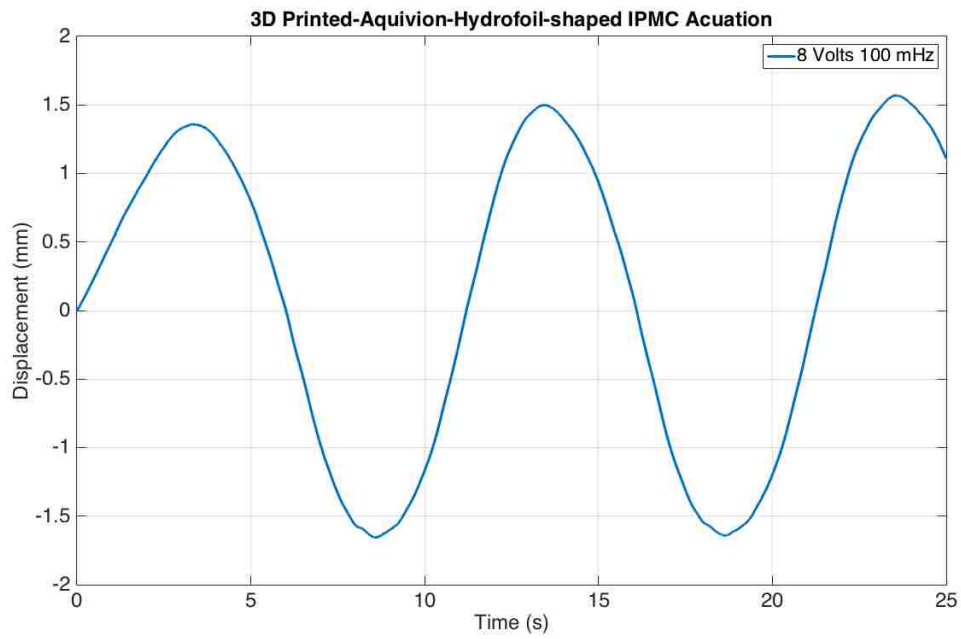


Figure 6.17. Applied voltage of 8 Volts 100 mHz to the 3D Printed-Aquivion-Hydrofoil-shaped IPMC.

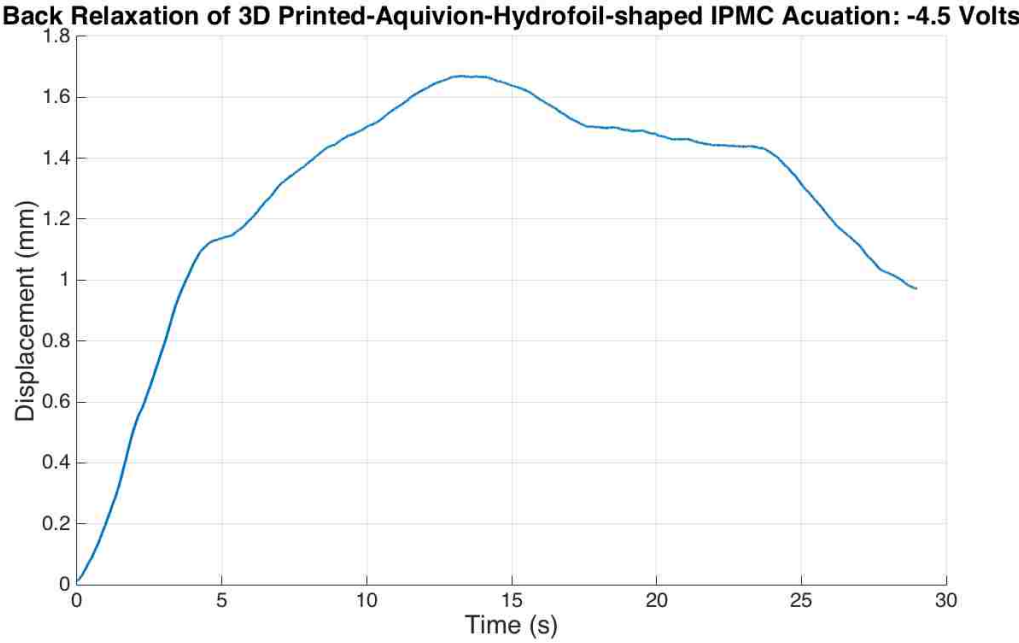


Figure 6.18. Back relaxation data of the 3D Printed-Aquivion-Hydrofoil-shaped IPMC with an applied voltage of -4.5 VDC.

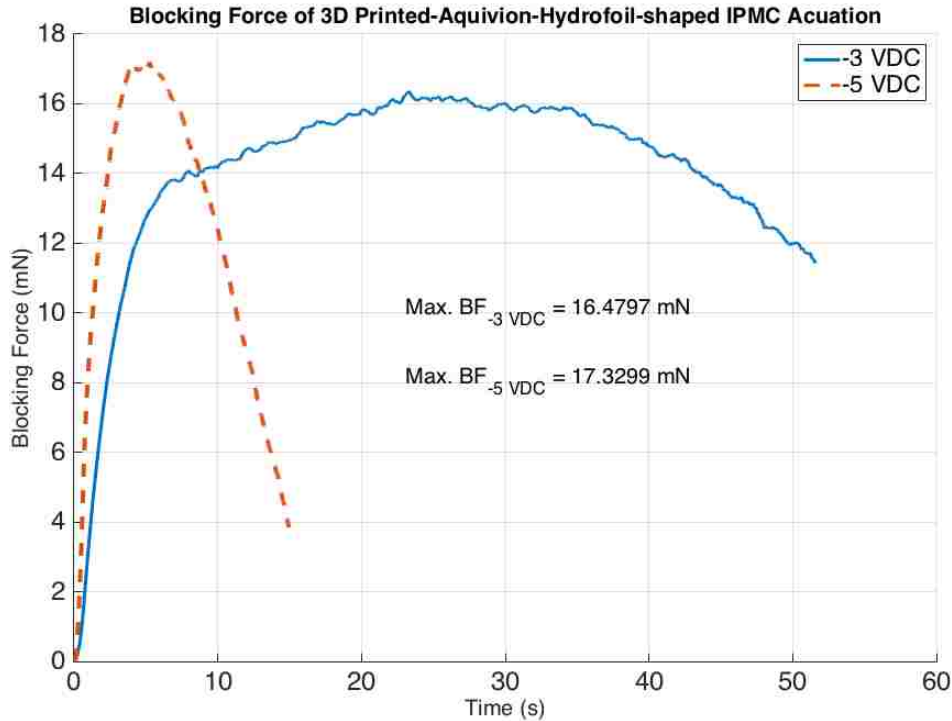


Figure 6.19. Blocking force results for the 3D Printed-Aquivion-Hydrofoil-shaped IPMC measured at the tip.

## 6.6. Conclusions and Future Work

This work has shown that it is possible to 3D print an ionomer shape for the use in IPMCs. A design was made to allow for the best print quality with what is available. The 3D Printed-Aquivion-Hydrofoil-shaped IPMC was successfully activated and plated with platinum. It was tested for its actuation and blocking force capabilities. The 3D Printed-Aquivion-Hydrofoil-shaped IPMC actuated up to 3 mm peak-to-peak and was able to produce good blocking forces. It is important to note that the asymmetry in the cross section hinders the 3D Printed Aquivion IPMC Hydrofoil from being able to actuate to its best ability. The largest thickness present in the cross section is 1.63 mm, which is considerably large compared to other IPMCs tested. The thinner portions of the cross sections show that they could potentially move further, but are limited because

of the thicker portion. It would be interesting to 3D print this same shape in Nafion to compare the performance.

Bed adhesion still needs to be perfected. At the moment, the best prints have been on Polyetherimide (PEI) or on double sided Kapton tape. Though PEI was a very good option, it is not able to withstand the high temperatures needed for Aquivion to stick. Double sided Kapton tape is not very reliable, since the adhesive burns off easily and may not be tacky enough to encourage a good initial layer. The first layer is the most important, since it needs to be a strong base for the rest of the layers to build on top of. Because Aquivion requires a high bed temperature, it is important to find a substrate that is similar to PEI, but can withstand the required high temperatures. One possible option is Polyether ether ketone (PEEK) and is available with adhesive backing from McMaster-Carr. Another point of interest is if a 3D structure is attempted, then it may be of interest to create a temperature controlled environment to continue encourage adhesion between the layers. This is important because as the layers move further away from the heated bed, it will not be at the required temperature to promote adhesion. It will be important to create a uniformly heated environment so prints do not fail.



## **Chapter 7. Conclusion**

A discussion was presented about potentially using Aquivion as a new option for IPMC actuators and sensors. Aquivion has a lower equivalent weight, due to its shorter side chain. This in turn allows for a higher ionic conductivity, potentially improving the IPMC performance. Theory was discussed to understand ion transport and its relationship to equivalent weight. An existing COMSOL model was used to verify the effects of the ionic conductivity and then verified with experimental tests. Aquivion was shown to improve the performance of the IPMC in both the COMSOL model and experimental testing.

This work provides a thorough material characterization of both Nafion and Aquivion in order to efficiently use them in different fabrication processes. The membrane form of ionomers was analyzed, but is not useful in thermal based processes, since it cannot melt. The precursor form can be melt, but not much information is available. Some time was taken to test the precursor forms of Nafion and Aquivion to understand their behavior once they begin to melt. It was shown that precursor Nafion is soft at room temperature, has a lower viscosity curve, and exhibits more liquid-like behavior. Precursor Aquivion on the other hand is significantly stiffer at room temperature, has a higher viscosity curve, and exhibits less liquid-like behavior. Because of these differences, precursor Aquivion is more “moldable” than precursor Nafion and could potentially be easier to work with in processes such as filament extrusion, hot pressing, and 3D printing. A complete study of the various material characteristics is provided for the field.

Spray-painting Nafion Water Dispersion was studied to create intricate shapes. It was shown it was possible to create different shapes by simply using vinyl-sticker stencils to produce the

thickness required. The samples were very similar to off-the-shelf membranes, other than being slightly stiffer. IPMCs were made using the painted-Nafion membranes and it was shown that the performance was not as good as traditionally made IPMCs, but this was mainly caused by the swelling effect present in painted-Nafion samples. This can be counteracted by producing membranes that are half of the desired thickness to allow for swelling to occur.

3D printing Aquivion precursor pellets was explored. Filament was extruded to be used in a slightly modified off-the-shelf 3D printer. It was shown that it is possible to print Aquivion precursor pellets using a set of specific printer settings. From there, printed-Aquivion samples were activated and plated with platinum. They were compared with a similarly dimensioned Nafion-based IPMCs and tested for back relaxation, blocking force, oscillatory actuation, and sensing. In all of the tests, the printed-Aquivion samples outperformed the Nafion-based IPMC. It was shown that the printed-Aquivion samples can overcome their large thickness to still produce large actuation and large blocking force.

To further explore 3D printing, a 3D Printed-Aquivion-Hydrofoil-shaped IPMC was designed and printed. It had an asymmetric cross section (thickest portion was measured to be 1.63 mm) and curved features. It was activated by hydrolysis and plated with platinum. The 3D Printed-Aquivion-Hydrofoil-shaped IPMC was tested for actuation and blocking force. It actuated up to 3 mm peak-to-peak. Its blocking force output was good, because of its large thickness.

## **Chapter 8. Future Work**

Though a baseline understanding of how Aquivion has a higher ionic conductivity has been studied, it would be interesting to further explore the underlying physics of ion transport. It would be important to know if there are any other differing values between Nafion and Aquivion to more accurately model them in COMSOL. This could be done by studying the cation concentration and the dielectric permittivity experimentally.

It would be interesting to attempt spray-painting Aquivion water dispersion. There are higher weight percent available on the market, some even made with purely water as the solvent. One thing to look for would be the swelling effect that was present in the painted-Nafion membranes. By using Aquivion, it could be possible to produce high-performance painted IPMCs that could overcome the swelling effect (if present).

3D printing can be moved towards pseudo-3D printing first. However, it is important to note that any design that is relatively tall could potentially cause problems. As the layers move further away from the heated bed, they will be at a much lower temperature than the extruder nozzle. This may cause issues in layer adhesion. One way to solve this is to provide a heated chamber to ensure the environment is warm enough to encourage layer adhesion. Designs that have overhang will need support. Introducing a secondary, cheaper plastic to act as support material could potentially contaminate the Aquivion sample, causing it to not be able to actuate. Using Aquivion as its own support material could be an option, but a lot of material could be wasted. Making designs that use minimal supports could solve this issue. The substrate of the heated bed could also be explored. One possible option is Polyether ether ketone (PEEK), which is a high temperature polymer that

could withstand the required temperature. The first layer of any print is extremely important so it is imperative to promote a strong initial layer.

The next step for the 3D Printed-Aquivion-Hydrofoil-shaped IPMC is to attempt to make a complete Hydrofoil-shape. This will provide users to have a completely active Hydrofoil shape. Measurements can be taken by testing the 3D Printed-Aquivion-Hydrofoil-shaped IPMC in a flow tank to see its performance as an active hydrofoil.

## Appendix A. Permission to use portion of a book chapter in Chapter 1 from CRC Press



Taylor & Francis Group, LLC

### GRATIS PERMISSION GRANT

March 15, 2018

Sarah Trabia  
351 Barletta Ave  
Las Vegas, NV 89123

Dear Sarah Trabia:

Taylor & Francis hereby grants you permission to

re-print Chapter 15: Guidelines for making Ionic Polymer-Metal Composite (IPMC) materials as artificial muscles by advanced manufacturing methods: State-of-the-Art on pages: 5-7

from *Advances in Manufacturing and Processing of Materials and Structures*

ISBN: 9781138035959

in your dissertation titled "Comprehensive Study of Spray-Painting and 3D Printing Fabrication Methods for Nafion® and Nafion® Equivalents in Ionic Polymer-Metal Composite Actuators and Sensors"

to be published by the University of Nevada, UNLV Theses, Dissertations, Professional Papers, and Capstones in May, 2018.

Permission is for world rights in the electronic format in the English language.

1. Permission is given on a one-time, **nonexclusive** basis. Future uses of the material must be applied for.
2. Each copy containing our material must bear a credit line in the following format (insert information as appropriate):

**Copyright (Insert © Year) From (Insert Title) by (Insert Author/Editor Name). Reproduced by permission of Taylor and Francis Group, LLC, a division of Informa plc.**

3. Electronically, this material may be displayed only and not accessible for users to print or download. In circumstances where this option is not available, the following citation must also be included:

**This material is strictly for personal use only. For any other use, the user must contact Taylor & Francis directly at this address: & Francis directly at this address: [permissions.mailbox@taylorandfrancis.com](mailto:permissions.mailbox@taylorandfrancis.com). Printing, photocopying, sharing via any means is a violation of copyright.**

4. This permission extends only to the usage specified above. Any other use (including re-use) requires additional permission from the publisher.
5. It is understood and contractually agreed upon that Taylor & Francis is the Rightsholder to this material.

Sincerely,

**Diana Taylor**

Permissions Coordinator | US Books Permissions Department

6000 Broken Sound Parkway NW, Suite 300 • Boca Raton, FL 33487  
Tel: (561) 994-0555 • Fax: (561) 241-7856  
[www.taylorandfrancis.com](http://www.taylorandfrancis.com)

an informa business

## Appendix B. Permission to reuse figures in Chapter 2



**Confirmation Number: 11696472**

### **Citation Information**

**Order Detail ID: 70979122**

**Smart Materials and Structures by IOP Publishing. Reproduced with permission of IOP Publishing in the format Thesis/Dissertation via Copyright Clearance Center.**

---

## Appendix C. Considered Multi-Physics for IPMC Actuators and COMSOL Procedure

When a voltage potential is applied to the surface of an IPMC, the cations and water molecules present will be attracted to the negatively charged side. This particular side of the IPMC will swell and force a bending motion. The motion of the cations can be controlled by using a sinusoidal or rectangular input, producing an oscillatory actuation. This phenomena is called electro-mechanical effect.

The underlying physics of how IPMCs work, in both the mechano-electrical and electro-mechanical effects, is the ionic current and the non-zero spatial charging within the electrodes [47], [125], [126]. To describe the ionic current, Nernst-Planck equation can be utilized:

$$\frac{\partial C}{\partial t} + \nabla \cdot (-D\nabla C - z\mu FC\nabla\phi - \mu C\Delta V\nabla P) = 0 \quad (12)$$

where  $C$  is the cation concentration,  $\mu$  is the mobility of the cations ( $\mu = \frac{D}{RT}$ ),  $D$  is the diffusion constant,  $F$  is the Faraday constant,  $z$  is the charge number,  $\Delta V$  is the molar volume that quantifies the cation hydrophilicity,  $P$  is the solvent pressure, and  $\phi$  is the electric potential in the polymer. Equation (12) includes the concentration gradient ( $\nabla C$ ), electric potential gradient ( $\nabla\phi$ ), and solvent pressure gradient ( $\nabla P$ ). By analyzing the cross-section of an IPMC, the direction of the gradients can be predicted based on the applied voltage (Figure C.1). The cation concentration is calculated with respect to time based on the three gradients present. The concentration gradient ( $\nabla C$ ) shows that this gradient is directly driven by the diffusion constant of the material. A higher diffusion constant would imply a higher concentration gradient. The electric potential gradient ( $\nabla\phi$ ) bring in the mobility of the cations and the applied potential to the IPMC. It should be noted that the diffusion constant is present in the mobility equation and has a potential effect on this term as well. The solvent pressure gradient ( $\nabla P$ ) is the due to the local strain in the polymer. However,

for the case of IPMC's electro-mechanic behavior, it is assumed that  $|F\nabla\phi| \gg |\Delta V\nabla P|$ , so the solvent pressure gradient is cancelled from the Nernst-Planck equation [47].

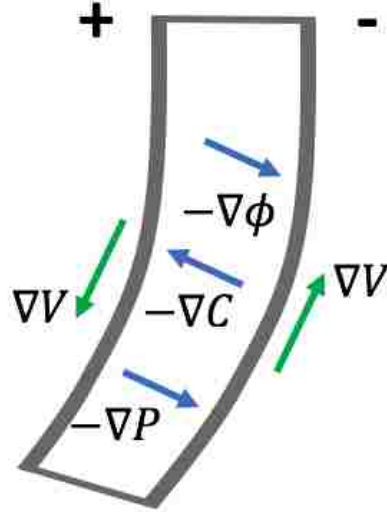


Figure C.1. Cross-section of an IPMC with an applied voltage and the effects on the gradients present in the smart material. It should be noted that  $\nabla V$  is the applied voltage potential. Figure redrawn from [47].

In order to accurately describe the potential gradient, it best to use Poisson's equation, which has been used widely to accurately understand the potential gradient due to charge density:

$$-\nabla^2\phi = \frac{\rho}{\varepsilon} \quad (13)$$

$\rho$  is the charge density:

$$\rho = F(C - C_a) \quad (14)$$

where  $C_a$  is the anion concentration.  $\varepsilon$  is the effective dielectric permittivity:

$$\varepsilon = \varepsilon_o\varepsilon_r \quad (15)$$



where  $\varepsilon_o$  is the dielectric permittivity in a vacuum ( $\varepsilon_o = 8.85 \times 10^{-12} \text{ Fm}^{-1}$ ) and  $\varepsilon_r$  is the relative permittivity. The anion concentration and the local volumetric strain ( $dV$ ) can be related to each other.  $dV$  is described by:

$$dV = \nabla \cdot \mathbf{u} \quad (16)$$

where  $\mathbf{u}$  is the local displacement vector. The anion concentration is:

$$C_a = C_o(1 - dV) \quad (17)$$

where  $C_o$  is the initial cation or anion concentration.

To calculate the displacement due to the applied voltage, the charge density must be related to the internal stress within the polymer. First, Newton's Second Law is defined as:

$$\rho_p \frac{\partial^2 \mathbf{u}}{\partial t^2} - \nabla \sigma = \mathbf{F}, \quad (18)$$

where  $\rho_p$  is the material's density and  $\mathbf{F}$  is the body force. The first term is the dynamic portion, including the acceleration of the material. The second term is stress gradient within the material.  $\mathbf{F}$  is the caused by the charge density due to the applied potential so it can be said that the induced stress inside the polymer is proportional to the charge density at the boundaries between the electrodes and the polymer [125]:

$$\sigma(\pm h, z, t) = \alpha \rho(\pm h, z, t). \quad (19)$$

Equation (19) can be related to the bending moment of the IPMC:

$$\sigma(\pm h, z, t) = \frac{\pm h M(z, t)}{I} \quad (20)$$

where  $I$  is the moment of inertia ( $I = \frac{2}{3W h^3}$ ).

The calculation first begins with an input, in this case, the applied voltage. The voltage waveform is determined by the user, depending on their application. From there, it is input in the Poisson-

Nernst-Planck equation and the equation is solved to find the cation concentration over time. The resulting charge density is then correlated with an internal stress. Then, the solid mechanics portion is solved with the calculated stress and the resulting output is solved: displacement. A flow chart is presented with the steps briefly described (Figure C.2).

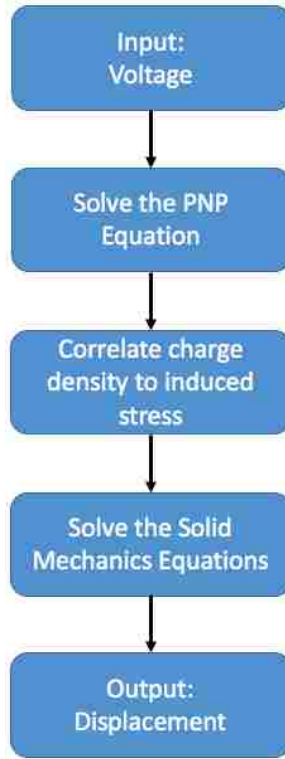


Figure C.2. Solution flow chart for the sets of equations for IPMC modeling.

### **COMSOL Model Procedure**

The model is built in COMSOL 5.2a and it combines the various physics involved to predict the motion of the IPMC with the applied voltage. To do this, the user will start with 2 Components: one in 1D and the other in 2D. The physics for the 1D component are Transport of Diluted Species, Electric Currents, and General Form PDE. This will model the Poisson-Nernst-Planck (PNP) equation, calculating the cation current with the applied voltage potential. The physics for the 2D

component is Solid Mechanics. In this component, the cation flux is converted to an applied boundary load. The reasoning behind modeling the PNP equation in 1D is that the cation current only varies within the thickness of the IPMC, but stays relatively constant along the length. So, by modeling one line through the thickness of the IPMC and understanding the flow of cations in that line, those values can be mapped throughout the rest of the IPMC along the length. This has shown to significantly reduce computational time from ~30 minutes to 1 minute in some cases. The “Study” for this model is “Time Dependent.”

The next step is to fill out the Global Parameters. This will make the setup for the rest of the model easier, as the user can easily change parameters to run different tests quickly. Most of these parameters were found by Pugal *et al.* [127]. Under the “Global Definitions” drop down menu, find “Parameters” and fill in the following parameters as shown in Figure C.3. The descriptions do not need to be added, but can be to help find the correct parameter to change later on.

Name	Expression	Value	Description
alpha	1000 [N/C]	1000 V/m	Electromechanical coupling coefficient
amp	1	1	Voltage Amplitude in waveform
buff_mesh	500	500	Elements in buffer region
clamp	10[mm]	0.01 m	Clamp length
conc_cat...	1200 [mol/m^3]	1200 mol/m <sup>3</sup>	Cation concentration
D_cat	7e-11 [m^2/s]	7E-11 m <sup>2</sup> /s	Diffusion coefficient
density	2000[kg/m^3]	2000 kg/m <sup>3</sup>	IPMC density
epsilon	2[mF/m]	0.002 F/m	Dielectric permittivity
Faraday	96485.3415 [s*A/mol]	96485 C/mol	Faraday's Constant
freq	1	1	Frequency of waveform
length	51.07 [mm]	0.05107 m	Length of IPMC
mem_buff	2*t_e	1.6E-5 m	Width of the buffer region
mem_mesh	250	250	Elements in bulk membrane
p	1	1	Parameter sweep variable
Poisson	0.49	0.49	Poisson's Ratio of IPMC
R	8.31 [J/(mol*K)]	8.31 J/(mol·K)	Universal Gas Constant
simtime	8	8	Simulation time
ster	0	0	Steric effect
T	293 [K]	293 K	Temperature
t_e	0.008[mm]	8E-6 m	Electrode thickness
t_p	0.57 [mm]	5.7E-4 m	Mmbrane thickness
timestep	0.05	0.05	Time step in simulation
width	9.94 [mm]	0.00994 m	Width of IPMC
Young	249 [MPa]	2.49E8 Pa	Young's Modulus of IPMC
z_cat	1	1	Charge number

Figure C.3. Parameters needed for the IPMC COMSOL model.

Next, the “Variables” needs to be set up. If the “Variables” option is not showing under “Global Definitions,” right click on “Global Definitions” and add “Variables.” In this tab, add the following variables shown in Figure C.4. For “Vpos,” “wv1” refers to the waveform that will be set up next. Right click on “Global Definitions” and add “Waveform.” Fill out the required information based on Figure C.5. Now, the shape of the applied voltage can be easily and quickly changed. The amplitude and frequency of the waveform can be modified in the “Parameters” tab.

Name	Expression	Unit	Description
my_cat	D_cat/(R*T)	s·mol/kg	Mobility
Vpos	wv1(t*1 [1/s])		Applied Voltage Potential
Vneg	0		Applied Voltage Potential

Figure C.4. Variables for the IPMC COMSOL model.

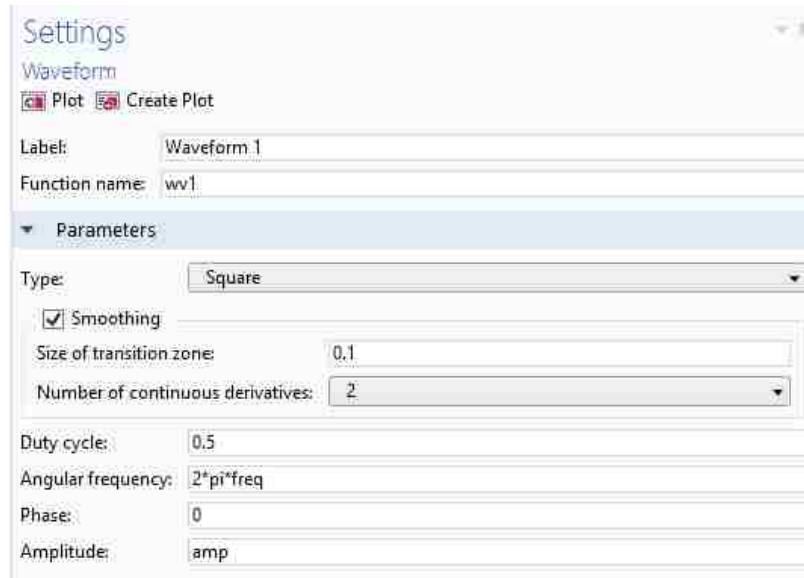


Figure C.5. Waveform to apply different kinds of voltage potential.

Under each component, the user will find a “Geometry” tab. First, the 1D component will be built. To define the thickness of the IPMC, it has been broken into five intervals (Figure C.6). For the first interval, right click on “Geometry” and add “Interval.” Label it “Pt 1” and set the “Left endpoint” to “0” and the “Right endpoint” to “t\_e.” Repeat these steps to create four more intervals by following the dimensions in Table C.1. When all have been added, click “Build All Objects.”

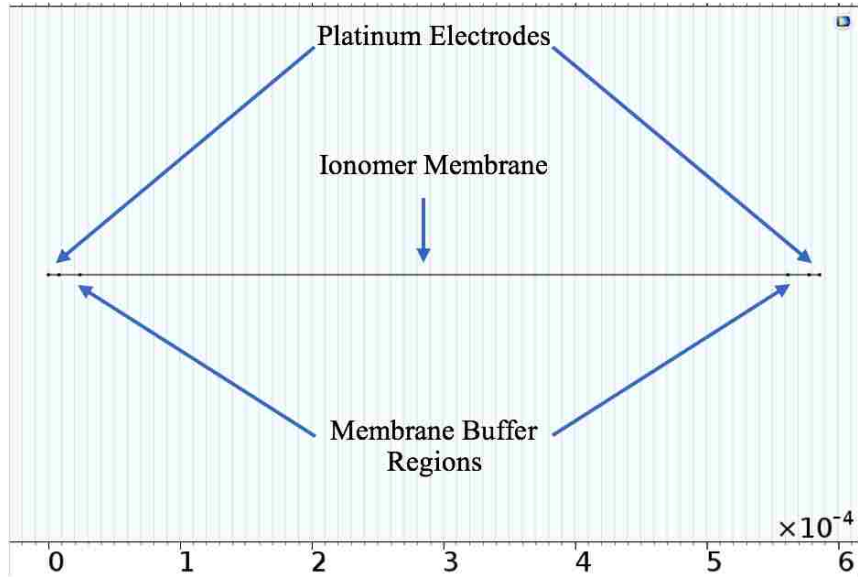


Figure C.6. 1D Component geometry breakdown.

Table C.1. Dimensions for the intervals in the 1D component geometry.

Interval #	Label Name	Left endpoint	Right endpoint
1	Pt 1	0	$t_e$
2	Membrane	$t_e$	$t_p+t_e$
3	Pt 2	$t_p+t_e$	$t_p+2*t_e$
4	Membrane buffer 1	$t_e$	$t_e+mem\_buff$
5	Membrane buffer 2	$t_e+t_p-mem\_buff$	$t_p+t_e$

For the 2D component (Figure C.7), four rectangles will be used to create the cross section of an IPMC. Right click on “Geometry” under the 2D component and add “Rectangle.” Label it “Membrane” and add the width and height found in Table C.2. Under the “Position” tab, be sure it is set to “Corner” and add the coordinates listed in Table C.2 for Rectangle 1. Repeat these steps for the three other rectangles. When they have all been set up, click “Build All Objects.”

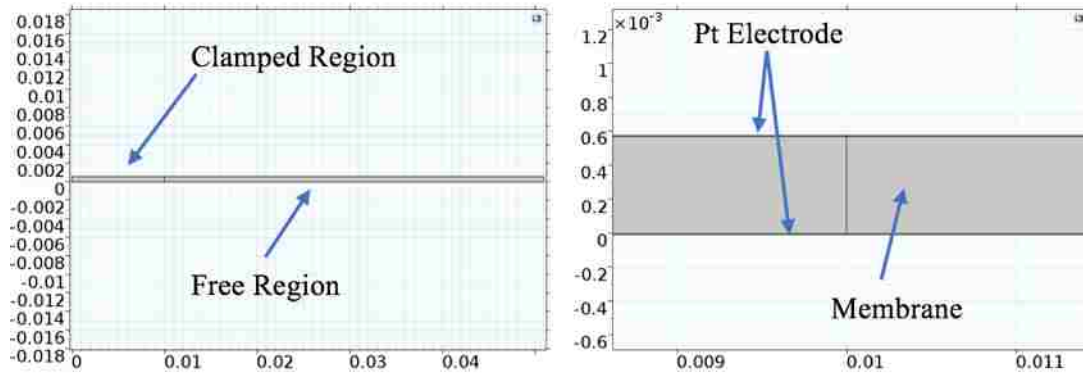


Figure C.7. 2D Component geometry breakdown.

Table C.2. Dimensions for the rectangles used to build the 2D component.

Rectangle #	Label	Width	Height	x	y
1	Membrane	length	t <sub>p</sub>	0	0
2	Electrode 1	length	t <sub>e</sub>	0	-t <sub>e</sub>
3	Electrode 2	length	t <sub>e</sub>	0	t <sub>p</sub>
4	Clamped Region	clamp	t <sub>p</sub> +2*t <sub>e</sub>	0	-t <sub>e</sub>

Now that the geometry for both components has been completed, the next step is to define the boundary conditions for the various physics. First, the 1D component will be set up. Under the 1D component, right click on “Definitions” and add “Variables.” Here is where resistivity and cation concentration will be introduced (Figure C.8). Right click on “Definitions” and add “Linear Extrusion”. This is what is used to map the PNP to the 2D domain. Follow Figure C.9 to set it up correctly.

Variables			
Name	Expression	Unit	Description
resist	$1/(1.1125[\text{ohm}^{-1}])^2[\text{cm}]$	$\Omega \cdot \text{m}$	
rho	$\text{Faraday} * (\text{c}2 - \text{conc\_cat\_mol})$	$\text{C}/\text{m}^3$	

Figure C.8. Variables for 1D component.

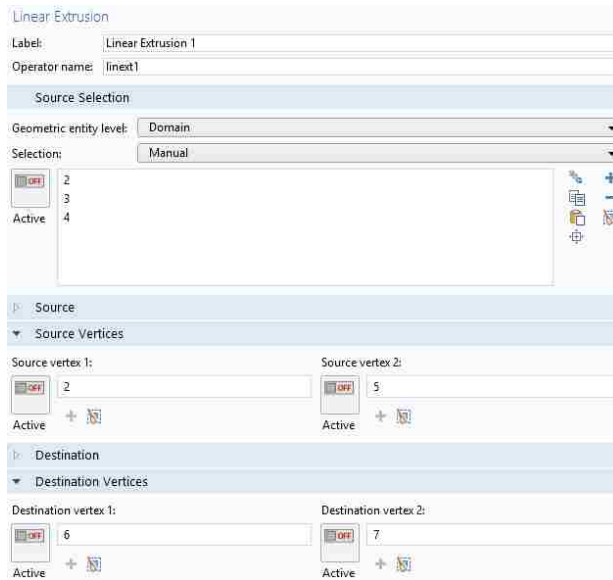


Figure C.9. Linear extrusion set up to map the PNP results to the 2D domain.

Next, the “General Form PDE” will be set up. Click on “General Form PDE” and select domains 2, 3, and 4 (Figure C.10). Under units, be sure that the “Dependent variable quantity” is set to “Electric potential (V)” and “Source term quantity” is set to “None.” Under “General Form PDE,” find “Conservative Flux” and add “-u3x.” Under “Source Term,” add “rho/epsilon.” “Damping or Mass Coefficient” and “Mass Coefficient” will be set to 0. For “Initial Values,” both u3 and its derivative will be set to 0. Right click on “General Form PDE” and add “Dirichlet Boundary Condition” and set “r” to “V2.” This completes the conditions needed for “General Form PDE.”



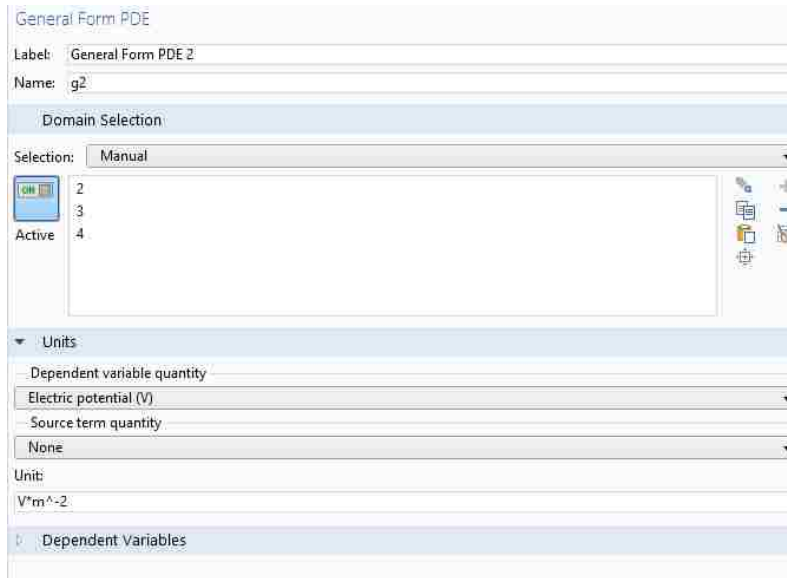


Figure C.10. Settings for General Form PDE.

Click on “Electric Currents” and select domains 1 and 5 (Figure C.11). For the “Cross-Section Area,” input “width\*length.” Under “Current Conservation,” ensure that the electrical conductivity is “user defined” and set to “1/resist.” The relative permittivity should also be “user defined” and set to “1.” Under “Initial Values,” the electric potential should be set to “0.” Right click on “Electric Currents” and add “Electric Potential.” Select Point 6 and set  $V_0$  to “Vpos.” Add another “Electric Potential”, select Point 1, and set  $V_0$  to “Vneg.” This represents the applied voltage potential.

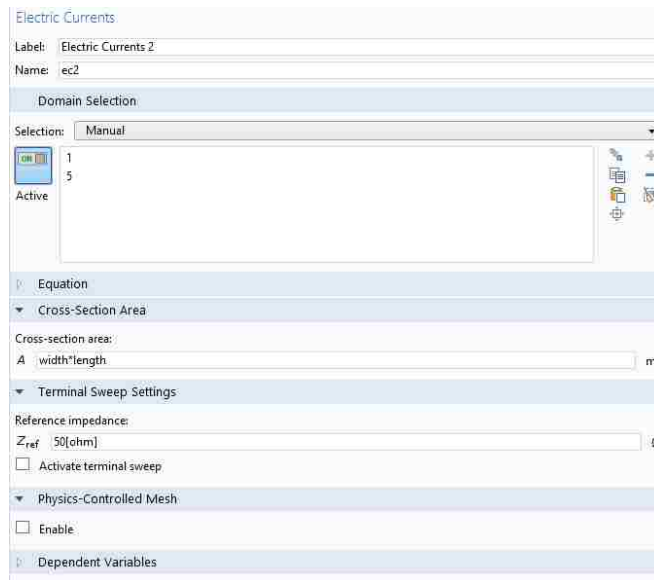


Figure C.11. Settings for the Electric Currents.

The last physics to set up for 1D is the Transport of Diluted Species. Select domains 2, 3, and 4 (Figure C.12). For the “Transport Mechanics,” ensure that the “Migration in electric field” is checked. Under “Transport Properties,” set “Electric potential” to “u3” and “Temperature” to “T.” For “Diffusion,” set Material to “None” and for the diffusion coefficient, it should be set to “User defined” and the value to  $p*D_{cat}*((1-2*ster)*conc_{cat\_mol})/(conc_{cat\_mol} - ster*(conc_{cat\_mol}+c2))$ . Here is where the scaling parameter “p” for the parameter sweep is first introduced. The reader will also note that the parameter “ster” is included, which is different from previous COMSOL models presented in literature. The parameter “ster” implements the steric effect of the cations, simulating the stacking effect of the cations during actuation. For this model, “ster” is set to “0” in the Parameters list, so this effect is not included in the simulation, but is available for the reader to implement for their own studies. For the “Migration in Electric Field” section, “Mobility” is “user defined” and set to  $p*my\_cat$ . Again, the scaling factor is introduced

to be able to run the parameter sweep. Finally, the “Charge number” is set to “z\_cat.” This completes the setup for the 1D component.

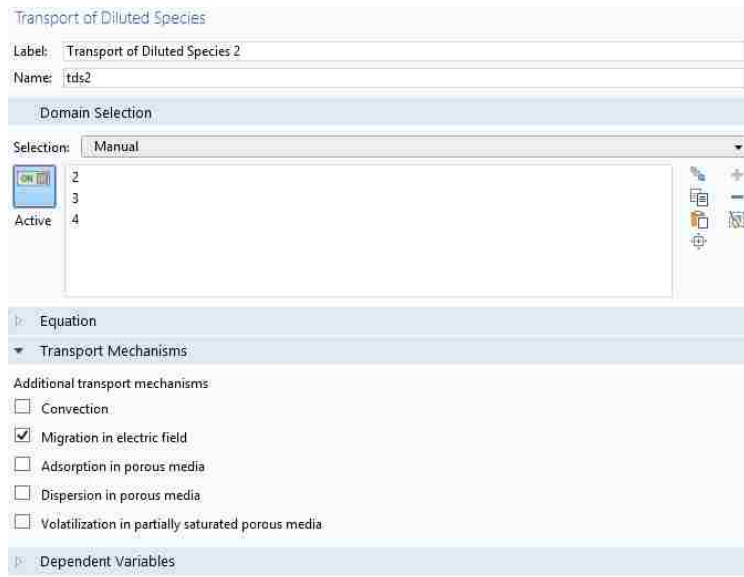


Figure C.12. Settings for Transport of Diluted Species.

The only physics to set up for the 2D component is the Solid Mechanics. First, it is important to set up the variable needed to tie the two physics together. Under “Definitions,” input a variable called “F\_alpha” equaling to “alpha\*comp3.linext1(comp3.rho)”. Please note that in our model, “comp3” refers to our 1D component. Please refer to your component list to see what you should be using. Figure C.13 shows the settings required to use the Solid Mechanics module. Select Domains 2, 4, 5, and 6 and ensure that “plane strain” is selected under “2D Approximation.” Under “Thickness,” set the value to “width.” For “Linear Elastic Material,” the various material properties of IPMCs should be added. Set the “Solid Model” to “Isotropic” and “Specify” to “Young’s modulus and Poisson’s ratio.” Set “Young’s Modulus,” “Poisson’s Ratio,” and “Density” to “Young,” “Poisson,” and “density,” respectively.

Variables			
Name	Expression	Unit	Description
F_alpha	$\alpha * \text{comp3.linext1}(\text{comp3.rho})$	N/m <sup>E</sup>	

Figure C.13. Variables for the 2D component.

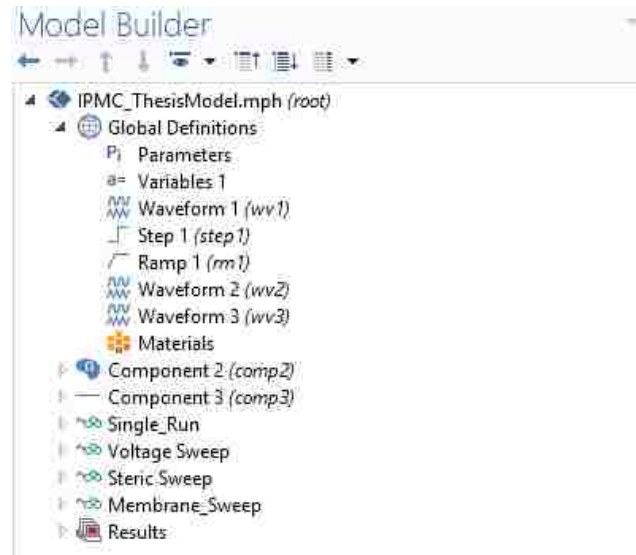


Figure C.14. Component list for this specific model.

Right click on “Linear Elastic Material” and add “External Stress”. This particular force loading creates a more accurate actuation behavior, since it evenly distributes the force to every element. Under the “External Stress,” ensure “Stress input” to “Stress tensor (Material).” For the “External stress tensor,” set it to “User defined” and set the value “-F\_alpha\*width” and “Isotropic.” Click on “Initial Values” and ensure that every value is set to “0.” Right click on “Solid Mechanics” and add “Fixed Constraint.” Select boundaries 3, 8, 10, and 12. This completes the setup of the Solid Mechanics Module.

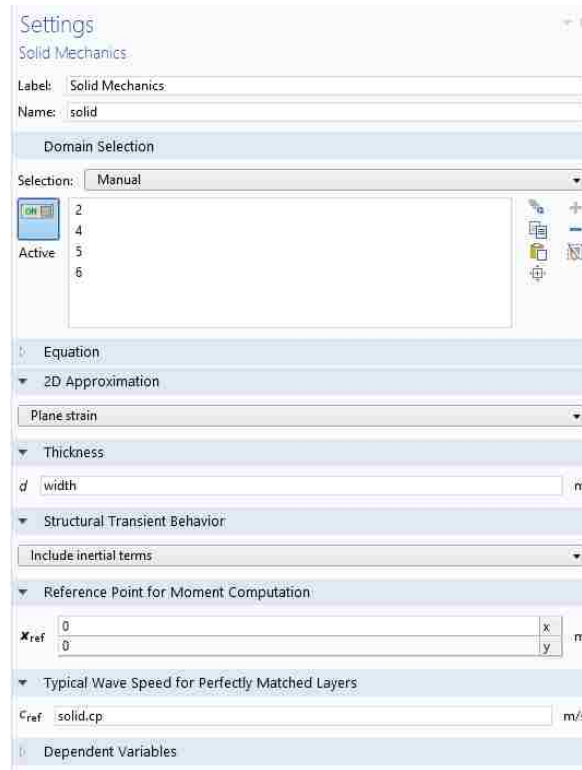


Figure C.15. Settings for Solid Mechanics.

With all of the boundary conditions set, the mesh now needs to be created for each component. First starting with the 1D component, right click on “Mesh” and add “Edge.” Right click on “Edge” and add “Distribution.” Here, select domains 1 and 5 and set the “Distribution properties” to “Fixed number of elements.” Set this value to “2.” Again, right click on “Mesh” and add “Edge,” then right click on “Edge” and add “Distribution.” Select domain “3” and set “Distribution properties” to “Predefined distribution type.” For “Number of elements,” set the value to “mem\_mesh.” The “Element ratio” is set to “5.” Be sure that “Distribution method” to “Geometric sequence” and to check “Symmetric distribution.” Add the last “Distribution” the same way as the previous ones. Select domains 2 and 4 and set the “Distribution properties” to “Fixed number of elements.” Set

this value to “buff\_mesh.” Once everything has been added, click “Build All.” This completes the mesh construction for the 1D component (Figure C.16).

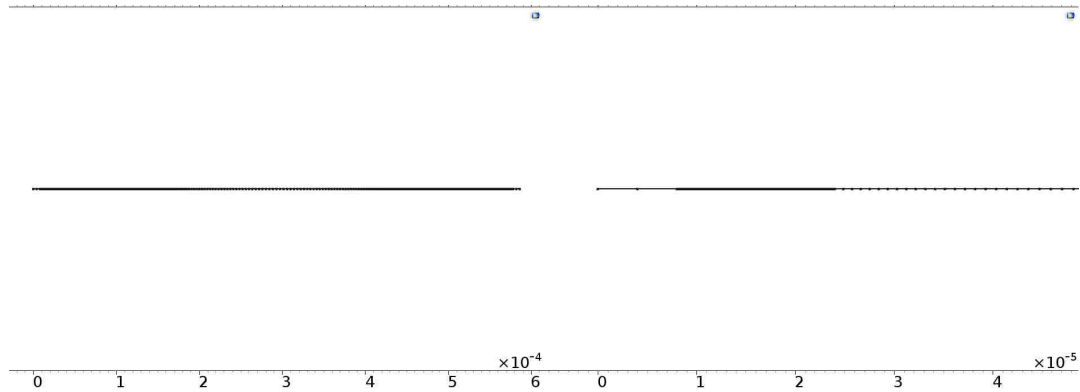


Figure C.16. Mesh for 1D Component (left) and zoomed in view of mesh (right).

The mesh for the 2D component is a similar process. Click on “Size” and set the “Predefined” to “Extremely fine.” Right click on “Mesh” and add “Edge,” then right click on “Edge” and add “Distribution.” Select all of the boundaries. Set “Distribution properties” to “Predefined distribution type.” For “Number of elements,” set the value to “20.” The “Element ratio” is set to “5.” Be sure that “Distribution method” to “Arithmetic sequence” and to check “Symmetric distribution.” Add another “Distribution” the same way as previously. Set “Distribution properties” to “Fixed number of elements.” For “Number of elements,” set the value to “2.” Right click on “Mesh” and add “Mapped,” then right click on “Mapped” and add “Size.” Under “Mapped,” set the “Geometric entity level” to “Remaining.” Under “Size,” set the “Geometric entity level” to “Entire Geometry.” Set the “Calibrate for” to “General Physics” and “Predefined” to “Extra fine.” Once everything has been added, click “Build All.” This completes the mesh construction for the 2D component (Figure C.17).

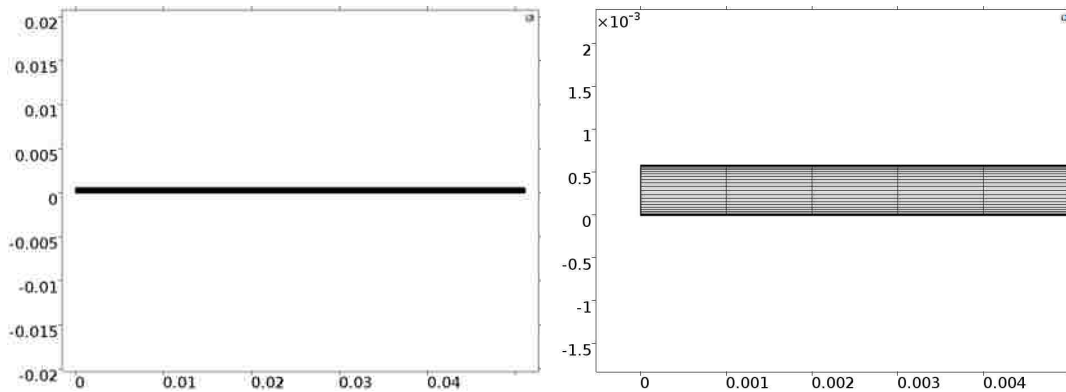


Figure C.17. Mesh for 2D Component (left) and zoomed in view of mesh (right).

To set up a parameter sweep, right click on “Study” and add “Parametric Sweep.” Under “Study Settings,” add a new row and select “p.” In the “Parameter value list,” indicated which values to be tested. For this model, 1 and 2.2 are listed to simulate Nafion and Aquivion, respectively (Figure C.18). Click on “Step 1: Time Dependent” and set up the simulation time. For “Times,” set the “Time unit” to “s” and input “range(0,timestep,simtime)” for “Times.” Be sure that all of the modules are checked (Figure C.19).

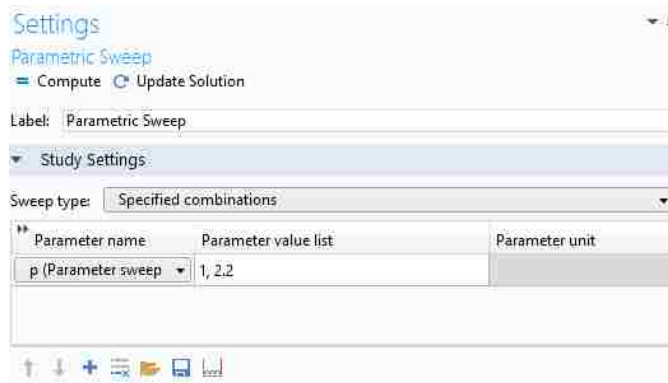


Figure C.18. Settings for parameter sweep.

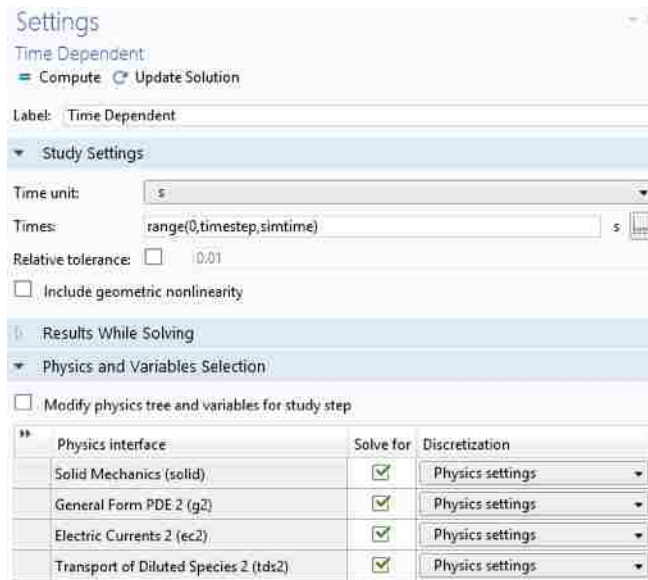


Figure C.19. Settings for the Time Dependent Study.

The model can be run with different inputs by simply changing the “Type” in “Waveform.” In this study, three inputs are implemented: sinusoidal, square, and triangular wave at 0.5 V at 1 Hz. To plot the results from the study and view both solutions at the same time, start by adding a “Point Graph.” Right click on “Results” and add “1D Plot Group.” Right click on this and add “Point Graph.” Click on this and label it “Nafion.” Under “Data,” set “Data Set” to the solution set called “Parametric Solutions.” The exact name will differ for every model built. For “Parameter Selection,” change it to “From List” and select “1.” This value simulates a Nafion-based IPMC. Under “Selection,” change it to “Manual” and select point 12. Change the units to “mm” and click “Plot.” Add a second “Point Graph” and repeat the previous steps, but for this one, label it “Aquivion” and select “2.2” for the parameter. Click “Plot” again and both lines should be in the plot now. The line type and color can be adjusted in the settings for each Point Graph (Figure C.20).



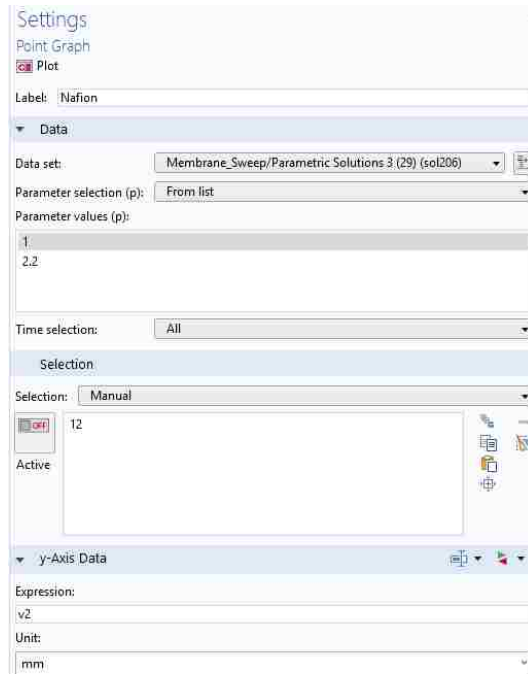


Figure C.20. Settings for the Point Graph in 1D Plot Group.

## Appendix D. Permission to use full article in Chapter 4 from IOP Publishing

### IOP Publishing LICENSE TERMS AND CONDITIONS

Feb 26, 2018

---

This is a License Agreement between Sarah Trabia ("You") and IOP Publishing ("IOP Publishing") provided by Copyright Clearance Center ("CCC"). The license consists of your order details, the terms and conditions provided by IOP Publishing, and the payment terms and conditions.

**All payments must be made in full to CCC. For payment instructions, please see information listed at the bottom of this form.**

License Number	4296560470540
License date	Jan 31, 2018
Licensed content publisher	IOP Publishing
Licensed content title	Smart Materials and Structures
Licensed content date	Jan 1, 1992
Type of Use	Thesis/Dissertation
Requestor type	Academic institution
Format	Electronic
Portion	chapter/article
The requesting person/organization is:	Sarah Trabia
Title or numeric reference of the portion(s)	Entire article
Title of the article or chapter the portion is from	"A fabrication method of unique Nafion® shapes by painting for ionic polymer-metal composites" DOI:10.1088/0964-1726/25/8/085006
Editor of portion(s)	N/A
Author of portion(s)	Sarah Trabia
Volume of serial or monograph.	N/A
Page range of the portion	
Publication date of portion	11 July 2016
Rights for	Main product
Duration of use	Life of current edition
Creation of copies for the disabled	no
With minor editing privileges	no
For distribution to	United States
In the following language(s)	Original language of publication
With incidental promotional	no

use

The lifetime unit quantity of new product Up to 499

Title Comprehensive Study of Spray-Painting, Extruding, and 3D Printing Fabrication Methods for Nafion® and Nafion® Equivalents in Ionic Polymer-Metal Composite Actuators and Sensors

Instructor name N/A

Institution name University of Nevada, Las Vegas

Expected presentation date Jan 2018

Billing Type Invoice

Billing Address Sarah Trabia  
351 Barletta Ave

Las Vegas, NV 89123  
United States  
Attn: Sarah Trabia

Total (may include CCC user fee) 0.00 USD

Terms and Conditions

### TERMS AND CONDITIONS

#### The following terms are individual to this publisher:

These special terms and conditions are in addition to the standard terms and conditions for CCC's Republication Service and, together with those standard terms and conditions, govern the use of the Works.

As the "User" you will make all reasonable efforts to contact the author(s) of the article which the Work is to be reused from, to seek consent for your intended use. Contacting one author who is acting expressly as authorised agent for their co-author(s) is acceptable.

User will reproduce the following wording prominently alongside the Work:

- the source of the Work, including author, article title, title of journal, volume number, issue number (if relevant), page range (or first page if this is the only information available) and date of first publication. This information can be contained in a footnote or reference note; and
- a link back to the article (via DOI); and
- if practicable, and IN ALL CASES for new works published under any of the Creative Commons licences, the words "© IOP Publishing. Reproduced with permission. All rights reserved"

Without the express permission of the author(s) and the Rightsholder of the article from which the Work is to be reused, User shall not use it in any way which, in the opinion of the Rightsholder, could: (i) distort or alter the author(s)' original intention(s) and meaning; (ii) be prejudicial to the honour or reputation of the author(s); and/or (iii) imply endorsement by the author(s) and/or the Rightsholder.

This licence does not apply to any article which is credited to another source and which does not have the copyright line '© IOP Publishing Ltd'. User must check the copyright line of the article from which the Work is to be reused to check that IOP Publishing Ltd has all the necessary rights to be able to grant permission. User is solely responsible for identifying and obtaining separate licences and permissions from the copyright owner for reuse of any such

third party material/figures which the Rightsholder is not the copyright owner of. The Rightsholder shall not reimburse any fees which User pays for a republication license for such third party content.

This licence does not apply to any material/figure which is credited to another source in the Rightsholder's publication or has been obtained from a third party. User must check the Version of Record of the article from which the Work is to be reused, to check whether any of the material in the Work is third party material. Third party citations and/or copyright notices and/or permissions statements may not be included in any other version of the article from which the Work is to be reused and so cannot be relied upon by the User. User is solely responsible for identifying and obtaining separate licences and permissions from the copyright owner for reuse of any such third party material/figures where the Rightsholder is not the copyright owner. The Rightsholder shall not reimburse any fees which User pays for a republication license for such third party content.

User and CCC acknowledge that the Rightsholder may, from time to time, make changes or additions to these special terms and conditions without express notification, provided that these shall not apply to permissions already secured and paid for by User prior to such change or addition.

User acknowledges that the Rightsholder (which includes companies within its group and third parties for whom it publishes its titles) may make use of personal data collected through the service in the course of their business.

If User is the author of the Work, User may automatically have the right to reuse it under the rights granted back when User transferred the copyright in the article to the Rightsholder. User should check the copyright form and the relevant author rights policy to check whether permission is required. If User is the author of the Work and does require permission for proposed reuse of the Work, User should select 'Author of requested content' as the Requestor Type. The Rightsholder shall not reimburse any fees which User pays for a republication license.

If User is the author of the article which User wishes to reuse in User's thesis or dissertation, the republication licence covers the right to include the Accepted Manuscript version (not the Version of Record) of the article. User must include citation details and, for online use, a link to the Version of Record of the article on the Rightsholder's website. User may need to obtain separate permission for any third party content included within the article. User must check this with the copyright owner of such third party content. User may not include the article in a thesis or dissertation which is published by ProQuest. Any other commercial use of User's thesis or dissertation containing the article would also need to be expressly notified in writing to the Rightsholder at the time of request and would require separate written permission from the Rightsholder.

User does not need to request permission for Work which has been published under a CC BY licence. User must check the Version of Record of the CC BY article from which the Work is to be reused, to check whether any of the material in the Work is third party material and so not published under the CC BY licence. User is solely responsible for identifying and obtaining separate licences and permissions from the copyright owner for reuse of any such third party material/figures. The Rightsholder shall not reimburse any fees which User pays for such licences and permissions.

As well as CCC, the Rightsholder shall have the right to bring any legal action that it deems necessary to enforce its rights should it consider that the Work infringes those rights in any way.

For STM Signatories ONLY (as agreed as part of the STM Guidelines)

Any licence granted for a particular edition of a Work will apply also to subsequent editions of it and for editions in other languages, provided such editions are for the Work as a whole

in situ and do not involve the separate exploitation of the permitted illustrations or excerpts.

**Other Terms and Conditions:**

**STANDARD TERMS AND CONDITIONS**

1. Description of Service; Defined Terms. This Republication License enables the User to obtain licenses for republication of one or more copyrighted works as described in detail on the relevant Order Confirmation (the “Work(s)”). Copyright Clearance Center, Inc. (“CCC”) grants licenses through the Service on behalf of the rightsholder identified on the Order Confirmation (the “Rightsholder”). “Republication”, as used herein, generally means the inclusion of a Work, in whole or in part, in a new work or works, also as described on the Order Confirmation. “User”, as used herein, means the person or entity making such republication.

2. The terms set forth in the relevant Order Confirmation, and any terms set by the Rightsholder with respect to a particular Work, govern the terms of use of Works in connection with the Service. By using the Service, the person transacting for a republication license on behalf of the User represents and warrants that he/she/it (a) has been duly authorized by the User to accept, and hereby does accept, all such terms and conditions on behalf of User, and (b) shall inform User of all such terms and conditions. In the event such person is a “freelancer” or other third party independent of User and CCC, such party shall be deemed jointly a “User” for purposes of these terms and conditions. In any event, User shall be deemed to have accepted and agreed to all such terms and conditions if User republishes the Work in any fashion.

**3. Scope of License; Limitations and Obligations.**

3.1 All Works and all rights therein, including copyright rights, remain the sole and exclusive property of the Rightsholder. The license created by the exchange of an Order Confirmation (and/or any invoice) and payment by User of the full amount set forth on that document includes only those rights expressly set forth in the Order Confirmation and in these terms and conditions, and conveys no other rights in the Work(s) to User. All rights not expressly granted are hereby reserved.

3.2 General Payment Terms: You may pay by credit card or through an account with us payable at the end of the month. If you and we agree that you may establish a standing account with CCC, then the following terms apply: Remit Payment to: Copyright Clearance Center, 29118 Network Place, Chicago, IL 60673-1291. Payments Due: Invoices are payable upon their delivery to you (or upon our notice to you that they are available to you for downloading). After 30 days, outstanding amounts will be subject to a service charge of 1-1/2% per month or, if less, the maximum rate allowed by applicable law. Unless otherwise specifically set forth in the Order Confirmation or in a separate written agreement signed by CCC, invoices are due and payable on “net 30” terms. While User may exercise the rights licensed immediately upon issuance of the Order Confirmation, the license is automatically revoked and is null and void, as if it had never been issued, if complete payment for the license is not received on a timely basis either from User directly or through a payment agent, such as a credit card company.

3.3 Unless otherwise provided in the Order Confirmation, any grant of rights to User (i) is “one-time” (including the editions and product family specified in the license), (ii) is non-exclusive and non-transferable and (iii) is subject to any and all limitations and restrictions (such as, but not limited to, limitations on duration of use or circulation) included in the Order Confirmation or invoice and/or in these terms and conditions. Upon completion of the licensed use, User shall either secure a new permission for further use of the Work(s) or immediately cease any new use of the Work(s) and shall render inaccessible (such as by deleting or by removing or severing links or other locators) any further copies of the Work (except for copies printed on paper in accordance with this license and still in User's stock at

the end of such period).

3.4 In the event that the material for which a republication license is sought includes third party materials (such as photographs, illustrations, graphs, inserts and similar materials) which are identified in such material as having been used by permission, User is responsible for identifying, and seeking separate licenses (under this Service or otherwise) for, any of such third party materials; without a separate license, such third party materials may not be used.

3.5 Use of proper copyright notice for a Work is required as a condition of any license granted under the Service. Unless otherwise provided in the Order Confirmation, a proper copyright notice will read substantially as follows: "Republished with permission of [Rightsholder's name], from [Work's title, author, volume, edition number and year of copyright]; permission conveyed through Copyright Clearance Center, Inc." Such notice must be provided in a reasonably legible font size and must be placed either immediately adjacent to the Work as used (for example, as part of a by-line or footnote but not as a separate electronic link) or in the place where substantially all other credits or notices for the new work containing the republished Work are located. Failure to include the required notice results in loss to the Rightsholder and CCC, and the User shall be liable to pay liquidated damages for each such failure equal to twice the use fee specified in the Order Confirmation, in addition to the use fee itself and any other fees and charges specified.

3.6 User may only make alterations to the Work if and as expressly set forth in the Order Confirmation. No Work may be used in any way that is defamatory, violates the rights of third parties (including such third parties' rights of copyright, privacy, publicity, or other tangible or intangible property), or is otherwise illegal, sexually explicit or obscene. In addition, User may not conjoin a Work with any other material that may result in damage to the reputation of the Rightsholder. User agrees to inform CCC if it becomes aware of any infringement of any rights in a Work and to cooperate with any reasonable request of CCC or the Rightsholder in connection therewith.

4. Indemnity. User hereby indemnifies and agrees to defend the Rightsholder and CCC, and their respective employees and directors, against all claims, liability, damages, costs and expenses, including legal fees and expenses, arising out of any use of a Work beyond the scope of the rights granted herein, or any use of a Work which has been altered in any unauthorized way by User, including claims of defamation or infringement of rights of copyright, publicity, privacy or other tangible or intangible property.

5. Limitation of Liability. UNDER NO CIRCUMSTANCES WILL CCC OR THE RIGHTSHOLDER BE LIABLE FOR ANY DIRECT, INDIRECT, CONSEQUENTIAL OR INCIDENTAL DAMAGES (INCLUDING WITHOUT LIMITATION DAMAGES FOR LOSS OF BUSINESS PROFITS OR INFORMATION, OR FOR BUSINESS INTERRUPTION) ARISING OUT OF THE USE OR INABILITY TO USE A WORK, EVEN IF ONE OF THEM HAS BEEN ADVISED OF THE POSSIBILITY OF SUCH DAMAGES. In any event, the total liability of the Rightsholder and CCC (including their respective employees and directors) shall not exceed the total amount actually paid by User for this license. User assumes full liability for the actions and omissions of its principals, employees, agents, affiliates, successors and assigns.

6. Limited Warranties. THE WORK(S) AND RIGHT(S) ARE PROVIDED "AS IS". CCC HAS THE RIGHT TO GRANT TO USER THE RIGHTS GRANTED IN THE ORDER CONFIRMATION DOCUMENT. CCC AND THE RIGHTSHOLDER DISCLAIM ALL OTHER WARRANTIES RELATING TO THE WORK(S) AND RIGHT(S), EITHER EXPRESS OR IMPLIED, INCLUDING WITHOUT LIMITATION IMPLIED WARRANTIES OF MERCHANTABILITY OR FITNESS FOR A PARTICULAR PURPOSE. ADDITIONAL RIGHTS MAY BE REQUIRED TO USE ILLUSTRATIONS,

GRAPHS, PHOTOGRAPHS, ABSTRACTS, INSERTS OR OTHER PORTIONS OF THE WORK (AS OPPOSED TO THE ENTIRE WORK) IN A MANNER CONTEMPLATED BY USER; USER UNDERSTANDS AND AGREES THAT NEITHER CCC NOR THE RIGHTSHOLDER MAY HAVE SUCH ADDITIONAL RIGHTS TO GRANT.

7. Effect of Breach. Any failure by User to pay any amount when due, or any use by User of a Work beyond the scope of the license set forth in the Order Confirmation and/or these terms and conditions, shall be a material breach of the license created by the Order Confirmation and these terms and conditions. Any breach not cured within 30 days of written notice thereof shall result in immediate termination of such license without further notice. Any unauthorized (but licensable) use of a Work that is terminated immediately upon notice thereof may be liquidated by payment of the Rightsholder's ordinary license price therefor; any unauthorized (and unlicensable) use that is not terminated immediately for any reason (including, for example, because materials containing the Work cannot reasonably be recalled) will be subject to all remedies available at law or in equity, but in no event to a payment of less than three times the Rightsholder's ordinary license price for the most closely analogous licensable use plus Rightsholder's and/or CCC's costs and expenses incurred in collecting such payment.

**8. Miscellaneous.**

8.1 User acknowledges that CCC may, from time to time, make changes or additions to the Service or to these terms and conditions, and CCC reserves the right to send notice to the User by electronic mail or otherwise for the purposes of notifying User of such changes or additions; provided that any such changes or additions shall not apply to permissions already secured and paid for.

8.2 Use of User-related information collected through the Service is governed by CCC's privacy policy, available online here:

<http://www.copyright.com/content/cc3/en/tools/footer/privacypolicy.html>.

8.3 The licensing transaction described in the Order Confirmation is personal to User.

Therefore, User may not assign or transfer to any other person (whether a natural person or an organization of any kind) the license created by the Order Confirmation and these terms and conditions or any rights granted hereunder; provided, however, that User may assign such license in its entirety on written notice to CCC in the event of a transfer of all or substantially all of User's rights in the new material which includes the Work(s) licensed under this Service.

8.4 No amendment or waiver of any terms is binding unless set forth in writing and signed by the parties. The Rightsholder and CCC hereby object to any terms contained in any writing prepared by the User or its principals, employees, agents or affiliates and purporting to govern or otherwise relate to the licensing transaction described in the Order Confirmation, which terms are in any way inconsistent with any terms set forth in the Order Confirmation and/or in these terms and conditions or CCC's standard operating procedures, whether such writing is prepared prior to, simultaneously with or subsequent to the Order Confirmation, and whether such writing appears on a copy of the Order Confirmation or in a separate instrument.

8.5 The licensing transaction described in the Order Confirmation document shall be governed by and construed under the law of the State of New York, USA, without regard to the principles thereof of conflicts of law. Any case, controversy, suit, action, or proceeding arising out of, in connection with, or related to such licensing transaction shall be brought, at CCC's sole discretion, in any federal or state court located in the County of New York, State of New York, USA, or in any federal or state court whose geographical jurisdiction covers the location of the Rightsholder set forth in the Order Confirmation. The parties expressly submit to the personal jurisdiction and venue of each such federal or state court. If you have

any comments or questions about the Service or Copyright Clearance Center, please contact us at 978-750-8400 or send an e-mail to [info@copyright.com](mailto:info@copyright.com).

v 1.1

**Questions? [customercare@copyright.com](mailto:customercare@copyright.com) or +1-855-239-3415 (toll free in the US) or +1-978-646-2777.**

---

---



## Appendix E. Permission to use full article in Chapter 5 from IOP Publishing

### IOP Publishing LICENSE TERMS AND CONDITIONS

Feb 26, 2018

---

This is a License Agreement between Sarah Trabia ("You") and IOP Publishing ("IOP Publishing") provided by Copyright Clearance Center ("CCC"). The license consists of your order details, the terms and conditions provided by IOP Publishing, and the payment terms and conditions.

**All payments must be made in full to CCC. For payment instructions, please see information listed at the bottom of this form.**

License Number	4296560409785
License date	Jan 31, 2018
Licensed content publisher	IOP Publishing
Licensed content title	Smart Materials and Structures
Licensed content date	Jan 1, 1992
Type of Use	Thesis/Dissertation
Requestor type	Academic institution
Format	Electronic
Portion	chapter/article
The requesting person/organization is:	Sarah Trabia
Title or numeric reference of the portion(s)	Entire article
Title of the article or chapter the portion is from	"Searching for a new ionomer for 3D printable ionic polymer-metal composites: Aquivion as a candidate"
Editor of portion(s)	N/A
Author of portion(s)	Sarah Trabia
Volume of serial or monograph.	N/A
Page range of the portion	
Publication date of portion	26 October 2017
Rights for	Main product
Duration of use	Life of current edition
Creation of copies for the disabled	no
With minor editing privileges	no
For distribution to	United States
In the following language(s)	Original language of publication
With incidental promotional use	no

The lifetime unit quantity of new product	Up to 499
Title	Comprehensive Study of Spray-Painting, Extruding, and 3D Printing Fabrication Methods for Nafion® and Nafion® Equivalents in Ionic Polymer-Metal Composite Actuators and Sensors
Instructor name	N/A
Institution name	University of Nevada, Las Vegas
Expected presentation date	Jan 2018
Billing Type	Invoice
Billing Address	Sarah Trabia 351 Barletta Ave  Las Vegas, NV 89123 United States Attn: Sarah Trabia
Total (may include CCC user fee)	0.00 USD

Terms and Conditions

### TERMS AND CONDITIONS

#### **The following terms are individual to this publisher:**

These special terms and conditions are in addition to the standard terms and conditions for CCC's Replication Service and, together with those standard terms and conditions, govern the use of the Works.

As the "User" you will make all reasonable efforts to contact the author(s) of the article which the Work is to be reused from, to seek consent for your intended use. Contacting one author who is acting expressly as authorised agent for their co-author(s) is acceptable.

User will reproduce the following wording prominently alongside the Work:

- the source of the Work, including author, article title, title of journal, volume number, issue number (if relevant), page range (or first page if this is the only information available) and date of first publication. This information can be contained in a footnote or reference note; and
- a link back to the article (via DOI); and
- if practicable, and IN ALL CASES for new works published under any of the Creative Commons licences, the words "© IOP Publishing. Reproduced with permission. All rights reserved"

Without the express permission of the author(s) and the Rightsholder of the article from which the Work is to be reused, User shall not use it in any way which, in the opinion of the Rightsholder, could: (i) distort or alter the author(s)' original intention(s) and meaning; (ii) be prejudicial to the honour or reputation of the author(s); and/or (iii) imply endorsement by the author(s) and/or the Rightsholder.

This licence does not apply to any article which is credited to another source and which does not have the copyright line '© IOP Publishing Ltd'. User must check the copyright line of the article from which the Work is to be reused to check that IOP Publishing Ltd has all the necessary rights to be able to grant permission. User is solely responsible for identifying and obtaining separate licences and permissions from the copyright owner for reuse of any such third party material/figures which the Rightsholder is not the copyright owner of. The

Rightsholder shall not reimburse any fees which User pays for a republication license for such third party content.

This licence does not apply to any material/figure which is credited to another source in the Rightsholder's publication or has been obtained from a third party. User must check the Version of Record of the article from which the Work is to be reused, to check whether any of the material in the Work is third party material. Third party citations and/or copyright notices and/or permissions statements may not be included in any other version of the article from which the Work is to be reused and so cannot be relied upon by the User. User is solely responsible for identifying and obtaining separate licences and permissions from the copyright owner for reuse of any such third party material/figures where the Rightsholder is not the copyright owner. The Rightsholder shall not reimburse any fees which User pays for a republication license for such third party content.

User and CCC acknowledge that the Rightsholder may, from time to time, make changes or additions to these special terms and conditions without express notification, provided that these shall not apply to permissions already secured and paid for by User prior to such change or addition.

User acknowledges that the Rightsholder (which includes companies within its group and third parties for whom it publishes its titles) may make use of personal data collected through the service in the course of their business.

If User is the author of the Work, User may automatically have the right to reuse it under the rights granted back when User transferred the copyright in the article to the Rightsholder. User should check the copyright form and the relevant author rights policy to check whether permission is required. If User is the author of the Work and does require permission for proposed reuse of the Work, User should select 'Author of requested content' as the Requestor Type. The Rightsholder shall not reimburse any fees which User pays for a republication license.

If User is the author of the article which User wishes to reuse in User's thesis or dissertation, the republication licence covers the right to include the Accepted Manuscript version (not the Version of Record) of the article. User must include citation details and, for online use, a link to the Version of Record of the article on the Rightsholder's website. User may need to obtain separate permission for any third party content included within the article. User must check this with the copyright owner of such third party content. User may not include the article in a thesis or dissertation which is published by ProQuest. Any other commercial use of User's thesis or dissertation containing the article would also need to be expressly notified in writing to the Rightsholder at the time of request and would require separate written permission from the Rightsholder.

User does not need to request permission for Work which has been published under a CC BY licence. User must check the Version of Record of the CC BY article from which the Work is to be reused, to check whether any of the material in the Work is third party material and so not published under the CC BY licence. User is solely responsible for identifying and obtaining separate licences and permissions from the copyright owner for reuse of any such third party material/figures. The Rightsholder shall not reimburse any fees which User pays for such licences and permissions.

As well as CCC, the Rightsholder shall have the right to bring any legal action that it deems necessary to enforce its rights should it consider that the Work infringes those rights in any way.

For STM Signatories ONLY (as agreed as part of the STM Guidelines)

Any licence granted for a particular edition of a Work will apply also to subsequent editions of it and for editions in other languages, provided such editions are for the Work as a whole in situ and do not involve the separate exploitation of the permitted illustrations or excerpts.

**Other Terms and Conditions:**  
**STANDARD TERMS AND CONDITIONS**

1. Description of Service; Defined Terms. This Republication License enables the User to obtain licenses for republication of one or more copyrighted works as described in detail on the relevant Order Confirmation (the “Work(s)”). Copyright Clearance Center, Inc. (“CCC”) grants licenses through the Service on behalf of the rightsholder identified on the Order Confirmation (the “Rightsholder”). “Republication”, as used herein, generally means the inclusion of a Work, in whole or in part, in a new work or works, also as described on the Order Confirmation. “User”, as used herein, means the person or entity making such republication.

2. The terms set forth in the relevant Order Confirmation, and any terms set by the Rightsholder with respect to a particular Work, govern the terms of use of Works in connection with the Service. By using the Service, the person transacting for a republication license on behalf of the User represents and warrants that he/she/it (a) has been duly authorized by the User to accept, and hereby does accept, all such terms and conditions on behalf of User, and (b) shall inform User of all such terms and conditions. In the event such person is a “freelancer” or other third party independent of User and CCC, such party shall be deemed jointly a “User” for purposes of these terms and conditions. In any event, User shall be deemed to have accepted and agreed to all such terms and conditions if User republishes the Work in any fashion.

**3. Scope of License; Limitations and Obligations.**

3.1 All Works and all rights therein, including copyright rights, remain the sole and exclusive property of the Rightsholder. The license created by the exchange of an Order Confirmation (and/or any invoice) and payment by User of the full amount set forth on that document includes only those rights expressly set forth in the Order Confirmation and in these terms and conditions, and conveys no other rights in the Work(s) to User. All rights not expressly granted are hereby reserved.

3.2 General Payment Terms: You may pay by credit card or through an account with us payable at the end of the month. If you and we agree that you may establish a standing account with CCC, then the following terms apply: Remit Payment to: Copyright Clearance Center, 29118 Network Place, Chicago, IL 60673-1291. Payments Due: Invoices are payable upon their delivery to you (or upon our notice to you that they are available to you for downloading). After 30 days, outstanding amounts will be subject to a service charge of 1-1/2% per month or, if less, the maximum rate allowed by applicable law. Unless otherwise specifically set forth in the Order Confirmation or in a separate written agreement signed by CCC, invoices are due and payable on “net 30” terms. While User may exercise the rights licensed immediately upon issuance of the Order Confirmation, the license is automatically revoked and is null and void, as if it had never been issued, if complete payment for the license is not received on a timely basis either from User directly or through a payment agent, such as a credit card company.

3.3 Unless otherwise provided in the Order Confirmation, any grant of rights to User (i) is “one-time” (including the editions and product family specified in the license), (ii) is non-exclusive and non-transferable and (iii) is subject to any and all limitations and restrictions (such as, but not limited to, limitations on duration of use or circulation) included in the Order Confirmation or invoice and/or in these terms and conditions. Upon completion of the licensed use, User shall either secure a new permission for further use of the Work(s) or immediately cease any new use of the Work(s) and shall render inaccessible (such as by deleting or by removing or severing links or other locators) any further copies of the Work (except for copies printed on paper in accordance with this license and still in User's stock at the end of such period).

3.4 In the event that the material for which a republication license is sought includes third party materials (such as photographs, illustrations, graphs, inserts and similar materials) which are identified in such material as having been used by permission, User is responsible for identifying, and seeking separate licenses (under this Service or otherwise) for, any of such third party materials; without a separate license, such third party materials may not be used.

3.5 Use of proper copyright notice for a Work is required as a condition of any license granted under the Service. Unless otherwise provided in the Order Confirmation, a proper copyright notice will read substantially as follows: "Republished with permission of [Rightsholder's name], from [Work's title, author, volume, edition number and year of copyright]; permission conveyed through Copyright Clearance Center, Inc." Such notice must be provided in a reasonably legible font size and must be placed either immediately adjacent to the Work as used (for example, as part of a by-line or footnote but not as a separate electronic link) or in the place where substantially all other credits or notices for the new work containing the republished Work are located. Failure to include the required notice results in loss to the Rightsholder and CCC, and the User shall be liable to pay liquidated damages for each such failure equal to twice the use fee specified in the Order Confirmation, in addition to the use fee itself and any other fees and charges specified.

3.6 User may only make alterations to the Work if and as expressly set forth in the Order Confirmation. No Work may be used in any way that is defamatory, violates the rights of third parties (including such third parties' rights of copyright, privacy, publicity, or other tangible or intangible property), or is otherwise illegal, sexually explicit or obscene. In addition, User may not conjoin a Work with any other material that may result in damage to the reputation of the Rightsholder. User agrees to inform CCC if it becomes aware of any infringement of any rights in a Work and to cooperate with any reasonable request of CCC or the Rightsholder in connection therewith.

4. Indemnity. User hereby indemnifies and agrees to defend the Rightsholder and CCC, and their respective employees and directors, against all claims, liability, damages, costs and expenses, including legal fees and expenses, arising out of any use of a Work beyond the scope of the rights granted herein, or any use of a Work which has been altered in any unauthorized way by User, including claims of defamation or infringement of rights of copyright, publicity, privacy or other tangible or intangible property.

5. Limitation of Liability. UNDER NO CIRCUMSTANCES WILL CCC OR THE RIGHTSHOLDER BE LIABLE FOR ANY DIRECT, INDIRECT, CONSEQUENTIAL OR INCIDENTAL DAMAGES (INCLUDING WITHOUT LIMITATION DAMAGES FOR LOSS OF BUSINESS PROFITS OR INFORMATION, OR FOR BUSINESS INTERRUPTION) ARISING OUT OF THE USE OR INABILITY TO USE A WORK, EVEN IF ONE OF THEM HAS BEEN ADVISED OF THE POSSIBILITY OF SUCH DAMAGES. In any event, the total liability of the Rightsholder and CCC (including their respective employees and directors) shall not exceed the total amount actually paid by User for this license. User assumes full liability for the actions and omissions of its principals, employees, agents, affiliates, successors and assigns.

6. Limited Warranties. THE WORK(S) AND RIGHT(S) ARE PROVIDED "AS IS". CCC HAS THE RIGHT TO GRANT TO USER THE RIGHTS GRANTED IN THE ORDER CONFIRMATION DOCUMENT. CCC AND THE RIGHTSHOLDER DISCLAIM ALL OTHER WARRANTIES RELATING TO THE WORK(S) AND RIGHT(S), EITHER EXPRESS OR IMPLIED, INCLUDING WITHOUT LIMITATION IMPLIED WARRANTIES OF MERCHANTABILITY OR FITNESS FOR A PARTICULAR PURPOSE. ADDITIONAL RIGHTS MAY BE REQUIRED TO USE ILLUSTRATIONS, GRAPHS, PHOTOGRAPHS, ABSTRACTS, INSERTS OR OTHER PORTIONS OF THE

WORK (AS OPPOSED TO THE ENTIRE WORK) IN A MANNER CONTEMPLATED BY USER; USER UNDERSTANDS AND AGREES THAT NEITHER CCC NOR THE RIGHTSHOLDER MAY HAVE SUCH ADDITIONAL RIGHTS TO GRANT.

7. Effect of Breach. Any failure by User to pay any amount when due, or any use by User of a Work beyond the scope of the license set forth in the Order Confirmation and/or these terms and conditions, shall be a material breach of the license created by the Order Confirmation and these terms and conditions. Any breach not cured within 30 days of written notice thereof shall result in immediate termination of such license without further notice. Any unauthorized (but licensable) use of a Work that is terminated immediately upon notice thereof may be liquidated by payment of the Rightsholder's ordinary license price therefor; any unauthorized (and unlicensable) use that is not terminated immediately for any reason (including, for example, because materials containing the Work cannot reasonably be recalled) will be subject to all remedies available at law or in equity, but in no event to a payment of less than three times the Rightsholder's ordinary license price for the most closely analogous licensable use plus Rightsholder's and/or CCC's costs and expenses incurred in collecting such payment.

**8. Miscellaneous.**

8.1 User acknowledges that CCC may, from time to time, make changes or additions to the Service or to these terms and conditions, and CCC reserves the right to send notice to the User by electronic mail or otherwise for the purposes of notifying User of such changes or additions; provided that any such changes or additions shall not apply to permissions already secured and paid for.

8.2 Use of User-related information collected through the Service is governed by CCC's privacy policy, available online here:

<http://www.copyright.com/content/cc3/en/tools/footer/privacypolicy.html>.

8.3 The licensing transaction described in the Order Confirmation is personal to User.

Therefore, User may not assign or transfer to any other person (whether a natural person or an organization of any kind) the license created by the Order Confirmation and these terms and conditions or any rights granted hereunder; provided, however, that User may assign such license in its entirety on written notice to CCC in the event of a transfer of all or substantially all of User's rights in the new material which includes the Work(s) licensed under this Service.

8.4 No amendment or waiver of any terms is binding unless set forth in writing and signed by the parties. The Rightsholder and CCC hereby object to any terms contained in any writing prepared by the User or its principals, employees, agents or affiliates and purporting to govern or otherwise relate to the licensing transaction described in the Order Confirmation, which terms are in any way inconsistent with any terms set forth in the Order Confirmation and/or in these terms and conditions or CCC's standard operating procedures, whether such writing is prepared prior to, simultaneously with or subsequent to the Order Confirmation, and whether such writing appears on a copy of the Order Confirmation or in a separate instrument.

8.5 The licensing transaction described in the Order Confirmation document shall be governed by and construed under the law of the State of New York, USA, without regard to the principles thereof of conflicts of law. Any case, controversy, suit, action, or proceeding arising out of, in connection with, or related to such licensing transaction shall be brought, at CCC's sole discretion, in any federal or state court located in the County of New York, State of New York, USA, or in any federal or state court whose geographical jurisdiction covers the location of the Rightsholder set forth in the Order Confirmation. The parties expressly submit to the personal jurisdiction and venue of each such federal or state court. If you have any comments or questions about the Service or Copyright Clearance Center, please contact

us at 978-750-8400 or send an e-mail to [info@copyright.com](mailto:info@copyright.com).  
v 1.1

**Questions? [customercare@copyright.com](mailto:customercare@copyright.com) or +1-855-239-3415 (toll free in the US) or  
+1-978-646-2777.**

---

---

## Appendix F. Injection Molding Ionomers

The last fabrication process that was to be explored was Injection Molding. This was first studied by a previous M.S. student [27]. Her work gave a preliminary start to this process, but showed some possibility of improvement. She set the injection molder temperature to 270°C and the mold was preheated in the oven at 270°C. The membranes show signs of degradation, which means they were most likely not processed at the correct temperatures or consistently through the process (Figure F.1). It was also noted that there may not have been enough air vents in the mold to allow the polymer to flow into the entire space.

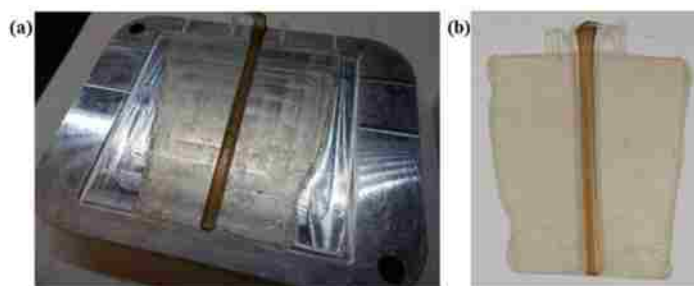


Figure F.1. Sample from the work done by Nelson [27].

The injection molder is a Galomb Benchtop Injection Molder with about 17 gram capacity (Figure F.2). The chamber for the pellets has a maximum temperature of 316°C. Once the pellets have melted, they are injected into the mold sitting below using the plunger. The chamber is easily cleaned out by removing the nozzle and pushing out the leftover polymer while it is all still heated. The mold can be made into any shape. For this project, it was of interest to make a curved membrane. Another point that was necessary to produce uncontaminated and usable ionomer membranes is that the mold must be heated to a similar or same temperature as the heated chamber. This will ensure that the ionomer is kept in a consistently heated environment. The mold was



designed with the help of Zakai Olsen. It was made into two sections to allow for ease in machining (Figure F.3). The curved membrane mold, a difficult task to machine, was made out of aluminum to make it easier to CNC-machine (Figure F.4). The outer sleeve was machined out of stainless steel 306 to hold the cartridge heaters. This was also CNC-machined. The completed mold set up with the cartridge heaters is shown in Figure F.5. The cartridge heaters are controlled by an external temperature controller.

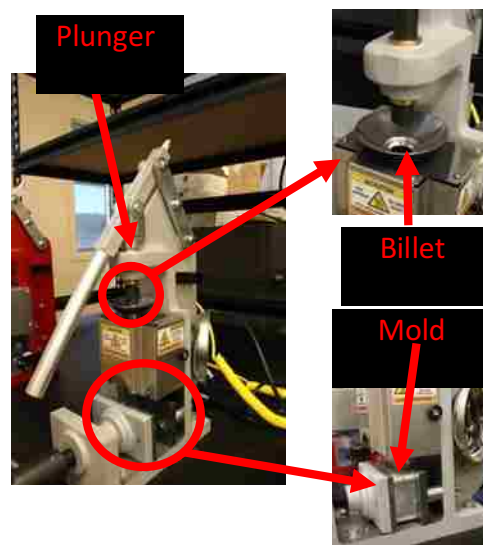


Figure F.2. Injection molder setup.

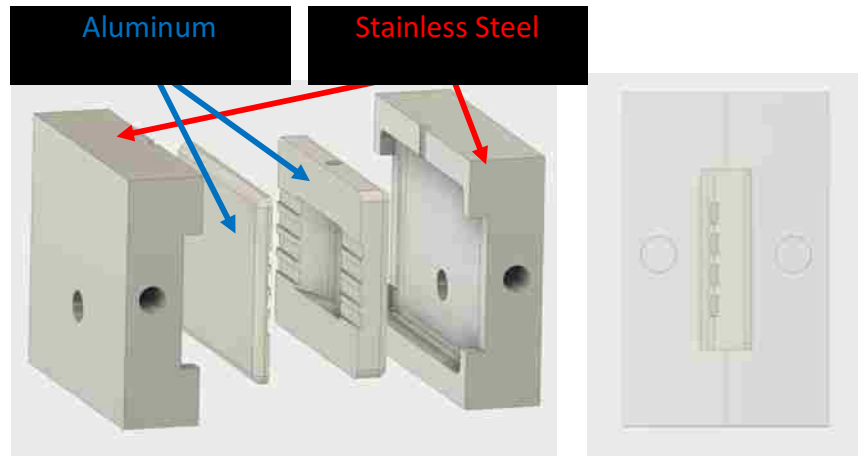


Figure F.3. New mold for creating curved membranes with two parts, one to hold the cartridge heaters (stainless steel) and the other to mold the ionomers (aluminum).



Figure F.4. Aluminum machined curved membrane molds.

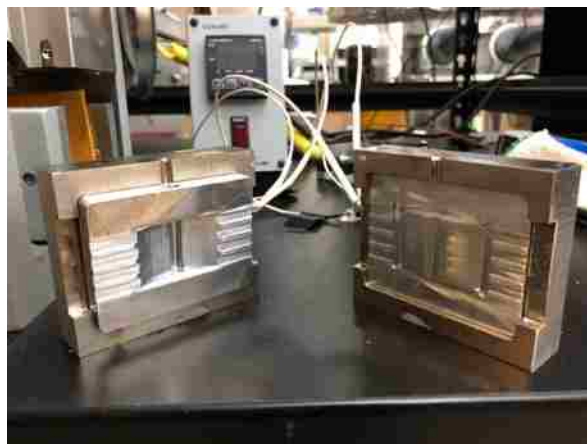


Figure F.5. Completed mold setup with the cartridge heaters installed.

The heated mold was tested to ensure that it was able to reach the desired temperatures for Nafion. From the IR image, it can be seen that the hot spots are centered on the chamber and the mold (Figure F.6). Nafion pellets were allowed to melt for 20 minutes and were compressed frequently. Then, the melted ionomer is injected into the mold at a steady rate. Once the mold has cooled down enough, it was opened to remove the membrane. The resulting sample is shown in Figure F.7 and there are many bubbles present, though the mold was successful in making a curved membrane (**Error! Reference source not found.**). The bubbles were most likely formed due to the packing formation of the pellets. Once they melt, they become a very viscous liquid, trapping the air pockets internally. An attempt to solve this was done by melting Nafion pellets in a vacuum oven for two hours. This was not able to solve the problem because the melted Nafion is still too viscous to pull the bubbles out (Figure F.9).



Figure F.6. IR image of the Injection Molder and Mold heated to 220°C for producing Nafion samples.



Figure F.7. Nafion sample with many bubbles throughout the membrane.

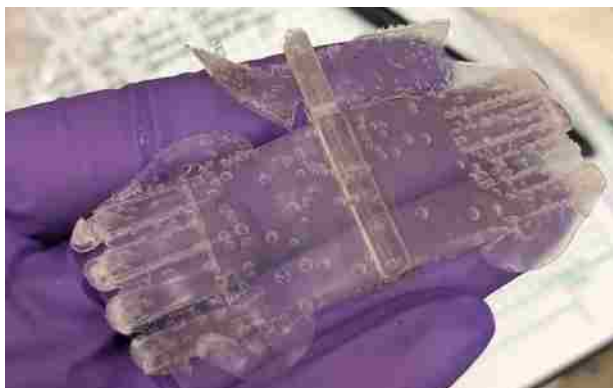


Figure F.8. Curved Nafion membrane.



Figure F.9. An attempt at producing a Nafion puck with no bubbles using the vacuum oven.

Aquivion precursor pellets was tested next at 255°C to see if the same issues were present. The entire setup was able to reach the desired temperature and the hot spots are again centered around the chamber and molds (Figure F.10). The pellets were allowed to sit for 20 minutes and were compressed frequently. It was injected into the mold at a steady rate. Once the mold has cooled off enough, the mold was opened up and the membrane was pulled out. The Aquivion membrane has more bubbles than the Nafion membrane (Figure F.11).



Figure F.10. IR image of the Injection Molder and Mold heated to 255°C for producing Aquivion samples.



Figure F.11. Aquivion curved membrane with many bubbles as well.

From the data gathered in Chapter 3, it was noted that the viscosity of the ionomers decreases as the temperature increases. To help remove the bubbles, the chamber was heated to 270°C for the next attempts. The mold was heated to 220 °C. Nafion pellets were heated and allowed to melt for 40 minutes. They were compressed every 5 minutes. Once it was ready, the ionomer was injected into the mold. From Figure F.12, it can be seen that there are still many bubbles present and the overall surface texture has worsened. A similar process was done for the second attempt with Aquivion pellets, except the mold was set to 255°C. The resulting samples was the worst sample produced with it having so many bubbles that the membrane was in two pieces (Figure F.13).

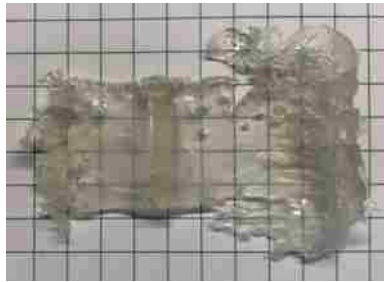


Figure F.12. Nafion membrane produced with bubbles present.

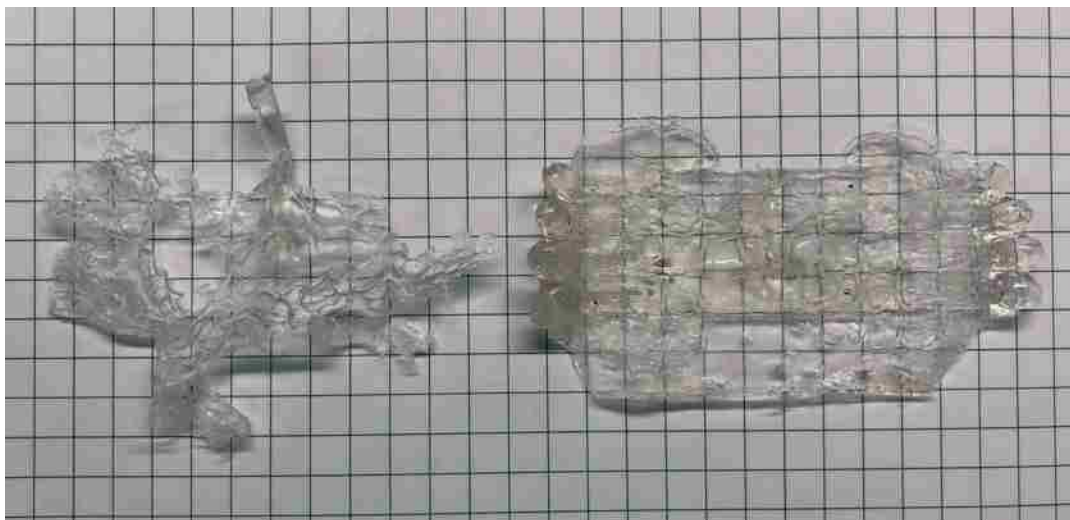


Figure F.13. Aquivion membrane produced with large bubbles throughout.

After the second attempt with Aquivion, the injection molder was cleaned out and the leftover ionomer was pulled out. There are many large bubbles in the polymer (Figure F.14). A single Nafion pellet was heated using a heat gun and it was noted that it showed signs of de-gassing (Figure F.15). Because of this, it was concluded that the ionomers may not be best in injection molding process. In order to use these ionomers, additional equipment that is not currently available in the lab are needed, such as a viscous liquid mixer or a vacuum line connected to the injection molder.



Figure F.14. Melted Aquivion pellets removed from the injection molder that has many bubbles.



Figure F.15. Nafion pellet heated up with a heat gun that shows de-gassing.

The produced samples were tested to compare with pure precursor pellets and 3D printed membranes. The Injection Molded Nafion (Nafion IM) matched very well compared with a Precursor Nafion pellet in FT-IR scans, where the bond stretches present are C-F, symmetric and asymmetric  $\text{CF}_2$ ,  $\text{CF}_2$ , and S-O (Figure F.16). The Injection Molded Aquivion (Aquivion IM) also matched well when compared to precursor Aquivion and printed Aquivion, where the bond



stretches present are C-F, symmetric and asymmetric  $\text{CF}_2$ ,  $\text{CF}_2$ , and S-O (Figure F.17). For the thermal degradation results, precursor Nafion and Nafion IM had similar degradation temperatures (Figure F.18), while the results for the Aquivion samples showed that the thermal degradation temperatures increase due to different thermal processes (Figure F.19). As discussed, the printed Aquivion sample has annealed due to the two heat processes: filament extrusion and printing. Interestingly, Aquivion IM showed a higher thermal degradation temperature. This could be attributed to the slow heating process and that it was sitting in the heated chamber for at least 20 minutes.

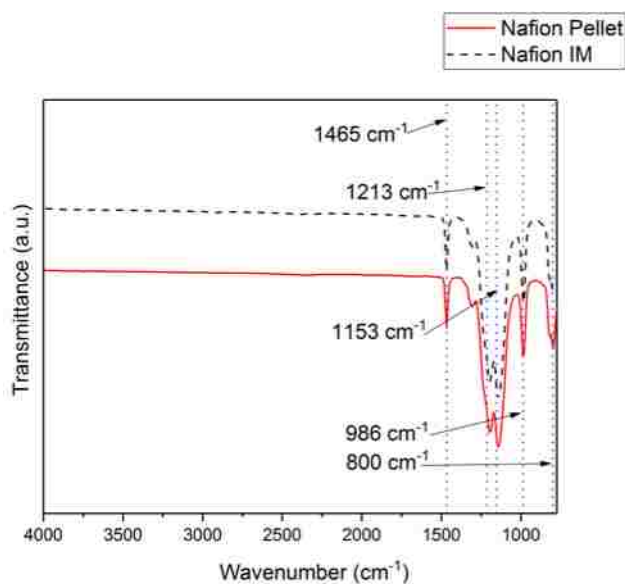


Figure F.16. FT-IR scans for precursor Nafion and Injection Molded Nafion with these bond stretches:  $1465 \text{ cm}^{-1}$  represents the C-F bond,  $1213 \text{ cm}^{-1}$  represents the symmetric  $\text{CF}_2$  bond,  $1153 \text{ cm}^{-1}$  represents the asymmetric  $\text{CF}_2$  bond,  $986 \text{ cm}^{-1}$  represents the C- $\text{F}_3$  bond,  $800 \text{ cm}^{-1}$  represents the S-O bond.

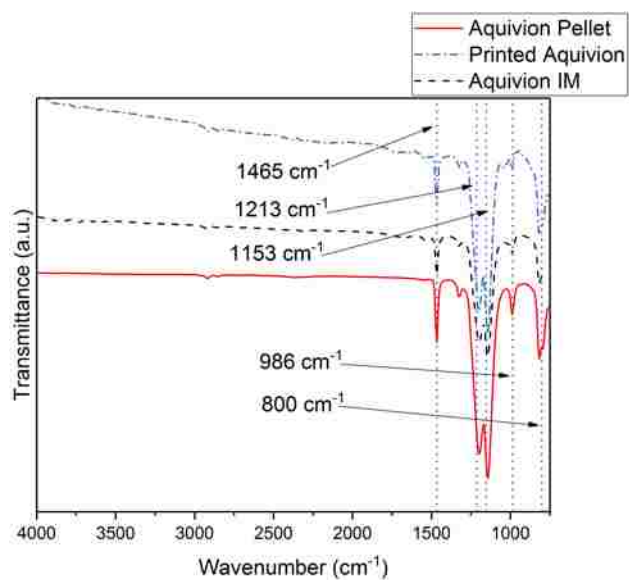


Figure F.17. FT-IR scans for precursor Aquivion, printed Aquivion, and Injection Molded Nafion with these bond stretches:  $1465\text{ cm}^{-1}$  represents the C-F bond,  $1213\text{ cm}^{-1}$  represents the symmetric  $\text{CF}_2$  bond,  $1153\text{ cm}^{-1}$  represents the asymmetric  $\text{CF}_2$  bond,  $986\text{ cm}^{-1}$  represents the C-F<sub>3</sub> bond,  $800\text{ cm}^{-1}$  represents the S-O bond.

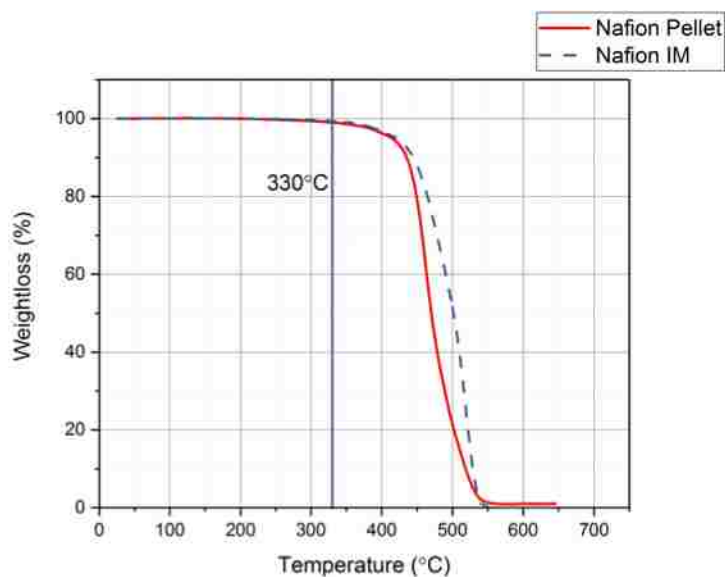


Figure F.18. TGA results for precursor Nafion and Nafion IM showing they have similar degradation temperatures and behaviors.

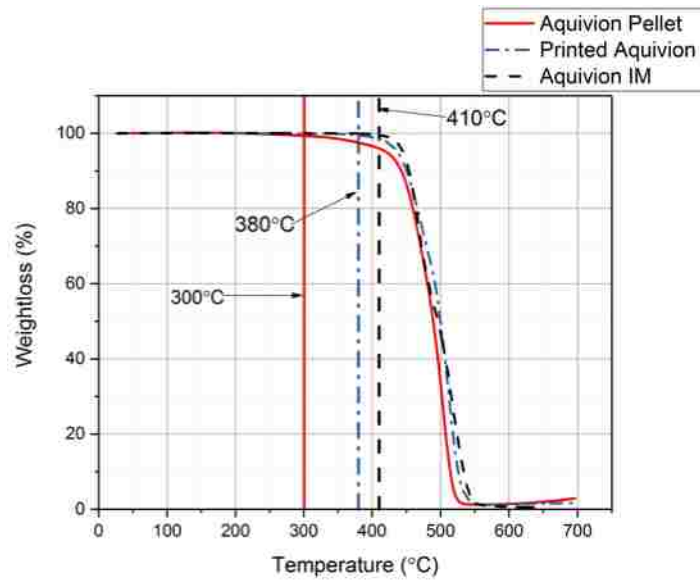


Figure F.19. TGA results for precursor Aquivion, printed Aquivion, and Aquivion IM showing that the thermal degradation temperature shifts.

## **Appendix G. Frequency Response for IPMCs in Sensing Applications**

As requested by the committee, a frequency response study was conducted to compare the Printed Aquivion-IPMC (Pr-Aq-IPMC) and Nafion-IPMC (N-IPMC) (Figure G.1). The tests were conducted in water with an applied amplitude of 3 mm at varying frequencies. It is interesting to note the different trends present in each sample. Over all, Pr-Aq-IPMC has a higher sensing voltage output than the N-IPMC. The Pr-Aq-IPMC sample response increases as the frequency increases, while the response of the N-IPMC decreases. This could be due to the difference in ionic conductivity of the two base ionomers. Aquivion has a higher ionic conductivity (~228 mS/cm) while Nafion has an ionic conductivity at (~100 mS/cm). Aquivion is potentially able to conduct more ions, even at higher frequencies. It would be interesting to attempt to use Aquivion in high frequency applications, such as vibration sensing. N-IPMC, on the other hand, with the lower ionic conductivity, is not able to conduct enough ions at higher frequencies to produce a high output. The N-IPMC response is noticeable and can be sensed, however it may be more useful in low frequency applications.

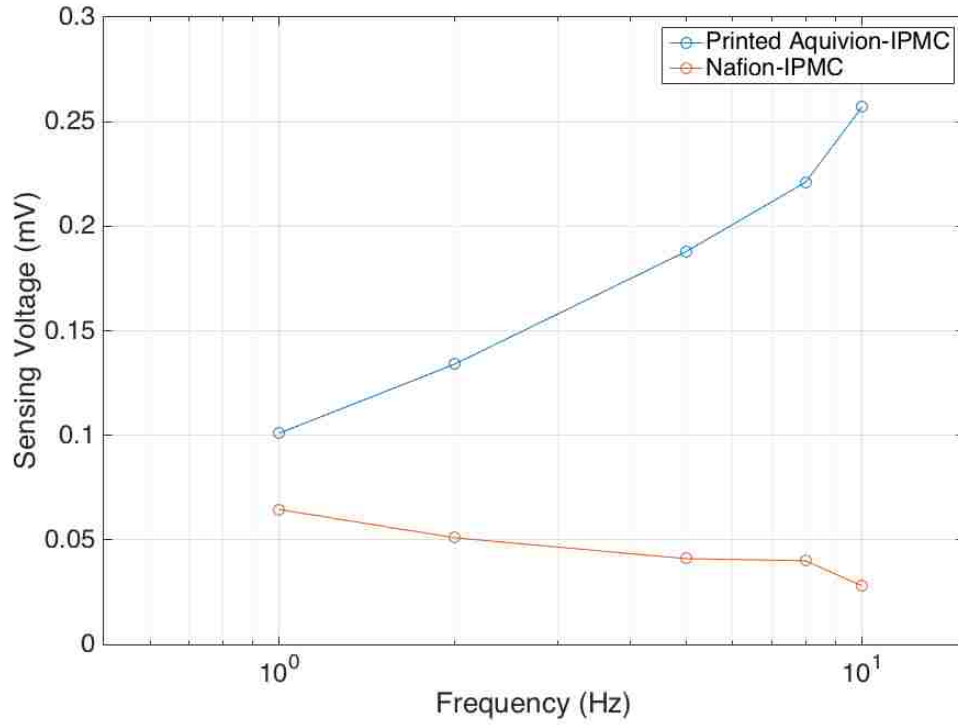


Figure G.1. Frequency response plot for a Printed Aquivion-IPMC and Nafion-IPMC in sensing application under 3mm amplitude with varying frequencies.

## Bibliography

- [1] M. Shahinpoor and K. J. Kim, "Ionic polymer-metal composites: I. Fundamentals," *Smart Mater. Struct.*, vol. 10, no. 4, pp. 819–833, Aug. 2001.
- [2] M. Shahinpoor, Y. Bar-Cohen, J. O. Simpson, and J. Smith, "Ionic polymer-metal composites (IPMCs) as biomimetic sensors, actuators and artificial muscles - a review," *Smart Mater. Struct.*, vol. 7, no. 6, pp. R15–R30, Dec. 1998.
- [3] R. Pelrine *et al.*, "Applications of dielectric elastomer actuators," 2001, no. July 2001, p. 335.
- [4] M. Shahinpoor and K. J. Kim, "Ionic polymer–metal composites: III. Modeling and simulation as biomimetic sensors, actuators, transducers, and artificial muscles," *Smart Mater. Struct.*, vol. 13, no. 6, pp. 1362–1388, 2004.
- [5] M. Shahinpoor and K. J. Kim, "Ionic polymer–metal composites: IV. Industrial and medical applications," *Smart Mater. Struct.*, vol. 14, no. 1, pp. 197–214, Feb. 2005.
- [6] K. Oguro, Y. Kawami, and H. Takenaka, "Bending of an ion-conducting polymer film-electrode composite by an electric stimulus at low voltage," *J. Micromachine Soc.*, vol. 5, pp. 27–30, 1992.
- [7] S. N. K. Sadeghipourt, R. Salomon, "Development of a novel electrochemically active membrane and ' smart ' material based vibration sensor / damper," *Smart Mater. Struct.*, vol. 172, no. 1, pp. 172–179, 1992.
- [8] R. Kanno, S. Tadokoro, M. Hattori, T. Takamori, M. Costafitis, and K. Oguro, "Dynamic model of ICPF (ionic conducting polymer film) actuator," *1995 IEEE Int. Conf. Syst. Man Cybern. Intell. Syst. 21st Century*, vol. 1, no. April, pp. 177–182, 1996.
- [9] M. Mojarad and M. Shahinpoor, "Biomimetic robotic propulsion using polymeric artificial

- muscles,” in *Proceedings of International Conference on Robotics and Automation*, 1997, vol. 3, no. April.
- [10] P. G. de Gennes, K. Okumura, M. Shahinpoor, and K. J. Kim, “Mechanoelectric effects in ionic gels,” *Europhys. Lett.*, vol. 50, no. 4, pp. 513–518, May 2000.
- [11] S. Nemat-nasser and J. Y. Li, “Electromechanical response of ionic polymer-metal composites,” *J. Appl. Phys.*, vol. 87, no. 7, pp. 3321–3331, 2000.
- [12] K. J. Kim and M. Shahinpoor, “Ionic polymer metal composites: II. Manufacturing techniques,” *Smart Mater. Struct.*, vol. 12, no. 1, pp. 65–79, Feb. 2003.
- [13] V. Palmre *et al.*, “An IPMC-enabled bio-inspired bending/twisting fin for underwater applications,” *Smart Mater. Struct.*, vol. 22, no. 1, p. 14003, Jan. 2013.
- [14] Z. Chen, T. I. Um, and H. Bart-Smith, “Bio-inspired robotic manta ray powered by ionic polymer–metal composite artificial muscles,” *Int. J. Smart Nano Mater.*, vol. 3, no. 4, pp. 296–308, Dec. 2012.
- [15] S.-W. Yeom and I.-K. Oh, “A biomimetic jellyfish robot based on ionic polymer metal composite actuators,” *Smart Mater. Struct.*, vol. 18, no. 8, p. 85002, 2009.
- [16] W. Yim, J. Lee, and K. J. Kim, “An artificial muscle actuator for biomimetic underwater propulsors,” *Bioinspir. Biomim.*, vol. 2, no. 2, pp. S31–S41, 2007.
- [17] S. Ruiz, B. Mead, V. Palmre, K. J. Kim, and W. Yim, “A cylindrical ionic polymer-metal composite-based robotic catheter platform: modeling, design and control,” *Smart Mater. Struct.*, vol. 24, no. 1, p. 15007, 2015.
- [18] J. Liu, Y. Wang, D. Zhao, C. Zhang, H. Chen, and D. Li, “Design and fabrication of an IPMC-embedded tube for minimally invasive surgery applications,” *Electroact. Polym. Actuators Devices*, vol. 9056, p. 90563K, 2014.

- [19] S. J. Lee, M. J. Han, S. J. Kim, J. Y. Jho, H. Y. Lee, and Y. H. Kim, “A new fabrication method for IPMC actuators and application to artificial fingers,” *Smart Mater. Struct.*, vol. 15, no. 5, pp. 1217–1224, 2006.
- [20] A. Punning, M. Kruusmaa, and A. Aabloo, “Surface resistance experiments with IPMC sensors and actuators,” *Sensors and Actuators*, vol. 133, no. 1, pp. 200–209, Jan. 2007.
- [21] G. H. Feng and J. W. Tsai, “3D omnidirectional controllable elastic IPMC tweezer with self-sensing and adjustable clamping force abilities for biomedical applications,” *2011 16th Int. Solid-State Sensors, Actuators Microsystems Conf. TRANSDUCERS’11*, vol. 3, pp. 1725–1728, 2011.
- [22] R. K. Jain, S. Majumder, and A. Dutta, “SCARA based peg-in-hole assembly using compliant IPMC micro gripper,” *Rob. Auton. Syst.*, vol. 61, no. 3, pp. 297–311, 2013.
- [23] S. Bhattacharya, B. Bepari, and S. Bhaumik, “Soft Robotic Finger Fabrication with PDMS and IPMC Actuator for Gripping,” in *SAI Computing Conference*, 2016, pp. 403–408.
- [24] W. Grot, “Manufacture,” in *Fluorinated Ionomers*, Second., Elsevier, 2011, pp. 11–48.
- [25] W. Grot, “Applications,” in *Fluorinated Ionomers*, Second., Elsevier, 2011, pp. 81–156.
- [26] M. Shahinpoor and K. J. Kim, “Ionic polymer metal composites: I. Fundamentals,” *Smart Mater. Struct.*, vol. 819, no. 833, pp. 819–833, 2001.
- [27] S. E. Nelson, “FEASIBILITY STUDY OF CUSTOM MANUFACTURING METHODS OF IONIC POLYMER-METAL COMPOSITE SENSORS,” University of Nevada, Las Vegas, 2013.
- [28] B. Kim *et al.*, “Analysis of mechanical characteristics of the ionic polymer metal composite (IPMC) actuator using cast ion-exchange film,” in *Proc SPIE Smart Materials and Structure*, 2003, vol. 5051, no. 1, p. 486.



- [29] K. Kim and M. Shahinpoor, "A novel method of manufacturing three-dimensional ionic polymer–metal composites (IPMCs) biomimetic sensors, actuators and artificial muscles," *Polymer (Guildf)*., vol. 43, no. 3, pp. 797–802, Feb. 2002.
- [30] B. Kim, J. Ryu, Y. Jeong, Y. Tak, B. Kim, and J.-O. Park, "A ciliary motion based 8-legged walking micro robot using cast IPMC actuators," in *International Conference on Robotics and Automation*, 2002, pp. 85–91.
- [31] T. Stalbaum, S. E. Nelson, V. Palmre, and K. J. Kim, "Multi degree of freedom IPMC sensor," in *Proceedings of the SPIE Smart Structures and Materials Symposium*, 2014, vol. 9056, p. 90562J.
- [32] C. Jo, D. Pugal, I. K. Oh, K. J. Kim, and K. Asaka, "Recent advances in ionic polymer-metal composite actuators and their modeling and applications," *Prog. Polym. Sci.*, vol. 38, no. 7, pp. 1037–1066, 2013.
- [33] V. Palmre, D. Pugal, K. J. Kim, K. K. Leang, K. Asaka, and A. Aabloo, "Nanothorn electrodes for ionic polymer-metal composite artificial muscles," *Sci. Rep.*, vol. 4, p. 6176, 2014.
- [34] M. Shahinpoor and K. J. Kim, "The effect of surface-electrode resistance on the performance of ionic polymer-metal composite (IPMC) artificial muscles," *Smart Mater. Struct.*, vol. 9, no. 4, pp. 543–551, 2000.
- [35] J.-W. Lee and Y.-T. Yoo, "Preparation and performance of IPMC actuators with electrospun Nafion®–MWNT composite electrodes," *Sensors Actuators B Chem.*, vol. 159, no. 1, pp. 103–111, Nov. 2011.
- [36] S. Lee and H. Park, "Performance improvement of IPMC (ionic polymer metal composites) for a flapping actuator," *Int. J. Control. Autom. Syst.*, vol. 4, no. 6, pp. 748–755, 2006.

- [37] S. J. Kim, I. T. Lee, and Y. H. Kim, "Performance enhancement of IPMC actuator by plasma surface treatment," *Smart Mater. Struct.*, vol. 16, no. 1, pp. N6–N11, 2007.
- [38] J. Park, V. Palmre, T. Hwang, K. Kim, W. Yim, and C. Bae, "Electromechanical performance and other characteristics of IPMCs fabricated with various commercially available ion exchange membranes," *Smart Mater. Struct.*, vol. 23, no. 7, p. 74001, Jul. 2014.
- [39] Y. Bahramzadeh and M. Shahinpoor, "Dynamic curvature sensing employing ionic-polymer–metal composite sensors," *Smart Mater. Struct.*, vol. 20, no. 9, p. 94011, Sep. 2011.
- [40] A. J. Duncan, D. J. Leo, and T. E. Long, "Beyond Nafion: Charged Macromolecules Tailored for Performance as Ionic Polymer Transducers," *Macromolecules*, vol. 41, no. 21, pp. 7765–7775, Nov. 2008.
- [41] R. Tiwari and E. Garcia, "The state of understanding of ionic polymer metal composite architecture: a review," *Smart Mater. Struct.*, vol. 20, no. 8, p. 83001, Aug. 2011.
- [42] Solvay, "Aquivion ® E87-05S." 2015.
- [43] Chemours, "Nafion 117 specifications," 2016. .
- [44] W. Y. Hsu and T. D. Gierke, "Ion Clustering and Transport in Nafion Perfluorinated Membranes," *J. Memb. Sci.*, vol. 13, pp. 307–326, 1983.
- [45] M. Chaplin, "Water Molecule Structure," 2000. [Online]. Available: [http://www1.lsbu.ac.uk/water/water\\_molecule.html](http://www1.lsbu.ac.uk/water/water_molecule.html).
- [46] S. Trabia, Z. Olsen, and K. J. Kim, "Searching for a new ionomer for 3D printable ionic polymer–metal composites: Aquivion as a candidate," *Smart Mater. Struct.*, vol. 26, no. 11, p. 115029, Nov. 2017.

- [47] D. Pugal, T. Stalbaum, V. Palmre, and K. J. Kim, "Chapter 5. Modeling Ionic Polymer Metal Composites with COMSOL: Step-by-Step Guide," in *RSC Smart Materials*, vol. 2016–Janua, no. 17, 2016, pp. 185–214.
- [48] Z. Olsen, "The Design, Modeling, and Optimization of a Biomimetic Soft Robot for Fluid Pumping and Thrust Generation Using Electroactive Polymer Actuators," 2018.
- [49] T. Mochizuki, K. Kakinuma, M. Uchida, S. Deki, M. Watanabe, and K. Miyatake, "Temperature- and Humidity-Controlled SAXS Analysis of Proton-Conductive Ionomer Membranes for Fuel Cells (supporting information)," *ChemSusChem*, vol. 7, no. 3, pp. S1–S8, 2014.
- [50] J. Peng and T. A. Zawodzinski, "Ion transport in phase-separated single ion conductors," *J. Memb. Sci.*, vol. 555, no. January, pp. 38–44, 2018.
- [51] K. Asaka and K. Oguro, "Bending of polyelectrolyte membrane platinum composites by electric stimuli. Part II. Response kinetics," *J. Electroanal. Chem.*, vol. 480, no. 1–2, pp. 186–198, 2000.
- [52] J. Lin, Y. Liu, and Q. M. Zhang, "Charge dynamics and bending actuation in Aquivion membrane swelled with ionic liquids," *Polymer (Guildf)*, vol. 52, no. 2, pp. 540–546, Jan. 2011.
- [53] R. B. Moore, K. M. Cable, and T. L. Croley, "Barriers to flow in semicrystalline ionomers. A procedure for preparing melt-processed perfluorosulfonate ionomer films and membranes," *J. Memb. Sci.*, vol. 75, no. 1–2, pp. 7–14, 1992.
- [54] K. A. Mauritz and R. B. Moore, "State of understanding of Nafion," *Chem. Rev.*, vol. 104, no. 10, pp. 4535–4585, 2004.
- [55] S. H. de Almeida and Y. Kawano, "Thermal Behavior of Nafion Membrane," *J. Therm.*

- Anal. Calorim.*, vol. 58, pp. 569–577, 1999.
- [56] Q. Zhao and J. Benziger, “Mechanical properties of perfluoro sulfonated acids: The role of temperature and solute activity,” *J. Polym. Sci. Part B Polym. Phys.*, vol. 51, no. 11, pp. 915–925, 2013.
- [57] W. Grot, “Properties,” in *Fluorinated Ionomers*, 2nd ed., Plastics Design Library, 2011, pp. 49–79.
- [58] J. A. Elliott *et al.*, “Hydrolysis of the Nafion® precursor studied by X-ray scattering and in-situ atomic force microscopy,” *e-Polymers*, vol. 1, no. 1, pp. 1–11, Jan. 2001.
- [59] D. D. Pugal, T. Stalbaum, V. Palmre, and K. J. Kim, “Chapter 5. Modeling Ionic Polymer Metal Composites with COMSOL: Step-by-Step Guide,” in *RSC Smart Materials*, vol. 2016–Janua, no. 17, 2016, pp. 185–214.
- [60] M. H. Kim, C. J. Glinka, S. A. Grot, and W. G. Grot, “SANS study of the effects of water vapor sorption on the nanoscale structure of perfluorinated sulfonic acid (NAFION) membranes,” *Macromolecules*, vol. 39, no. 14, pp. 4775–4787, 2006.
- [61] Solvay, “Aquivion ® E87-05S Data Sheet.” 2015.
- [62] W. Grot, “Manufacture,” in *Fluorinated Ionomers*, 2011, pp. 11–48.
- [63] Solvay, “Aquivion ® P87S-SO2F Data Sheet.” 2015.
- [64] T. Stalbaum *et al.*, “Physics-based modeling of mechano-electric transduction of tube-shaped ionic polymer-metal composite,” *J. Appl. Phys.*, vol. 117, pp. 1–8, 2015.
- [65] J. D. Carrico, N. W. Traeden, M. Aureli, and K. K. Leang, “Fused filament 3D printing of ionic polymer-metal composites (IPMCs),” *Smart Mater. Struct.*, vol. 24, no. 12, p. 125021, 2015.
- [66] T. Xie, “Tunable polymer multi-shape memory effect.,” *Nature*, vol. 464, no. 7286, pp.

- 267–270, 2010.
- [67] S. Goodyer, “Measuring Polymers using a Rotational Rheometer in Oscillatory Mode.” Anton Paar Ltd., pp. 1–35.
- [68] A. V. Shenoy and D. R. Saini, *Thermoplastic Melt Rheology and Processing (Plastics Engineering)*. CRC Press, 1996.
- [69] C. A. Hieber and H. H. Chiang, “Shear-rate-dependence modeling of polymer melt viscosity,” *Polym. Eng. Sci.*, vol. 32, no. 14, pp. 931–938, 1992.
- [70] M. Shahinpoor, “Biomimetic robotic Venus flytrap ( *Dionaea muscipula* Ellis ) made with ionic polymer metal composites,” *Bioinspir. Biomim.*, vol. 6, no. 4, p. 46004, Dec. 2011.
- [71] Q. Shen, T. Wang, J. Liang, and L. Wen, “Hydrodynamic performance of a biomimetic robotic swimmer actuated by ionic polymer – metal composite,” *Smart Mater. Struct.*, vol. 22, pp. 1–13, 2013.
- [72] M. Aureli, V. Kopman, and M. Porfiri, “Free-locomotion of underwater vehicles actuated by ionic polymer metal composites,” *IEEE/ASME Trans. Mechatronics*, vol. 15, no. 4, pp. 603–614, 2010.
- [73] Q. Shen, T. Wang, and K. J. Kim, “A biomimetic underwater vehicle actuated by waves with ionic polymer–metal composite soft sensors,” *Bioinspir. Biomim.*, vol. 10, no. 5, p. 55007, Sep. 2015.
- [74] M. Ul Haq, Z. Gang, and H. Muhammad Waqas, “A Comprehensive Review of the Biomimetic Applications of Ionic Polymer Metal Composite,” *J. Biomimetics, Biomater. Biomed. Eng.*, vol. 23, pp. 47–58, Jun. 2015.
- [75] M. Ul Haq, Z. Gang, F. E. Ahad, A. Ur Rehman, and M. Hussain, “Inverse Kinematic Analysis of Three Link Mechanism for Fin Actuation of Fish Like Micro Device,” *J.*

- Biomimetics, Biomater. Biomed. Eng.*, vol. 24, pp. 77–81, Jul. 2015.
- [76] R. Tiwari and E. Garcia, “The state of understanding of ionic polymer metal composite architecture: a review,” *Smart Mater. Struct.*, vol. 20, no. 8, p. 83001, Aug. 2011.
- [77] P. J. C. Branco and J. a Dente, “Derivation of a continuum model and its electric equivalent-circuit representation for ionic polymer–metal composite (IPMC) electromechanics,” *Smart Mater. Struct.*, vol. 15, no. 2, pp. 378–392, Apr. 2006.
- [78] T. Yang and Z. Chen, “Development of 2D maneuverable robotic fish propelled by multiple ionic polymer-metal composite artificial fins,” in *2015 IEEE International Conference on Robotics and Biomimetics (ROBIO)*, 2015, pp. 255–260.
- [79] M. A. Tsugawa, V. Palmre, J. D. Carrico, K. J. Kim, and K. K. Leang, “Slender tube-shaped and square rod-shaped IPMC actuators with integrated sensing for soft mechatronics,” *Meccanica*, vol. 50, no. 11, pp. 2781–2795, 2015.
- [80] R.-J. Chung, T.-S. Chin, L.-C. Chen, and M.-F. Hsieh, “Preparation of gradually componential metal electrode on solution-casted Nafion<sup>TM</sup> membrane,” *Biomol. Eng.*, vol. 24, no. 5, pp. 434–437, Nov. 2007.
- [81] Q. He, M. Yu, L. Song, H. Ding, X. Zhang, and Z. Dai, “Experimental Study and Model Analysis of the Performance of IPMC Membranes with Various Thickness,” *J. Bionic Eng.*, vol. 8, no. 1, pp. 77–85, Mar. 2011.
- [82] T. Hwang, V. Palmre, J. Nam, D.-C. Lee, and K. J. Kim, “A new ionic polymer–metal composite based on Nafion/poly(vinyl alcohol- co -ethylene) blends,” *Smart Mater. Struct.*, vol. 24, no. 10, p. 105011, 2015.
- [83] R. Jiang, H. R. Kunz, and J. M. Fenton, “Composite silica/Nafion® membranes prepared by tetraethylorthosilicate sol–gel reaction and solution casting for direct methanol fuel

- cells,” *J. Memb. Sci.*, vol. 272, no. 1–2, pp. 116–124, Mar. 2006.
- [84] T. D. Gierke, G. E. Munn, and F. C. Wilson, “The morphology in nafion perfluorinated membrane products, as determined by wide- and small-angle x-ray studies,” *J. Polym. Sci. Polym. Phys. Ed.*, vol. 19, no. 11, pp. 1687–1704, Nov. 1981.
- [85] R. B. Moore and C. R. Martin, “Procedure for preparing solution-cast perfluorosulfonate ionomer films and membranes,” *Anal. Chem.*, vol. 58, no. 12, pp. 2569–2570, Oct. 1986.
- [86] M. Fujimura, T. Hashimoto, and H. Kawai, “Small-angle x-ray scattering study of perfluorinated ionomer membranes. 1. Origin of two scattering maxima,” *Macromolecules*, vol. 14, no. 5, pp. 1309–1315, Sep. 1981.
- [87] L. Shen, Z. Sun, Y. Chu, J. Zou, and M. Deshusses, “Novel sulfonated Nafion®-based composite membranes with pillararene as selective artificial proton channels for application in direct methanol fuel cells,” *Int. J. Hydrogen Energy*, vol. 40, no. 38, pp. 13071–13079, Oct. 2015.
- [88] F. Zhang, Z. Zhang, Y. Liu, H. Lu, and J. Leng, “The quintuple-shape memory effect in electrospun nanofiber membranes,” *Smart Mater. Struct.*, vol. 22, no. 8, p. 85020, Aug. 2013.
- [89] V. Di Noto, R. Gliubizzi, E. Negro, and G. Pace, “Effect of SiO<sub>2</sub> on Relaxation Phenomena and Mechanism of Ion Conductivity of [Nafion/(SiO<sub>2</sub>)<sub>x</sub>] Composite Membranes†,” *J. Phys. Chem.*, vol. 110, no. 49, pp. 24972–24986, Dec. 2006.
- [90] K. Ketpang, S. Shanmugam, C. Suwanboon, N. Chanunpanich, and D. Lee, “Efficient water management of composite membranes operated in polymer electrolyte membrane fuel cells under low relative humidity,” *J. Memb. Sci.*, vol. 493, pp. 285–298, Nov. 2015.
- [91] L. Sha Wang, A. Nan Lai, C. Xiao Lin, Q. Gen Zhang, A. Mei Zhu, and Q. Lin Liu, “Orderly

- sandwich-shaped graphene oxide/Nafion composite membranes for direct methanol fuel cells,” *J. Memb. Sci.*, vol. 492, pp. 58–66, Oct. 2015.
- [92] Q. Deng, C. A. Wilkie, R. B. Moore, and K. A. Mauritz, “TGA–FTi.r. investigation of the thermal degradation of Nafion® and Nafion®/[silicon oxide]-based nanocomposites,” *Polymer (Guildf)*., vol. 39, no. 24, pp. 5961–5972, Nov. 1998.
- [93] J. Zheng, Q. He, C. Liu, T. Yuan, S. Zhang, and H. Yang, “Nafion-microporous organic polymer networks composite membranes,” *J. Memb. Sci.*, vol. 476, pp. 571–579, Feb. 2015.
- [94] C. Chen and T. F. Fuller, “The effect of humidity on the degradation of Nafion® membrane,” *Polym. Degrad. Stab.*, vol. 94, no. 9, pp. 1436–1447, Sep. 2009.
- [95] M. Shahinpoor, “Conceptual design, kinematics and dynamics of swimming robotic structures using ionic polymeric gel muscles,” *Smart Mater. Struct.*, vol. 1, no. 1, pp. 91–94, Mar. 1992.
- [96] Q. Shen, T. Wang, J. Liang, and L. Wen, “Hydrodynamic performance of a biomimetic robotic swimmer actuated by ionic polymer–metal composite,” *Smart Mater. Struct.*, vol. 22, no. 7, p. 75035, Jul. 2013.
- [97] B. Kim, D.-H. Kim, J. Jung, and J.-O. Park, “A biomimetic undulatory tadpole robot using ionic polymer–metal composite actuators,” *Smart Mater. Struct.*, vol. 14, no. 6, pp. 1579–1585, Dec. 2005.
- [98] Z. Chen, T. I. Um, and H. Bart-smith, “Bio-inspired robotic manta ray powered by ionic polymer – metal composite artificial muscles,” vol. 5411, no. April, 2012.
- [99] W. Yim, J. Lee, and K. J. Kim, “An artificial muscle actuator for biomimetic underwater propulsors,” *Bioinspir. Biomim.*, vol. 2, no. 2, pp. S31–S41, Jun. 2007.
- [100] N. Kamamichi, M. Yamakita, K. Asaka, and Zhi-Wei Luo, “A snake-like swimming robot



- using IPMC actuator/sensor,” in *Proceedings 2006 IEEE International Conference on Robotics and Automation, 2006. ICRA 2006.*, 2006, vol. 2006, no. May, pp. 1812–1817.
- [101] M. Shahinpoor and K. J. Kim, “Design, development, and testing of a multifingered heart compression/assist device equipped with IPMC artificial muscles,” in *Smart Structures and Materials 2001: Electroactive Polymer Actuators and Devices*, 2001, vol. 4329, p. 411.
- [102] D. Pugal, K. Jung, A. Aabloo, and K. J. Kim, “Ionic polymer-metal composite mechanoelectrical transduction: review and perspectives,” *Polym. Int.*, vol. 59, no. 3, pp. 279–289, Jan. 2010.
- [103] A. T. Abdulsadda and X. Tan, “An artificial lateral line system using IPMC sensor arrays,” *Int. J. Smart Nano Mater.*, vol. 3, no. 3, pp. 226–242, Sep. 2012.
- [104] B. Paola, L. Fortuna, P. Giannone, S. Graziani, and S. Strazzeri, “IPMCs as vibration sensors,” in *Conference Record - IEEE Instrumentation and Measurement Technology Conference*, 2008, pp. 2065–2069.
- [105] Z. Chen, T. I. Um, and H. Bart-Smith, “Bio-inspired robotic manta ray powered by ionic polymer–metal composite artificial muscles,” *Int. J. Smart Nano Mater.*, vol. 3, no. 4, pp. 296–308, Dec. 2012.
- [106] T. Yang and Z. Chen, “Development of 2D maneuverable robotic fish propelled by multiple ionic polymer-metal composite artificial fins,” in *2015 IEEE International Conference on Robotics and Biomimetics (ROBIO)*, 2015, pp. 255–260.
- [107] V. Palmre *et al.*, “An IPMC-enabled bio-inspired bending/twisting fin for underwater applications,” *Smart Mater. Struct.*, vol. 22, no. 1, p. 14003, Jan. 2013.
- [108] K. Kim and M. Shahinpoor, “A novel method of manufacturing three-dimensional ionic polymer–metal composites (IPMCs) biomimetic sensors, actuators and artificial muscles,”

- Polymer (Guildf)*., vol. 43, no. 3, pp. 797–802, Feb. 2002.
- [109] J. Nam, T. Hwang, K. J. Kim, and D. Lee, “A new high-performance ionic polymer–metal composite based on Nafion/polyimide blends,” *Smart Mater. Struct.*, vol. 26, no. 3, p. 35015, Mar. 2017.
- [110] S. Trabia, T. Hwang, and K. J. Kim, “A fabrication method of unique Nafion® shapes by painting for ionic polymer–metal composites,” *Smart Mater. Struct.*, vol. 25, no. 8, p. 85006, 2016.
- [111] J. D. Carrico and K. K. Leang, “Fused Filament 3D Printing of Ionic Polymer-Metal Composites for Soft Robotics,” in *SPIE Proceedings*, 2017.
- [112] B. N. Turner, R. Strong, and S. A. Gold, “A review of melt extrusion additive manufacturing processes: I. Process design and modeling,” *Rapid Prototyp. J.*, vol. 20, no. 3, pp. 192–204, Apr. 2014.
- [113] M. Khandelwal and M. M. Mench, “Direct measurement of through-plane thermal conductivity and contact resistance in fuel cell materials,” *J. Power Sources*, vol. 161, no. 2, pp. 1106–1115, Oct. 2006.
- [114] Chemours, “Nafion Membrane Data Sheet.” 2016.
- [115] Solvay, “Aquivion ® P87S-SO2F.” 2015.
- [116] R. Shankar, T. K. Ghosh, and R. J. Spontak, “Dielectric elastomers as next-generation polymeric actuators,” *Soft Matter*, vol. 3, no. 9, p. 1116, 2007.
- [117] NASA, “Effect of Shape on Lift.” .
- [118] O. Lilienthal and G. Lilienthal, “Der Vogelflug als Grundlage der Fliegekunst. Ein Beitrag zur Systematik der Flugtechnik.” 1889.
- [119] S. Heathcote, D. Martin, and I. Gursul, “Flexible Flapping Airfoil Propulsion at Zero

- Freestream Velocity,” *AIAA J.*, vol. 42, no. 11, pp. 2196–2204, 2004.
- [120] J. M. Miao and M. H. Ho, “Effect of flexure on aerodynamic propulsive efficiency of flapping flexible airfoil,” *J. Fluids Struct.*, vol. 22, no. 3, pp. 401–419, 2006.
- [121] R. Unger, M. C. Haupt, P. Horst, and R. Radespiel, “Fluid-structure analysis of a flexible flapping airfoil at low Reynolds number flow,” *J. Fluids Struct.*, vol. 28, pp. 72–88, 2012.
- [122] E. Abdullah, C. Bil, and S. Watkins, “Application of Smart Materials for Adaptive Airfoil Shape Control,” in *47th AIAA Aerospace Sciences Meeting including The New Horizons Forum and Aerospace Exposition*, 2009, pp. 1–11.
- [123] A. Fontanazza, R. Talling, M. Jackson, R. Dashwood, D. Dye, and L. Iannucci, “Morphing wing technologies research,” *Seas DTC first Conf.*, 2006.
- [124] J. Scheller *et al.*, “A Combined Smart-Materials Approach for Next-Generation Airfoils,” *Solid State Phenom.*, vol. 251, pp. 106–112, 2016.
- [125] Q. Shen, K. J. Kim, and T. Wang, “Electrode of ionic polymer-metal composite sensors: Modeling and experimental investigation,” *J. Appl. Phys.*, vol. 115, no. 19, p. 194902, May 2014.
- [126] Q. Shen, V. Palmre, T. Stalbaum, and K. J. Kim, “A comprehensive physics-based model encompassing variable surface resistance and underlying physics of ionic polymer-metal composite actuators,” *J. Appl. Phys.*, vol. 118, no. 12, p. 124904, Sep. 2015.
- [127] D. Pugal, K. J. Kim, and A. Aabloo, “An explicit physics-based model of ionic polymer-metal composite actuators,” *J. Appl. Phys.*, vol. 110, no. 8, p. 84904, Oct. 2011.

## Curriculum Vitae

### Sarah Trabia

Ph.D. Candidate in Mechanical Engineering

sarahtrabia@gmail.com

[LinkedIn](#)

[Google Scholar](#)

[ORCID](#)

### Education

- Ph.D. University of Nevada, Las Vegas, “*Comprehensive Study of Spray-Painting, Extruding, and 3D Printing Fabrication Methods for Nafion® and Nafion® Equivalents for Ionic Polymer-Metal Composite Actuators and Sensors,*” Mechanical Engineering, May 2018 (Expected), GPA: 3.83  
Advisor: Dr. Kwang Kim
- M.S. University of Nevada, Las Vegas, “*Analytical and Experimental Analysis of Magnetorheological Elastomers,*” Mechanical Engineering, August 2014, GPA: 4.0  
Advisor: Dr. Woosoon Yim
- B.S. University of Nevada, Las Vegas, Honors Thesis: “*The Design and Testing of a Solar Autoclave with Broad Spectrum Sterilization Capabilities,*” Mechanical Engineering, December 2012, Magna Cum Laude, GPA: 3.76  
Advisor: Dr. Robert Boehm

### Journal Publications

1. **Trabia, S.**; Choi, K.; Olsen, Z.; Hwang, T.; Nam, J.; Kim, K. Understanding the Thermal Properties of Precursor-Ionomers to Optimize Fabrication Processes for Ionic Polymer-Metal Composites (IPMCs). *Materials* (Basel). 2018, 11, 665, DOI:10.3390/ma11050665.
2. An, H., Karas, D., Kim, B.-W., **Trabia, S.**, Moon, J. (2017) Flexible n-type thermoelectric composite films with enhanced performance through interface engineering and post-treatment. *Nanotechnology*. (Accepted).
3. **Trabia, S.**, Olsen, Z., and Kim, K. J. (2017). Searching for a new ionomer for 3D printable ionic polymer-metal composites: Aquivion® as a candidate. *Smart Materials and Structures*. 26(11), 1-17. DOI: 10.1088/1361-665X/aa919f.
4. Stalbaum, T., Hwang, T., **Trabia, S.**, Shen, Q., Hunt, R., Olsen, Z., & Kim, K. J. (2017) Bioinspired Travelling Wave Generation in Soft-Robotics using Ionic Polymer-Metal Composites. *International Journal of Intelligent Robotics and Applications*, 1(1), 1-13. DOI: 10.1007/s41315-017-0015-9.
5. Kim, K. J., Palmre, V., Stalbaum, T., Hwang, T., Shen, Q., & **Trabia, S.** (2016). Promising Developments in Marine Applications with Artificial Muscles: Electrodeless Artificial Cilia Microfibers. *Marine Technology Society Journal*, 50(5), 24-34. DOI: 10.4031/MTSJ.50.5.4.
6. **Trabia, S.**, Hwang, T., & Kim, K. J. (2016). A fabrication method of unique Nafion® shapes by painting for ionic polymer-metal composites. *Smart Materials and Structures*, 25(8), 085006. DOI: 10.1088/0964-1726/25/8/085006.
7. Shen, Q., **Trabia, S.**, Stalbaum, T., Palmre, V., Kim, K., & Oh, I. K. (2016). A multiple-shape memory polymer-metal composite actuator capable of programmable control, creating complex 3D motion of bending, twisting, and oscillation. *Scientific Reports*, 6. DOI: 10.1038/srep24462.

### Conference Publications

1. **Trabia, S.**, Olsen, Z., Hwang, T., & Kim, K. J. (2017, May). Producing intricate IPMC shapes by means of spray-painting and printing (Conference Presentation). In *SPIE Smart Structures and Materials+ Nondestructive Evaluation and Health Monitoring* (pp. 101630J-101630J). International Society for Optics and Photonics.
2. Shen, Q., Stalbaum, T., **Trabia, S.**, Hwang, T., Hunt, R., & Kim, K. (2017, April). Modeling of a soft multiple-shape-memory ionic polymer-metal composite actuator. In *SPIE Smart Structures and Materials+ Nondestructive Evaluation and Health Monitoring* (pp. 101650C-101650C). International Society for Optics and Photonics.
3. **Trabia, S.**, Shen, Q., Stalbaum, T., Hunt, R., Hwang, T., & Kim, K. (2016, October). Numerical and experimental investigation of a biomimetic robotic jellyfish actuated by Ionic Polymer-Metal Composite. In *Ubiquitous Robots and Ambient Intelligence (URAI), 2016 13th International Conference on* (pp. 204-205). IEEE.
4. Hwang, T., Palmre, V., Stalbaum, T. P., Shen, Q., **Trabia, S.**, & Kim, K. J. (2016, March). IPMC cilia system for artificial muscle applications. In *SPIE Smart Structures and Materials+ Nondestructive Evaluation and Health Monitoring* (pp. 979818-979818). International Society for Optics and Photonics.
5. Hwang, T., Nam, J., Shen, Q., **Trabia, S.**, Suhr, J., Lee, D. C., & Kim, K. J. (2016, March). Property modification of Nafion via polymer blending with ethylene vinyl alcohol polyimide. In *SPIE Smart Structures and Materials+ Nondestructive Evaluation and Health Monitoring* (pp. 979820-979820). International Society for Optics and Photonics.
6. **Trabia, S.**, Hwang, T., & Kim, K. J. (2016, March). A fabrication method of unique Nafion shapes by painting for ionic polymer-metal composites (Conference Presentation). In *SPIE Smart Structures and Materials+ Nondestructive Evaluation and Health Monitoring* (pp. 979817-979817). International Society for Optics and Photonics.
7. Stalbaum, T., **Trabia, S.**, Shen, Q., & Kim, K. J. (2016, March). Fluid flow sensing and control with ionic polymer-metal composites. In *SPIE Smart Structures and Materials+ Nondestructive Evaluation and Health Monitoring* (pp. 97982E-97982E). International Society for Optics and Photonics.
8. **Trabia, S.**, Palmre, V., & Kim, K. J. (2015, October). Development of self-sensing Ionic Polymer-Metal Composite soft robotic actuator integrated with gallium-indium alloy. In *Ubiquitous Robots and Ambient Intelligence (URAI), 2015 12th International Conference on* (pp. 368-369). IEEE.
9. **Trabia, S.**, Hwang, T., & Yim, W. (2014, March). Programmable variable stiffness 2D surface design. In *SPIE Smart Structures and Materials+ Nondestructive Evaluation and Health Monitoring* (pp. 90580X-90580X). International Society for Optics and Photonics.

### Book Chapters

1. Stalbaum, T., **Trabia, S.**, Hwang, T., Olsen, Z., Nelson, S., Shen, Q., Lee, D., Kim, K. J., Carrico, J., Leang, K., Palmre, V., Nam, J., Park, I., Tiwari, R., Kim, D., Kim, S. (2017). Guidelines for making Ionic Polymer-Metal Composite (IPMC) materials as artificial muscles by advanced manufacturing methods: State-of-the-Art. In *Advances in manufacturing and processing of materials and structures*. (Accepted; Under Revision)

### Experimental Expertise

During my undergraduate and graduate studies, I have gained knowledge and expertise in a wet lab environment as well as conducted various experiments. I have learned how to use a variety of laboratory equipment, including Contact Angle Analyzer (KSV Instruments Cam 200), Differential Scanning Calorimetry (DSC Q 10), Dynamic Mechanical Analysis (Pyris Diamond DMA), Fourier Transform Infrared Spectroscopy (IRPrestige-21), Scanning Electron Microscope (TM3030), and Thermogravimetric Analysis (TGA Q 500). I also have worked with many different 3D printers, including Form 2, Raised N2 Plus, and Zortrax M200.

### Programs Proficiency

Throughout my graduate studies, I have learned how to use different programs, including MATLAB, Solidworks, and COMSOL.

### Research Experience

- 2014 - present    Research Assistant, *Active Material and Smart Living Laboratory* University of Nevada, Las Vegas
- Conduct research on fabrication methods (spray-painting, extruding, and additive manufacturing) for ionomeric polymers to produce unique shapes for applications in soft robotics, specifically Ionomer Polymer-Metal Composites (IPMC)
- June, 2016        Research Assistant, NASA Langley Research Center
- Studied the use of thin films for increased radiation shielding for space shuttles in long-term expeditions
- 2013 - 2014      Graduate Assistant, Department of Mechanical Engineering, University of Nevada, Las Vegas
- Developed a device that uses magnetic field to control the stiffness of Magnetorheological elastomers.
- Jan. 2011 –      Research Assistant, Center for Materials and Structures, University of Nevada,  
August 2011    Las Vegas
- Tested composite cylinders for compressive strength at room and elevated temperatures (400°F and 750°F).

### Teaching Experience

- Spring 2015        Taught ME 330 “Analysis of Dynamic Systems” and designed the lectures, homework assignments, project, and exams
- Spring 2014 and    Taught Engineering Measurements and Automatic Controls undergraduate  
Fall 2014            labs. Duties include developing lab manuals

## Honors and Awards

- NASA Fellowship Spring 2014 and Spring 2016
- Member of Tau Beta Pi and Phi Kappa Phi honor societies

## Hobbies

I enjoy photography in my past time as well as traveling. I also enjoy taking care of my 20-gallon aquarium with various fish. I recently picked up crocheting and have started a few projects to work on in my past time.

## References

Dr. Kwang Kim, NV Energy Professor of Energy and Matter, and CoRE Fellow

- UNLV, Department of Mechanical Engineering
- [kwang.kim@unlv.edu](mailto:kwang.kim@unlv.edu), 702-774-1419

Dr. Woosoon Yim, Professor in Mechanical Engineering

- UNLV, Department of Mechanical Engineering
- [woosoon.yim@unlv.edu](mailto:woosoon.yim@unlv.edu), 702-895-0956

Dr. Ji Su, Researcher

- NASA Langley Research Center
- [ji.su-1@nasa.gov](mailto:ji.su-1@nasa.gov), 757-864-8336